UNIVERSIDADE FEDERAL DE SÃO CARLOS
CENTRO DE CIÊNCIAS EXATAS E DE TECNOLOGIA
DEPARTAMENTO DE QUÍMICA
PROGRAMA DE PÓS-GRADUAÇÃO EM QUÍMICA

Calibration strategies for elemental determination using direct solid analysis by X-ray spectroscopy and Laser-induced breakdown spectroscopy

Diego Victor de Babos*

Tese apresentada como parte dos requisitos para obtenção do título de DOUTOR EM CIÊNCIAS, área de concentração: QUÍMICA ANALÍTICA.

Orientador: Prof. Dr. Edenir Rodrigues Pereira Filho

*** bolsista CNPq**

São Carlos - SP
2020

UNIVERSIDADE FEDERAL DE SÃO CARLOS

Centro de Ciências Exatas e de Tecnologia
Programa de Pós-Graduação em Química

Folha de Aprovação

Defesa de Tese de Doutorado do candidato Diêgo Victor de Babos, realizada em 30/07/2020.

Comissão Julgadora:

Prof. Dr. Edenir Rodrigues Pereira Filho (UFSCar)

Profa. Dra. Cassiana Seimi Nomura (USP)

Prof. Dr. Hudson Wallace Pereira de Carvalho (CENA/USP)

Profa. Dra. Roberta Cerasi Urban (UFSCar)

Profa. Dra. Poliana Macedo dos Santos (UTFPR)

O presente trabalho foi realizado com apoio da Coordenação de Aperfeiçoamento de Pessoal de Nível Superior - Brasil (CAPES) - Código de Financiamento 001.
O Relatório de Defesa assinado pelos membros da Comissão Julgadora encontra-se arquivado junto ao Programa de Pós-Graduação em Química.

"Ainda que eu falasse as línguas dos homens e dos anjos, e não tivesse amor, seria como o metal que soa ou como o sino que tine.
E ainda que tivesse o dom de profecia, e conhecesse todos os mistérios e toda a ciência, e ainda que tivesse toda a fé, de maneira tal que transportasse os montes, e não tivesse amor, nada seria.
E ainda que distribuísse toda a minha fortuna para sustento dos pobres, e ainda que entregasse o meu corpo para ser queimado, e não tivesse amor, nada disso me aproveitaria.
O amor é sofredor, é benigno; o amor não é invejoso; o amor não trata com leviandade, não se ensoberbece.
Não se porta com indecência, não busca os seus interesses, não se irrita, não suspeita mal;
Não folga com a injustiça, mas folga com a verdade;
Tudo sofre, tudo crê, tudo espera, tudo suporta.
O amor nunca falha; mas havendo profecias, serão aniquiladas; havendo línguas, cessarão; havendo ciência, desaparecerá;
Porque, em parte, conhecemos, e em parte profetizamos;
Mas, quando vier o que é perfeito, então o que o é em parte será aniquilado.
Quando eu era menino, falava como menino, sentia como menino, pensava como menino, mas, logo que cheguei a ser homem, acabei com as coisas de menino.
Porque agora vemos por espelho em enigma, mas então veremos face a face; agora conheço em parte, mas então conhecerei como também sou conhecido.
Agora, pois, permanecem a fé, a esperança e o amor, estes três, mas o maior destes é o amor."

I Coríntios 13, 1-13

Dedico esse trabalho a Deus, minha família, amigos e professores.

AGRADECIMENTOS

A Deus honra e glória eternamente! Obrigado pelo dom da Vida, por me sustentar e sentir sua presença! “Louvado seja o Nosso Senhor Jesus Cristo!”

Á minha família, pelo carinho, por me incentivar e por não medir esforços em ajudar a concretizar os meus sonhos: aos meus pais Iracy e Nizia, o meu irmão Jeferson, avós e demais familiares. Muito obrigado, amo vocês!

A minha amada Bruna, pelo amor, confiança, companheirismo e todo carinho.

Ao Professor Edenir, muito obrigado pela oportunidade de conhecer, trabalhar, aprender, ser orientado em todos os aspectos (profissional e pessoal) e poder conviver com você. A “oportunidade” concedida proporcionou um novo norte em minha vida profissional. Você é um ser humano fantástico! Obrigado por tudo!

Ao Professor Jesús Anzano, pela oportunidade, orientação e atenção durante a realização do estágio de doutorado no exterior. Aos amigos Abrahan Velásquez, Andrés Cruz e Flávio Nakadi. A Universidad de Zaragoza - Espanha por toda a infraestrutura necessária. ¡Muchas gracias!

Aos amigos, colegas e professores que o Grupo de Análise Instrumental Aplicada me proporcionou durante esses quatro anos de curso: Ariane Barros, Vinícius, Ariane Neiva, Raimundo, Fernanda, Matheus, Eduardo, Raquel, Jeyne, Daniel, Marco, Amanda, Alisson, José Augusto, Wendel, Ana Beatriz, Julymar, Ívero, Mykaelli, Herick, Beatriz, Cibeli, Alex, Ana Rita, Lucimar e Joaquim. Vocês são especiais! Com vocês, o café, as reuniões de grupo e as análises são melhores...

Aos membros da banca por aceitarem o convite e por avaliarem esta tese. O meu muito obrigado pela contribuição de cada um de vocês!

Ao Programa de Pós-graduação em Química, secretárias e coordenação pelo apoio.

A Universidade Federal de São Carlos e ao Departamento de Química pela estrutura necessária no desenvolvimento desse trabalho.

Ao Conselho Nacional de Desenvolvimento Científico e Tecnológico - CNPq pela bolsa concedida, e a todos os brasileiros que com a contribuição tributária patrocinaram essa bolsa de estudo.

As editoras Elsevier e Royal Society of Chemistry pela autorização do uso dos artigos publicados e apresentados nesta tese.

Ao Laboratório Nacional de Luz Síncrotron - LNLS pela oportunidade de realizar experimentos na linha de espectroscopia de absorção de raios-X (XAS) - número do projeto SXS-20170074.

O presente trabalho foi realizado com apoio da Coordenação de Aperfeiçoamento de Pessoal de Nível Superior - CAPES, código de financiamento 001.

Muito obrigado!

This PhD thesis is based on the following publications which are presented in the original format:

"Direct determination of calcium and phosphorus in mineral supplements for cattle by wavelength dispersive X-ray fluorescence (WD-XRF)"
Diego Victor Babos, Vinícius Câmara Costa, Marco Aurelio Sperança and Edenir Rodrigues Pereira-Filho, *Microchemical Journal* 137 (2018) 272-276.

"Wavelength dispersive X-ray fluorescence (WD-XRF) applied to speciation of sulphur in mineral supplement for cattle: evaluation of the chemical and matrix effects"
Diego Victor Babos, Vinícius Câmara Costa and Edenir Rodrigues Pereira-Filho, *Microchemical Journal* 147 (2019) 628-634.

"Determination and speciation of phosphorus in fertilizers and mineral supplements for cattle by X-ray absorption near-edge structure spectroscopy: a simple nondestructive method"
Diego Victor Babos, Jeyne Pricylla Castro, Daniel Fernandes Andrade, Vinicius Câmara Costa and Edenir Rodrigues Pereira Filho, *Analytical Methods* 11 (2019) 1508-1515.

"Calibration strategies to overcome matrix effects in laser-induced breakdown spectroscopy: direct calcium and phosphorus determination in solid mineral supplements"
Diego Victor Babos, Ariane Isis Barros, Joaquim Araújo Nóbrega and Edenir Rodrigues Pereira-Filho, *Spectrochimica Acta Part B* 155 (2019) 90-98.

"**Direct Determination of Al and Pb in waste printed circuit boards (PCB) by Laser-induced breakdown spectroscopy (LIBS): evaluation of calibration strategies and economic-environmental questions"**
Diego Victor Babos, Andrés Cruz-Conesa, Edenir Rodrigues Pereira-Filho and Jesús Manuel Anzano, *Journal of Hazardous Materials* 399 (2020) 122831.

LIST OF ACRONYMS

A_{ki}	transition probability between the upper and lower levels of the transition
ANN	artificial neural network
$C_{analyte}$	concentration of analyte
CF	calibration-free
cps	count *per* second
CRM	certified reference material
$C_{standard}$	concentration of standard
Cδ graphs	Csigma graphs
d	interplanar space of diffracting planes
EC	external calibration
ED XRF	energy dispersive X-ray fluorescence
eV	electron volt
EXAFS	extended X-ray absorption fine structure spectroscopy
f	function
FPC	flow proportional counter
fs	femtosecond
HCA	hierarchical cluster analysis
HR-CS F AAS	high-resolution continuum source flame atomic absorption spectrometry
I	X-ray intensity transmitted
I/Δλ	Intensity divided by Lorentzian width
I_0	X-ray incident intensity
ICP OES	inductively coupled plasma optical emission spectrometry
I_F	X-ray fluorescence
IS	internal standardization
J cm^{-2}	Joule *per* centimeter squared
K	Kelvin
KNN	k-nearest neighbor

kPCR	kernel principal component regression
λ	wavelength
LAMIS	laser-induced breakdown isotopic molecular spectroscopy
lasso	least absolute shrinkage and selection operator regression
LCF	linear combination fitting
LDA	linear discriminant analysis
LIBS	laser-induced breakdown spectroscopy
LTE	local thermodynamic equilibrium
μ	mass attenuation coefficient
μ(E)	X-ray absorption coefficient
μg	microgram
μm	micrometer
μs	microsecond
μ-XRF	micro X-ray fluorescence
MCR-ALS	multivariate curve resolution alternating least-squares algorithm
MEC	multi-energy calibration
MIP OES	microwave-induced plasma optical emission spectrometry
MLR	multiple linear regression
MMC	matrix-matching calibration
n	order of the diffracted
NIPALS	nonlinear interactive partial least square
NIR	near-infrared spectroscopy
nm	nanometer
ns	nanosecond
OP GSA	one-point gravimetric standard addition
OP MLC	one-point and multi-line calibration
OP-CF	one-point calibration-free
PARAFAC	parallel factor analysis
PCA	principal component analysis

PCB	printed circuit board
PCR	principal component regression
PLS	partial least squares
PLS-1	partial least squares- single response model
PLS-2	partial least squares- multiple response model
PLS-DA	partial least squares discriminant analysis
RFR	random forest regression
RSD	relative standard deviation
s	second
SA	standard addition
SC	scintillation counter
SIMCA	soft independent modeling of class analogy
$\mathbf{slope_{sample}}$	slope calculated for linear model obtained for the sample
$\mathbf{slope_{standard}}$	slope calculated for linear model obtained for the standard
SRC	slope ratio calibration
SSC	single-sample calibration
SVR-line	support vector regression with linear kernel
SVR-poly	support vector regression with second order polynomial kernel
T XRF	total reflection X-ray fluorescence
TP CT	two-point calibration transfer
WD XRF	wavelength dispersive X-ray fluorescence
WT-RF	wavelength transform-random forest
x	sample thickness
XANES	X-ray absorption near-edge structure
δl	line cross section
θ	Bragg angle

LIST OF FIGURES

RESUMO

ESTRATÉGIAS DE CALIBRAÇÃO PARA DETERMINAÇÃO ELEMENTAR EMPREGANDO ANÁLISE DIRETA DE SÓLIDOS POR *X-RAY SPECTROSCOPY* E *LASER-INDUCED BREAKDOWN SPECTROSCOPY*. A análise direta de amostras sólidas empregando as técnicas como *wavelength dispersive X-ray fluorescence* (WD XRF), *X-ray absorption near-edge structure* (XANES) *spectroscopy* e *laser-induced breakdown spectroscopy* (LIBS), apresentam muitas vantagens para o desenvolvimento de novos métodos analíticos. Contudo, como a amostra é analisada integralmente (analito e matriz presente na porção analisada) por estas técnicas, fortes efeitos de matriz e preparo inadequado dos padrões de calibração sólidos, podem ocorrer e comprometer a determinação com exatidão e precisão necessárias. Várias estratégias de calibrações univariada e multivariada, e diferentes preparos de padrões de calibração sólidos, foram avaliadas para a determinação direta de i) Ca, P e S em suplementos minerais para bovinos por WD XRF, incluindo a análise de especiação de S (espécies enxofre elementar e sulfato); ii) de espécies de P (fosfato and fosfito) em fertilizantes e suplementos minerais para bovinos por espectroscopia XANES, e iii) de Ca e P em suplementos minerais, e de Al e Pb em resíduos eletroeletrônico, utilizando a LIBS. As estratégias avaliadas foram calibração com compatibilização de matriz, padronização interna, *calibration-free*, *single-sample calibration*, *one-point and multi-line calibration*, *two-point calibration transfer*, *partial least squares regression* e *linear combination fitting*. Duas novas estratégias de calibrações univariadas foram propostas para a análise direta de sólidos por LIBS: i) *multi-energy calibration* e *one-point gravimetric standard addition*. Estratégias estas que possibilitam uma eficiente compatibilização de matriz e minimizam os efeitos de matriz. Considerando as vantagens e limitações das estratégias de calibração avaliadas, das características intrínsecas das amostras analisadas e dos analitos determinados, associadas a ferramentas quimiométricas apropriadas; novos métodos de determinação e de análise de especiação química são propostos nesta tese, com excelentes parâmetros de desempenho analítico.

ABSTRACT

CALIBRATION STRATEGIES FOR ELEMENTAL DETERMINATION USING DIRECT SOLID ANALYSIS BY X-RAY SPECTROSCOPY AND LASER-INDUCED BREAKDOWN SPECTROSCOPY. Direct analysis of solid samples using techniques such as wavelength dispersive X-ray fluorescence (WD XRF), X-ray absorption near-edge structure (XANES) spectroscopy and laser-induced breakdown spectroscopy (LIBS); have many advantages for the development of new analytical methods. However, as the sample is analyzed in its entirety (analyte and matrix present in the analyzed portion) by these techniques, strong matrix effects and inadequate preparation of the solid calibration standards can occur and compromise the determination with the necessary accuracy and precision. Several univariate and multivariate calibration strategies and different preparations of solid calibration standards were evaluated for the direct determination of i) Ca, P and S in mineral supplements for cattle by WD XRF, including the speciation analysis of S (elemental sulfur and sulfate species); ii) species of P (phosphate and phosphite) in fertilizers and mineral supplements for cattle XANES spectroscopy, and iii) of Ca and P in mineral supplements, and Al and Pb in electronics waste using LIBS. The evaluated strategies were matrix-matching calibration, internal standardization, calibration-free, single-sample calibration, one-point and multi-line calibration, two-point calibration transfer, partial least squares regression and linear combination fitting. Two new univariate calibration strategies have been proposed for the direct analysis of solids by LIBS: i) multi-energy calibration and one-point gravimetric standard addition. These strategies enable efficient matrix-matching and minimize matrix effects. Considering the advantages and limitations of the evaluated calibration strategies, the intrinsic characteristics of the analyzed samples and the determined analytes, associated with appropriate chemometric tools; new methods of determination and analysis of chemical speciation were proposed in this thesis, with excellent parameters of analytical performance.

SUMMARY

Chapter 1 – Introduction

1. Introduction

Direct analysis of solid samples has many advantages and some limitations when used for elements determination by atomic spectroscopy. In order to obtain good figures of merit, calibration strategies for elements determination must efficiently overcome or minimize matrix effects from the solid sample integrally analyzed. In this section, the intrinsic characteristics of the direct solid analysis will be discussed, as well as univariate and multivariate calibration strategies, both employed for the techniques of direct analysis by wavelength dispersive X-ray fluorescence (WD XRF) and laser-induced breakdown spectroscopy (LIBS).

1.1. Direct solid analysis

The possibility of obtaining qualitative and quantitative information on the analyte by directly analyzing a solid sample, with none or minimal treatment, is attractive to analysts and employed using different analytical techniques such as WD XRF, LIBS, among others.[1]

Direct solid analysis is a term used in Analytical Chemistry, when the solid sample is integrally analyzed, that is, in the portion of the sample used for analysis, the analyte and matrix are present. The solid analysis procedure can be obtained from a pressed pellet, fused discs (fusion), suspension, loose powder, or directly from the sample.[1,2] Several advantages of this procedure make it attractive to be used in the development of analytical methods, when compared to traditional wet sample preparation methods (acid decomposition, for example), highlighting:

i- simplification of sample pre-treatment, reducing the time spent on this stage of the analytical sequence, and thus increasing the analytical frequency;

ii- nondestructive / semi-destructive analysis;

iii- greater detectability of analytes by analytical techniques, because the sample is not diluted;

iv- minimizing the risk of contamination and loss of analytes by volatilization or adsorption on the walls of the flasks, because flasks and reagents are not used for sample decomposition;

v- less danger to the analyst as it does not require toxic or corrosive reagents, such as oxidant acids that are normally used;

vi- less waste generation, according to the principles of “green chemistry”; and

vii- possibility of analyzing a small amount of the sample (e.g. µg, using LIBS), making it possible to evaluate the sample's micro-homogeneity.[1-3]

However, some factors are critical in the development of the analytical method and should be considered when using direct solid analysis, highlighting the homogeneity and the sample mass. Sample homogeneity is directly associated with particle size and distribution of the analyte in the sample. Thus, the smaller the particle size distribution interval (preferable <10 µm) and its diameter the better the sample homogeneity and distribution of contained analytes.[3]

Homogeneity can be obtained using an adequate milling procedure considering the intrinsic characteristics of the sample and the mills. Thus, the particle size makes it possible to obtain homogeneity in the distribution of the analyte in the sample, which directly reflects on the precision of the measurements.[3]

An example of how the sample's homogeneity reflects in the distribution of the analyte is shown in Figure 1.1. Using a mineral supplement for cattle, two pellets were prepared, one without homogenization and other with the sample homogenized in mortar and pistil. Using 100 LIBS spectra collected (matrix 10x10), a spectral image was obtained.[4] From the emission intensity of each spectrum, for P I 213.63 nm line, an spectral image was obtained, being possible to visualize the spatial distribution of P macronutrient in the solid sample.

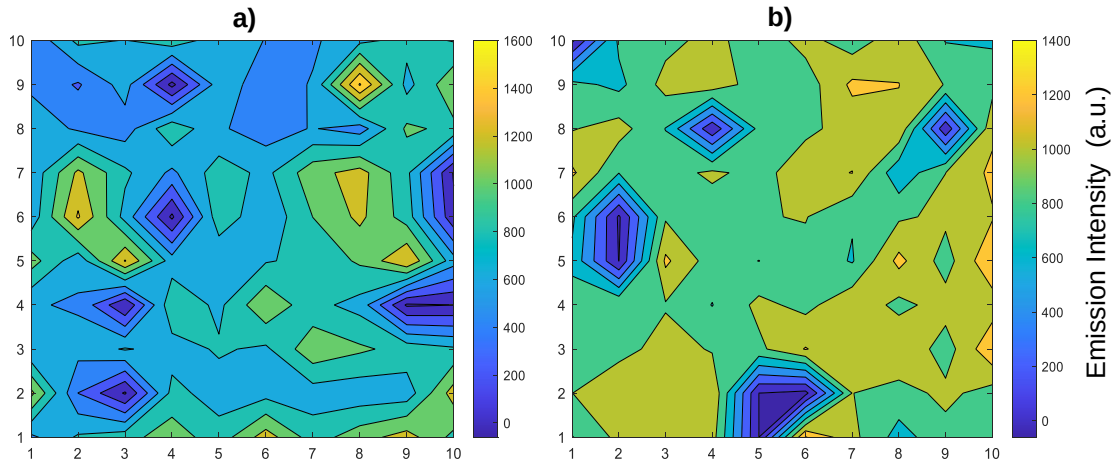

FIGURE 1.1 Spectral image for P I 213.63 nm using LIBS spectra obtained for a non-homogenized (a) mineral supplement for cattle pellet and other homogenized (b) in mortar and pistil (500 mg of sample, 2.7 J cm^{-2} laser fluence and 1 µs delay time).

When the sample has been homogenized (Fig. 1.1b), phosphorus is homogeneously distributed on the sample surface, indicating that there is no significant influence of the particle size on the spatial distribution of this element. However, when the sample was not properly homogenized (Fig. 1.1a), many clusters, depicted by colors yellow and blue, of element are observed in certain regions of the sample. In addition, the relative standard deviation (RSD) values of the emission intensities of the spectra obtained in the homogenized sample showed an adequate RSD value (16%), when compared to the non-homogenized sample (RSD = 25%), which will reflect directly in the accuracy and precision of LIBS determinations.

Other factor that is highlighted is the sample mass analyzed, as the portion taken for analysis must be representative of the whole to ensure the precision and accuracy of the analytical results.[2,3] In LIBS, masses around 500 mg are used to obtain cohesive pellets, however only µg of sample *per* laser pulse is analyzed. Thus, a considerable number of laser pulses (usually above 50 pulses) are performed in different regions of the sample, to obtain a representative analysis.

Another example of how the mass of the analyzed sample is important in direct solid analysis is when WD XRF technique is used. For the quantitative analysis by WD XRF, the amount of sample to be pelleted (when necessary) must be standardized so that samples and calibration standards are

subjected to the same pressure, and thus obtain cohesive pellets with similar densities, so that the emission of X-rays is not affected.[2] In addition, the mass attenuation coefficient (μ) that is related to the depth of penetration of electromagnetic radiation in a material, and depends on the mass and density of the sample; it must be similar for sample and standards, in order to obtain satisfactory accuracy and precision.[5]

Matrix effects must also be considered and may limit the use of direct solid analysis in the development of some analytical methods. The sample matrix can influence the interaction of electromagnetic radiation with the analyte of different magnitudes and forms, and thus influence the obtaining of the analytical signal.[1] The main matrix effects in the direct solid analysis are associated with spectral and non-spectral interferences. The non-spectral matrix effects are related to the physical and chemical properties of the sample, such as humidity, presence of easily ionizable elements, irregular surface, particle size, and elements that attenuate or intensify the analytical signal.[2,5-9] However, a way to overcome the matrix effects, and to make adequate determinations feasible, is to use appropriate calibration strategies.

1.2. Calibration strategies employed in direct solid analysis

Method calibration for quantitative analysis is an important step in the analytical method, and should be performed after considering the intrinsic properties of the analytical technique employed, the analyte and the sample. Difficulties in choosing the best calibration strategy to be used are found mainly when using direct solid analysis. When the sample matrix is integrally present in the analyzed portion, matrix effects can strongly influence the monitored analytical signals. Thus, the matrix effects will consequently influence the accuracy and precision of the analyte determination. However, the use of solid calibration standards and appropriate calibration strategies can minimize or to overcome matrix effects and allow good parameters for analytical performance.[1,10]

Various calibration strategies i) traditional, ii) non-traditional and iii) multivariate are widely used, and others have recently been proposed.[1,10-12] The choice of the calibration strategy for the method and the preparation of the solid

calibration standards to be used, strongly depend on the behavior of the analyte and the matrix when interacting with electromagnetic radiation. In the following paragraphs I will describe the main univariate and multivariate calibration strategies used in direct analysis of solids in both LIBS and WD XRF techniques.

Matrix-matching calibration (MMC) is probably the most used strategy when direct solid analysis is performed. Solid calibration standards are usually prepared using a sample set with analyte concentrations determined by a reference method, a set of certified reference materials (CRMs), or sample dilution (with known analyte concentration) in sample concomitants. This strategy permits to minimize the matrix effects, since the physic-chemical properties of the calibration standards and samples are similar.[10,13-16] Some limitations of MMC are related to the i) difficulty of obtaining a set of samples or CRMs with reference concentrations, due to the costs and availability of CRMs and some analytical techniques; and ii) most commercial CRMs do not ensure homogeneity for sample masses below 100 mg (a problem for LIBS which uses sample masses generally <10 mg). In addition, some solid samples are difficult to prepare and analyze by other techniques to obtain reference values.[10,11,14]

The standard addition (SA) calibration is a strategy that corrects strong matrix effects, since the preparation of the calibration standards used to obtain the analytical curve, are made for each sample by the known addition of a standard containing the analyte. As the sample matrix will be present in all calibration standards, the matrix effects will be circumvented and thus allow determinations with appropriate accuracy.[11,17,18] The requirement of considerable amount of sample for the preparation of the standards, an effective procedure of homogenization of the sample and solid standard containing the analyte and low analytical frequency, are examples of limitations of the use of SA.[14]

Internal standardization (IS) calibration minimizes matrix effects and correct instrumental fluctuations during the acquisition of the analytical signal. The ratio of the analyte signal to the internal standard signal is used to obtain a calibration curve. It is advisable that the analyte and the element used as an internal standard should have similar physic-chemical properties, and that the concentration of the internal standard is constant in the prepared solid

standards and samples. In this case the magnitude of the matrix effects and instrumental fluctuations are efficiently corrected / normalized. Difficulties in the selection and addition of internal standard in the sample prevents the use of IS in some applications for direct solid analysis.[11,13,19-22]

Surely MMC, SA and IS are the traditional univariate calibration strategies most applied for chemical elements determination using direct analysis of solid samples in LIBS and WD XRF. However, multivariate calibration strategies are also applied to both techniques, such as partial least squares (PLS),[23-26] principal component regression (PCR)[23,26] and data fusion.[27,28]

In multivariate calibration, chemometric tools try to find the relationship between samples (scores) and variables (loadings)[29] and thus propose a calibration model with good predictive ability of the analyte concentration, for example. Thus, several variables are measured for a set of samples (for example, spectral intervals of atomic emission or X-ray fluorescence), and from the vector measured for each sample (first order calibration) are used to propose a model capable of determining all types of variation in these data.

The main advantages of multivariate calibration are related to i) exploratory aspects, where several parameters obtained can be used to improve, understand and investigate the model generated (for example, based on the score values, it is possible to identify an outlier, which may be related to the different chemical composition of a particular sample in the sample set), ii) noise reduction using multiple responses, improving model robustness and precision and iii) inclusion of variables related to interferences in the model, which provides greater robustness to the model, since it is possible to obtain good predictive capacity when in the calibration model the interferents are considered, which can be generated by the sample matrix.[29-31]

PLS regression is a multivariate technique that permits to obtain a calibration model in the presence of interferents, but not to correct it. Using nonlinear interactive partial least square (NIPALS) as algorithm for data processing, the PLS regression uses a selected number of latent variables to decompose not only the **X** matrix (independent variables) with n samples and m variables ($\mathrm{X} = \mathrm{TP}^{\mathrm{T}} + \mathrm{E}$, where **T** is the score matrix, **P** is the loading matrix and

E is the matrix of residuals) but also the vector y (dependent variables) with n rows (reference concentration) ($y = UQ^T + F$, where **U** is scores, **Q** is loadings and **F** is residuals for y). Therefore, the PLS calculates the correlation between **X** and y maximizing the covariance between the scores. After this decomposition, the scores and loadings are used to calculate the regression coefficients b for the prediction of a vector ŷ, $\hat{y} = Xb$, where b is a vector of regression coefficients, and ŷ corresponds to predicted concentrations of the element of interest.[31-33] This strategy was successfully used for methods using the LIBS and WD XRF techniques, as in the direct determination and analysis of speciation of Cr in soil, plastic and paint by WD XRF;[23] and rare earth elements in hard disk magnets by LIBS,[25] among others.

PCR regression is another multivariate calibration tool used in the analysis of solid samples.[23,26] PCR is a regression based on the same decomposition as the PCA. First, the algorithm decomposes a matrix $X = TP^T + E$, with *n* samples and *m* pixels or variables. In the case of LIBS, the variables are the emission lines signals recorded and for WD XRF, the transition energies (Kα, Kβ, Lβ, …). Through a selection of principal components, important information is retained in the score matrix **T**. After this decomposition, the scores and loadings are used to calculate the regression coefficients *b* for the prediction of a vector ŷ with *n* rows, and predicted concentration of analyte.[31-33]

An advanced approach for multivariate calibration is data fusion. This strategy combines multiple data sources obtained from different analytical techniques, for samples and standards, in a new single model with fused data. In addition, data fusion makes it possible to obtain more information on data and analytical parameters.[27,28] An interesting method was proposed by GAMELA et al. (2020), using the data fusion by LIBS and WD XRF, and the multivariate model generated by multiple linear regression (MLR), as a calibration strategy for the direct determination of K, Mg and P in bean seed samples. Good analytical performance parameters were obtained with the data fusion obtained by direct analysis of the samples, when compared with the matrix-matching calibration univariate strategy.[27]

In the study by DE OLIVEIRA et al. (2019),[28] the data fusion from the spectra obtained by LIBS and near-infrared spectroscopy (NIR), using the PLS multivariate model was successfully applied in the direct analysis of

vegetable samples for determination of micro- and macronutrients. The elementary information obtained by the LIBS spectra merged with the spectral information regarding the molecular composition of the samples by NIR, made it possible to obtain a model with exact predictions of the concentration of the analytes.[28]

There are many calibration strategies proposed for direct solid analysis, and all of them have advantages and limitations in their implementation. However, the choice of the best strategy is directly related with the ability of the calibration to overcome and / or minimize the matrix effects for each analyte. Although LIBS and WD XRF techniques allow for multi elementary determinations, not necessarily a given calibration strategy will allow good analytical performance parameters for all analytes. This can occur because the magnitude and complexity of the matrix effects (spectral or non-spectral) can act differently for each analyte. Thus, it is necessary to evaluate the preparation of the solid calibration standards, the available strategies and develop new calibration strategies that permits to overcome these effects, and thus directly analyze the solid sample and determine all analytes with satisfactory precision and accuracy.

Others calibration strategies that are specific and recently proposed for the WD XRF and LIBS techniques will be discussed in detail in the Chapters 2 and 3, respectively.

Chapter 2 – X-ray spectroscopy

2. X-ray spectroscopy

X-ray spectroscopy is the study of the interaction of electromagnetic radiation called X-ray with the matter. X-rays can be defined as electromagnetic radiation of wavelengths (λ) in the range of approximately 10^{-6} to 10 nm, produced by deceleration of high-energy electrons and/or by electron transitions in the inner orbitals of atoms.[6]

The interaction of X-rays with matter can be described in different ways, highlighting scattering (coherent or incoherent), transmission, diffraction and absorption.[6] When absorbed, they can produce other X-rays due to the photoelectric effect, as illustrated in Figure 2.1 for a sulphur atom. This phenomenon is very important for X-ray fluorescence spectrometry, which is based on the measurement of the characteristic X-ray fluorescence by atoms present in the sample.

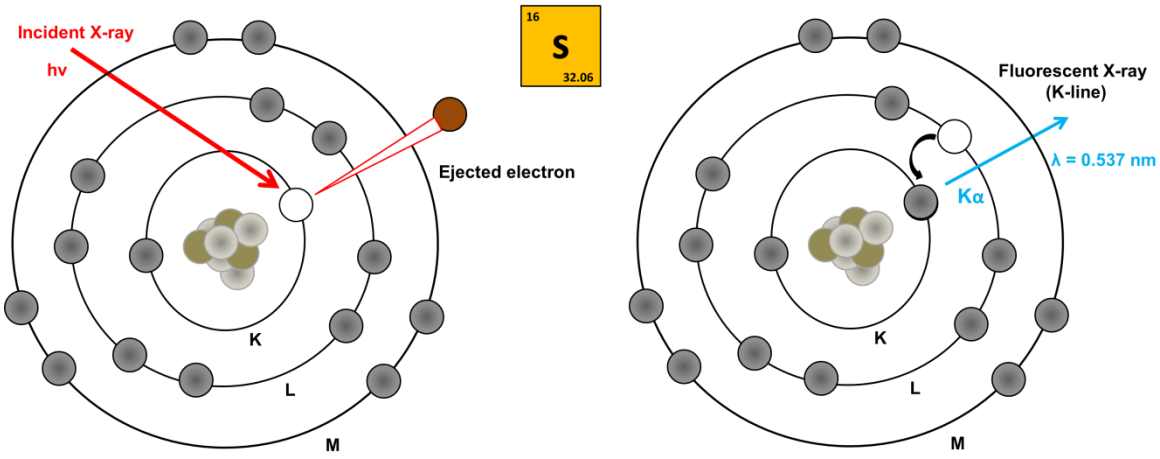

FIGURE 2.1 Representation of the X-ray fluorescence phenomenon for a sulphur atom.

Primary X-ray photons, from an X-ray tube or synchrotron radiation, for example; when absorbed by an electron in the innermost layer of the atom, provoke electron ejection, forming a vacancy. Subsequently, an electron from a higher energy level fills this vacancy and emits a characteristic fluorescent X-ray photon (line) resulting from this electronic transition. Electron transitions are virtually instantaneous, taking place within 10^{-12} to 10^{-14} s of the creation of an electron vacancy.[6] The energy (referring to the given λ) and the intensity of this emitted photon are used in X-ray fluorescence spectrometry for the qualitative and quantitative analysis.

When an X-ray photon interacts with sample containing sulphur, for example, X-ray fluorescence can occur (Fig. 2.1). And if the L layer electron fills the electronic vacancy in the K layer, we will have an electronic transition called SKα and an X-ray fluorescence line at λ = 0.537 nm.

Several techniques can be used to obtain X-ray fluorescence or X-ray absorption measurements, the most used are wavelength dispersive X-ray fluorescence (WD XRF), energy dispersive X-ray fluorescence (ED XRF), total reflection X-ray fluorescence (T XRF), micro X-ray fluorescence (μ-XRF), X-ray absorption near-edge structure spectroscopy (XANES) and extended X-ray absorption fine structure spectroscopy (EXAFS). These techniques differ mainly in the detection mode and source of the primary X-ray generation, review articles and books can be consulted for further details about the state of the art.[1,2,5,6,34-36]

In the experimental procedure performed in this PhD thesis, were used one X-ray fluorescence technique (WD XRF) and one X-ray absorption technique (XANES), as analytical tools for the direct solid analysis (mineral supplements for cattle) and suspensions (fertilizers) in order to evaluate i) calibration strategies, ii) preparation of solid calibration standards, iii) analysis of chemical speciation, iv) evaluation of matrix and chemical effects and v) elementary determination.

2.1 Wavelength dispersive X-Ray Fluorescence

Wavelength dispersive X-ray fluorescence (WD XRF) is an attractive multi-element, non-destructive analytical technique that enables direct solid analysis of many types of samples.[1] A simplified representation of the instrumental arrangement of a WD XRF spectrometer is shown in FIGURE 2.2

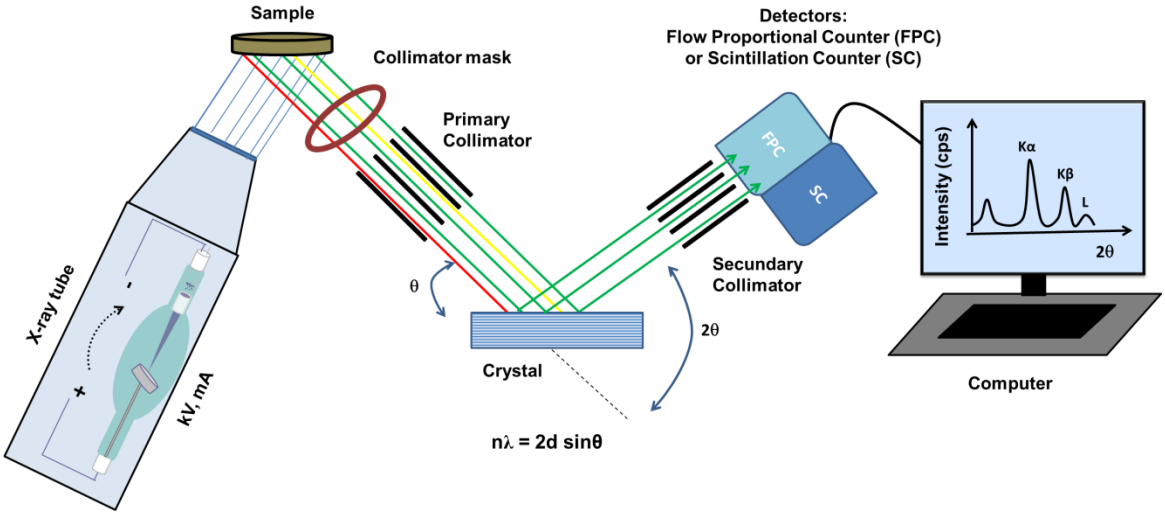

FIGURE 2.2 Simplified representations of the components of a WD XRF spectrometer.

Using an appropriate current and voltage, the primary X-ray emission can be produced by the deceleration of high-energy electrons, from a W filament, on a metallic target (for example, from Rh target). The interaction of primary X-rays focused on the sample surface, promotes electronic transitions and X-ray fluorescence of the elements present in the sample. In addition, the deceleration of primary X-rays by atom's electron field produces white or continuous radiation.[6]

Subsequently, the primary collimator intercepts divergent X-ray from the sample (fluorescent and continuous radiation) to ensure that an effectively parallel beam arrives at both the analyzing crystal. Using an appropriate crystal analysis (from different materials such as LiF, Ge, among others) this radiation is dispersed at different wavelengths according to Bragg's law: $n\lambda = 2d\,sin\theta$, where *n* is order of the diffracted beam and is numerically equal to the path difference, in wavelengths, for two successive planes; λ is wavelength, *d* is interplanar space of diffracting planes and θ is Bragg angle, the angle between the incident X-ray and the diffraction planes. The choice of analyzing crystal should consider the intrinsic characteristics of the analyte and the crystal (as desired resolution and sensitivity).[5,6]

The different diffracted λ are sent to the detector using a secondary collimator. The detection of X-rays by WD XRF can be sequential or simultaneous, and is usually done using the flow proportional counter (FPC) detector or scintillation counter (SC) detector. An X-ray detector transduces,

converts X-ray photons (a form of energy) into electrical voltages pulses that can be measured electronically.[5,6] So a multi-element X-ray fluorescence spectrum (intensity in count per second (cps) *versus* 2θ degrees) that can be used for qualitative and quantitative purposes.

WD XRF has been used in several qualitative analysis proposals, such as i) acquisition of spectral image of Ni and Cu analyzing Ni film on a Cu plate, using a spectrometer equipped with a high sensitivity imaging sensor and 10s counting time;[37] and Cu, Br, Sn and Pb spectral image of an electric device;[38] ii) particulate matter in filters for the acquisition of elementary information used in environmental monitoring;[39] iii) human hair to assess the chemical composition after cosmetic treatment;[40] among others.

I highlight in qualitative analysis by WD XRF the possibility of carrying the analysis of chemical speciation of certain elements using high resolution-energy spectrometers and the direct solid analysis. X-ray spectra are sensitive to the oxidation states of the analyte, due to the electronic transitions resulting from the electrons of the analyte and their interaction with the ligands (chemical effects). After appropriate data treatment and suitable instrumental conditions, WD XRF can be an excellent analytical tool for chemical speciation analysis, due to the minimal manipulation of the sample and non-destructive analysis, which minimizes one of the main problems observed in this type of analysis: the inter-conversion of chemical species of the analyte and laborious sample preparation. By monitoring different electronic transitions it was possible, for example, to analyze the speciation of S (S 0 and S +VI; S –II and S +VI),[41-43] Cr (Cr +III and Cr +VI),[23] Fe (Fe +II and Fe +III)[43] and Mn (Mn +II, Mn +III and Mn +IV).[44]

For quantitative analysis, analytes in the concentration range of ug g^{-1} to % can be determined by WD XRF. This technique has been used in the analysis of different samples as i) human placenta to verify correlations between the neonate weight and maternal age;[45] ii) bivalve mollusks for direct determination of Ca, K, Mg, Na, P, S, Fe and Zn nutrients;[16] iii) plant material for determination of major, trace and non-essential elements;[46] iv) sediment for determination of bromine;[22] v) silicate rocks and soils employing fused glass discs for determination of 26 major and trace elements;[47] vi) hard drive disks from electronic waste for determination of Nd,[48] among others.

Although WD XRF is an excellent analytical tool in the development of quantitative methods, efforts are necessary to select efficient calibration strategies and preparation procedure of the solid calibration standards that make it possible to overcome matrix and chemical effects.

The quantification method using the fused glass discs is generally effective to reduce secondary X-ray absorption and enhancement (matrix effect) by coexisting elements in a sample.[49] However, some algorithms, available in some WD XRF spectrometer software, allow corrections of absorption and enhancement effects, with theoretical calculation, such as fundamental parameter method, fundamental algorithm and theoretical α coefficient method.[11,50] Some calculations were proposed to establish the relationship between concentrations of elements and measured intensities, such as Sherman formula and De Jongh formula.[11,50] However, other matrix effects related to measured intensity (or peak width and peak positions) and matrix composition is complicated, and the influence of effects cannot be evaluated quantitatively. Thus, the use of appropriate calibration strategies is necessary. Univariate and multivariate calibration strategies such as MMC, SA, IS and PLS, when used in WD XRF, make it possible to correct the matrix effects and provide excellent analytical performance parameters.

Recently three new calibration strategies for WD XRF were proposed by CASTRO et al. (2020).[48] The strategies i) one-point gravimetric standard addition - OP GSA, ii) multi-energy calibration - MEC and iii) two-point calibration transfer - TP CT, were evaluated for the direct determination of Nd in hard drive disks magnets samples. In these new calibration strategies only one calibration standard is required for TP CT and two solid calibration standards for MEC and OP GSA. Using five different electronic transitions of the analyte (Nd $L\gamma_1$, Nd $L\beta_2$, Nd $L\beta_3$, Nd $L\beta_4$ and Nd $L\alpha_1$) is obtained a linear model for MEC. Using only an electronic transition to OP GSA and TP CT it was possible to obtain a calibration curve or linear model. These new univariate strategies make it possible to efficiently matrix-matching method (MEC and OP GSA), identify spectral interference (MEC), require few solid calibration standards (only one for TP CT) and obtain results with satisfactory precision and accuracy.

2.1.1 Direct determination of calcium and phosphorus in mineral supplements for cattle by wavelength dispersive X-ray fluorescence (WD-XRF). Microchemical Journal 137 (2018) 272-276.

Microchemical Journal 137 (2018) 272–276

Contents lists available at ScienceDirect

Microchemical Journal

journal homepage: www.elsevier.com/locate/microc

Direct determination of calcium and phosphorus in mineral supplements for cattle by wavelength dispersive X-ray fluorescence (WD-XRF)

Diego Victor Babos, Vinícius Câmara Costa, Marco Aurelio Sperança, Edenir Rodrigues Pereira-Filho *

Group of Applied Instrumental Analysis, Department of Chemistry, Federal University of São Carlos, São Carlos, São Paulo State 13565-905, Brazil

ARTICLE INFO

Article history:
Received 23 October 2017
Received in revised form 3 November 2017
Accepted 4 November 2017
Available online 6 November 2017

Keywords:
Solids direct analysis
Matrix-matching
Mineral supplements for cattle
WD-XRF
Animal nutrition

ABSTRACT

The current study describes a simple and rapid method for the direct determination of Ca and P in mineral supplements for cattle by wavelength dispersive - X-ray fluorescence (WD-XRF). For calibration, solid standards obtained through a set of reference materials (RMs) of mineral supplements for cattle with concentrations of Ca ranged from 120 to 223 g kg^{-1} ($r = 0.9809$) and P ranged from 29 to 95 g kg^{-1} ($r = 0.9957$) were used. For Ca, the matrix-matching using the RM 18/03 diluted in Na_2CO_3: NaCl (1:1 w/w) in the range of 0–204 g kg^{-1} ($r = 0.9975$) was also used as calibration strategy. The proposed method presented limits of detection of 47 mg kg^{-1} for Ca and 36 mg kg^{-1} for P using calibrations with RMs and 61 mg kg^{-1} to Ca using matrix-matching calibration strategy. Accuracy was assessed by the analysis of four RM of mineral supplements for cattle. A statistical evaluation using student's *t*-test showed that there is no significant difference between the value obtained with the proposed method and the certified value, at 95% confidence level. The method was successfully applied and is a good alternative to conventional acid digestion routine analysis for determination of Ca and P in mineral supplements for cattle.

1. Introduction

The agricultural sector is one of the main Brazilian highlights in the agribusiness world scenario, being responsible for a substantial part of the gross domestic product. However, P deficiency in the bovine herd is a significant factor for low milk and meat productivity, therefore, animal supplementation with this element is nearly mandatory. P is the macronutrient that represents the highest cost in the composition of the mineral supplement and together with the Ca take place directly of the animal bone composition [1,2]. The Ministry of Agriculture, Livestock and Supply (MAPA) regulates the manufacture of mineral supplements regarding their classification, composition, registration and inspection in the market [3]. Monitoring of Ca and P in mineral supplements for cattle must be carried out to control the quality of these inputs, thus generating greater confidence in the entire production chain until reaching the consumer.

Several analytical techniques such as, atomic absorption spectrometry (AAS) [4,5] inductively coupled plasma optical emission spectrometry (ICP OES) [6], ion chromatography (IC) [7] and spectrophotometry in the UV–Vis [8], have been applied to determine the elemental concentration in mineral supplements for cattle. These techniques require a sample pre-treatment to convert the solid material to a homogeneous aqueous solution through the procedures of acid digestion using open or closed systems [9,10]. In addition, a sample dilution is necessary to reduce the acidity and, depending on the analytical technique employed, sensitivity is compromised. Systematic errors can also be introduced due to contamination, sample manipulation or analyte losses by volatilization, which affect the accuracy of the results [11].

In contrast to intensive sample preparation procedures and manipulation involving acid digestion, direct analysis of solid samples with minimal manipulation is a reliable alternative and presents important advantages, such as: 1) improvement of the analytical frequency, where several samples (around 20–50) can be processed per hour; 2) drastically reduction of the chance of contamination, since reagents are not used; 3) minimization of errors related to sample manipulation and exposure to the laboratory environment; 4) minimization of analyte losses (mainly those that are volatile); 5) the operator avoids the used of toxic or corrosive acids; 6) less chemical residues generation; 7) increased detection capability, as the samples are not diluted; and 8) the use of small amounts of sample (<1 g) [12,13].

In this sense, wavelength dispersive - X-ray fluorescence (WD-XRF) is an attractive technique being used in direct analysis of several types of complex samples [14–19]. WD-XRF is a well-established technique that allows direct and non-destructive analysis in solid sample. In addition, it can conduct simultaneous multi-element measurements (typically from sodium to uranium) and allows the analysis of solid and liquid samples. It is considered a selective technique with simple spectra when compared to ultraviolet emission.

* Corresponding author.
E-mail address: erpf@ufscar.br (E.R. Pereira-Filho).

https://doi.org/10.1016/j.microc.2017.11.002
0026-265X/

Direct analysis by WD-XRF presents relative standard deviation (%RSD) greater than or equal those obtained by conventional techniques such as FAAS and ICP OES [20]. However, to obtain these levels of RSD, the availability of solid calibration standards, whose chemical and physical composition are similar to the samples or adequate methods to compensate for the main X-ray fluorescence matrix, effects (absorption or intensification phenomena of X-ray) [21,22] is low. In this sense, some calibration strategies are used, such as internal standardization (IS) [16], matrix-matching of the samples by fusion [22], and the use of a set of the samples as reference and certified reference materials (CRMs) [23–27].

However, the above-mentioned calibration strategies require care when implemented. The IS, for example, requires that analyte and internal standard have similar physicochemical properties for this strategy to be used effectively; in the matrix-matching by fusion (much used in the treatment of mineralogical samples) the use of large amount of flux can be a source of contamination, in addition to loss of analyte by volatilization during heating. In some cases, there is no CRMs that can be used, as these are not compatible with the sample, and present a high cost that difficult their use [16,22–27]. Hence, strategies of simple and fast calibration that employ the direct analysis of solids by WD-XRF must be implemented.

In this regard, the goal of this study is to develop a simple and fast procedure for the direct analysis in mineral supplements for cattle for the determination of Ca and P by WD-XRF employing different calibration strategies. Moreover, the proposed method minimizes the use of reagents, sample manipulation, time and costs.

2. Materials and methods

2.1. Instrumentation

A Perform-X ARL (Thermo Fischer, Madison, WI, USA) wavelength dispersive - X-ray fluorescence (WD-XRF) was used for directly analyses of the samples. Samples were irradiated with X-ray emission provided by an Rh tube with a maximum of 4200 W. In addition, the X-rays emitted from the electronic transitions of the elements enter into the optical section of the equipment, passing first through collimators, and then they are reflected by specific crystals. The detectors register the counts per second of the X-ray emission lines that correspond to each crystal used. Each crystal in the equipment can reflect different regions of wavelength, ranging from 0.124 Å (LiF220) to 162.662 Å (AX16c). There are 5 crystals that can be used in the wavelength dispersion, and the choice is based on which crystal can disperse the characteristic wavelength from the element studied. The instrument is also equipped with 4 different collimators (0.15 mm, 0.40 mm, 1.00 mm and 2.60 mm) and 2 detectors: a flow proportional counter (FPC) and a scintillation counter (SC). For all elements evaluated in this study, only the electronic transition Kα was considered. In order to obtain the data the following fluorescence emission signals were measured (n = 3): Ca Kα and P Kα. The current and the voltage applied to the X-ray source was evaluated at intervals of 50 to 100 mA at 30 and 60 kV, respectively. The other instrumental conditions of analysis are described in Table 1.

Table 1
Instrumental parameters used for the direct determination of Ca and P in mineral supplements for cattle by WD-XRF.

Parameters	Ca	P
λ (Å)	3.359	6.158
2θ (°)	113.086	141.035
Crystal	LiF200	Ge111
Collimator (mm)	0.150	0.400
Elliptical mask (mm)	10	10
Counting time (s)	20	20
Detector	FPC[a]	

[a] Flow proportional counter.

Reference Ca and P concentrations were obtained using an inductively coupled plasma optical emission spectrometer (ICP OES) (iCAP 6000, Thermo Scientific, Waltham, MA, USA), after acid digestion of the samples (n = 3). This instrument allows sequential emission signals collection using both axial and radial viewing. A pneumatic nebulizer was used and the instrumental conditions were established as the manufacturer recommendations, as follow: power (1.15 kW), plasma gas flow (12 L min^{-1}), auxiliary gas flow (0.5 L min^{-1}), nebulizer gas flow (0.7 L min^{-1}) and sample introduction flow rate (2.1 mL min^{-1}). Emission lines monitored were: Ca 317.93 nm and P 178.28 nm.

2.2. Reagents, solutions and samples

Ultrapure water (18.2 ΩM cm^{-1} resistivity) produced by a Milli-Q® Plus Total Water System (Millipore Corp., Bedford, MA, USA) was used to prepare all the solutions. Nitric acid (HNO_3) was previously purified using a sub-boiling distillation system Distillacid™ BSB-939-IR (Berghof, Eningen, Germany). All glassware and polypropylene flasks were washed with soap, soaked in 10% v/v HNO_3 for 24 h, rinsed with deionized water prior to use. Standard solutions containing 250 mg L^{-1} Ca and 75 mg L^{-1} P were prepared by diluting standard stock solutions containing 10,000 mg L^{-1} Ca and 1000 mg L^{-1} P (Specsol, São Paulo, Brazil), and acidified with HNO_3 10% v/v.

Salts of NaCl (Merck, Darmstadt, Germany) and Na_2CO_3 (Mallinckrodt, Missouri, USA) were used as diluents in the preparation of the calibration solid standards. To evaluate the accuracy of the proposed method, mineral supplements for cattle reference materials (RMs) were analyzed: RM 17/03, RM 18/06, RM 18/09 and RM SM03/2010; all obtained from Embrapa Southeast Livestock (São Carlos - SP).

Six different samples of bovine mineral supplements were obtained commercially (Rio Paranaíba - MG and São Carlos - SP). These samples were dried to a constant mass and later homogenized in mortar and pistil. Subsequently, the solid samples and all calibration standards (500 mg) were packed into 13-mm-diameter pellets using a hydraulic press (GS15011, Specac), applying 10 t of pressure for 2 min.

2.3. Proposed method and calibration strategies

The evaluation of the power applied at the primary X-ray source on the intensity of fluorescence emission for Ca and P was performed in the scanning mode. The counting time on the precision of the measurements was evaluated in the range of 5 to 65 s. Samples pellets (n = 3) were positioned in cassettes with a 10-mm- diameter aperture, and were placed to be analyzed directly in the WD-XRF analysis chamber.

For the calibration, four analytical curves were constructed, approaching two strategies: (1) calibration using RMs set of mineral supplements for cattle in the range of 120–223 g kg^{-1} for Ca and 29–95 g kg^{-1} for P; (2) calibration using matrix-matching with RM 18/03 (204.40 ± 19 g kg^{-1} Ca and 94.80 ± 5 g kg^{-1} P) diluted in Na_2CO_3: NaCl (1:1 *w*/w); (3) matrix-matching with RM 18/03 diluted in NaCl; (4) matrix-matching with RM 18/03 diluted in Na_2CO_3.

2.4. Sample preparation for determination by ICP OES

The concentrations of Ca and P in mineral supplements for cattle were determined by ICP OES, after partial acid decomposition of the samples. The determined concentrations were used as reference values (n = 3). For partial acid decomposition of the samples the following procedure was employed: 300 mg of homogenized mineral supplement for cattle was accurately weighed in falcon tubes and kept overnight (approximately 16 h) with 2.0 mL of 65% v/v HNO_3 at room temperature. Then, 20 mL of high purity water were added, and the solution filtered on qualitative filter paper 80 g m^{-2} (Unifil, Germany).

3. Results and discussion

3.1. WD-XRF analysis

WD-XRF operational parameters such as the X-ray spot size and measurement time were proper selected. X-ray fluorescence measurements were performed using characteristic line for the Ca Kα ($\lambda = 3.359$ Å and $2\theta = 113.086°$) using a LiF 200 crystal and 0.15 mm collimator. For the P, the characteristic line P Kα ($\lambda = 6.158$ Å and $2\theta = 141.035°$), crystal Ge 111 and collimator 0.40 mm were used. For both analytes, an FPC (*flow proportional counter*) detector and elliptical mask of Ø10 mm were used. The tube voltage, current and counting time were as follows: 30 kV, 100 mA and 20 s for the analysis of Ca and P, respectively.

3.2. Matrix effects and calibration strategies

One of the greatest difficulties in the direct analysis of solid samples is the calibration, because when direct sampling of solids is used, the sample matrix is integrally present in the portion to be analyzed, therefore influencing the phenomenon of X-ray fluorescence and, consequently, the analytical signal. The calibrations commonly used in direct sampling of solids are: solid certified reference materials; (ii) solid synthetic samples; and (iii) analyte addition method [28]. Thus,

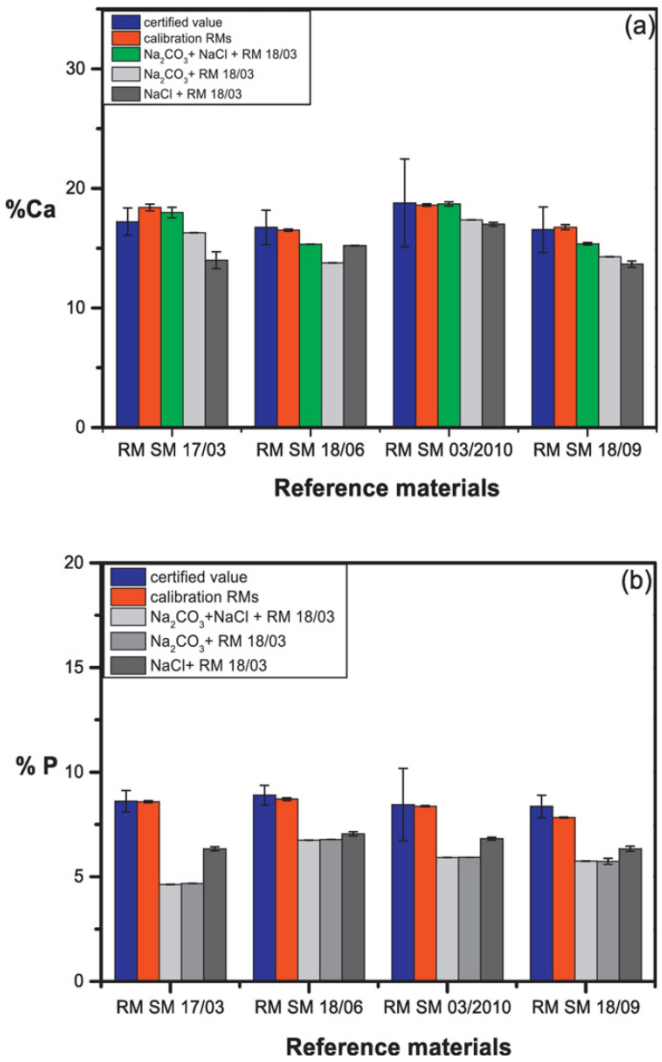

Fig. 1. Results for determination of (a) Ca and (b) P (%) in the reference materials by the proposed WD-XRF method.

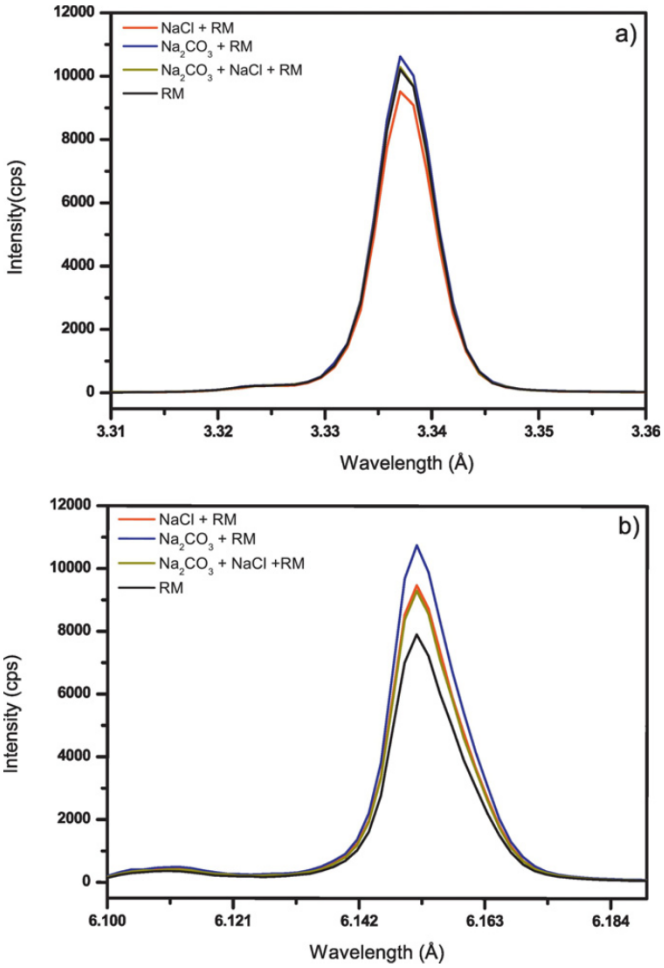

Fig. 2. Profile of transient signals fluorescence X-ray obtained for (a) Ca and (b) P at different solid media.

the influence of possible matrix effects on the calibration of the proposed methods was investigated. In this sense, two calibration strategies were evaluated: (1) calibration using set of RMs of mineral supplements and (2) matrix-matching with RM using different diluents (NaCl, NaCl and Na_2CO_3, and Na_2CO_3).

The analytical curves build for Ca and P using set of RMs of mineral supplements for cattle presented good linear correlation coefficients ($r \geq 0.9809$). For calibration, using matrix-matching, the diluents Na_2CO_3 and NaCl were used. Analytical curves using the RM 18/03 diluted in Na_2CO_3: NaCl (1:1 w/w) ($r \geq 0.9970$); in NaCl ($r \geq 0.9898$); and Na_2CO_3 ($r \geq 0.9835$), also obtained good linear correlation coefficients. The performance of the proposed methods was evaluated by analyzing four RMs of mineral supplements for cattle using the strategies described in section "*Proposed method and calibration strategies*". According to Fig. 1a it is possible to observe that for Ca the calibration

Table 2
Parameters of analytical performance for the direct determination of Ca and P by WD-XRF employing calibration with solid standards.

Parameters	Ca		P
Calibration mode	RMs	RM 18/03 diluted in Na_2CO_3:NaCl (1:1 w/w)	RMs
Linear ranger (g kg^{-1})	120–223	0–204	29–95
R	0.9809	0.9975	0.9957
LOD (mg kg^{-1})	47	61	36
LOQ (mg kg^{-1})	141	183	109
RSD (%)	0.5–2	0.1–2	0.3–3

Table 3
Concentrations determined (average ± standard deviation, n = 3) of Ca and P in mineral supplements for cattle by the proposed method WD-XRF, and by ICP OES as reference method.

Samples	Ca (g kg^{-1})			P (g kg^{-1})		Ca:P ratio
	WD-XRF		ICP OES	WD-XRF	ICP OES	
	Calibration 1*	Calibration 2*		Calibration 1*		
Supplement 1	158 ± 1	157 ± 1	153 ± 6	45 ± 0.3	47 ± 1	3:1
Supplement 2	218 ± 2	219 ± 2	220 ± 6	29 ± 0.4	29 ± 1	7.5:1
Supplement 3	194 ± 1	195 ± 1	187 ± 5	105 ± 1	104 ± 4	1.8:1
Supplement 4	301 ± 5	286 ± 6	294 ± 22	162 ± 2	173 ± 6	1.8:1
Supplement 5	210 ± 3	216 ± 0.4	214 ± 6	68 ± 1	70 ± 3	3:1
Supplement 6	299 ± 7	288 ± 8	291 ± 2	176 ± 4	173 ± 2	1.7:1

Calibration 1*: Set of RMs; Calibration 2*: RM 18/03 diluted in Na_2CO_3: NaCl (1:1 w/w).

strategies using the RMs set and matrix-matching using the RM18/03 diluted in Na_2CO_3:NaCl presented the best results. For P (see Fig. 1b) the best calibration strategy was that applying only the RMs set.

X-ray fluorescence intensity spectra for Ca (180 g kg^{-1}) and P (84.5 g kg^{-1}) in different solid media were obtained. Analyzing the profiles of transient signals and intensities (see Fig. 2a–b) of X-ray fluorescence, it is possible to evaluate one of the main effects of matrix in WD-XRF: phenomenon of absorption or intensification of X-rays [20]. The similarity in the profiles and intensities suggests that there is no significant influence of the matrix on the X-rays produced by the analyte in the solid matrix.

For Ca (Fig. 2a), the X-ray fluorescence emission intensities and the profiles of the transient signals in the solid media of RM 18/03 and RM 18/03 diluted in Na_2CO_3: NaCl (1:1 w/w) were similar, demonstrating that there is no significant influence of the sample matrix on the production of X-ray fluorescence of the analyte, therefore enabling the use of these two calibration strategies with solid standards in the determination of Ca by direct sampling of solids. However, for P (Fig. 2b) it is observed that the X-ray fluorescence emission intensities were different for all media in which matrix-matching with diluent was used compared to the standards used in the calibration with set of RM 18/03, thus indicating the possibility of using only this calibration mode for P.

3.3. Analytical parameters for the proposed methods using WD-XRF

The analytical performance parameters of the proposed methods were calculated using the calibrations with solid standards for Ca and P, monitoring their respective analytical lines, and they are shown in Table 2. Limits of detection (LOD) and quantification (LOQ) were calculated according software OXSAS®, using the Eqs. (1) and (2):

$$LOD = 3 \times \sqrt{\frac{BEQ}{Q \times t}} \quad (1)$$

$$LOQ = \left(3 \times \sqrt{\frac{BEQ}{Q \times t}}\right) \times 3 \quad (2)$$

where *BEQ* is the background equivalent concentration, *Q* is the analytical sensitivity (cps/%) and *t* is the counting time (s).

The values of RSD were up to 3%, demonstrating good precision of measurements. LOQ values were approximately 400 times lower than the minimum concentrations for P (40 g kg^{-1}) permitted by Brazilian legislation [3], which makes the proposed method an excellent tool for P quality control in mineral supplements. The analytical parameters presented in Table 2 are considered satisfactory for the analytical methods of determination of Ca and P employing the direct sampling of solid samples in mineral supplements for cattle.

3.4. Determination of Ca and P in real samples

The methods developed were applied in the determination of Ca and P in different commercial formulations of mineral supplements for cattle using the direct sampling of solids, and the results are shown in Table 3. The results obtained by the proposed method WD-XRF and by ICP OES (reference method) were concordant at the 95% level (paired *t*-test). As expected the LOD for Ca and P using ICP OES (0.03 and 0.8 mg L^{-1}, respectively) were lower than those presented by WD-XRF.

Concentrations of Ca and P ranged from 157 to 301 g kg^{-1} and 29 to 176 g kg^{-1}, respectively. The MAPA, through Normative Instruction N°.12 of November 30, 2004, establishes the minimum levels in the final mixture for lactating bovine in 73 g kg^{-1} P and for bovine and other categories of dairy bovine in 40 g kg^{-1} P, and that the Ca:P ratio is 1:1 to 7:1 [3]. Only one sample did not present results within the specifications of the current legislation, because in its final formulation the concentration of P was 29.2 ± 0.4 g kg^{-1} and the ratio, 7.5 to Ca: 1 to P.

4. Conclusions

WD-XRF is an excellent tool to evaluate the quality of mineral supplements for cattle, because it offers good analytical frequency (20 samples/h), operational simplicity and robustness to the analytical methods. These advantages are necessary because the presented results have already shown that the current legislation on the minimum levels of Ca and P is not being observed. Direct analysis of mineral supplements using WD-XRF was possible using simple and fast calibration strategies as a set of RM and compatibility with a suitable diluent. The influence of the sample matrix on the X-ray fluorescence production of the analytes can significantly influence the calibration employed using solid standards, however after systematic investigations of the matrix effect it was possible to employ direct sampling of mineral supplements for cattle to determine Ca and P by WD-XRF, with satisfactory precision and accuracy.

Acknowledgments

This study was supported by the São Paulo Research Foundation (FAPESP, 2016/01513-0) and the Conselho Nacional de Desenvolvimento Científico e Tecnológico (CNPq, 141311/2017-7, 401074/2014-5, 305637/2015-0 and 160152/2015-1). The authors are grateful to Analítica and Thermo Scientific for their instrument loans (ICP OES and WD-XRF) and EMBRAPA Southeast Livestock for donating the reference materials.

References

[1] Ministério da Agricultura, Pecuária e Abastecimento (MAPA), Bovinos e bubalinos. Brasília, DFAvailable in: http://www.agricultura.gov.br/animal/especies/bovinos-e-bubalinos 2010, Accessed date: 16 August 2016.

[2] W.S. Marçal, B.C. Oliveira Junior, V.V. Ortunho, Levels of phosphorus and fluorine in mineral salt preparations commercialized in the State of Paraná, Brazil. Acta Sci. Vet. 33 (2005) 315–319.
[3] Ministério da Agricultura, Pecuária e Abastecimento (MAPA), Legislação. Brasília, DFAvailable in: http://sistemasweb.agricultura.gov.br/sislegis/action/detalhaAto.do?method=visualizarAtoPortalMapa&chave=2062798598 2004, Accessed date: 8 September 2016.
[4] L. Gaste, W.S. Marçal, M.R. Do Nascimento, Values of lead in mineral salt commercialized in Paraná State, Arch. Vet. Sci. 7 (2002) 43–48.
[5] W.S. Marçal, L. Gaste, M.R.L. Nascimento, H.S. Oliveira, Teores de chumbo em suplementos comercializados no Estado de Mato Grosso do Sul, Ciênc. Rural. 33 (2003) 775–778.
[6] W.S. Marçal, L. Gaste, M. Liboni, P.E. Pardo, M.R. Do Nascimento, C.S. Hisasi, Concentration of lead in mineral salt mixtures used as supplements in cattle food, Exp. Toxicol. Pathol. 53 (2001) 7–9.
[7] T. Taflik, F.A. Duarte, E.L.M. Flores, F.G. Antes, J.N.G. Paniz, E.M.M. Flores, V.L. Dressler, Determination of bromine, fluorine, and iodine in mineral supplement using pyrohydrolysis for sample preparation, J. Braz. Chem. Soc. 23 (2012) 488–495.
[8] W.S. Marçal, L. Gaste, M.C. Carvalho, M.S. Fortes, W.P. Junior, Avaliações da relação fósforo: flúor em suplementos minerais para bovinos comercializadas na região nordeste do Paraná, Arq. Ciênc. Vet. zool. UNIPAR. 7 (2004) 103–107.
[9] M.D.G.A. Korn, E.S.B. Morte, D.C.M.B. Santos, J.T. Castro, J.T.P. Barbosa, A.P. Teixeira, A.P. Fernandes, B. Welz, W.P.C. Santos, E.B.G.N. Santos, M. Korn, Sample preparation for the determination of metals in food samples using spectroanalytical methods — a review, Appl. Spectrosc. Rev. 43 (2008) 67–92.
[10] S.L.C. Ferreira, L.O.B. Silva, F.A. De Santana, M.M.S. Junior, G.D. Matos, W.N.L. Dos Santos, A review of reflux systems using cold finger for sample preparation in the determination of volatile elements, Microchem. J. 106 (2013) 307–310.
[11] C.A. Bizzi, M.F. Pedrotti, J.S.S. Oliveira, J.S. Barin, J.A. Nobrega, E.M.M. Flores, Microwave-assisted digestion methods: towards greener approaches for plasma-based analytical technique, J. Anal. At. Spectrom. 32 (2017) 1448–1466.
[12] F.J. Krug, F.R.P. Rocha, Métodos de preparo de amostras, Fundamentos sobre o preparo de amostras orgânicas e inorgânicas para análise elementar, Editora, EditSBQ, 2016.
[13] M. West, A.T. Ellis, P.J. Potts, C. Streli, C. Vanhoofe, P. Wobrauschekc, 2014 atomic spectrometry update — a review of advances in X-ray fluorescence spectrometry, J. Anal. At. Spectrom. 29 (2014) 1516–1563.
[14] J. Malherbe, F. Claverie, Toward chromium speciation in solids using wavelength dispersive X-ray fluorescence spectrometry Cr Kβ lines, Anal. Chim. Acta 773 (2013) 37–44.
[15] T.A.P. Fernandes, J.A.A. Brito, L.M.L. Gonçalves, Analysis of micronutrients and heavy metals in Portuguese infant milk powders by wavelength dispersive X-ray fluorescence spectrometry (WDXRF), Food Anal. Method. 8 (2015) 52–57.
[16] G.V. Pashkova, T.S. Aisueva, A.L. Finkelshtein, E.V. Ivanov, A.A. Shchetnikov, Analytical approaches for determination of bromine in sediment core samples by X-ray fluorescence spectrometry, Talanta 160 (2016) 375–380.
[17] L. Yanhong, X. Dingshuai, W. Hongyue, A new sample preparation method for WD-XRF analysis of sulfide ores by fusion techniques: a BN crucible for protection against contamination and quantitative retention of sulfur, Anal. Methods 8 (2016) 1299–1306.
[18] M.F. Gazulla, M.J. Ventura, M. Orduna, M. Rodrigo, M.P. Gomez, Analysis of corrosion residues by WDXRF, X-Ray Spectr. 46 (2017) 271–276.
[19] C.M. Figueiredo, J.P. Castro, M.A. Sperança, L.L. Fialho, J.A. Nobrega, E.R. Pereira-Filho, Qualitative and quantitative chemical investigation of orthopedic alloys by combining wet digestion, spectroanalytical methods and direct solid analysis, J. Bras. Chem. Soc. (2017)https://doi.org/10.21577/0103-5053.20170182.
[20] F.J. Holler, D.A. Skoog, S.R. Crouch, Principles of Instrumental Analysis, 6th edition Thomson Brooks/Cole, 2006.
[21] J. An, K. Ko-Hyun, Y. Hye-On, J. Seo, Application of the wavelength dispersive X-ray fluorescence technique to determine soil fluorine with consideration of iron content in the matrix, Spectrochim. Acta Part B. 69 (2012) 8–43.
[22] A.K. Krishna, T.C. Khanna, K.R. Mohan, Rapid quantitative determination of major and trace elements in silicate rocks and soils employing fused glass discs using wavelength dispersive X-ray fluorescence spectrometry, Spectrochim. Acta Part B. 122 (2016) 65–171.
[23] I. Shintaro, M. Takehaya, N. Toshihiro, Assessment of metal elements in final drug products by wavelength dispersive X-ray fluorescence spectrometry, Anal. Methods 3 (2011) 1468–1470.
[24] J. Na, J. Lee, H.O. Yoon, Strategies for overcoming limitations associated with fluorine determination in solid materials by conventional wavelength dispersive X-ray fluorescence spectrometry, Microchem. J. 122 (2012) 76–81.
[25] L.C. Peruchi, L.C. Nunes, G.G.A. De Carvalho, M.B.B. Guerra, E. De Almeida, I.A. Rufini, D. Santos, F.J. Krug, Determination of inorganic nutrients in wheat flour by laser-induced breakdown spectroscopy and energy dispersive X-ray fluorescence spectrometry, Spectrochim. Acta B 100 (2014) 129–136.
[26] P.S.R. Devi, A.C. Trupti, A. Nicy, A.A. Dalvi, K.K. Swain, D.N. Wagh, R. Verma, Evaluation of uncertainty in the energy dispersive X-ray fluorescence determination of platinum in alumina, Anal. Methods 7 (2015) 5345–5351.
[27] G.B. Brito, L.S.G. Teixeira, M.G.A. Korn, Direct analysis of marine macroalgae for determination of macro minerals by energy dispersive X-ray fluorescence, Microchem. J. 134 (2017) 35–40.
[28] U. Kurfürst, Solid Sample Analysis: Direct and Slurry Sampling Using GFAAS and ETV-ICP, Springer-Verlag, Berlin, 1998.

2.1.2 Wavelength dispersive X-ray fluorescence (WD-XRF) applied to speciation of sulphur in mineral supplement for cattle: evaluation of the chemical and matrix effects. Microchemical Journal 147 (2019) 628-634.

Microchemical Journal 147 (2019) 628–634

Contents lists available at ScienceDirect

Microchemical Journal

journal homepage: www.elsevier.com/locate/microc

Wavelength dispersive X-ray fluorescence (WD-XRF) applied to speciation of sulphur in mineral supplement for cattle: Evaluation of the chemical and matrix effects

Diego Victor Babos, Vinicius Câmara Costa, Edenir Rodrigues Pereira-Filho*

Group for Applied Instrumental Analysis, Department of Chemistry, Federal University of São Carlos, P.O. Box 676, São Carlos, São Paulo State 13560-905, Brazil

ARTICLE INFO

Keywords:
Matrix-matching method
Speciation
Mineral supplements
Sulphur
Matrix effects

ABSTRACT

A nondestructive method for speciation of sulphur (S), elemental sulphur and sulphate; and determination of total sulphur in mineral supplements for cattle by wavelength dispersive X-ray fluorescence (WD-XRF) spectrometry is proposed. Using direct solids analysis it was possible to perform S speciation with high analytical frequency, simplicity and precision. The intensities ratio for the different electronic transitions (S $K\alpha_{1,2}$, S Kβ and S Kβ′) and principal component analysis (PCA) of the spectra obtained for samples and standards of different inorganic species of S allowed the speciation and quantification of S in mineral supplements for cattle. Matrix effects were minimized using matrix-matching method and univariate and partial least squares (PLS) treatments. The samples containing predominantly sulphate species were used as standards for calibration. For mineral supplement samples that contain predominantly elemental sulphur species, a sample set or S_8 diluted in Na_2CO_3: NaCl (1:1 w/w) were used with standards. No statistically significant difference was observed between method proposed and inductively coupled plasma optical emission spectrometry (ICP OES) reference values at 95% confidence level (Student's *t*-test, $n = 3$). The limits of quantification $\leq 2\ g\ kg^{-1}$ S, standard error of calibration $\leq 3.5\ g\ kg^{-1}$ S, standard error of Cross Validation $\leq 4.7\ g\ kg^{-1}$ S values obtained for the models proposed. The relative standard error ≤ 9% were obtained for the proposed method, demonstrating good precision. The method was successfully applied and a good alternative to direct speciation and analysis for determination of S in mineral supplements for cattle.

1. Introduction

Sulphur (S) is an essential macronutrient that must be supplied to herds due to its relation with protein and vitamin production. It is a component of amino acids as methionine, cystine and cysteine, and also occurs in animal tissues like sulphate. In addition, sulphur is the constituent of vitamins biotin and thiamin [1,2]. Diets that present deficiency in S lead to a reduction in the synthesis of microbial protein, causing malnutrition, affecting food consumption and, consequently, animal weight gain [1]. Thus, the mineral supplements offered to the herds usually employ sulphate and elemental sulphur as sources of this element. However, studies have been demonstrated that sulphate sources are readily available for animal microbial metabolism, whereas elemental sulphur has limited bioavailability [3]. In this context the speciation of S is necessary to evaluate the source and bioavailability in formulations of commercially available mineral supplements.

The main problems that can affect chemical speciation are related to the stability of the species, from the step of sampling to the analysis. Thus, some experimental conditions are critical for elemental speciation as: i) type of reagents (acids, hydroxides, salts, among others); ii) pH; iii) temperature and; iv) solvents that when improperly used can provide the oxidation or reduction of a particular species, conversion of chemical species, and making it impossible to perform chemical speciation with reliability [4].

In contrast to intensive chemical speciation procedure, the speciation using solid direct analysis without or with minimal sample preparation is an excellent alternative for minimizing cross-conversion of chemical species and reliable determinations. Some analytical techniques as X-ray absorption near edge structure (XANES) [5,6], X-ray photoelectron spectroscopy (XPS) [7] and X-ray fluorescence (XRF) spectrometry [8–13]; make possible the chemical speciation using direct analysis of several complex samples.

Through the wavelength dispersive X-ray fluorescence (WD-XRF) spectrometry, it is possible to obtain K X-ray fluorescence spectrum

* Corresponding author.
E-mail address: erpf@ufscar.br (E.R. Pereira-Filho).

https://doi.org/10.1016/j.microc.2019.03.077
Received 1 November 2018; Received in revised form 5 March 2019; Accepted 25 March 2019
Available online 26 March 2019

originates from radiative electron transitions either from a core or from a valence state to the K hole. The main K transitions are the electric dipole $K\alpha_{1,2}$ and the $K\beta_{1,3}$ transitions, which correspond to the 2p and 3p shell electron transition to the 1 s shell core hole, respectively [13,14]. The energies of Kα and Kβ transitions of some elements, provides information about its oxidation state and can be used for elemental speciation.

The WD-XRF was successfully used in the speciation and determination of Chromium (Cr VI) in soil, paint and polymer, monitoring the transitions Cr $K\beta_{1,3}$; Kβ′ and $K\beta_{2,5}$ and employing principal component analysis (PCA), partial least square regression (PLS) and principal component regression (PCR) [15]. The strong Kβ″ and the absence of Kβ′ satellites structures are fingerprints for the presence of hexavalent Cr [13].

For sulphur, some methods are reported in the literature for the direct speciation and determination employing WD-XRF [12]. The WD-XRF was used for estimation of the ratio between sulphide and total sulphur in sulphide ores monitoring the S $K\alpha_{1,2}$ and S $K\beta_{1,3}$ lines and satellites S Kβ′ and S $K\alpha_{3,4}$. The samples were pelleted using boric acid substrate and analyzed further [8]. In another study, univariate predictive models of binary mixtures of sulphur species were proposed, including Thiosulphate [10]. Uhlig et al. proposed a method of analysis of synthetic samples prepared using rock material as carrier for sulphide-sulphate mixtures. Limit of detection for sulphide species of 10 g kg^{-1} was obtained, and report that spectral interferences for sulphur in S Kβ′ line with lead (Pb Mβ' line) may compromise the determinations [11]. Even with these reports, we did not find in the scientific literature the development of analytical methods for the determination and speciation of S in livestock inputs such as mineral supplement for cattle, and with a systematic study of the effects of matrix and chemicals in the determination of total sulphur in these samples.

The WD-XRF presents other advantages, besides the possibility of direct speciation and determination of sulphur, as i) low consumption of reagents, as it does not require the decomposition of the sample for later analysis; ii) low generation of waste; and iii) requires small amounts of samples (< 1 g) [16]. Some limitations of the use of this technique are related to the quantitative analysis, because as the sample is analyzed integrally, the sample matrix can act on the phenomenon of X-ray fluorescence of the analyte and make difficult the determination of the analyte with required precision and accuracy. However, these matrix effects can be minimized by correctly employing some calibration strategies, as matrix-matching method, and multivariate calibration as PLS [14,15].

In this context, we developed a simple method for speciation of sulphur (elemental sulphur and sulphate) and determination of total S in mineral supplements for cattle by WD-XRF. In addition to employing solid direct analysis, different calibration strategies (univariate and multivariate) were evaluated for minimizing matrix effects.

2. Material and methods

2.1. Instrumentation

A Perform-X ARL (Thermo Fischer, Madison, WI, USA) wavelength dispersive - X-ray fluorescence (WD-XRF) was used for direct analyses of the samples. Samples were irradiated with X-ray emission provided by an Rh tube with a maximum power of 4200 W. The maximum voltage and current applied to the X-ray source are 70 kV and 180 mA, respectively. The operational values must be selected to obtain a power lower than 4200 W. The instrument is equipped with five different crystals that can be used in the wavelength dispersion, ranging from 0.124 Å (LiF220) to 162.662 Å (AX16c), and the choice is based on which crystal can disperse the characteristic wavelength from the analyte. The instrument is also equipped with four different collimators (0.15 mm, 0.40 mm, 1.00 mm and 2.60 mm) and two detectors: a flow proportional counter (FPC) and a scintillation counter (SC). The electronic transitions S $K\alpha_{1,2}$, S $K\beta_1$ and S Kβ′ were monitored. The current and the voltage applied to the X-ray source was of 100 mA and 30 kV (3000 W), respectively.

Reference total sulphur concentrations were obtained using an inductively coupled plasma optical emission spectrometer (ICP OES) (iCAP 6000, Thermo Scientific, Waltham, MA, USA), after acid digestion of the samples ($n = 3$). This instrument allows sequential emission signals collection using both axial and radial viewing. A pneumatic nebulizer was used and the instrumental conditions were established as the manufacturer recommendations: power (1.15 kW), plasma gas flow (12 L min^{-1}), auxiliary gas flow (0.5 L min^{-1}), nebulizer gas flow (0.7 L min^{-1}) and sample introduction flow rate (2.1 mL min^{-1}). Emission line monitored was S 180.7 nm using axial viewing.

2.2. Reagents, solutions and samples

All solutions used in the comparative ICP OES determinations were prepared using high purity water (18.2 MΩ cm resistivity) obtained from a Milli-Q® Plus Total Water System (Millipore Corp., Bedford, MA, USA). Nitric acid was purified by a Distillacid™ BSB-939-IR sub-boiling distillation system (Berghof, Eningen, Germany) and used to partially digest the samples in the comparative study. All glassware and polypropylene vessels were decontaminated prior to use by detergent washing, soaking in 10% (v/v) HNO_3 for 24 h, and then thorough rinsing with distilled-deionized water.

Working standard solutions, containing 100 mg L^{-1} S, used to build the ICP OES calibration curve was prepared by the appropriate dilution of stock standard solutions containing 1000 mg L^{-1} S (SpecSol, São Paulo, Brazil) in 10% (v/v) HNO_3.

Sodium carbonate (Merck, Darmstadt, Germany) and NaCl (Merck) were used as diluent, and elemental sulphur (S_8, Sigma-Aldrich, Saint Louis, USA), $CuSO_4{\cdot}5H_2O$ (Sigma-Aldrich), $MnSO_4{\cdot}H_2O$ (Sigma-Aldrich), $ZnSO_4{\cdot}7H_2O$ (Sigma-Aldrich), $(NH_4)_2SO_4$ (Sigma-Aldrich), $CoSO_4{\cdot}7H_2O$ (Sigma-Aldrich), $MgSO_4{\cdot}7H_2O$ (Sigma-Aldrich), Na_2SO_4 (Qhemis, Jundiaí, São Paulo, Brazil), FeS (B. Herzog, Rio de Janeiro, Brazil), $Na_2S_2O_4{\cdot}5H_2O$ (Sigma-Aldrich), Na_2SO_3 (Sigma-Aldrich), $Na_2S_2O_5$ (Sigma-Aldrich), $(NH_4)_2S_2O_8$ (Sigma-Aldrich), were used as solid standards to obtain reference spectra for the different inorganic sulphur species.

Eleven samples of cattle mineral supplement purchased in local markets of Rio Paranaíba (Minas Gerais State, Brazil) and provided by the Empresa Brasileira de Pesquisa Agropecuária (Brazilian Agricultural Research Corporation, São Carlos, São Paulo State, Brazil) were analyzed. All the cattle mineral supplements are composed of both macro- and microminerals (*e.g.*, Ca, P, S, Na, Cu, Fe, Mn and Zn), as well as < 42% protein equivalent.

2.3. Sample preparation for sulphur total determinations by ICP OES

A ICP OES was used as an analytical technique to determine the reference concentrations of total sulphur in cattle mineral supplements after partial acid decomposition of the samples. The samples were homogenized with a pestle and mortar, and then partially decomposed with HNO_3 65% v/v. Approximately 300 mg of sample was accurately weighed in polypropylene tubes and kept overnight (approximately 16 h) in contact with 2.0 mL of HNO_3 65% v/v at room temperature. Then 20 mL of high purity water was added and the solutions were filtered using an 80 g m^{-2} qualitative filter paper (Unifil, Germany).

2.4. Sample preparation and methods for speciation of Sulphur

Approximately 500 mg of mineral supplement sample or solid standard was weighed using an analytical balance (model AY 220, Shimadzu, Kyoto, Japan), and then pressed for 2 min under 80 kN to form pellets with a 12 mm diameter and *ca.* 3 mm thickness. Using the

counting time of 5 s, 0.40 mm collimator, elliptical mask of 10 mm, 0.15° increment, Ge 111 as diffraction crystal, all samples and solid standards were analyzed in the scan mode by monitoring spectral windows for diffraction angles between 105 and 115° (electronic transition S $K\alpha_{1,2}$), and 95 to 105° (electronic transition S $K\beta_1$ and S Kβ′). The X-ray fluorescence spectra obtained for the samples and the different inorganic species of S, monitoring the different electronic transitions, were used to propose models of prediction of the sulphur oxidation state in the samples of mineral supplements, using the ratios of the intensities of fluorescence of the different species and employing PCA for data interpretation.

Three univariate models for the prediction of the oxidation state of the S in the bovine mineral supplement for cattle samples were proposed using the X-ray intensities ratios for the different electronic transitions (S Kβ′/S $K\beta_1$, S Kβ/S $K\alpha_{1,2}$ and S Kβ′/S $K\alpha_{1,2}$) for the different species of inorganic sulphur (S-II, S0, S + II, S + IV and S + VI).

To generate the PCA the spectra were previously mean-center. The spectral range included the electronic transitions S $K\beta_1$ and S Kβ′ (68 variables), and all calculations were performed using Pirouette software, version 4.5 (Infometrix, Bothell, WA).

2.5. Calibration strategies for determination of total sulphur

As calibration strategy for the determination of total sulphur using WD-XRF, the matrix-matching method was evaluated. Solid calibration standards were prepared in three different ways: i) using a sample set of mineral supplements for cattle, ii) S_8 diluted in Na_2CO_3:NaCl (1:1 w/w); and iii) Na_2SO_4 diluted in Na_2CO_3: NaCl (1:1 w/w). The standards were homogenized with a pestle and mortar. All solid standards, in the concentration range of 0 to 32.1 g kg^{-1} S, were then pressed for 2 min under 80 kN to form pellets with approximately 500 mg (n = 3).

The precision (n = 3) was calculated using all samples. Limits of detection (LOD) and quantification (LOQ) were calculated according software OXSAS®, using the Eqs. (1) and (2):

$$LOD = 3x\sqrt{\frac{BEQ}{Qx\,t}} \quad (1)$$

$$LOQ = \left(3x\sqrt{\frac{BEQ}{Qx\,t}}\right) \times 3 \quad (2)$$

where BEQ is the background equivalent concentration, Q is the analytical sensitivity (cps/%) and t is the counting time (s).

Two forms of data treatment were evaluated, univariate (using X-ray fluorescence intensity) and multivariate (using PLS models). For PLS models 68 variables were used, and as data pretreatment the spectra were mean-center, and calculations were processed using Pirouette software. For proposition of the PLS models, the data set was subdivided into 5 or 6 standards for calibration:

- 5 standards for calibration using sample set and 6 standards prepared in S_8 or Na_2SO_4 diluted in Na_2CO_3:NaCl,
- 6 or 11 samples for validation (6 samples for calibration using sample set and 11 samples for calibration with standards prepared using S_8 or Na_2SO_4 diluted in Na_2CO_3:NaCl).

For the quantitative analysis, all samples and standards were analyzed in triplicate and using 20 s of counting time.

3. Results and discussion

3.1. Direct speciation of Sulphur by WD-XRF: chemical effects

Sulphur has several inorganic species, where the oxidation state can be S-II, S0, S + II, S + IV and S + VI, as shown in Table 1. Using WD-XRF as monitoring technique for these species, it is possible to observe spectral variations from the phenomenon of X-ray fluorescence for the S, that are related to the different inorganic chemical species. The so-called chemical effects that are related to displacements of the position of peak of some main lines of sulphur spectrum (S $K\alpha_{1,2}$, S $K\beta_1$) and predominantly for the Kβ lines. This phenomenon is due to the fact that the Kβ lines result from electron transitions from the unfilled 3p orbitals which are involved in chemical bonding [14].

Satellite SKβ' is preconditioned by transition from the molecular orbitals, which, in addition to 3p electrons of sulphur, is considerably contributed by 2 s and 2p electrons of the element chemically bonded with sulphur. S Kα1,2 and S Kβ1 can be observed for all species, S Kβ′ satellites only for species with coordinated oxygen (thiosulphate, sulphite and sulphate) [10], as showed in Fig. 1. In sulphate (S + IV) spectra, S Kβ′ satellite intensity reaches 40% of that of S$K\beta_1$ line (Fig. 1b), but in sulphide (S-II) spectra this satellite is practically absent [8].

Thus, the inherent characteristics of the WD-XRF technique makes it an excellent analytical tool for the development of methods for direct speciation of S in complex samples such as mineral supplements for cattle samples.

From the utilization of different salts (describe in Section 2.2 Reagents, solutions and samples) as solid standards the different inorganic sulphur species, and their respective reference spectra were obtained as showed in Fig. 1. The intensities ratio for the different electronic transitions (S Kβ′/S $K\beta_1$, S Kβ/S $K\alpha_{1,2}$ and S Kβ′/S $K\alpha_{1,2}$), of different species of inorganic sulphur were calculated and three univariate regression models were obtained for the prediction of the oxidation state of the predominant species present in the eleven samples of mineral supplements for cattle. By the interpolation of the calculated ratio for the samples, using the different electronic transitions the chemical speciation was performed.

For the three models calculated, the best one was a polynomial calculated with the intensity ratio of the S Kβ′/S $K\beta_1$ lines, whose coefficient of determination (R^2) was 0.9755, Fig. 2. Of the eleven samples analyzed, the model predicted six samples that have elemental sulphur (S_8 − S0) as the predominant specie, and the other five samples as the predominant species being the sulphate (SO_4^{2-} − S + VI).

The spectra obtained by monitoring S Kβ′ and S $K\beta_1$ lines for all eleven samples together with three solid standards with different concentrations of S in species S_8 and SO_4^{2-} (0.5, 1.0 and 1.5 g kg^{-1} S) were used to calculate PCA. The PCA showed, two classes obtained for reference samples formulated predominantly by elemental sulphur or sulphate, Fig. 3.

The scores and loadings of the first two principal components (PC) were evaluated. Fig. 3a presents the score plot for PC1 × PC2 of different samples with 98.0% of the explained variance, and an ellipse (green line) with 95% confidence interval [17] was applied in PCA score plot, showing that the samples are within the 95% confidence limit. Fig. 3b presents the loadings plot for PC1 and PC2 using different S Kβ′ and S $K\beta_1$ spectra. In Fig. 3a, there is separation between the two classes of samples according to the different sulphur species present. The samples composed predominantly of sulphate (S + VI) are separated from the samples that are composed of predominantly elemental sulphur (S 0).

This differentiation was possible due to the chemical effects: i) S Kβ′ satellites that are observed only for the sulphate specie, and ii) displacement of the position of peak for S $K\beta_1$ line, for SO_4^{2-} and S_8 species. The PC1 loadings (Fig. 3b) plot shows a positive peak in the region from 100.762 ± 0.150° coinciding with the shift of the position of peak for SO_4^{2-} (S + VI). This observation is also confirmed with the scores plot (Fig. 3a). The PC2 loading plot shows a positive peak that coincides with a sulphate spectrum, referent the S Kβ′ satellites and negative peak referent a position of peak for S $K\beta_1$ line for S_8 (S0), and similar results are observed for the scores plot.

The data obtained by the polynomial model were confirmed using the PCA method for speciation of S. Thus, five mineral supplements for

Table 1
Different inorganic sulphur species and some monitoring characteristics by WD-XRF.

Specie	Oxidation state of Sulphur	Electronic distribution	Observed spectral lines		
			S $K\alpha_{1,2}$	S $K\beta_1$	S Kβ′
			110.688°	100.762°	101.390°
			5.373 Å/0.537 nm	5.031 Å/0.503 nm	5.054 Å/0.505 nm
Sulphide/S^{2-}	-II	[Ne] $3s^23p^6$	Yes	Yes	Not observable
Elemental $Sulphur_8$	0	[Ne] $3s^23p^4$	Yes	Yes	Not observable
Thiosulphate/$S_2O_3^{2-}$	+II	[Ne] $3s^23p^2$	Yes	Yes	Yes
Sulphite/SO_3^{2-}	+IV	[Ne] $3s^2$	Yes	Yes	Yes
Sulphate/SO_4^{2-}	+VI	[Ne]	Yes	Yes	Yes

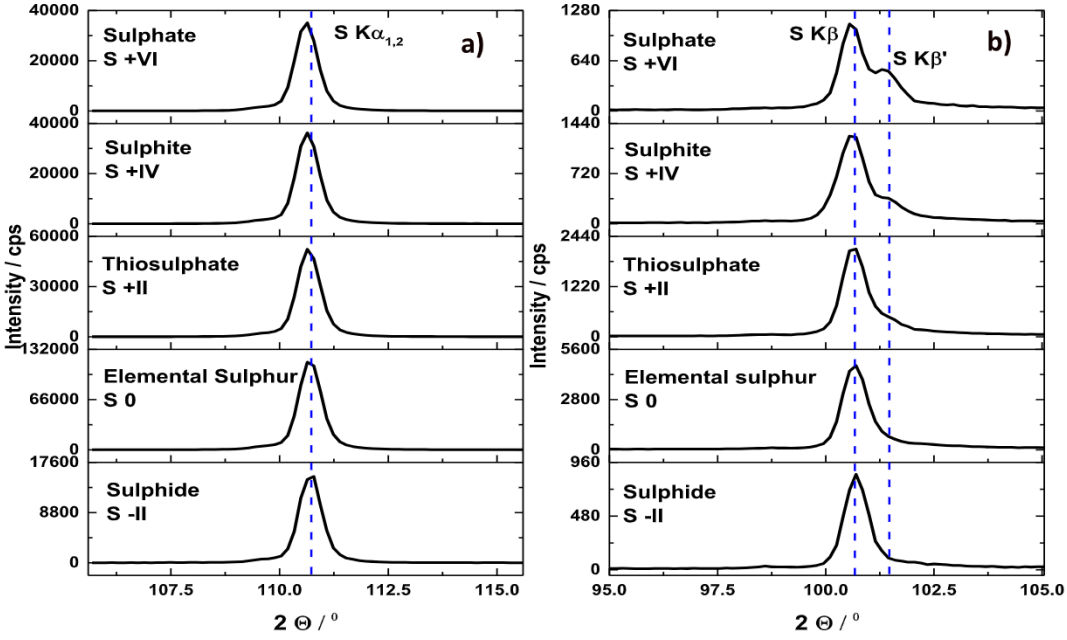

Fig. 1. X-ray fluorescence spectra for different inorganic sulphur species, monitoring (a) S $K\alpha_{1,2}$, (b) S $K\beta_1$ and S Kβ′ lines.

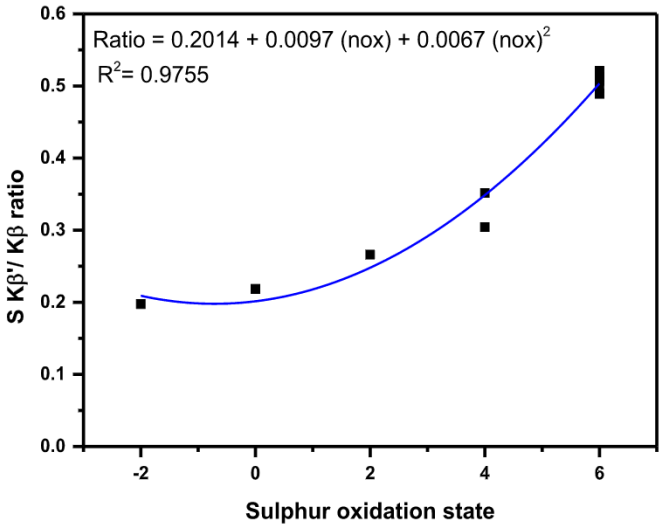

Fig. 2. Polynomial model obtained with the intensity ratio of the S Kβ′/S $K\beta_1$ lines (using different inorganic sulphur species), for prediction of the oxidation state of the predominant species present in the samples of mineral supplements for cattle.

cattle samples analyzed present majority the sulphate species in its formulation, and six samples the elemental sulphur specie. Studies have shown that sulphate species is recommended as a source of S in mineral supplements, considering that this species presents good bioavailability to cattle when compared to S_8. In this way, WD-XRF can contribute to a direct, fast and simple verification of the predominant sulphur species in the commercialized formulations of these supplements, conferring greater reliability and safety in the commercialization of these livestock inputs.

3.2. Calibration strategies to overcome matrix effects in WD-XRF

In direct analysis of solid, the sample matrix and analytes are analyzed integrally. Thus, the matrix can influence the X-ray fluorescence phenomenon, and consequently the analyte signal obtained may contain uncertainties regarding the identity (spectral interferences) and the amount of the analyte present in the analyzed portion. The main matrix effects described in the literature for X-ray fluorescence are related to i) elemental interactions (absorption and enhancement) and ii) physical effects (particle size and surface effects, and effects due to chemical state) [14].

Thus, we evaluated the matrix-matching method (MMC) as a calibration strategy for the determination of total S in mineral supplements for cattle. In this case, matrix effects can be minimized when the physical properties of the calibration standards closely match those of the

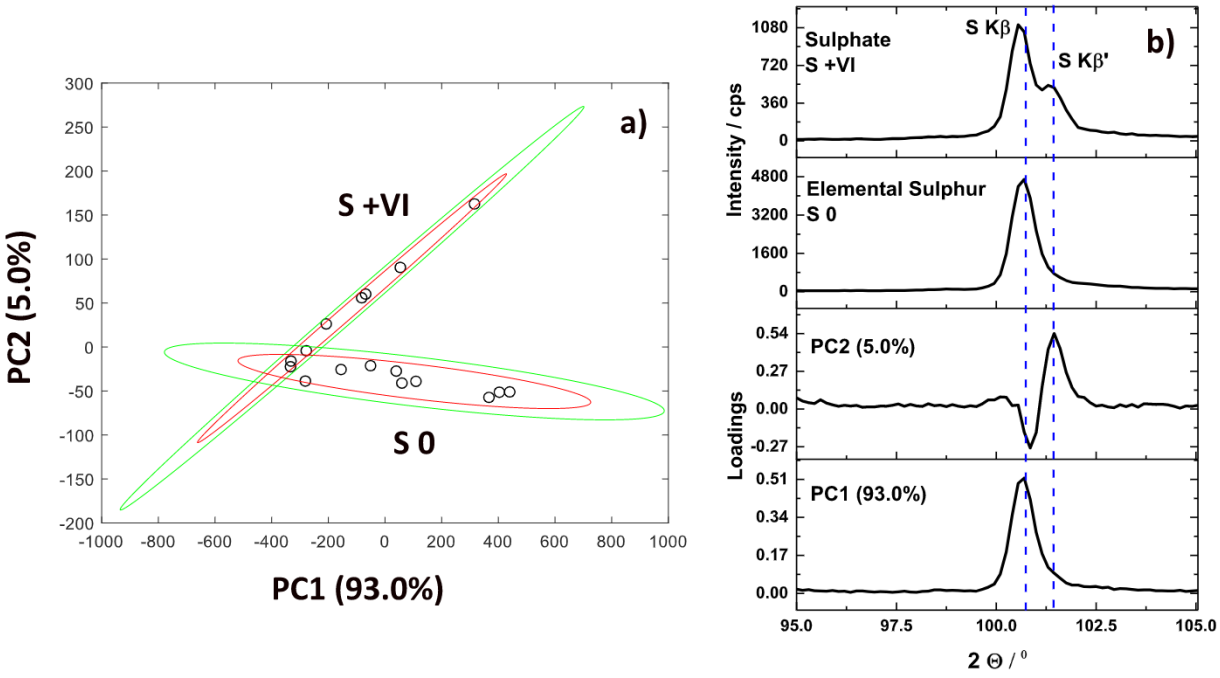

Fig. 3. Principal component analysis: (a) scores and (b) loadings.

samples being analyzed. The calibration standards were prepared in three different forms: i) using a sample set of mineral supplements for cattle ($R^2 \geq 0.8568$); ii) S_8 diluted in Na_2CO_3: NaCl (1:1 w/w) ($R^2 \geq 0.9921$); and iii) Na_2SO_4 diluted in Na_2CO_3: NaCl (1:1 w/w) ($R^2 \geq 0.9979$). As can be noted all models presented good determination coefficients.

Through the spectral profiles of X-ray fluorescence obtained for S, in two samples of mineral supplements, #SM 02 and #SM 18/09, and standards prepared using the reagents S_8, Na_2SO_4, Na_2CO_3 and NaCl; we can see some matrix effects, Fig. 4.

Fig. 4a and b presents the spectral profiles and X-ray fluorescence intensities obtained by monitoring the S $K\alpha_{1,2}$, S $K\beta_1$ and S $K\beta'$ lines, for the #SM 18/09 mineral supplement and the standard prepared with S_8 diluted in Na_2CO_3:NaCl (1:1 w/w), both with 32.1 g kg^{-1} S, in the elemental sulphur species (S 0). As can be noted, there are similarities, indicating negligible influence of the matrix on the X-rays produced by

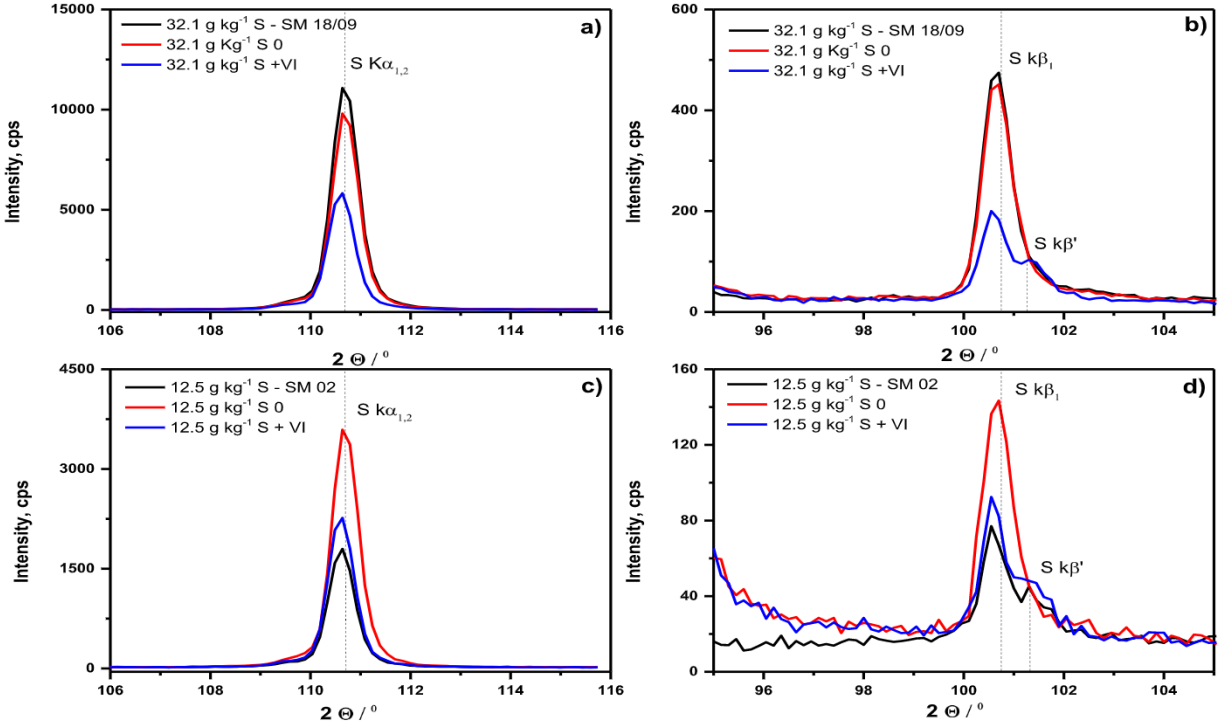

Fig. 4. Profile of X-ray fluorescence spectra obtained for sulphur species at different solid media, for available matrix effects. In a) and b) spectra obtained for SM02 mineral supplement and standards both with 32.1 g kg^{-1} S (S_8 and SO_4^{2-} species). In c) and d) spectra obtained for #SM 02 mineral supplement and standards both with 12.5 g kg^{-1} S (S_8 and SO_4^{2-} species).

the analyte in the solid matrix [18]. In this way calibration standards prepared using a sample set or S_8 diluted in Na_2CO_3:NaCl (1:1 w/w) (S 0) can be used for the determination of total S, using the MMC.

However, for the #SM 02 sample, that contains predominantly SO_4^{2-} specie, the enhancement and chemical effects are observed from the spectral profiles. Standards prepared using S_8 or Na_2SO_4 diluted in Na_2CO_3:NaCl (1:1 w/w), present an enhancement effect, approximately 2 and 1.3-fold greater intensity of x-ray fluorescence when compared to the intensity of the sample (monitoring the S $K\alpha_{1,2}$ line), Fig. 4c and d. The energies of the characteristic lines of the matrix elements exceed the binding energies of the analyte element lines, and analyte atoms emit extra characteristic radiation in addition to that from the primary exciting radiation [14]. Moreover, by the chemical effects, we can observe the S Kβ′ satellites only for S + VI, which can also compromise the determination of total S. In this way it is recommended to use only calibration standards prepared using a sample set for the determination of total S, using the MMC.

In addition to univariate calibration, we evaluated the multivariate approach through PLS regression. The PLS regression presents as main advantages the possibility of proposing a calibration model in the presence of the possible concomitants. The SEC (SE of Calibration) and SECV (SE of Cross Validation) values obtained for the models proposed were ≤ 3.5 g kg^{-1} S and ≤ 4.7 g kg^{-1} S, respectively. When reference and predicted values were compared, good linear determination coefficient (R^2) values were obtained for the models proposed ($R^2 \geq 0.8886$). The latent variables used in the PLS models, were 1 for model calculated using samples set and Na_2SO_4 diluted in Na_2CO_3:NaCl for S $K\beta_1$ line; and 2 latent variables for all others models.

3.3. Parameters of analytical performance

Some parameters of analytical performance were calculated for the proposed method, and can be observed in Table 2. Limits of detection (LOD) and quantification (LOQ) were calculated according software OXSAS® [18]. Good coefficients of determination were obtained for univariate ($R^2 \geq 0.8568$) and PLS models ($R^2 \geq 0.8886$). The LOQ values were approximately 25 and 670-fold lower, depending on the monitored line, than the recommended values of total S in formulations of bovine mineral supplements (40–50 g kg^{-1} S) [1,2].

The lower limits of detection were obtained by monitoring the most sensitive electronic transition S $K\alpha_{1,2}$ (LOQ = 0.06 g kg^{-1} S) and using the solid standards prepared with S_8 diluted in Na_2CO_3:NaCl (1:1 w/w).

When the calibration curve was prepared with Na_2SO_4 diluted in Na_2CO_3: NaCl (1:1 w/w) and monitoring the S Kβ1 the obtained LOD value was 0.5 g kg^{-1}.

The values of RSD were up to 9% for WD-XRF analysis, demonstrating good precision of measurements, when compared with ICP OES analysis (RSD ≤ 8%). Thus from these calculated parameters, the proposed analytical method proves to be an excellent tool to determine total S in samples of mineral supplements for cattle.

3.4. Determination of total sulphur in mineral supplement for cattle

The proposed method was applied for the determination of total S in 11 samples of mineral supplements for cattle, Table 3. For the samples of supplements containing S_8 as the predominant species of S in the formulations marketed, it was employed the analytical strategies using S_8 diluted in NaCl:Na_2CO_3 (1:1 w/w). The concentrations of total sulphur determined were between 6.6 and 39.5 g kg^{-1} S (both applying PLS), and trueness between 76 and 123% when compared to the reference values obtained by the ICP OES technique.

In the case of samples of mineral supplements containing SO_4^{2-} as the predominant S species in the formulations, the determined total sulphur concentrations were between 7.9 (using PLS) to 22.9 (using univariate) g kg^{-1} S, and trueness between 66 and 116%. It is important to mention that for samples containing SO_4^{2-} it was necessary to use a sample set to propose calibration models.

Given the complexity of bovine mineral supplement samples, and even using the matrix-matching method, some samples may contain variations in their matrix composition. Thus, we consider satisfactory recoveries between 66 and 76% for four samples (total of 11 samples) analyzed by the proposed method.

It is observed that no sample analyzed had total S concentration recommended in the final formulations of mineral supplement for cattle that would be between 40 and 50 g kg^{-1} S.

4. Conclusions

A simple and fast (20 s of counting time) method is proposed for sulphur speciation, elemental sulphur or sulphate. Using PCA or intensities ratio from X-ray fluorescence it is possible to perform Sulphur speciation in mineral supplements for cattle. These species can be monitored using the electronic transitions S Kβ′ and S $K\beta_1$ by WD-XRF and employing direct sampling of solids. Matrix and chemical effects can be minimized in the determination of total sulphur using the matrix-matching method and using appropriate calibration standards as a function of the predominant sulphur species in the bovine mineral supplement formulation. The two forms of treatment of the data evaluated, using X-ray fluorescence intensity and PLS regressions, were appropriate for direct determination of total sulphur in samples. The method proposed presents an excellent tool to evaluate the quality of mineral supplements for cattle, due to the chemical speciation and sulphur concentration present.

Acknowledgments

This study was supported by the Conselho Nacional de Desenvolvimento Científico e Tecnológico (CNPq, 141311/2017 and

Table 2
Parameters of analytical performance for the direct determination of S by WD-XRF employing matrix-matching method.

Parameter	S total					
	Samples set		S_8 diluted in Na_2CO_3: NaCl (1:1 w/w)		Na_2SO_4 diluted in Na_2CO_3: NaCl (1:1 *w/w*)	
Line	S $K\alpha_{1,2}$	S $K\beta_1$	S $K\alpha_{1,2}$	S $K\beta_1$	S $K\alpha_{1,2}$	S $K\beta_1$
Linear response range (g kg^{-1})	8.2–32.1	8.2–32.1	0–32.1	0–32.1	0–32.1	0–32.1
Calibration curve linear equation	y = 4.22[S] − 1.75	y = 0.13[S] − 0.022	y = 3.19[S] +0.13	y = 0.12[S] + 0.029	y = 1.83[S] − 0.019	y = 0.050[S] − 0.016
R^2	0.9395	0.8568	0.9924	0.9921	0.9982	0.9979
PLS model (reference × predicted)	y = 0.95[S] − 1.1	y = 0.94[S] + 1.0	y = 1.4[S] – 8.5	y = 1.34[S] − 14.8	y = 4.1[S] – 28.1	y = 2.3[S] − 11.4
R^2	0.9599	0.9416	0.9530	0.8886	0.8994	0.9524
LOD (g kg^{-1})	0.05	0.3	0.02	0.3	0.03	0.5
LOQ (g kg^{-1})	0.1	0.7	0.06	0.9	0.08	2
SEC (g kg^{-1})	3.5	2.2	1.2	1.0	0.9	1.7
SEV (g kg^{-1})	4.5	2.4	3.3	4.7	1.1	2.1
RSD (%)	0.4–8.7	1.2–4.6	0.2–5.5	0.3–6.8	0.2–8.4	0.8–5.0

Table 3
Concentrations determined (average, n = 3) of total S in mineral supplements for cattle by the proposed method WD-XRF, and by ICP OES as reference method. Values in parenthesis are the mean trueness in %.

Sample	Specie	Reference value (ICP OES)	Univariate		Multivariate (PLS)		
			Sample set	S_8 diluted in NaCl: Na_2CO_3 (1:1 w/ w)	Sample set	S_8 diluted in NaCl: Na_2CO_3 (1:1 w/ w)	
		g kg^{-1}	S $K\alpha_{1,2}$	S $K\alpha_{1,2}$	S $K\alpha_{1,2}$	S $K\beta_1$	S $K\alpha_{1,2}$
SM 18/03	Elemental Sulphur	20.5 ± 0.4	–	15.5 ± 0.04 (76)	–	–	15.5 (76)
SM 18/06	Elemental Sulphur	13.0 ± 0.2	–	11.3 ± 0.1 (87)	–	–	12.8 (98)
SM 18/09	Elemental Sulphur	32 ± 2	–	35.5 ± 0.5 (110)	–	–	39.5 (123)
SM 03/10	Elemental Sulphur	8.2 ± 0.4	–	7.7 ± 0.04 (94)	–	–	6.6 (81)
SM 17/09	Elemental Sulphur	32 ± 2	33 ± 3 (102)	38.4 ± 0.2 (114)	30.1 (94)	32.3 (101)	39.2 (122)
SM 01	Elemental Sulphur	27 ± 2	19.1 ± 0.8 (71)	19.4 ± 1 (72)	22.5 (83)	19.5 (72)	23.2 (86)
SM 17/06	Sulphate	30 ± 2	–	–	–	–	–
SM 17/03	Sulphate	20.1 ± 0.6	22.9 ± 0.1 (114)	–	21.1 (105)	20.0 (100)	–
SM 02	Sulphate	12.5 ± 0.3	9.2 ± 0.05 (74)	–	8.4 (67)	10.9 (87)	–
SM 03	Sulphate	8.7 ± 0.1	9.6 ± 0.4 (110)	–	10.0 (115)	10.1 (116)	–
SM 04	Sulphate	11.9 ± 0.3	8.5 ± 0.2 (72)	–	7.9 (66)	11.1 (93)	–

305637/2015-0). The authors are grateful to EMBRAPA Southeast Livestock for donating the mineral supplements for cattle samples, and Analítica and Thermo Scientific for their instrument loan (WD-XRF). This study was financed in part by the Coordenação de Aperfeiçoamento de Pessoal de Nível Superior - Brasil (CAPES) - Finance Code 001. The authors are also grateful to São Paulo Research Foundation (FAPESP), grant number 2016/01513-0.

References

[1] M.A.A. Balsalobre, A.L.M. Martins, A. E. Cruz, C. Sevilla, Formulação de misturas minerais para bovinos, available in: http://grupoapb.com.br/pdf/Formulacao_de_misturas_minerais_para_bovinos.pdf, Accessed date: 20 September 2018.
[2] M.L.F. Nicodemo, Cálculos de misturas minerais para bovinos, 2001, available in: https://www.infoteca.cnptia.embrapa.br/handle/doc/325195. Accessed date: 13 october 2018.
[3] T.S.J. Kahlon, J.C. Meiske, R.D. Goodrich, Sulphur metabolism in ruminants: I. In vitro availability of various chemical forms of Sulphur, J. Anim. Sci. 41 (1975) 1147–1153.
[4] F.J. Krug, F.R.P. Rocha, Métodos de preparo de amostras, Fundamentos sobre o preparo de amostras orgânicas e inorgânicas para análise elementar, Editora, EditSBQ, 2016.
[5] A.K. Eriksson, D. Hesterberg, W. Klysubun, J.P. Gustafsson, Phosphorus dynamics in Swedish agricultural soils as influenced by fertilization and mineralogical properties: insights gained from batch experiments and XANES spectroscopy, Sci. Total Environ. 566–567 (2016) 1410–1419.
[6] E.M. Kroukamp, T. Wondimu, P.B.C. Forbes, Metal and metalloid speciation in plants: overview, instrumentation, approaches and commonly assessed elements, Trends Anal. Chem. 77 (2016) 87–99.
[7] E. Catoa, A. Rossi, N.C. Scherrer, E.S.B. Ferreira, An XPS study into Sulphur speciation in blue and green ultramarine, J. Cult. Herit. 29 (2018) 30–35.
[8] V. Chubarov, A. Amosova, A. Finkelshtein, X-ray fluorescence determination of Sulphur chemical state in sulphide ores, X-Ray Spectrom. 45 (2016) 352–356.
[9] M.F. Gazulla, M.P. Gómez, M. Orduna, M. Rodrigo, New methodology for Sulphur analysis in geological samples by WD-XRF spectrometry, X-Ray Spectrom. 38 (2009) 3–8.
[10] S. Hennings, A. Pleßow, Distinction and quantification of inorganic Sulphur species including thiosulphate by X-ray fluorescence (WD-XRF), X-Ray Spectrom. 47 (2018) 144–152.
[11] S. Uhlig, R. Möckel, A. Pleßow, Quantitative analysis of sulphides and sulphates by WD-XRF: capability and constraints, X-Ray Spectrom. 45 (2016) 133–137.
[12] S. Imai, Y. Yamomoto, T. Yamamoto, K. Kodoma, J. Nishimoto, Y. Kikuchi, Sulphur chemical state and chemical composition of insoluble substance in soft rime, hard rime, and snow collected in remote and rural areas in Japan using wavelength dispersive X-ray fluorescence, Anal. Sci. 34 (2018) 589–598.
[13] D.F. Anagnostopoulos, X-ray emission spectroscopy optimization for chemical speciation in laboratory, Spectrochim. Acta B 148 (2018) 83–91.
[14] J.P. Willis, A.R. Ducan, Understanding XRF spectrometry, Basic concepts and instrumentation, 1 PANalytical B.V., 2008.
[15] J. Malherbe, F. Claverie, Toward chromium speciation in solids using wavelength dispersive X-ray fluorescence spectrometry Cr Kβ lines, Anal. Chim. Acta 773 (2013) 37–44.
[16] M. West, A.T. Ellis, P.J. Potts, C. Streli, C. Vanhoofe, P. Wobrauschekc, 2014 atomic spectrometry update - a review of advances in X-ray fluorescence spectrometry, J. Anal. At. Spectrom. 29 (2014) 1516–1563.
[17] F. Husson, S. Le, J. Pages, Confidence ellipse for the sensory profiles obtained by principal component analysis, Food Qual. Prefer. 16 (2005) 245–250.
[18] D.V. Babos, V.C. Costa, M.A. Sperança, E.R. Pereira-Filho, Direct determination of calcium and phosphorus in mineral supplements for cattle by wavelength dispersive X-ray fluorescence (WD-XRF), Microchem. J. 137 (2018) 272–276.

2.2 X-ray absorption near-edge structure spectroscopy

Using X-ray absorption near-edge structure (XANES) spectroscopy and employing direct solid analysis, information regarding the identity, quantity, oxidation state and coordination geometry of an element in a sample can be obtained. With XANES, measurements are made of the X-ray absorption coefficient, μ(E), in function of the incident energy, that comes energy from a synchrotron radiation source. When a beam of X-ray photons passes through a material, the intensity of the incident X-rays decreases according to the absorption characteristics of the irradiated material.[35] The μ(E), gives the probability that X-rays will be absorbed according to Lambert-Beer's law, $I = I_0 e^{-\mu(E)x}$, where *I* is the X-ray intensity transmitted through the sample, I_0 is the incident intensity, and x the sample thickness.[35,51,52]

X-ray absorption phenomenon occurs when an electron, from the innermost layer of an atom (i.e. 1s or 2p levels), absorbs a photon with quantized energy and promotes that electron to unoccupied higher energy levels (photoelectric effect),[35,53] as illustrated in the FIGURE 2.3.a.

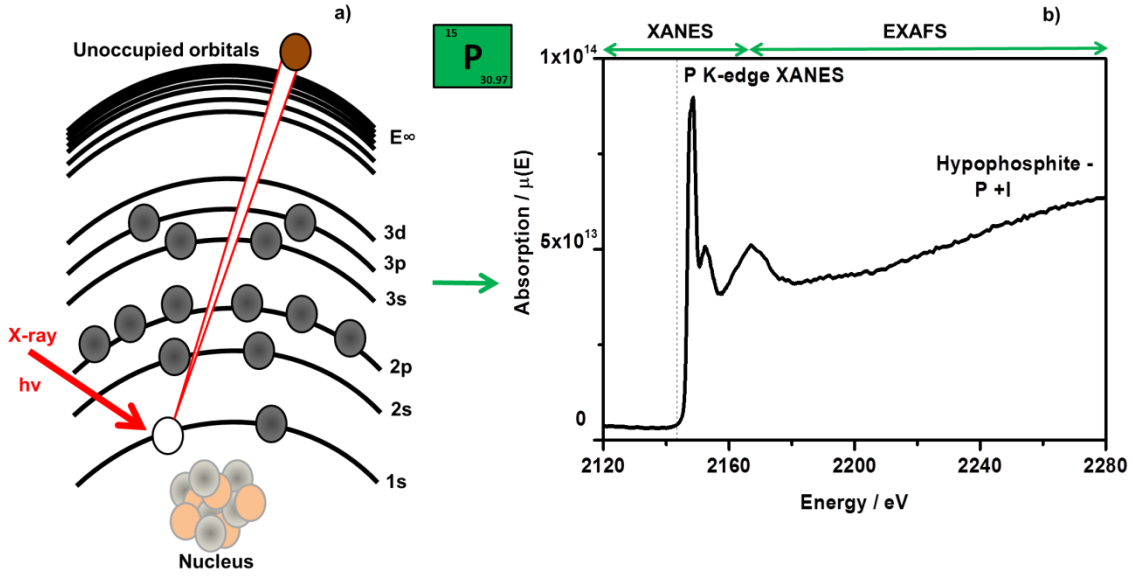

FIGURE 2.3 Illustration of (a) X-ray absorption phenomenon and (b) K-edge XANES spectrum obtained for a phosphorus atom (hypophosphite species - P +I).

X-ray absorption spectra (XANES spectrum) are obtained by scanning using different values of incident energy (FIGURE 2.3.b). When an abrupt increase in the absorption coefficient of the material as a function of the

incident energy is observed, its indicates that the energy of the incident X-ray photon has enough energy to eject electrons from a certain internal electronic layer of the absorber atom. Them, the probability of the electron absorbing these X-ray photons and promoting this electronic transition is high.[51,53]

This abrupt increase in the absorption coefficient is called the absorption edges, and they are named according to the origin of the electron that was ejected (electronic transition). The energy related to this absorption edge will depend on the element and its oxidation state. Thus, the K edge is related to the electron ejection of the principal quantum level 1 (1s). For elemental phosphorus (P 0), for example, the absorption edge K XANES refers to energy of 2145 eV, while for the hypophosphite species (P +I) is around 2148 eV. P K-edge position requires greater energy with increasing oxidation state (P 0 = 2145 eV, P +I = 2148 eV, P +III = 2149 eV and P +V = 2150 eV) and can be affected by nature of the ligand attached to P.[53]

Considering the edge position and presence of particular fingerprint peaks it is possible to identify different chemical species of the analyte. In this way, the XANES spectrum (referring to the energy range of -50 to +200 eV in relation to the absorption edge) can be an excellent analytical tool for the analysis of chemical speciation, since information is obtained regarding the oxidation state, electron in orbitals, coordinating geometry of a given element.[51] After this absorption edge (referring to the energy range of +200 to +1000 eV) oscillations in the spectrum referring to information on the molecular structure location (distance between the absorbing atom and neighboring atoms) can be obtained through the extended X-ray absorption fine structure (EXAFS) spectroscopy (FIGURE. 2.3.b); and widely used in the characterization of matter.[51,52]

The source of synchrotron radiation is appropriate to be used in XANES and EXAFS spectroscopy, making possible to obtain high energy and intensity of monochromatic X-ray radiation, necessary to occur the X-ray absorption phenomenon; and detectors with appropriate resolution in the acquisition of the spectra.[35,53] A simplified example of the instrumental components in a soft X-ray spectroscopy beamline, required to obtain XANES measurements, is illustrated in FIGURE 2.4. In Brazil, the National Synchrotron

Light Laboratory, in Campinas - São Paulo, makes it possible to obtain XANES spectra using the available instrumentation.

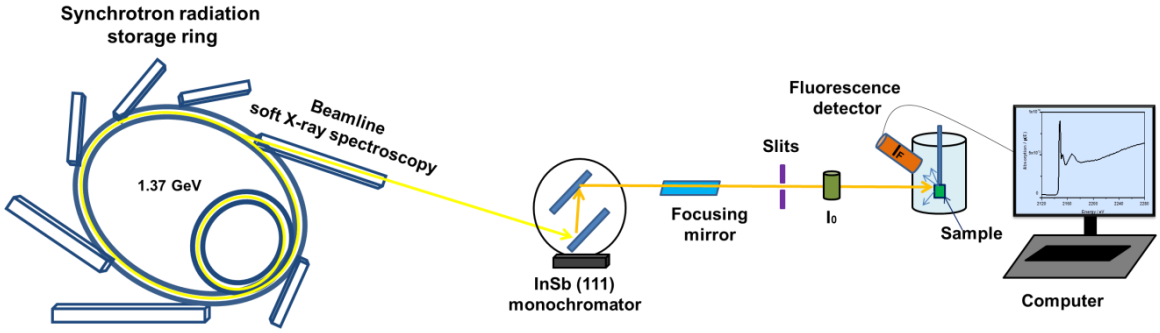

FIGURE 2.4 Simplified representations of the components of a soft X-ray spectroscopy beamline using synchrotron radiation and detection in X-ray fluorescence mode.

Two detection modes can be used for X-ray absorption measurements, i) the most usual are the measurements of photons transmitted through the sample by monitoring the incident and transmitted photon flux with photodiodes; and ii) X-ray fluorescence mode (more sensitive) using a solid-state detector of X-ray at 90° with respect to the incoming beam. In X-ray fluorescence mode, the absorption coefficient is measured as a function of the X-ray fluorescence yield I_F normalized by X-ray incident (I_0) in the sample ($\mu(E) = I_F/I_0$), thus avoiding the spectroscopically irrelevant elastic scattering contribution.[52,54]

These techniques allow direct, non-destructive analysis with minimal preparation of different types of samples in solid, liquid and gas.[35] Some limitations of this technique are the longtime of acquisition of the spectra (above 5 min), and availability to use the instrument in beamline of synchronous radiation.

The XANES spectra obtained can be used for qualitative and quantitative analysis. The qualitative analysis highlights the analysis of chemical speciation of different elements in different types of samples, as in i) analysis of asphaltenes and resins from Argentinian petroleum to identify nine organic and inorganic species of S;[55] ii) in obtaining spectral images for the species Fe +II and Fe +III in brain gliomas;[56] iii) soil analysis for speciation and quantification of Cr +III and Cr +VI;[57] iv) different plant parts and rhizospheric soil to determine the forms of Zn +II at the root-soil interface and inside the plant, resulting from

the different Zn complexes formed;[58] v) industrial waste for speciation of Sb +III and Sb +V;[59] vi) an arsenite-oxidizing bacterium (*Comamonas terrae*) isolated from agricultural soil for speciation and assessment of the biotransformation of As +III into the less-toxic As +V specie;[60] vii) sphalerit ores to verify the occurrence of Ge +IV, Cu +I and Fe +II monitoring the K-edges XANES for all elements;[61] among other samples.

In elementary determinations using XANES spectroscopy, concentrations of the analyte in the order of μg g^{-1} are determined with accuracy and precision. The use of chemometric tools are essential and widely used for appropriate interpretation and processing of XANES spectra, highlighting the linear combination fitting (LCF),[55,62-64] PCA,[64,65] PLS regression,[57,64,66] and multivariate curve resolution alternating least-squares algorithm (MCR-ALS);[54,67-70] in addition to software suitable for data processing (spectral normalization) and database, as ATHENA, ARTEMIS and HEPHAESTUS.[71]

The LCF is an essential tool for the semi-quantitative and qualitative analysis of the oxidation state and the chemical environment of the analyte present in the samples. From LCF of the different XANES spectra obtained for the known standard species with the XANES spectrum obtained in the sample, weights are obtained for each chemical species of the analyte in the sample, which represent the proportion-contribution of each reference species in the sample analyzed after fitting.[55,62] This strategy has been used successfully, for example, in the determination of six forms of phosphorus (phosphate adsorbed on aluminum (hydr)oxides, phosphate adsorbed on iron (hydr)oxides, crystalline aluminum phosphates, crystalline iron phosphates, calcium phosphates and organic P (lecithin)) in unfertilized and fertilized soils.[63]

The PCA is used to interpret the XANES spectra obtained and to verify spectral similarities, as in the analysis of phosphorus speciation in fertilizers and mineral supplements, where using the P K-edge XANES and PCA was possible to observe three clusters referring to the samples that contains in its formulations, the chemical species phosphate, phosphite and both.[64] And in the study by LEVINA et al. (2015), anti-diabetic vanadium complexes containing V +IV and V +V were monitored by V K-edge XANES after reaction with blood and its components; and using PCA, differences in the biotransformation products of the complexes were observed.[65]

However, PLS regression is used as a multivariate calibration strategy in XANES spectroscopy. This strategy was used in the analysis of toxic metal speciation such as; i) Cr +III and Cr +VI, and in the determination of total Cr in contaminated soils with Cr concentration above 10 ug g^{-1};[57] ii) Cd +II in soils monitoring the transition Cd L_3-edge XANES;[66] and major metals such as iii) iron from pyrite, olivine and goethite minerals in estuarine sediments, with a standard error of prediction ≤ 1.7%.[72]

Another chemometric tool used for the quantitative speciation of chemical species in mutual transformation is the multivariate curve resolution alternating least-squares algorithm (MCR-ALS). Multivariate curve resolution (MCR) methods allow modeling an experimental dataset as the product of a spectral matrix $\mathbf{S}$, composed of a minimal-uncorrelated set of pure spectra, for their signal-related concentration profiles, ordered in a matrix $\mathbf{C}$. This kind of data factorization can be calculated through an iterative alternating least-squares algorithm (ALS).[54,67-68] MCR-ALS was employed for the determination of the spectra of pure constituents and respective concentration profiles characterizing the time evolution of X-ray absorption spectra in speciation of Cu during the reduction of Cu-based catalyst supported in alumina (reduction of Cu +II to Cu 0 involving a Cu +I species at 250 °C) with hierarchical porosity.[68]

The combination of PCA, MCR-ALS, W L_3-edge and Mo K-edge XANES spectra allowed to determine the number of intermediate species, their chemical nature and concentration profiles during sulfidation of the $H_4SiMo_3W_9O_{40}$ catalyst supported in alumina.[69] In another study, the quantification of the number of intermediate species and identification during the sulfidation process of the two catalysts (Mo/Al_2O_3 and $CoMo/Al_2O_3$) was investigated by time-resolved X-ray absorption spectroscopy and using the chemometric methods mentioned previously.[70] These studies highlight the importance of XANES spectroscopy and the synergy with chemometric tools for pattern recognition and multivariate calibration for the characterization of different materials (mainly catalysts) and direct analysis of chemical speciation in analytical chemistry.

2.2.1 Determination and speciation of phosphorus in fertilizers and mineral supplements for cattle by X-ray absorption near-edge structure spectroscopy: a simple nondestructive method. Analytical Methods 11 (2019) 1508-1515.

Analytical Methods

PAPER

View Article Online
View Journal | View Issue

Cite this: *Anal. Methods*, 2019, **11**, 1508

Determination and speciation of phosphorus in fertilizers and mineral supplements for cattle by X-ray absorption near-edge structure spectroscopy: a simple nondestructive method†

Diego Victor Babos, Jeyne Pricylla Castro, Daniel Fernandes Andrade, Vinicius Câmara Costa and Edenir Rodrigues Pereira-Filho *

X-ray absorption near-edge structure (XANES) spectroscopy is an excellent analytical tool for the determination of the direct speciation of phosphorus in complex matrices as agricultural inputs. The use of linear combination fitting (LCF), principal component analysis (PCA) and partial least squares (PLS) enabled the development of a simple nondestructive method for the quantitative determination of different species of phosphorus in fertilizers and mineral supplements for cattle. The samples were classified into three classes using PCA: the samples containing phosphite, the samples containing phosphate and the samples containing both these species. The LCF is an interesting strategy for the qualitative and quantitative analyses of chemical species by XANES spectroscopy. Using LCF, the trueness of the phosphite and phosphate species added to the samples was found to be in the range of 96–113%. The strong matrix effects in the mechanism of X-ray absorption for P K-edge XANES spectroscopy prevented the determination of the phosphorus species in the fertilizers (trueness was in the range of 65–121%) and mineral supplements for cattle (trueness was in the range of 12–48%) using the PLS models.

Received 12th December 2018
Accepted 10th February 2019

DOI: 10.1039/c8ay02704h

rsc.li/methods

1. Introduction

Brazilian agriculture and cattle breeding have received worldwide importance either by addressing the food demand or due to the technology that has been developed and used in this economical sector. To increase the quality of agricultural products and herd and crop productivity, phosphorus-based inputs have been increasingly employed.[1] The use of phosphorus in the form of phosphite in agricultural activities has several advantages, such as high phosphorus solubility and absorption by the plant, as compared to the case of phosphate products, which directly influence metabolism and physiology.[2,3] In addition to the low relative cost of the raw material, many studies have shown that phosphite can act as a fungicide, providing remarkable results in the control of plant diseases.[1–3]

In cattle breeding, phosphorus deficiency is a significant factor for low milk and meat productivity. Thus, mineral supplementation of animals with phosphorus is necessary because phosphorus is a nutrient that directly affects the animal bone composition.[4,5] Phosphorus is the most expensive mineral supplement for cattle, and the phosphate rock needs to be industrially processed for the removal of potential toxic elements, such as F and Pb, before it can be safely used as a source of this nutrient.[4] Many alternative sources of this element have been introduced to reduce the price, which can pose risks to the animal and consumer health.[4–6]

The analytical methods used to determine the speciation of phosphorus usually require sequential extraction,[7,8] separation,[9,10] and conversion of solid samples into solutions.[11,12] Conventional wet or dry solid sample preparation procedures are often time-consuming, laborious (approximately 16 hours are required for the extraction of an analyte from the sample),[13] vulnerable to contamination and analyte loss, require a large amount of reagents and energy, and generate a significant volume of toxic waste.

In addition, an inadequate sample preparation method for speciation may change the oxidation states of the analyte, interconvert the species and result in the generation of erroneous chemical identifications; although most of the procedures for the determination of phosphite require the conversion of phosphite to phosphate (using appropriate oxidizing agents) for spectrophotometric determination, erroneous conclusions in the determination of phosphite can be obtained if this conversion is not efficiently conducted.[12,14] Thus, procedures that allow minimum manipulation of the sample and

Group of Applied Instrumental Analysis, Department of Chemistry, Federal University of São Carlos, São Carlos, São Paulo State, 13565-905, Brazil. E-mail: erpf@ufscar.br; Tel: +55 16 3351-8092

† Electronic supplementary information (ESI) available. See DOI: 10.1039/c8ay02704h

techniques that permit non-destructive analysis should be evaluated as they present an excellent alternative to the conventional methods of phosphorus speciation. X-ray absorption near-edge structure (XANES) spectroscopy is a technique that presents many advantages that allow its use in the development of elementary speciation methods.

XANES spectroscopy using synchrotron radiation is a well-established technique that provides information regarding the electronic (oxidation state), structural (coordination geometry) and magnetic properties of matter.[15,16] XANES spectroscopy measurements can be performed on solids, gases, or liquids, including moist or dry soils, mineral suspensions, and aqueous solutions.[9,16] Some methods of chemical speciation by XANES spectroscopy in different samples have been reported in the literature: for example, for the speciation of Cr,[17,18] Ni,[19] Sb,[20] As,[21] Cd,[22,23] Fe,[24] S,[25,26] Ce,[27] and Zn;[28] phosphorus speciation by P K-edge XANES spectroscopy has been extensively explored in the analysis of complex environmental samples such as sediments, soils and minerals.[7,8,13,29–32] However, to the best of our knowledge, analytical methods for the speciation of P in agricultural inputs, such as mineral supplement samples for cattle and fertilizers, by XANES spectroscopy have not been reported in the scientific literature.

Quantitative data of the chemical species are obtained by XANES spectroscopy for environmental samples regardless of their physical state provided that the integrity of the original species is maintained throughout the entire analytical procedure.[18] Although this technique has significant potential in the identification of chemical species, its analytical sensitivity still needs to be improved.[19] Another challenge associated with quantitative XANES methods is the choice of the calibration strategy because the availability of certified reference materials that can be used in calibration by matrix matching is limited. However, linear combination fitting (LCF) and chemometric tools, such as partial least squares (PLS) regression,[18,33] multivariate curve resolution (MCR)[34] and artificial neural network,[33] are being successfully employed in the quantitative analysis of chemical species by XANES spectroscopy.

In this context, the development of new analytical methods for the determination of phosphite and phosphate content in fertilizers and mineral supplements for cattle will improve the quality control of these agricultural and cattle breeding inputs and thus generate more confidence not only in the entire production chain but also for the consumer. In this study, simple nondestructive methods for the determination and phosphorus speciation were developed using XANES spectroscopy. The PLS models and LCF for the quantitative analysis of phosphite and phosphate were also compared and evaluated.

2. Experimental

2.1 ICP OES instrumentation and determination of total phosphorus in fertilizers

An inductively coupled plasma optical emission spectrometer (iCAP 6000, Thermo Scientific, Waltham, MA, USA) was used to determine the amount of total phosphorus in fertilizer samples ($n = 3$). The instrumental conditions were established according to the manufacturer's recommendations and previous experience. The following procedure was employed to analyze the samples: 250 mg of fertilizer was accurately weighed in falcon tubes and diluted in 50 mL of 1% HNO_3 (v/v). The emission line of phosphorus was monitored at 213.6 nm at the radial viewing mode. The concentrations determined by ICP OES were used as reference values ($n = 3$) for total phosphorus.

2.2 Reagents, analytical solutions and samples

All solutions were prepared using high-purity water (18.2 MΩ cm^{-1} resistivity) obtained *via* the Milli-Q® Plus Total Water System (Millipore Corp., Bedford, MA, USA). Standard solutions of 120 mg L^{-1} P were prepared *via* suitable dilution of the stock standard solution containing 1000 mg L^{-1} P (Specsol, São Paulo, Brazil) and used to construct the calibration curve for ICP OES measurements.

The salts $K_2HPO_4 \cdot 3H_2O$ (≥99.0%, Merck, Darmstadt, Germany) and $Na_2(HPO_3) \cdot 5H_2O$ (≥98.0%, Riedel-de Haën, Germany) were used as standards to prepare the calibration solutions containing phosphorus in the form of phosphate (PO_4^{3-}) and phosphite (HPO_3^{2-}) species, respectively. For the LCF and PLS models, calibration solutions in the following concentrations were used: 0, 0.05, 0.075, 0.1, 0.125 and 0.15% P (w/w) in the phosphate and phosphite species.

All the glass and polypropylene vessels were washed with detergent, soaked in 10% HNO_3 (v/v) for 24 h, and then thoroughly rinsed with deionized water prior to use.

Herein, five samples of liquid fertilizers, containing macro and micro nutrients or only potassium phosphite, were commercially acquired from Rio Paranaíba (Minas Gerais, Brazil) and São Carlos (São Paulo, Brazil), and five reference materials (RM) of the mineral supplements (RM 17-03, RM 18-03, RM 18-06, RM 18-09 and RM SM 03-10) for cattle were provided by Empresa Brasileira de Pesquisa Agropecuária (Brazilian Agricultural Research Corporation). The analyzed mineral supplements for cattle were also composed of macro- and microminerals (*e.g.*, P, Ca, Cu, Fe, Mn and Zn) as well as less than 42% protein equivalent.

2.3 Preparation of samples for the speciation of phosphorus by XANES spectroscopy

The phosphorus standard solutions, containing the phosphate and phosphite species, and all the analyzed samples (fertilizers and mineral supplements for cattle) were prepared using only ultra-pure water. The fertilizer samples # 1, # 2, # 3, # 4 and # 5 were diluted 1-, 1-, 5-, 10- and 50-fold, respectively. All mineral supplement samples for cattle were diluted 60-fold with water. The dilution of the samples is necessary to ensure that the self-absorption phenomenon does not occur during the P K-edge XANES measurements.

The accuracy of the proposed methods was also evaluated *via* addition/recovery tests. The fertilizer and mineral supplement samples were spiked with 0.077% P (w/w) in the phosphate and phosphite species; the fertilizers samples # 1 and # 4 were diluted 2- and 20-fold, respectively, and the mineral

supplements for both the cattle samples # 1 and # 2 were diluted 150-fold.

The samples, standard solutions and blanks (only ultra-pure water) were added to the sample port of the Teflon plates. Samples were conditioned in the sample port using an o-ring and a lid (stainless steel or copper) with the Ultralene® film. Then, the sample port containing a rod was inserted into the sampling chamber initially pressurized with N_2 gas for further analysis.

2.4 XANES data collection

The spectral data for phosphorus K-edge XANES were obtained at the beamline of soft X-ray spectroscopy (SXS) at the Brazilian Synchrotron Light Laboratory (LNLS), Campinas, São Paulo, Brazil. The LNLS storage ring was operated at the energy of 1.37 GeV with the electron beam currents between 130 and 250 mA. The beamline SXS, with the energy range of 1–5 keV, was equipped with a dual crystal-type InSb (111) monochromator under high vacuum (5×10^{-8} mbar).

XANES spectra were obtained in the fluorescence mode using a silicon drift diode detector (Ampetek – X123SDD). A fluorescence detector was used to reduce the amount of elastic scattered background and thus improve the signal-to-noise ratio. The measurements were conducted under standard operating conditions, *i.e.*, after calibrating the X-ray energy to the K-edge of P using $Ca_3(PO_4)_2$ as a standard (0.1% P (w/w) and 0.28 g $Ca_3(PO_4)_2$ diluted in 2.25 g BN), the spectrum was assigned a reference energy (E_0) value of 2150.7 eV using the maximum peak.

All the fluorescence yield spectra were obtained in the energy range between 2120 and 2280 eV. The energy step resolution was 1 eV between 2120 and 2143 eV, 0.2 eV between 2144 and 2160 eV, and 1 eV between 2161 and 2280 eV. All measurements were conducted using a dwell time of 1 s per energy step. Moreover, nine scans were measured for each sample.

The XANES data were processed using the Athena software suite, version 0.9.25.[35] Multiple spectra were merged and normalized using the following procedure: a linear baseline function was subtracted from the pre-edge spectral region (between −30 and −8 eV relative to E_0), and a quadratic function was used to create background-corrected spectra across the post-edge region between 15 and 130 eV relative to E_0 for each sample.

2.5 Principal component analysis (PCA)

Principal component analysis of the first derivative and mean-centered spectra in the 2120–2280 eV range (225 variables) was conducted using the Pirouette software, version 4.5 (Infometrix, Bothell, WA).

After performing the calculation, the variables have been projected to the principal components (PCs), and each PC (from 1 to the number of initial variables) is a vector that explains the higher variance in the data. PCs are calculated in the decreasing order of explained variance, and the main requirement is to select an appropriate number of PCs smaller than the number of the original variables. The PCA provides the weights needed to obtain a new variable that best explains the variation in the whole dataset in a certain sense. This new variable including the defining weights is called the first principal component.[36]

2.6 Linear combination fitting (LCF) analysis

The linear combination fitting of the fertilizers and mineral supplements for cattle in the XANES spectra was conducted in the spectral region from 2120 to 2190 eV using the Athena software, version 0.9.25. The calculations were performed using weighted combinations of the spectra from two known standards, $K_2HPO_4 \cdot 3H_2O$ (PO_4^{3-} and P^{5+}) and $Na_2(HPO_3) \cdot 5H_2O$ (HPO_3^{2-} and P^{3+}), to fit the sample spectra.

The parameter R factor can be used to verify the goodness-of-fit for the LCF. The R factor is the sum of the squares of the differences between the data and the fit at each data point divided by the sum of the squares of the data at each corresponding point. This parameter represents the mean square misfit between the data and the fit for both the real and the imaginary parts of the Fourier transform and has been defined in eqn (1).[16]

$$R\ \text{factor} = \frac{\sum_i (\text{data}_i - \text{fit}_i)^2}{\sum_i \text{data}_i^2} \quad (1)$$

In general, the R factor values less than 0.05 are considered to reflect a reasonable fit.

Using the weights ($\text{weight}_{\text{specie}}$) assigned to the XANES spectra of the sample with the phosphate or phosphite species obtained by LCF and the total concentration of phosphorus, $[P]_{\text{total}}$, in the samples determined by ICP OES, the concentration of the phosphate or phosphite species, $[P]_{\text{specie}}$, determined in the sample is given by eqn (2).

$$[P]_{\text{specie}} = \text{weight}_{\text{specie}} \times [P]_{\text{total}}. \quad (2)$$

2.7 Partial least squares (PLS)

The calibration models were obtained by the partial least squares (PLS) regression of the sample data set using the Pirouette software, version 4.5. In the application of PLS, the data set was divided into 11 samples for calibration, *i.e.* 6 standards for phosphate (in the concentration range from 0 to 0.15% w/w P) and 5 standards for phosphite (in the concentration range from 0 to 0.125% w/w P), and 14 samples for validation: 5 fertilizers, 5 mineral supplements for cattle, 2 fertilizers and 2 mineral supplements for the cattle samples both fortified with the phosphate and phosphite standards as described in section 2.3 Preparation of samples for the speciation of phosphorus by XANES spectroscopy.

The first derivative was applied to the obtained spectra for the standards, the samples and the blank. Later, the data was mean-centered. All the PLS models were constructed using 225 independent variables representing the data points of the K-edge XANES spectra in the energy range between 2120 and 2280 eV. To predict the concentration of P in the unknown analyzed samples, the regression was made by the obtained XANES spectra in the proposed models.

The standard error of calibration (SEC) and the standard error cross-validation (SECV) were calculated using the following equations:

$$\mathrm{SEC} = \sqrt{\frac{\sum_{i=1}^{N_{\mathrm{cal}}} (y_i - \hat{y}_i)^2}{N_{\mathrm{cal}} - k - 1}} \quad (3)$$

where y_i and $\hat{y}_i$ are the reference and predicted values, respectively, N_{cal} and k are the number for the standards 11 (phosphite) and 12 (phosphate) in this study and the number of latent variables, respectively.

$$\mathrm{SECV} = \sqrt{\frac{\sum_{i=1}^{N_{\mathrm{cv}}} (y_i - \hat{y}_i)^2}{N_{\mathrm{cv}}}} \quad (4)$$

where N_{cv} is the number of samples used in the cross-validation process (1 in this study).

2.8 Limits of speciation and method detection limits in XANES spectroscopy

The limit of speciation (LOS) of the method for phosphate and phosphite was determined according to the recommendations of Bacquart *et al.*[37] and Porcaro *et al.*[38] LOS corresponds to 10 times the standard deviation (SD) of the blank measurements evaluated ($\mathrm{LOS} = 10 \times \mathrm{SD}_{\mathrm{blank}}$). For phosphate and phosphite, the values of E_0 at 2150 eV and 2149 eV, respectively, were used to calculate the standard deviation of the normalized X-ray absorptions (norm $\mu(E)$) for the blank measurements ($n = 8$).

The method detection limit (MDL)[40] was evaluated *via* XANES analysis. The MDL is defined as the standard deviation (SD) of the blank measurements ($n = 8$) multiplied by the t value of the $n - 1$ sample (for a 99% confidence level) ($\mathrm{MDL} = t$ value $\times \mathrm{SD}_{\mathrm{blank}}$).

3. Results and discussion

3.1 Principal component analysis and discrimination of phosphorus species

Phosphorus has a variety of oxidation states between P^0 in it is elemental form and P^{5+} as PO_4^{3-}. The position of the P K-edge (~2140–2190 eV) can shift by ~8 eV (ref. 39) depending on the oxidation state (higher energy with increasing oxidation) and can be affected by the nature of the ligand attached to P. The P K-edge XANES spectra consisted of one sharp transition arising from an electron transition from the ls core level to the t_2^* (p-like) antibonding orbital.[16]

The K-edge XANES spectra for the phosphate – PO_4^{3-} (P^{5+}) and phosphite – HPO_3^{2-} (P^{3+}) species show spectral differences that can be observed in Fig. 1. The E_0 values for phosphite and phosphate were 2149 eV and 2150 eV, respectively. The P K-edge XANES spectra for fertilizers, F (Fig. S1a†), and mineral supplements, S (Fig. S1b†), are shown in the ESI† (Appendix).

By analyzing the PCA (Fig. 2) of the P K-edge XANES spectra for the fertilizers and mineral supplements, the presence of phosphate and phosphite was identified.

Herein, three classes of samples (samples formulated by phosphate, phosphite and with both species) were analyzed to assess the P K-edge XANES spectra. The scores and loadings of the first two principal components were evaluated. Fig. 2a presents the score plot for PC1 × PC2 of different samples with

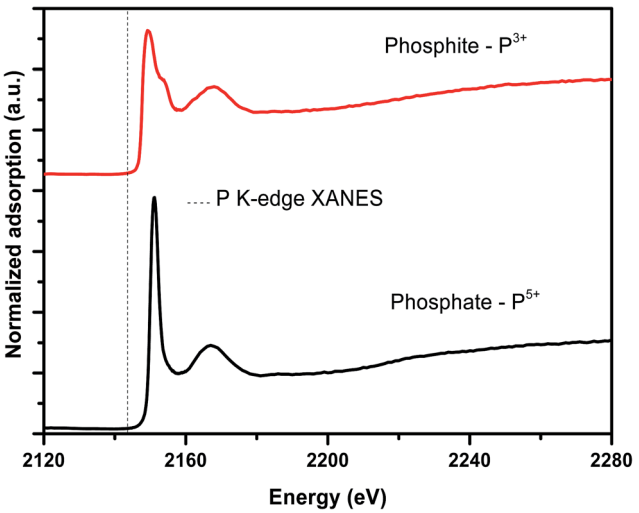

Fig. 1 The phosphorus K-edge XANES spectra for phosphate ($K_2HPO_4 \cdot 3H_2O$, PO_4^{3-}) and phosphite ($Na_2(HPO_3) \cdot 5H_2O$, HPO_3^{2-}), both at 0.125% P (w/w).

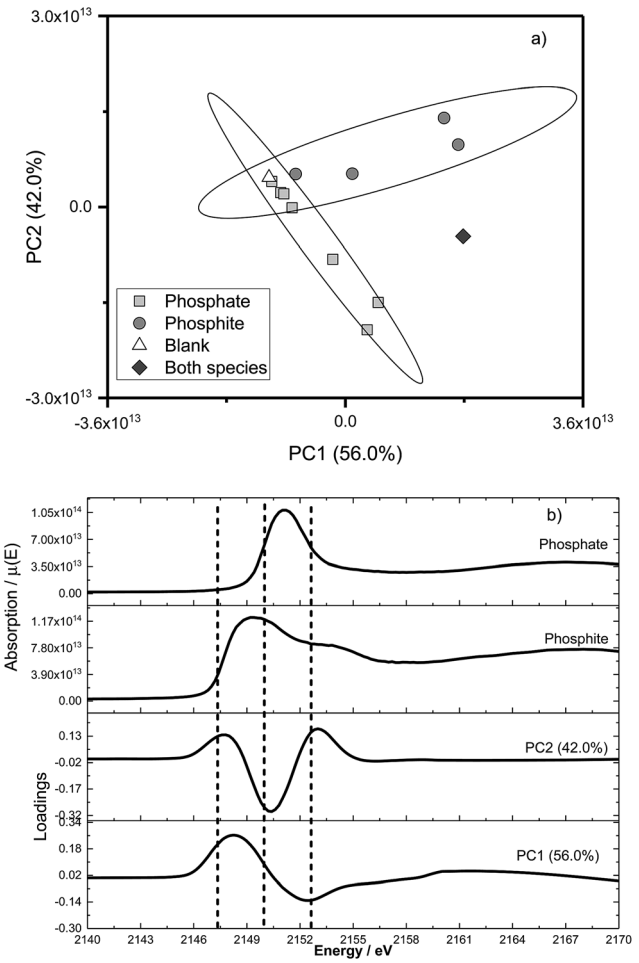

Fig. 2 Characterization of samples as a function of the phosphorus species present in the formulation. Scores (a) and loading (b) plots of the first two principal components from the PCA.

Table 1 Results (mean ± standard deviation) for phosphate and phosphite determined ($n = 9$) in fertilizers and mineral supplements for cattle by the proposed linear combination fitting P K-edge XANES method

		LCF weight		% w/w P specie		Total% w/w P				
Sample	*R* factor	Phosphate	Phosphite	Phosphate	Phosphite	LCF found[a]	Reference value (ICP OES)	Trueness (%)	Sample label description	Species founded by the proposed method
Fertilizer 1	0.026	0.14 ± 0.18	0.86 ± 0.18	0.012 ± 0.016	0.074 ± 0.016	0.086 .00.022	0.086 ± 0.001	100	Phosphite	Phosphite
Fertilizer 2	0.076	0.08 ± 0.09	0.92 ± 0.09	0.001 ± 0.002	0.017 ± 0.002	0.018 .00.002	0.018 ± 0.0004	100	Both species	Phosphite
Fertilizer 3	0.028	0.37 ± 0.01	0.63 ± 0.01	0.296 ± 0.010	0.504 ± 0.010	0.800 .80.014	0.801 ± 0.006	100	Both species	Both species
Fertilizer 4	0.059	1	0	1.24	0	1.24	1.23 ± 0.020	101	Phosphate	Phosphate
Fertilizer 5	0.054	0.02 ± 0.04	0.98 ± 0.04	0.137 ± 0.237	6.48 ± 0.24	6.62 .60.33	6.40 ± 0.08	103	Both species	Phosphite
Supplement 1	0.868	1	0	8.65	0	8.65	8.61 ± 0.51	100	Phosphate	Phosphate
Supplement 2	0.125	1	0	8.30	0	8.30	8.90 ± 0.47	93	Phosphate	Phosphate
Supplement 3	0.342	0.94 ± 0,10	0.06 ± 0.10	7.55 ± 0.83	0.48 ± 0.83	8.03 .01.17	8.45 ± 0.17	95	Phosphate	Phosphate
Supplement 4	0.077	0.97 ± 0.06	0.03 ± 0.06	7.72 ± 0.46	0.26 ± 0.46	7.98 .90.61	8.36 ± 0.54	95	Phosphate	Phosphate
Supplement 5	0.061	0.91 ± 0.15	0.09 ± 0.15	8.03 ± 1.33	0.77 ± 1.33	8.80 .81.88	9.48 ± 0.51	93	Phosphate	Phosphate

[a] Total% w/w P = [phosphite] + [phosphite].

98.0% of the explained variance, and an ellipse with a 95% confidence interval[41] was applied in the PCA score plot, showing that the samples were within the 95% confidence limit. Fig. 2b presents the loading plots for PC1 and PC2 obtained using different P K-edge XANES spectra. In Fig. 2a, there is a separation between the three classes of samples according to the different phosphorus species present in this study. The samples composed of only phosphate (square) or phosphite (circle) were separated from the sample that was composed of both species (fertilizer #3, gray lozenge). This differentiation was possible because the energies of the X-ray absorption edges were distinct for phosphite (2149 eV) and phosphate (2150 eV). The PC1 loading plots (Fig. 2b) showed a positive peak in the region from 2146 to 2149 eV that coincided with the spectrum of phosphite. This observation was also confirmed by the scores plot (Fig. 2a), in which the samples with phosphate were in the negative part of the scores. The PC2 loading plot showed a positive peak from 2149 to 2150 eV that coincided with the phosphate spectrum, and similar results were observed for the scores plot.

3.2 Linear combination fitting of the P K-edge XANES spectra

The linear combination fitting (LCF) models the spectrum for a sample of unknown species with a linear combination of spectra from the standards of known structure and composition that are candidate species within the sample. Another possible use of the LCF would be to determine the species and quantities of standards in a heterogeneous sample.[16,35]

The standard spectra of phosphate and phosphite (both 0.125% P (w/w), Fig. 1) were applied for the linear combination fitting of the fertilizer and mineral supplement samples. Ideally, the scaling factor (weight) obtained from the LCF represents the fractions of each standard species within the unknown sample. The accuracy of the fitting results is limited by the accuracy of the standards in representing the chemical species present in the sample and the uniqueness of the XANES spectral features between standards.[16]

The LCF for fertilizer #3 and mineral supplement for cattle #5 is shown in the ESI Fig. S2a and S2b† (Appendix), respectively. The LCF results identified the weights (proportions) of standards that yielded the best fit to the data. For fertilizer #3 (Table 1), the *R* factor value was 0.028, indicating a good fit, and the weights for phosphate and phosphite were 0.37 ± 0.01 and 0.63 ± 0.01, respectively. For the mineral supplement #5 (Table 1), the *R* factor value was 0.061, and the weights for phosphate and phosphite were 0.91 ± 0.15 and 0.09 ± 0.15, respectively. Using these weights, it was concluded that fertilizer #3 had both phosphorus species (PO_4^{3-} and HPO_3^{2-}) in its formulation, whereas the mineral supplement for cattle #5 only contained the phosphate species.

Using these weights and eqn (2), the concentrations of both PO_4^{3-} and HPO_3^{2-} species were determined for all the samples and are presented in Table 1. The measured concentrations ranges were 0.017–6.48% P (w/w) for phosphite and 0.29–1.24% P (w/w) for phosphate in the fertilizers. Moreover, the measured concentrations ranges were 0.48–0.77% P (w/w) for phosphite

and 7.55–8.03% P (w/w) for phosphate in the mineral supplements for cattle.

The specifications of all the tested supplement samples were consistent with the information described on the labels; the mineral supplements for cattle were composed of only phosphate as the source of phosphorus. However, for the fertilizers, the determined values for the PO_4^{3-} and HPO_3^{2-} species were not in agreement with the label specifications of the fertilizers #2 and #5, as shown in Table 1.

The trueness of the total phosphorus determined by LCF as compared to that determined by the ICP OES technique and the informative values for the reference materials were in the range of 93–103%. These values demonstrate satisfactory accuracy of the proposed method.

The LCF and P K-edge XANES spectroscopy were demonstrated to be excellent analytical tools for the speciation and determination of phosphate and phosphite in phosphorus-based agricultural inputs.

3.3 Partial least squares regression models for the determination of phosphite and phosphate

Multivariate calibration models for the determination of phosphate and phosphite species in the analyzed samples were calculated using partial least squares (PLS). The first derivative was applied to the obtained spectra for the standards, samples and blanks. The first derivatives for the fertilizers and mineral supplements are shown in the ESI Fig. S3a and S3b† (Appendix), respectively. After this, the data were mean-centered, and cross validation (leave-one-out) was carried out to select the adequate number of latent variables (LV). In the PLS models, the calculation for phosphate and phosphite used 1 and 2 LV, respectively.

The SEC (SE for calibration) and SECV (SE for cross validation) values obtained for the models proposed were 0.0198% P (w/w) and 0.018% P (w/w), respectively, for phosphite. For phosphate, an SEC of 0.0075% P (w/w) and an SECV of 0.0083% P (w/w) were obtained. When the reference and predicted values were compared, the linear equations for the PLS models obtained were $y = 0.0087 + 0.9129x$ (phosphite) and $y = 0.0155 + 0.9244x$ (phosphate). Good linear determination coefficient (R^2) values were obtained for the models proposed for phosphite ($R^2 = 0.8558$) and phosphate ($R^2 = 0.9511$).

The concentrations of the PO_4^{3-} and HPO_3^{2-} species were determined using the PLS models for all samples and are shown in Table 2. The measured concentration ranges were 0.022–4.36% P (w/w) for phosphite, 0.38–1.22% P (w/w) for phosphate for the fertilizers and 0.97–4.18% P (w/w) for phosphate for the mineral supplements for cattle. In the case of the supplement samples, the concentrations of the phosphite species were lower than the SECV (0.018% P (w/w)). It was concluded that the information provided by the manufacturers of the mineral supplements for cattle was consistent because these samples were composed of only phosphate as the source of phosphorus.

The trueness of total phosphorus determined by PLS as compared to that determined by the ICP OES technique or the values of the reference materials were in the range of 65–121% for fertilizers and 12–48% for the mineral supplements for cattle.

The trueness was not satisfactory for the predictions of phosphate concentrations in the mineral supplement samples by PLS. The matrix effects may have interfered with the sensitivity of the measured analytical signals of the X-ray absorption because all supplement samples contain a solid material in the suspension. The model generated was sensitive to these fluctuations in the obtained analytical signal. For this reason, the trueness obtained was not satisfactory.

3.4 Addition/recovery tests

Further tests were performed to verify the accuracy of the analytical methods developed for the determination of phosphorus species by LCF and PLS. The tests were performed for the fertilizer and supplement samples spiked with 0.077% P (w/w) in the phosphite and phosphate species.

The trueness of the phosphite and phosphate species added to the samples varied in the range of 96–113% for the LCF method (Table 3), demonstrating the accuracy of the

Table 2 Results (mean) for phosphate and phosphite determined ($n = 9$) in fertilizers and mineral supplements for cattle by the proposed PLS models P K-edge XANES method[a]

	PLS model		Total% w/w P				
Sample	Phosphate	Phosphite	PLS found	Reference values (ICP OES)	Trueness (%)	Sample label description	Species founded by the proposed method
Fertilizer 1	<SECV	0.057	0.057	0.086 ± 0.001	65	Phosphite	Phosphite
Fertilizer 2	<SECV	0.022	0.022	0.018 ± 0.0004	121	Both species	Phosphite
Fertilizer 3	0.375	0.280	0.655	0.801 ± 0.006	82	Both species	Both species
Fertilizer 4	1.22	<SECV	1.22	1.23 ± 0.020	99	Phosphate	Phosphate
Fertilizer 5	0.689	4.362	5.05	6.40 ± 0.08	76	Both species	Both species
Supplement 1	<SECV	<SECV	—	8.61 ± 0.51	—	Phosphate	—
Supplement 2	0.97	<SECV	0.97	8.90 ± 0.47	12	Phosphate	Phosphate
Supplement 3	1.05	<SECV	1.05	8.45 ± 0.17	13	Phosphate	Phosphate
Supplement 4	1.69	<SECV	1.69	8.36 ± 0.54	21	Phosphate	Phosphate
Supplement 5	4.18	<SECV	4.18	9.48 ± 0.51	48	Phosphate	Phosphate

[a] Phosphate SECV: 0.0083% w/w P. Phosphite SECV: 0.018% w/w P.

Table 3 Recovery tests results (mean ± standard deviation) for phosphate and phosphite (% P, w/w) determined ($n = 9$) in fertilizers and mineral supplements for cattle by the LCF and PLS methods

Sample	% w/w P in the sample	% w/w P added		Found by LCF (trueness, %)		Found by PLS (trueness, %)	
		Phosphate	Phosphite	Phosphate	Phosphite	Phosphate	Phosphite
Fertilizer 1	0.042	0.077	—	0.087 ± 0.004 (113)	—	0.088 (114)	—
Fertilizer 1	0.042	—	0.077	—	0.075 ± 0.004 (97)	—	0.066 (86)
Fertilizer 4	0.062	0.077	—	0.077 (100)	—	0.070 (91)	—
Fertilizer 4	0.064	—	0.077	—	0.077 ± 0.006 (100)	—	0.057 (74)
Supplement 1	0.058	0.077	—	0.075 ± 0.001 (97)	—	0.44 (76)	—
Supplement 1	0.057	—	0.077	—	0.074 ± 0.005 (96)	—	0.132 (171)
Supplement 2	0.058	0.075	—	0.075 ± 0.001 (100)	—	0.026 (35)	—
Supplement 2	0.058	—	0.077	—	0.076 ± 0.001 (99)	—	0.115 (149)

measurements for all the samples using LCF. For the PLS method, the trueness of phosphite and phosphate added to the fertilizers and the mineral supplement samples for cattle varied in the range of 74–114% and 35–149%, respectively.

The trueness of the species in the mineral supplement samples was not satisfactory for the PLS calibration method due to matrix effects. This may be related to the quality of the spectra obtained for phosphate and phosphite in these samples by XANES. Possible interferences in the acquisition of the spectra, which generated fluctuations in the analytical signals obtained, affected the calibration model proposed by the PLS regression.

3.5 Limits of speciation and method detection limits for phosphite and phosphate

The calculated limits of speciation (LOSs) of the method for phosphate and phosphite were 11 and 14 mg L^{-1}, respectively. This value is helpful in estimating the feasibility of further experiments.

The standard deviations of 1.13 and 1.35 were obtained for phosphate and phosphite, respectively, for the maximum normalized absorption (norm $\mu(E)$) P K-edge XANES spectra. For eight analyses with seven degrees of freedom and a 99% confidence level, the value of the Student's t test was 3.499. From this analysis, the method detection limit (MDL) values for the phosphate and phosphite species were found to be 4.0 and 4.7 mg L^{-1}, respectively. The MDL depends on multiple factors such as the atomic number of the analyte, the energy of the incoming beam, the integration time, and the detector characteristics. Therefore, the value reported herein specifically applies to the analytes and instrumental parameters evaluated in this study.

4. Conclusions

XANES spectroscopy is an excellent analytical tool for the direct speciation of phosphorus in complex matrices as agricultural inputs. The use of LCF, PCA and PLS aided in the development of a simple nondestructive method for the speciation and determination of phosphorus in fertilizers and mineral supplements for cattle. Linear combination fitting is an interesting strategy and efficient method for the qualitative and quantitative analysis in chemical speciation by XANES spectroscopy. Strong matrix effects in the mechanism of X-ray absorption for P K-edge XANES spectroscopy prevented the determination of the phosphorus species in the mineral supplements for cattle using the PLS models. The proposed methods are environmentally friendly since the direct sample analysis reduces the environmental impact caused by the use of hazardous reagents commonly employed for sample preparation in speciation.

Conflicts of interest

There are no conflicts to declare.

Acknowledgements

This study was supported by the São Paulo Research Foundation (FAPESP, 2016/01513-0, 2016/17221-8 and 2016/17304-0) and the Conselho Nacional de Desenvolvimento Científico e Tecnológico (CNPq, 141311/2017-7, 401074/2014-5 and 305337/2015-0). We are also thankful to the Brazilian Synchrotron Light Laboratory (LNLS) for the XAS measurements (process number SXS-20170074) and EMBRAPA Southeast Livestock for donating the reference materials. We would like to thank Dr Flávio C. Vicentin and Felipe A. Del Nero for assistance during LNLS experiments. This study was financed in part by the Coordenação de Aperfeiçoamento de Pessoal de Nível Superior – Brasil (CAPES) – Finance Code 001.

References

1 J. Zhu, M. Li and M. Whelan, *Sci. Total Environ.*, 2018, **612**, 522–537.
2 F. C. Gómez-Merinoa and L. I. Trejo-Téllez, *Sci. Hortic.*, 2015, **196**, 82–90.
3 M. Manna, V. M. Achary, T. Islam, P. K. Agrawal and M. K. Reddy, *Sci. Rep.*, 2016, **6**, 24941.
4 W. S. Marçal, B. C. Oliveira Junior and V. V. Ortunho, *Acta Sci. Vet.*, 2005, **33**, 315–319.
5 D. V. Babos, V. C. Costa, M. A. Sperança and E. R. Pereira-Filho, *Microchem. J.*, 2018, **137**, 272–276.

6 T. Taflik, F. A. Duarte, E. L. M. Flores, F. G. Antes, J. N. G. Paniz, E. M. M. Flores and V. L. Dressler, *J. Braz. Chem. Soc.*, 2012, **23**, 488–495.
7 L. Luo, Y. Ma, R. L. Sanders, C. Xu, J. Li and S. C. B. Myneni, *Nutr. Cycling Agroecosyst.*, 2017, **107**, 215–226.
8 N. Siebers, J. Kruse and P. Leinweber, *Water, Air, Soil Pollut.*, 2013, **224**, 1–13.
9 M. Gräfe, E. Donner, R. N. Collins and E. Lombi, *Anal. Chim. Acta*, 2014, **822**, 1–22.
10 A. P. Miller and Y. Arai, *Geoderma*, 2017, **305**, 62–69.
11 E. D. Roy, N. T. Nguyen and J. R. White, *Sci. Total Environ.*, 2017, **609**, 1248–1257.
12 J. Kruse, M. Abraham, W. Amelung, C. Baum, R. Bol, O. Kuhn, H. Lewandowski, J. Niederberger, Y. Oelmann, C. Ruger, J. Santner, M. Siebers, N. Siebers, M. Spohn, J. Vestergren, A. Vogts and P. Lienweber, *J. Soil Sci. Plant Nutr.*, 2015, **178**, 43–88.
13 Y. Hashimoto and Y. Watanabe, *Geoderma*, 2014, **230–231**, 143–150.
14 R. A. Barco, D. G. Patil, W. Xu, L. Ke, C. S. Khachikian, G. Hanrahan and T. M. Salmassi, *Talanta*, 2006, **69**, 1292–1299.
15 G. S. Henderson, F. M. F. de Groot and B. J. A. Moulton, *Rev. Mineral. Geochem.*, 2014, **78**, 75–138.
16 *Methods of Soil Analysis Part 5-Mineralogical Methods*, ed. A. L. Ulery and L. R. Drees, Soil Science of America, Madison, 2008.
17 L. F. Oliveira, N. T. Canevari, M. B. B. Guerra, F. M. V. Pereira, C. E. G. R. Schaefer and E. R. Pereira-Filho, *Microchem. J.*, 2013, **109**, 165–169.
18 R. E. Shaffer, J. O. Cross, S. L. Rose-Pehrsson and W. T. Elam, *Anal. Chim. Acta*, 2001, **442**, 295–304.
19 E. M. Kroukamp, T. Wondimu and P. B. C. Forbes, *Trends Anal. Chem.*, 2016, **77**, 87–99.
20 P. Kappena, G. Ferrando-Miguel, S. M. Reichmand, L. Innes, E. Welter and P. J. Pigram, *J. Hazard. Mater.*, 2017, **329**, 131–140.
21 K. Chitpirom, A. Akaracharanya, S. Tanawupawat, N. Leeptpatpiboon, K. W. Kim, J. Hormes and A. Prange, *J. Food, Agric. Environ.*, 2017, **15**, 44–47.
22 N. Siebers, J. Kruse, K. U. Eckhardt, Y. Hu and P. Leinweber, *J. Synchrotron Radiat.*, 2012, **19**, 579–585.
23 M. P. Isaure, B. Leyh, M. Salomé, G. J. Krauss, D. Schaumlöffel and D. Dobritzsch, *Spectrochim. Acta, Part B*, 2017, **137**, 85–92.
24 O. L. G. Alderman, M. C. Wilding, A. Tamalonis, S. Sendelbach, S. M. Heald, C. J. Benmore, C. E. Johnson, J. A. Johnson, H. Y. Hah and J. K. R. Weber, *Chem. Geol.*, 2017, **453**, 169–185.
25 S. S. Yekta, J. Gustavsson, B. H. Svensson and U. Skyllberg, *Talanta*, 2012, **89**, 470–477.
26 A. Prance, B. Birzele, J. Kramer, H. Modrow, R. Chauvistré, J. Hormes and P. Kohler, *J. Agric. Food Chem.*, 2003, **51**, 7431–7438.
27 M. L. Lopez-Moreno, G. Rosa, J. A. Hernandez-Viezcas, J. R. Peralta-Videa and J. R. Gardea-Torresdey, *J. Agric. Food Chem.*, 2010, **58**, 3689–3693.
28 R. Terzano, Z. A. Chami, B. Vekemans, K. Janssens, T. Miano and P. Ruggiero, *J. Agric. Food Chem.*, 2008, **56**, 3222–3231.
29 A. K. Eriksson, D. Hesterberg, W. Klysubun and J. P. Gustafsson, *Sci. Total Environ.*, 2016, **566–567**, 1410–1419.
30 C. Giguet-Covex, J. Poulenard, E. Chalmin, F. Arnaud, C. Rivard, J. P. Jenny and J. M. Dorioz, *Geochim. Cosmochim. Acta*, 2013, **118**, 129–147.
31 S. Sato, D. Solomon, C. Hyland, Q. M. Ketterings and J. Lehmann, *Environ. Sci. Technol.*, 2005, **39**, 7485–7491.
32 W. Wisawapipat, K. Charoensri and J. Runglerttrakoolchai, *J. Agric. Food Chem.*, 2017, **65**, 704–710.
33 A. Kuno and M. Matsuo, *Anal. Sci.*, 2000, **16**, 597–602.
34 A. Voronov, A. Urakawa, W. van Beek, N. E. Tsakoumis, H. Emerich and M. Rønning, *Anal. Chim. Acta*, 2014, **840**, 20–27.
35 B. Ravel and M. Newville, *J. Synchrotron Radiat.*, 2005, **12**, 537–541.
36 R. Bro and A. K. Smilde, *Anal. Methods*, 2014, **6**, 2812–2831.
37 T. Bacquart, G. Deve`s, A. Carmona, R. Tucoulou, S. Bohic and R. Ortega, *Anal. Chem.*, 2007, **79**, 7353–7359.
38 F. Porcaro, S. Roudeau, A. Carmona and R. Ortega, *Trends Anal. Chem.*, 2018, **104**, 22–41.
39 APHA, American Water Works Association, Water Environment Federation, *Standard Methods for the Examination of Water and Wastewater*, American Public Health Association, Washington, 19th edn, 1995.
40 E. D. Ingall, J. A. Brandes, J. M. Diaz, M. D. de Jonge, D. Paterson, I. McNulty, W. C. Elliotte and P. Northrup, *J. Synchrotron Radiat.*, 2011, **18**, 189–197.
41 F. Husson, S. Le and J. Pages, *Food Qual. Prefer.*, 2005, **16**, 245–250.

Electronic Supplementary Material (ESI) for Analytical Methods.

Determination and speciation of phosphorus in fertilizers and mineral supplements by cattle by X-ray absorption near edge structure spectroscopy: a simple nondestructive method

Diego Victor Babos, Jeyne Pricylla Castro, Daniel Fernandes Andrade,

Vinicius Câmara Costa and Edenir Rodrigues Pereira-Filho*

Group of Applied Instrumental Analysis, Department of Chemistry, Federal University of São Carlos, São Carlos, São Paulo State, 13565-905, Brazil

*Corresponding author: Group of Applied Instrumental Analysis, Department of Chemistry, Federal University of São Carlos, São Carlos, São Paulo State 13565-905, Brazil

Phone number: +55 16 3351-8092

E-mail: erpf@ufscar.br (E.R. Pereira-Filho)

Appendix A. Supplementary data

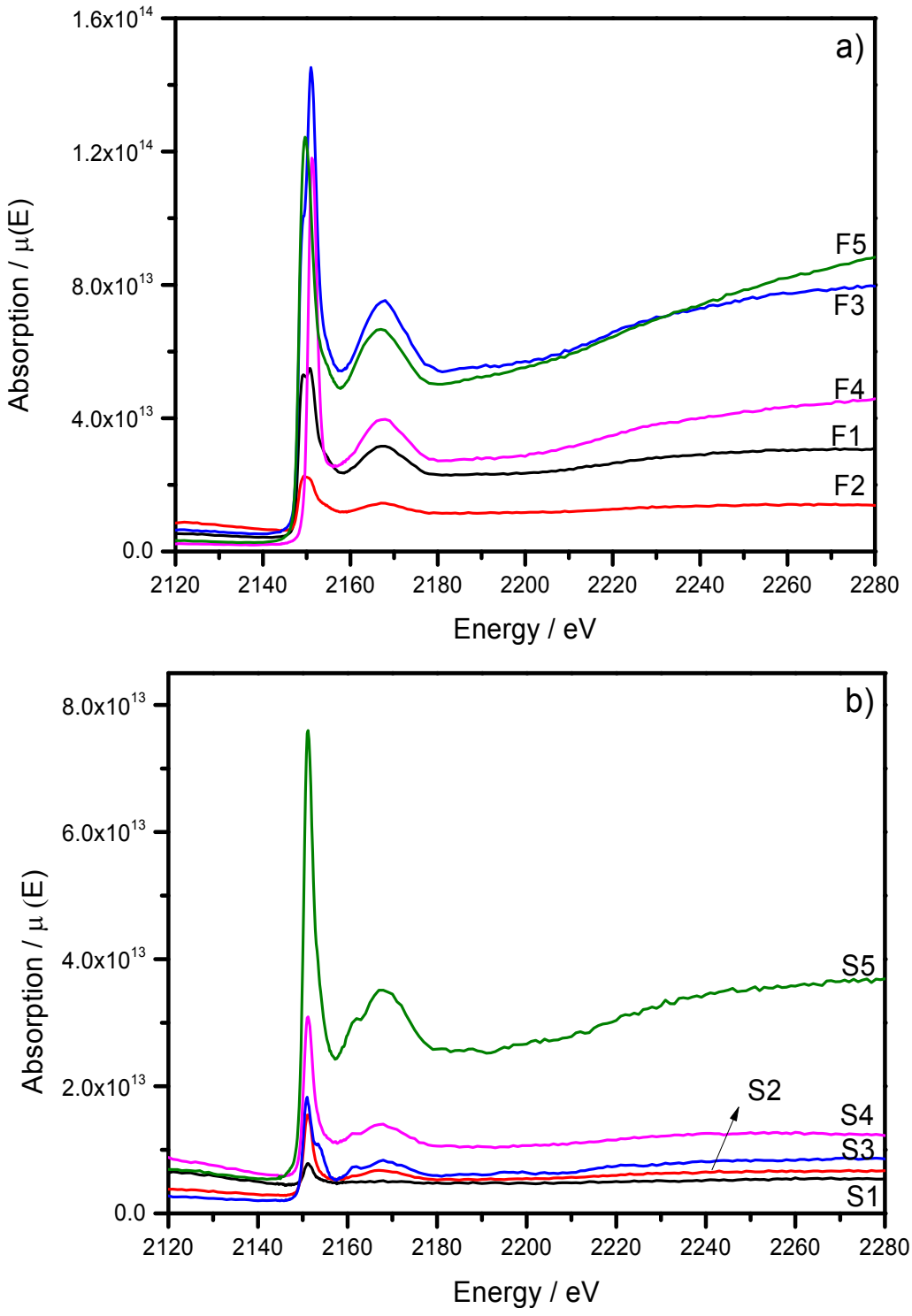

Figure S1. Phosphorus K-edge XANES spectra for fertilizers (F) (a) and mineral supplement for cattle (S) (b).

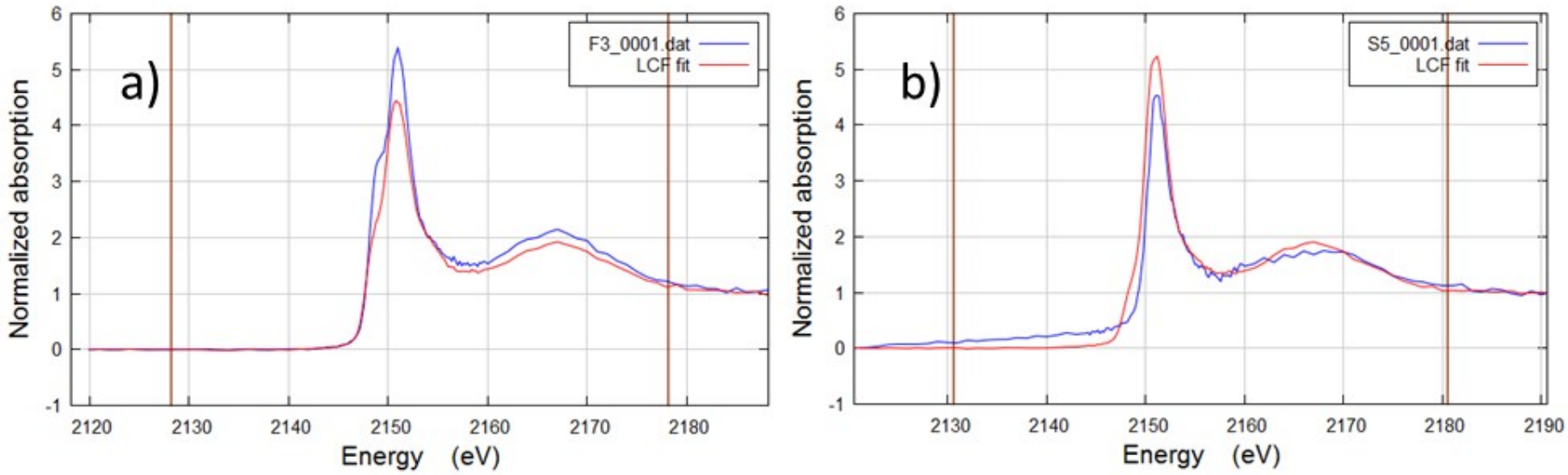

Figure S2. Linear combination fitting using two standards (phosphite and phosphate) for (a) fertilizer #3 and (b) mineral supplement for cattle #5.

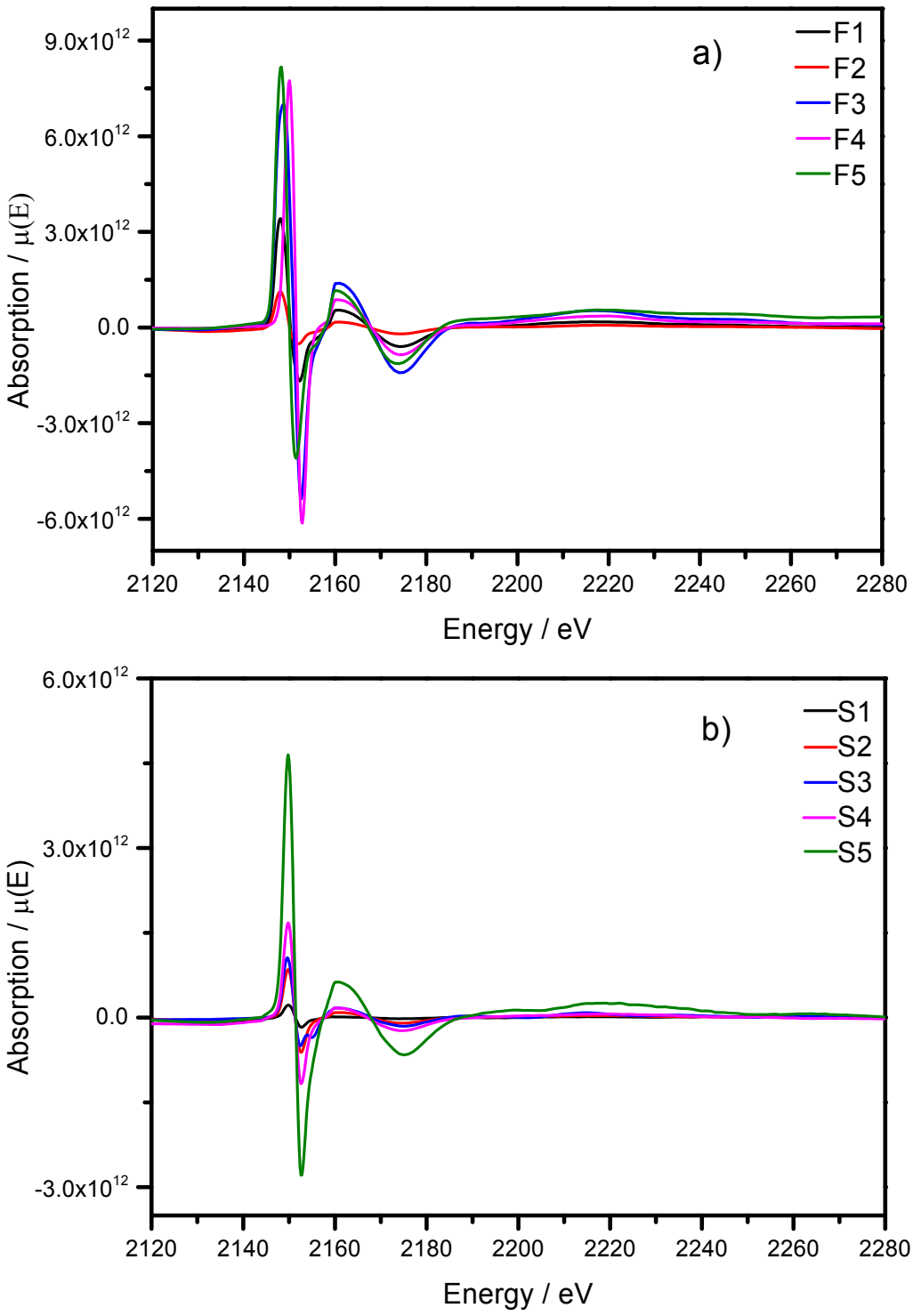

Figure 3S. First derivative of the P K-edge XANES spectra of the (a) fertilizers (F) and (b) mineral supplement for cattle (S) samples analyzed by the proposed PLS models.

Chapter 3 – Laser-induced breakdown spectroscopy

3.1 Laser-induced breakdown spectroscopy

Laser-Induced breakdown spectroscopy (LIBS) is a technique that has been widely used in direct analysis of solid, liquid or gaseous samples, to obtain qualitative and quantitative multi-element information of its constituents.[1,2,7,73]

LIBS have interesting advantages when compared to other plasma-based spectroscopic techniques, which have made it an excellent analytical tool in proposing new methods. I highlight as main characteristics: i) the possibility of being used to directly analyze solid samples with none or minimal treatment; ii) allows multi-elementary analysis of surfaces and different depths in solid samples, with spatial resolution of a few μm; iii) the sampled masses are in the range of 0.1 to 100 μg, or more, depending on the characteristics of the sample and the laser; iv) can be used in unhealthy environments and for remote monitoring of potentially dangerous samples; v) fast analysis with short spectrum acquisition time (1 to 10 spectra *per* second, depending on the laser repetition rate); vi) the cleaning and / or removal of films on the surface to be analyzed can be carried out in a programmed way, applying some pulses with the laser itself; vii) use of few consumable materials (no Argon or Nitrogen gas required for plasma generation); and viii) the technique can be used both in the laboratory and in field analysis (portable LIBS).[1,2,7,10,12,73-75]

Despite these attractions, LIBS still requires considerable efforts in quantitative analysis, due to: i) calibration difficulties, preparation of standards, and the absence of reference materials with certified properties for masses <0.1 mg; ii) limits of detection in the order of 50 μg g^{-1}, which may make it impossible to use the technique in elementary determination whose analyte concentration is less than this quantity; iii) strong matrix effects (spectral and non-spectral) that compromise quantitative determination with required precision and accuracy; and iv) poor reproducibility due to sample heterogeneity (high values of relative standard deviation).[1,2,8,10,12,73-75]

The instrumental arrangement of the LIBS technique is basically composed of a laser source (light amplification by stimulated emission of radiation), sample holder, optical components, spectrometer, detector and

computer for system control and recording of the LIBS emission spectrum, as shown in FIGURE 3.1.

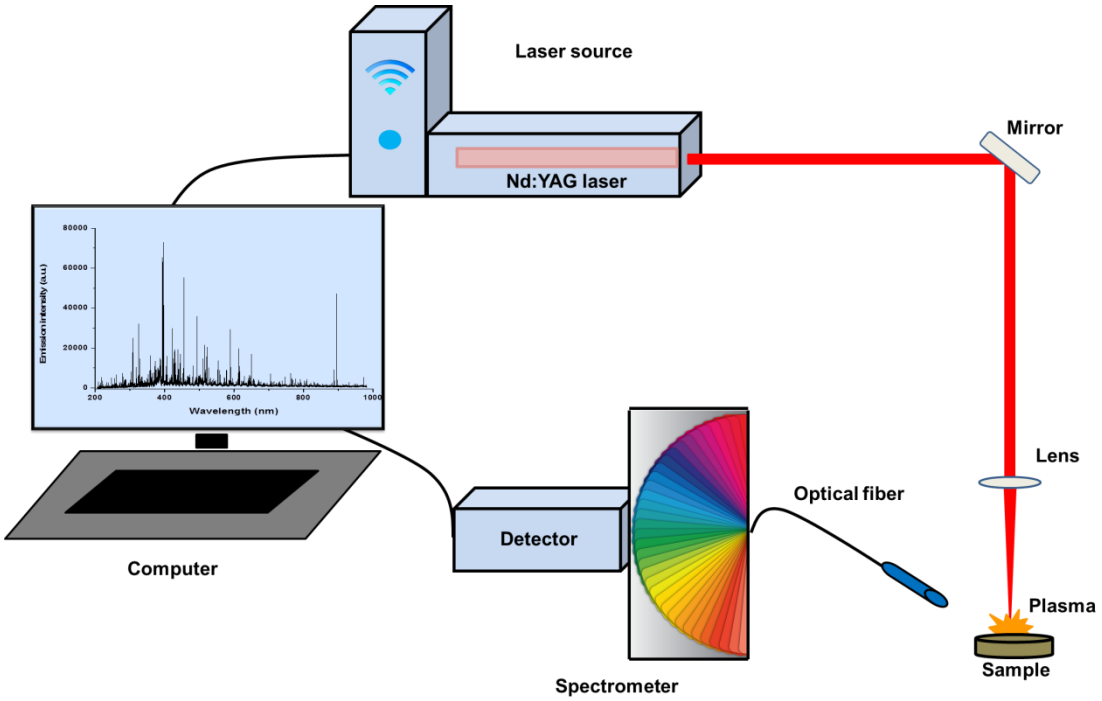

FIGURE 3.1 Simplified representations of the instrumental components of a LIBS system.

When firing a laser pulse over the surface of a given sample, several phenomena occurred due to the interaction of electromagnetic radiation with the sample. The formation of a microplasma (with temperatures in the order of 10000 K) and the emission of radiation characteristic of the species present in this plasma (ions, atoms and molecules) can be considered the two phenomena that contribute significantly in the search for chemical information of a given sample.[1,7,10,73]

The chemistry of plasma induced by laser is of great complexity and a very rich source of chemical information. The multi-element spectra obtained by this technique contain the following information i) chemistry of the sample analyzed, such as identity (specific wavelengths) and concentration of analytes (emission intensity); and ii) physical properties, such as the temperature and electronic density of the plasma formed.[10,73] FIGURE 3.2 shows the main processes that occur due to the interaction of the laser pulse in a given material, in a LIBS system.

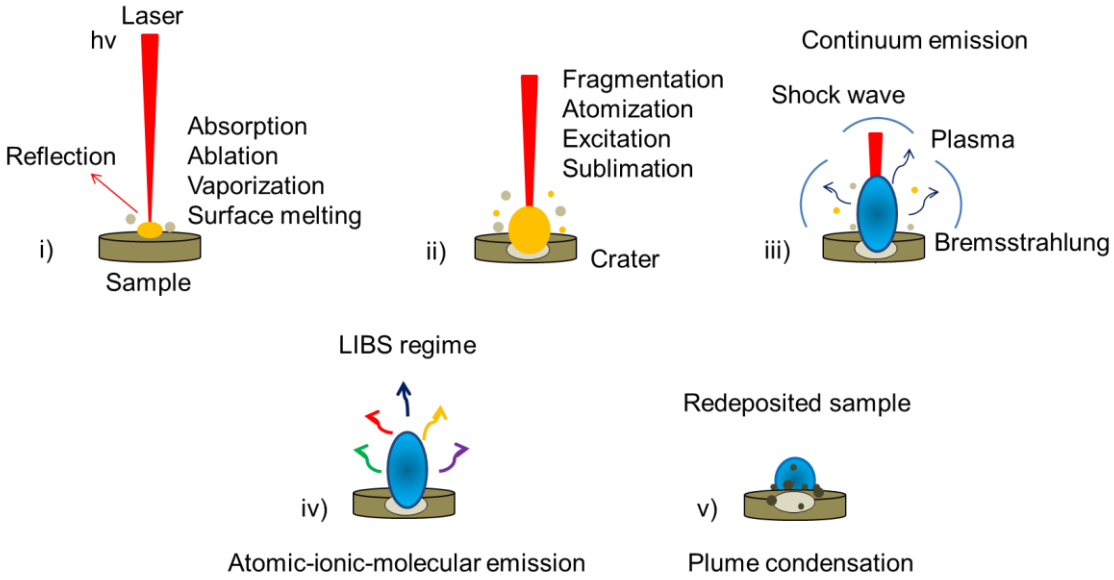

FIGURE 3.2 Main processes that occur due to the interaction of a laser pulse in a given sample.

Each sample has a unique chemical composition and structure, resulting from the presence, nature and position of its atoms, which when irradiated by a laser pulse determine all the processes resulting from this interaction, as result, take place the decomposition and vaporization mechanisms of the particles, the extent of fragmentation, atomization, excitation and plasma formation; which will directly reflect on the atomic, ionic and molecular band emissions of the analytes by LIBS.[1,2,10,73]

All these processes, described in Figure 3.2, occur quickly, with a time of less than 1s. For analytical purposes, the delay time to start collecting chemical information and the acquisition time of the analytical signal, from the moment a laser pulse was given, are important variables and should be optimized considering the characteristics of the sample and the analyte, so that all processes take place and reproducible measures are obtained. In addition, other variables such as laser fluence (laser pulse energy *per* unit area, J cm^{-2}) and the number of pulses in the sample must be optimized to obtain quantitative and representative ablations.[73,75]

FIGURE 3.3 shows the profile of the analytical signal obtained (emission intensity) in relation to the time required for the phenomena to occur after the laser pulse on the sample surface.[75] I highlight the time required for the emission related to the *continuum* (background emission, due to the

recombination of free electrons and ions in the plasma, for example) and emission of the ionic, atomic and molecular species of the analyte. An optimized delay time allows to obtain a good signal-to-background ratio of the lines and/or emission bands of the analyte.[2,75]

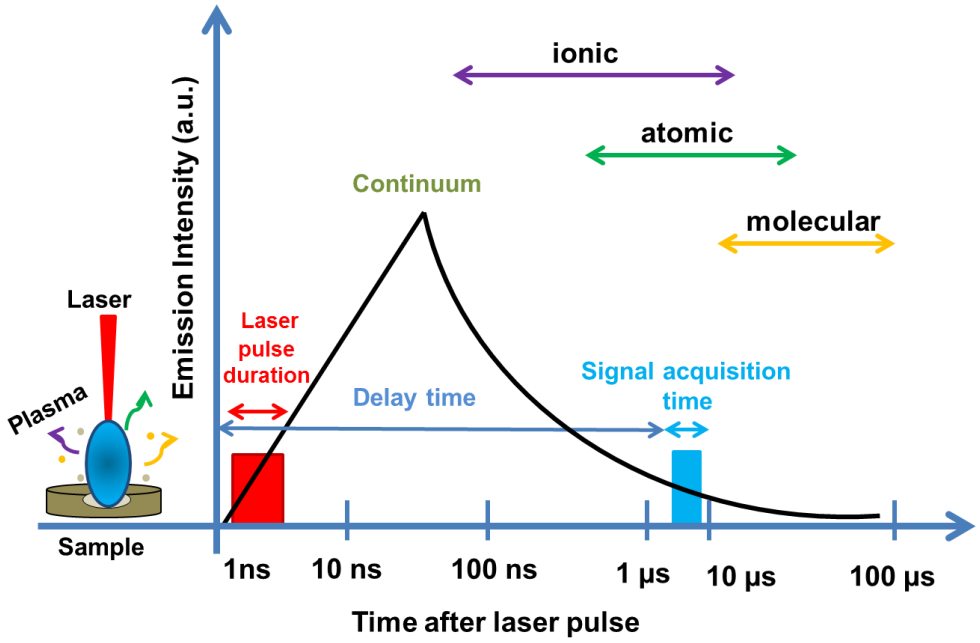

FIGURE 3.3 Temporal evolution of some processes that occur in the plasma and related variables (delay time and signal acquisition time).

However, some physical-chemical processes may not be allowed; others, when they occur, can be suppressed and subordinate to the presence of specific species that act as precursors in the plasma. In addition, the quantity and type of excited species that populate the plasmas produced by laser are strongly determined by several variables,[10] such as the type of molecular solid (predominantly organic or inorganic),[76] the composition of the surrounding atmosphere (O_2, N_2, Ar, H_2, air), as well as the applied pressure, where the plasma evolves,[77,78] and laser irradiation parameters such as wavelength (266, 532 or 1064 nm),[79] pulse duration (femtoseconds (fs) or nanoseconds (ns))[77,79] and laser fluence.[80]

This multiplicity of factors are critical especially when using qualitative analysis to monitor molecular emission, as they make it very difficult to assign a specific molecular emission profile to each molecule. The complexity of plasma chemistry was verified by SERRANO et al. (2016),[79] and according to them, four routes can lead to the formation and optical emission of diatomic

molecules present in plasma from LIBS: a) from the portion of fragmented molecules, i) decomposition reactions (ABCD → AB + CD); and b) the portion of atomized molecules, ii) atomic recombination (A_{native} + C_{native} → AC); iii) single displacement reactions (A^*_2 + $C_{native/\ environment}$ → AC + A), and iv) double displacement reactions (A^*_2 + BC → AC + AB).[79] Great efforts have been made to investigate the mechanisms of formation of diatomic molecules, as well as their connections with the binding structure of molecular solids, aiming at many qualitative and quantitative applications.

In the qualitative analysis I highlight the advance of laser-induced breakdown isotopic molecular spectroscopy (LAMIS). PIESTCH et al. (1998),[81] used LAMIS, based on the optimization of predetermined instrumental parameters, for the isotopic analysis of ^{235}U - ^{238}U in uranium sample, monitoring the ionic line at 424.42 nm, with an isotopic shift of 0.025 nm. In another study, the detection of isotopes of ^{1}H - ^{2}H (OH and OD), ^{10}B - ^{11}B (BO), ^{12}C - ^{13}C (CN and C_2) and ^{16}O - ^{18}O (OH), and the determination of B isotopes using PLS regression were demonstrated by RUSSO et al. (2011), using LAMIS.[82]

In the direct qualitative analysis I also highlight the use of LIBS in the acquisition of spectral and hyperspectral images.[4,83-84] These images are important for the analysis of superficial and in depth characterization of the sample (see FIGURE 1.1), aiming at the identification and location of essential, toxic, strategic, major elements, among others. Using a hyperspectral image, obtained through the score maps from a PCA, it was possible to verify the distribution of macronutrients (Ca, K, Mg, Na and P) on the surfaces and in depth of different edible seeds,[84] and of toxic, precious and strategic metals in electronic waste electronic circuit board,[4] for example. And recently NARDECCHIA et al. (2020),[85] proposed a new spectral analysis strategy, called embedded k-means clustering in order to explore a big LIBS imaging data set (millions spectra) acquired from mineral sample.

The LIBS spectra associated with chemometric tools for the recognition of unsupervised patterns (hierarchical cluster analysis - HCA and PCA) and supervised (partial least squares discriminant analysis (PLS-DA), k-nearest neighbor (KNN), linear discriminant analysis (LDA) and soft independent modeling of class analogy (SIMCA)) are used in many qualitative

applications. For example, CASTRO & PEREIRA-FILHO (2016)[86] used SIMCA, KNN and PLS-DA to classify samples of steel and alloy, according to the concentration of Fe. And BELLOU et al. (2020),[87] classified olive oil samples and verified the authentication of their geographic origin and detection of adulteration, using PCA and LDA.

In quantitative analysis, LIBS is a fantastic analytical tool employing direct analysis of solids, due to the advantages already mentioned. However, the choice of the calibration strategy, the matrix effects and the preparation of solid calibration standards are still major challenges that must be evaluated and circumvented, to ensure quantitative results with good figures of merit.

Normalization strategies of the LIBS emission spectra and appropriate chemometric tools have also contributed to the successful use of calibration strategies. Spectral normalizations are used to improve analytical performance, as they can correct or compensate some instrumental fluctuations in the obtained signals (area or height), baseline corrections when necessary, and sample matrix differences during data acquisition; that reflect repeatability, accuracy and precision of measurements.[86,88]

Various types of matrices were analyzed by LIBS for quantitative analysis, and using different calibration strategies, such as: i) sunscreen to determine Ti, evaluating four calibration strategies (MMC, MLR, PLS and PCR);[26] ii) biochar-based fertilizers to determine N by monitoring the CN molecule and using MMC,[89] and iii) human hair to determine Cu and Zn using standard addition.[90]

FIGURE 3.4 shows the main univariate (highlighting the number of solid calibration standards required) and multivariate (most used and new approaches) calibration strategies reported in the scientific literature for LIBS. All strategies have advantages and limitations that must be verified for the development of a new analytical method, also considering the characteristics of the sample analyzed and the analyte by LIBS technique. In the next pages, I briefly describe the advantages, limitations and applications of each of these calibration strategies.

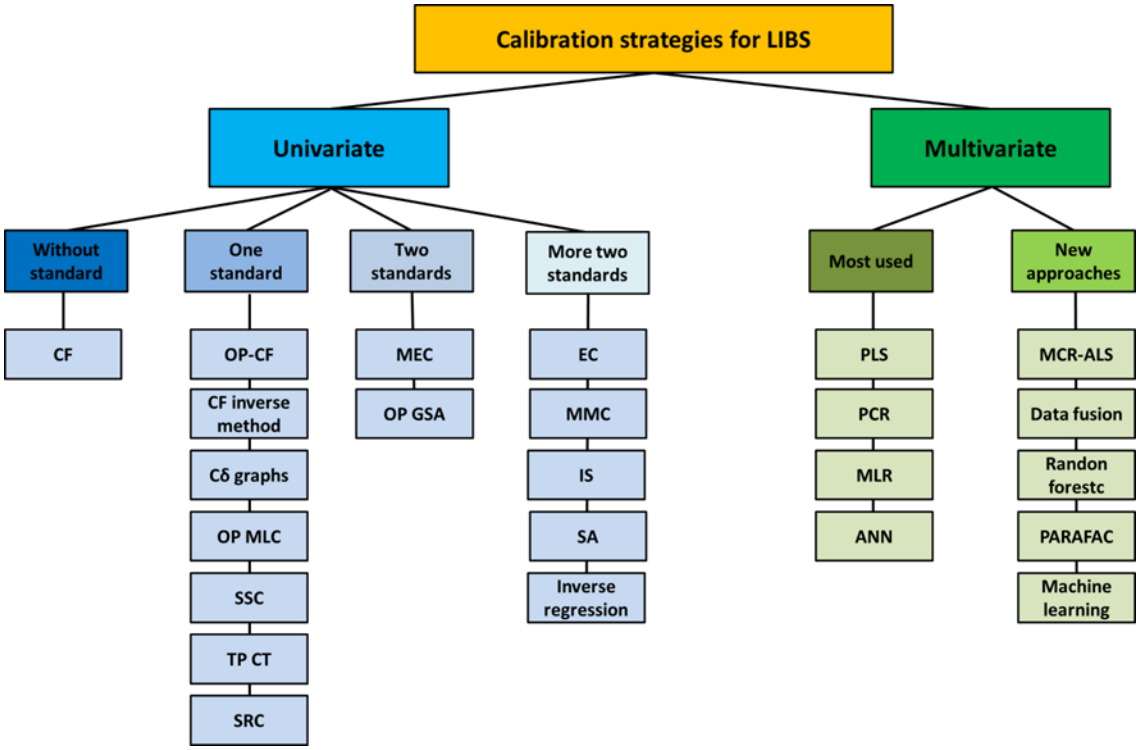

FIGURE 3.4 Calibration strategies i) univariate (calibration-free - CF, one-point calibration-free - OP-CF, calibration-free inverse method, Cδ graphs, one-point and multi-line calibration - OP MLC, single-sample calibration - SSC, two-point calibration transfer - TP CT, slope ratio calibration - SRC, multi-energy calibration - MEC, one-point gravimetric standard addition - OP GSA, external calibration - EC, matrix-matching calibration - MMC, Internal standardization - IS, standard addition - SA and inverse regression) and ii) multivariate (partial least squares - PLS, principal component regression - PCR, multiple linear regression - MLR, artificial neural network - ANN, multivariate curve resolution alternating least-squares algorithm - MCR-ALS, data fusion, random forest regression, parallel factor analysis - PARAFAC and machine learning regressions) used in LIBS method.

Calibration-free - CF, proposed in 1999 by CIUCCI et al.,[91] considers the principles and equations that govern the emission of plasmas in the local thermodynamic equilibrium (LTE) for the quantitative analysis by LIBS. The CF LIBS assumes that there a stoichiometric ablation and complete atomization, thermal equilibrium, homogeneous plasma, thin radiation and detection of all elements. In LTE, excited levels and ionization states are populated according to the Boltzmann distribution and Saha-Boltzmann equilibrium equation, respectively. The graphical representation of a group of spectral lines in a Boltzmann plane is commonly used to determine the plasma temperature.[91-93]

The McWhirter criterion is very used to verify the LTE validity of the analyzed plasma. It is based on the requirement that in LTE the rate of collision processes must be dominant over the radiative processes.[92] LTE is valid if when the electron number density calculated is of the order of 10^{17}-10^{18} cm^{-3}.

The main advantage of CF is that it does not require solid calibration standards (for a matrix-matching, for example), because it requires only physic-chemical parameters of the plasma and the intensity of the integrated signal of the analyte emission line and all others elements present in the plasma, for the determination of the analyte.[93] This advantage is very interesting for the analysis of samples with complex matrices, without solid commercial calibration standards or with a small number of samples (which could be analyzed and used as standards). The main limitations of CF are related to the self-absorption effect, matrix effects, difficulties in obtaining results with accuracy for minority analytes and laborious processing.[93] The absorption of photons within the laser-induced plasma is called self-absorption.[93] This phenomenon is observed mainly for emission lines where the lower level of transition is equal or close to the ground state. Self-absorption phenomenon underestimates the concentration of the analyte and consequently impairs the accuracy in the determinations using the CF.

The CF was a strategy used successfully in the analysis of modern bronzes,[93] seafood,[94] titanium alloys,[95] oxide materials[96] among others.

One-point calibration-free - OP-CF,[97] calibration-free inverse method[98] and Cδ graphs[99] are strategies that use LTE principles, as CF.

However, these three calibration strategies use only one solid calibration standard, with a similar matrix to that of the samples, in order to obtain instrumental parameters that provide greater accuracy in LIBS determinations.[93]

In OP-CF, the parameters referring to the knowledge of the response curve of the spectrometer in the spectral regions and of the spectral A_{ki} (transition probability between the upper and lower levels of the transition) parameter are obtained with greater precision, from the analysis of a standard with known composition. In addition, the possible variations in the LIBS plasma parameters obtained in the samples, in relation to the standard (one-point), such as plasma temperature, density of the number of electrons, amount of mass ablated; will be taken into account and fully compensated in the analysis.[93,97] The OP-CF was used as a calibration strategy in the analysis of copper-based alloys[97] and modern bronzes,[93] for example.

In the calibration-free inverse method,[98] using the LTE equations, the concentration of the analytes in a reference sample is determined using different temperatures, and assuming that the real electronic temperature of the plasma is the one that provides the determinations of the analytes in accordance with the reference values. Thus, the plasma temperature value obtained with accuracy in this procedure is used in the analyte determination calculations in other similar matrix samples and ablated under the same conditions as the reference sample.[93] CF inverse method was used in the analysis of archeological findings of copper-based alloys (proof concept),[98] modern bronzes,[93] and depth profiles of copper-based alloys,[100] for example.

The Csigma (Cδ) graphs approach, proposed by ARAGÓN & AGUILERA (2014),[99] can be considered a calibration curve for LIBS that allows to include several lines of emission of different elements in the same ionization state in many concentrations. The method is based on the Boltzmann, Saha and radiative transfer equations for plasmas in LTE. Cδ graphs are based on the calculation of a line cross section (δI) for each of the experimental data, starting from the atomic data of the line, the temperature and the electron density. The Cδ curve represents the dependence of the line intensities, divided by their Lorentzian width (I/Δλ) as a function of Cδ, and is determined using the spectral lines measured on a single standard of known composition.[93,99] From this characterization the intensity and self-absorption of a given spectral line of

an element at a certain concentration may be determined by LIBS.[99] The Cδ graphs was used to determine Fe, Mn, Mg, Si and Cr in fused glass samples,[99] Cu, Pb, Sn and Zn in modern bronzes,[93] and Si, Fe, Cu, Mn, Mg, Cr, Ni, Zn, Ti and Ca in aluminum alloys,[101] for example.

One-point and multi-line calibration - OP MLC, recently proposed by HAO et al. (2018),[102] uses a single solid standard for matrix-matching and several analyte emission lines to obtain a linear calibration model. From the plot on the x-axis of the emission intensities of lines of different sensitivities of the analyte in the standard (with a matrix similar to that of the analyzed samples and with known analyte concentration, $C_{standard}$) and on the y-axis the intensities of the emission lines of the analyte in the sample with unknown concentration, a linear calibration model is obtained. From the slope of this model it is possible to calculate the concentration of the analyte, $C_{analyte}$ in the sample ($C_{analyte}$ = slope x $C_{standard}$).[102]

The limitations of the strategy are related to the difficulty of choosing a standard with appropriate concentration, which can compromise determinations with satisfactory accuracy, if the samples show great variability of analyte concentration; and choice of emission lines with low sensitivity (more susceptible to spectral interference).[103,104] However, OP MLC was the calibration strategy used to determine Cr, Mn, Ni and Ti in low-alloy steel samples,[102] Ca, K and Mg in cocoa beans,[103] and direct determination of Al and Pb in waste printed circuit board (PCB).[104]

Single-sample calibration - SSC proposed by YUAN et al. (2019)[105] is a strategy based on a simple correlation between emission intensities of the analyte and other elements present in the analyzed plasma of the unknown concentration sample, with the concentrations of the analyte and other elements and their respective emission intensities obtained in the analysis of single calibration standard. Based on the Lomakin-Scherbe formula, it is possible to use this correlation from parameters obtained from only one calibration standard, with a matrix similar to that of the samples, for matrix-matching and direct determination of the analyte by LIBS.[104,105]

Some limitations of SSC are related to the use of emission lines with spectral interference, so they must be chosen very carefully to overcome this limitation; and samples and standard with significant variability in physical

and chemical properties, which can compromise the accuracy of the determinations.[103,104] However using SSC, analytes in samples of brass, steel, nickel-based alloy,[105] cocoa beans[103] and waste PCB [104] were determined.

Slope ratio calibration - SRC proposed by NUNES et al. (2019)[106] and posteriorly the Two-point calibration transfer - TP CT proposed by CASTRO et al. (2019)[25] are strategies based on the increase of the ablated mass with the number of accumulated laser pulses on a single solid calibration standard. However, in TP CT, only two sets of accumulated pulses are needed to obtain a linear calibration model, simplifying and facilitating the treatment of the data, while in SRC five sets of accumulated pulses are used.

The emission intensity is directly proportional to the analyte amount in the ablated sample mass, which, in turn, is proportional to the number of laser pulses.[106] Thus, two linear models are obtained for SRC and TP CT. The plot in the x-axis of the number of accumulated spectra, and in the y-axis the intensity obtained by the sum of the intensity (monitored by the analyte in each set of accumulated spectra) obtained for the sample and single standard calibration (with known analyte concentration, $C_{standard}$ and matrix similar to the sample). From these models, two slopes are calculated (referring to the model obtained for the sample and the other for the standard) and used in the calculation of the analyte concentration in the sample ($C_{analyte} = (slope_{sample} / slope_{standard}) \times C_{standard}$) by LIBS.[25,106]

The main advantages of these strategies are that they require a single solid calibration standard and correct matrix effects. However, the difficulty of choosing a standard with appropriate concentration of the analyte is a limitation of these strategies, because the concentration of the standard used in the calculation can under or over-estimates the concentration of the analyte in the sample.

SRC was used in the analysis of plant material in order to determine macro and micronutrients.[106] The TP CT was used in the direct determination of B, Fe, Dy, Gd, Nd, Pr, Sm and Tb in hard disk magnets,[25] Al and Pb in waste PCB,[104] and Ca, K and Mg in cocoa beans.[103]

Multi-energy calibration - MEC proposed by VIRGILIO et al. (2017)[107] was evaluated for the spectrometric techniques inductively coupled plasma optical emission spectrometry (ICP OES), high-resolution continuum

source flame atomic absorption spectrometry (HR-CS FAAS) and microwave-induced plasma optical emission spectrometry (MIP OES); and BABOS et al. (2019),[14] proposed MEC for direct solid analysis by LIBS.

The MEC is an efficient matrix compatibility strategy that uses only two solid calibration standards prepared for each sample and many analyte emission lines (of different sensitivities) to obtain a linear calibration model. As the two standards are prepared using the sample itself, strong matrix effects are corrected and provide results with satisfactory accuracy.[14]

The first standard is a pellet that contains an i) portion of sample and another portion of diluent (blank) that can be a salt, oxide, binder or a sample that does not contain analytes, for example. And the second standard is a pellet that contains a ii) portion of sample and a standard containing the analytes which can be CRM, salts or sample with reference values of the analytes; and it is mandatory that the two standards (i and ii) have the same proportion, sample: blank and sample: standard.[13,14]

By plotting the emission intensities of the analyte obtained on the analysis of the second standard on the x-axis (sample: standard) and on the y-axis the emission intensities obtained for the first standard (sample: blank), it is possible to calculate the slope of this linear model. As the concentration of the standard added to the sample is known, and using the slope calculated for the linear model it is possible to determine the concentration of the analyte in the sample ($C_{analyte}$ = (slope x $C_{standard}$) / (1- slope)). [13,14,107]

The main advantages of MEC are related to the possibility of identifying emission lines with spectral interferences (an outlier is observed in the linear model), using only two solid calibration standards for each sample and efficient matrix-matching. The main limitations are the difficulty in choosing the appropriate blank and requiring efficient homogenization of the two standards, to ensure the precision of the measurements.[13,14,107]

MEC LIBS was used in the direct analysis of different matrices to determine different elements such as: Ca, Cu, Fe, Mn and Zn,[14] and Ca and P,[13] both in mineral supplements for cattle; Ca, K and Mg in dietary supplements,[108] Al, Fe and Ti in high-silicon-content samples,[109] In in liquid crystal display,[110] Ni and Cr in nickeliferous ores,[111] and B, Fe, Dy, Gd , Nd, Pr, Sm and Tb in hard disk magnets.[25]

One-point gravimetric standard addition - OP GSA, proposed by Babos et al. (2019),[13] like MEC, uses only two solid calibration standards for each sample to obtain the calibration curve: i) sample + diluent and ii) sample + standard. Differently conventional standard addition (SA) calibration, which employs around five solid calibration standards, OP GSA requires only one standard addition point. By extrapolating the analytical curve obtained, it is possible to determine the concentration of the analyte in the sample.[13]

The use of only one standard addition point by OP GSA has some advantages when compared to SA, because i) it needs a small amount of sample to prepare the standards and consequently there is ii) increased analytical frequency.[13] The F-test is performed in order to observe the significance of the calculated models and their linearity.[112] However, an efficient homogenization of the diluent or of the standard in the sample is required to obtain adequate precision of the measurements (low RSD value).[13,25]

OP GSA was the calibration strategy employed in the direct determination of Ca and P in mineral supplements for cattle,[13] and of base and some rare earth elements in hard disk magnets.[25]

External calibration - EC is very useful in the development of analytical methods using direct LIBS analysis. However, obtaining solid calibration standards is difficult to perform EC. Ideally, EC is a strategy that should be applied using calibration standards, where the sample matrix does not interfere with stoichiometric ablation and have a linear behavior of the emission signals of standards and samples, that is, there are no matrix effects. However, obtaining solid calibration standards without these requirements is difficult, and so most methods that use EC employ the matrix-matching calibration (MMC) method.[7,13]

Examples that demonstrate the difficulty of obtaining standards for EC and the need to use MMC, were reported by MILLAR et al. (2018),[113] for the determination of Cl in cement-bound materials by LIBS. In this study, the authors evaluate different compositions containing different Cl-salts, water-to-cement ratios and additives, for the process of preparing solid standards. The authors demonstrated that the use and preparation of calibration standards using Portland cement, a water to cement ratio of 0.5 and added NaCl in the mixing water, allows to obtain determinations with accuracy. In another study,

MARTINEZ & BAUDELET (2020),[114] prepared a solution of alginic acid and keratin, spiked with ZnO nanoparticles, which was cross-linked and dried to obtain a hard film, as calibration standards. Using these standards it was possible to determine Zn in human nail by LIBS using the normalization of the Zn line by C I 193.09 nm and matrix-matching; due to the similarities of the plasma and crater properties obtained for sample and standard.

Recently DUPONCHEL, et al. (2020),[115] proposed the calibration for LIBS using the Inverse regression. From sets of soils and glass samples, used as calibration standards, an inverse regression model (concentration = f (analyte emission signal), where f is function) was obtained, compared to the simple regression model (signal of analyte emission = f (concentration)); and used to determine Ca in soils and Na in glass.[115]

The authors demonstrated that, i) the predictive capacity of the models using inverse regression provided better statistical parameters when compared to simple regression (using specific experimental conditions); ii) that the lower the signal-to-noise ratio, the greater the differences between the regressions, and iii) advised the researchers to use the inverse regression when the number of calibration standards is small.[115]

The matrix-matching calibration - MMC, internal standardization - IS, standard addition - SA, partial-least squares - PLS, principal component regression - PCR, multiple linear regression - MLR, data fusion, have been detailed in section *2.1. Calibration strategies employing in direct solid analysis* and descriptions of the advantages and limitations of all these strategies can be obtained.

Chemometric tools are employed as multivariate calibration strategies and are reported in the scientific literature for LIBS.[10,12] The most used are PLS, PCR, MLR and artificial neural network - ANN.

The ANN is able to propose a calibration model based on nonlinear and complex relationships, especially when the nonlinear relationships between experimental data are unknown. Similar to the way the human brain recognizes, manages and learns patterns; in experimental data the artificial neural network can learn and recognize the relationships between the set of input data (dependent variables with a certain associated weight) and generate a response corresponding to the variable, that is, the output

parameter.[10,116,117] The ANN was used, for example, to determine Cu in soils,[116] and Al, Ca, Cu and Fe in soils with errors of prediction lower than 20%.[117]

Limitations of this strategy are associated with the need for training and expertise of the analyst, in addition to taking care not to over-adjust the model, attributing erroneous weights to the input data, for example, as they may compromise the figures of merit the method.[10]

Multivariate curve resolution alternating least-squares algorithm - MCR-ALS, as well as XANES, is also used in LIBS for quantitative and qualitative analysis. El HADDAD et al. (2019),[118] used MCR-ALS applied to the LIBS data allowed the identification, quantification and imaging of minerals on rock tiles, even in the presence of 10 mixed mineral phases. The method presented a mineral quantification root mean square error below 10% for the main minerals.

In another study, EL RAKWE et al. (2016),[119] explored the temporal and spectral dimensions of the LIBS spectra obtained from the analysis of metallic Al, using MCR-ALS and independent component analysis (ICA). Thus, the temporal evolution of the LIBS signal was measured between 0.2 and 15 µs after the laser pulse, to assess mainly the kinetics of ionic recombination and molecular formation (AlO) within the plasma.

The main advantage of MCR-ALS over other chemometric methods for multivariate calibration is that it requires relatively fewer calibration standards to obtain regression models. However, treatments require expertise from the analyst, and difficulties in determining the number of factors or components that cause the variability in the data set, can be observed.[118,119]

Machine learning regression is closely related to computational statistics, is the study of algorithms that improve automatically through experience. Machine learning algorithms build a mathematical model based on sample data, known as "training data", in order to make predictions or decisions without being explicitly programmed to do so.[120,121] Several machine learning algorithms are used in LIBS determinations, using the mentioned principles.

An interesting example is described by BOUCHER et al. (2015).[121] In this study, the authors evaluated and described nine machine learning regression methods for the determination of ten major elements in rocks by LIBS; the linear regression methods being: i) partial least squares- PLS-1

(single response model), ii) PLS-2 (multiple response model), iii) PCR, iv) least absolute shrinkage and selection operator (lasso) regression, v) elastic net, and vi) support vector regression with linear kernel (SVR-line), and nonlinear regression methods including vii) kernel PCR (kPCR), viii) SVR with second order polynomial kernel (SVR-poly) and ix) k-nearest neighbor (kNN) regression.

Random forest regression - RFR is an advanced algorithm of machine learning, proposed by by LEO BREIMAN in 2001,[122] that have been used for LIBS. A random forest is a classifier consisting of a collection of tree-structured classifiers ($h(\mathbf{x}, \theta_k)$, k=1,…) where the (θ_k) are independent identically distributed random vectors and each tree casts a unit vote for the most popular class at input **x**. It is based upon an ensemble of decision trees, from which the prediction of a continuous variable is proved as average of the predictions of all trees. Some advantages of this regression are the good tolerance for the noise, as well as avoid over-fitting of the regression however; it requires analyst expertise for its implementation.[122,123]

The RFR was used as multivariate calibration strategy in the direct determination of Cr, Cu, Ni, Mn and Si in steel by LIBS. In this study, the authors mention that the RFR model can eliminate the influence of nonlinear factors due to self-absorption in the plasma and provide a better predictive result.[123] And other applications as i) in the determination of nonmetals, P and S in steel samples using RFR,[124] and ii) Cu, Zn, Cr and Ni in oily sludge samples, using wavelet transform-random forest (WT-RF), were also observed in the scientific literature.[125]

The parallel factor analysis - PARAFAC was recently applied to LIBS data by CASTRO et al. (2020),[126] to characterize and assist in the determination of Al, Ag, Au and Cu in PCB. PARAFAC is a decomposition method applied for multi-way data (higher order data arranged in arrays). It can estimate the spectra and concentration profiles of the underlying chemical analytes if the data behave according to the model. The decomposition uses trilinear components, with each component consisting of one score and two loading vectors.[126,127]

For LIBS data, the authors evaluated the trilinear components: samples *versus* variables (emission lines) *versus* depths (laser pulses from 1 to

10). Using PARAFAC was possible i) to identify spectral interference in the Cu emission line, due to the presence of Ti, ii) using multi-way data was possible to create a map of the PCB colored by concentration, and visualize where the element is predominantly located in sample, and iii) use classification models for Au and Ag using PLS-DA after removal of the interferents.[126] Thus, PARAFAC and LIBS present a synergy and advantages that should be increasingly explored in the direct analysis of solids.

The multivariate calibration chemometric tools are very important and have significantly contributed to the development of analytical methods using the direct analysis of solids by LIBS, due to all the advantages described previously.

However, a question is valid: what is the best calibration strategy for LIBS? From the above, considering the advantages and limitations of each of the univariate and multivariate calibration strategies, I believe that the best calibration strategy to be employed will depend on trained human resources to identify and understand some phenomena resulting from the laser-sample interaction (mainly matrix effects), as well as the intrinsic characteristics of: i) each of the available calibration strategies, ii) the analytes; iii) the sample analyzed and that iv) provides results with satisfactory precision and accuracy.

It is an apparent trend for LIBS calibration to use few solid calibration standards and greater exploration of instrumental parameters, of the properties of laser-induced plasma, associated with chemometric treatments, in proposing new calibration strategies that can significantly contribute to the development of analytical methods of quantification using the direct solid analysis by LIBS.

3.1.1 Calibration strategies to overcome matrix effects in laser-induced breakdown spectroscopy: direct calcium and phosphorus determination in solid mineral supplements. Spectrochimica Acta Part B 155 (2019) 90-98.

Spectrochimica Acta Part B 155 (2019) 90–98

Contents lists available at ScienceDirect

Spectrochimica Acta Part B

journal homepage: www.elsevier.com/locate/sab

Calibration strategies to overcome matrix effects in laser-induced breakdown spectroscopy: Direct calcium and phosphorus determination in solid mineral supplements

Diego Victor Babos, Ariane Isis Barros, Joaquim Araújo Nóbrega, Edenir Rodrigues Pereira-Filho*

Group for Applied Instrumental Analysis, Department of Chemistry, Federal University of São Carlos, P.O. Box 676, São Carlos, SP 13560-270, Brazil

ARTICLE INFO

Keywords:
Matrix-matching calibration
Internal standardization
Multi-energy calibration
One-point standard addition calibration
Matrix effects

ABSTRACT

Several calibration strategies were evaluated for Ca and P determination in mineral supplements for cattle using direct solids analysis by laser-induced breakdown spectroscopy (LIBS). Matrix-matching calibration (MMC), internal standardization (IS), multi-energy calibration (MEC) and a new calibration strategy named one-point gravimetric standard addition (OP GSA) were evaluated in order to correct for matrix effects normally observed in measurements by LIBS. The MEC and OP GSA were the calibrations strategies that led to better recoveries for Ca (86–109% MEC and 72–117% OP GSA) and for P (80–108% MEC and 82–111% OP GSA). Applying both strategies only two calibration standards were used and the presence of the sample itself in the calibration standards contributes for correcting for matrix effects. For MEC several atomic emission wavelengths with different sensitivities were used to determine the analyte concentration in the sample and also to identify spectral interferences that showed up as outliers points in the calibration curve. However, for OP GSA, only one atomic emission wavelength is used to build the calibration curve, simplifying data handling when compared to the MEC method. A statistical evaluation using student's *t*-test showed that there is no significant difference at 95% confidence level between the value determined and the reference value (reference material or ICP OES data) when using MEC or OP GSA calibrations. Both MEC and OP GSA can be used for direct determination of Ca and P in mineral supplements for cattle allowing proper quality control in order to support the Brazilian Regulation Normative Instruction No. 12, 2004.

1. Introduction

Since 2010 laser-induced breakdown spectroscopy (LIBS) has been widely used for elemental analysis in analytical chemistry. Beyond the possibility of direct analysis of solid, liquid and gaseous samples, there are outstanding advantages, high as analytical frequency, low-cost analysis, simultaneous and multielementar capacity, possibility of in-situ and real time analysis [1–5]. However, calibration by LIBS is still a challenge. In the analysis by LIBS, a sample fraction is analyzed integrally, so the matrix can influence the atomic or ionic emission phenomena of the analyte and, consequently, the analytical signals. Moreover, differences among chemical and physical properties of samples and standards can cause deviations among emission lines intensities or peak areas and analytes concentrations, these effects are commonly named in the literature as matrix effects [6].

Usually matrix effects are more pronounced for complex samples, as mineral supplements for cattle feeding, which is composed of different amounts of mixtures of refractory oxides, carbonates, sulfates and phosphates [7]. The different forms of each analyte in the sample can affect chemical and physical processes in the generated plasma by LIBS [8,9]. Furthermore, mineral supplements can differ in their physical properties, such as water content, granulometry, homogeneity and others. These differences can affect the ablation process and hence the detection of the analytes [8].

To overcome these matrix effects and allow direct analysis of the sample by LIBS, with proper precision and accuracy, multivariate regression [10], machine learning [11] and univariate calibration strategies have been used as well as matrix-matching calibration (MMC) [12,13], internal standardization (IS) [14], standard additions (SA) [15] and, more recently, multi-energy calibration (MEC) [16].

In MMC method the calibration standards are matched with sample matrix, usually employing certified reference materials (CRMs), set of samples or by matching solid standards by adding the concomitants that are causing interferences. In some cases, the matching of the

* Corresponding author.
E-mail address: erpf@ufscar.br (E.R. Pereira-Filho).

https://doi.org/10.1016/j.sab.2019.03.010
Received 14 September 2018; Received in revised form 18 March 2019; Accepted 19 March 2019
Available online 21 March 2019
0584-8547/

sample and standards is not enough to avoid or to correct for matrix effects, for this reason MMC have been combined with internal standardization [17,18]. Morais et al. [13] used MMC combined with IS for Ca determination in biochar-based fertilizers by LIBS; the matrix matching was performed using eucalyptus biochar and the Na naturally present in the matrix was used as internal standard.

Other calibration strategy frequently used for correcting for matrix effects is the SA method. In this method the sample itself is used as calibration standard, hence matrix effects can be corrected. Usually the analyte is added to the sample in gradually increasing concentrations that are plotted in the x-axis and analytical signals (S) are plotted in the y-axis. A mathematical equation is used to calculate the analyte concentration in the unknown sample, considering the intercept (b), slope (m), the concentration of standard (C_S) as well as the volumes (V_S) of the standard and unknown sample (C_x), Eq. (1) [19].

$$C_x = \frac{bV_sC_S}{mV_x} \quad (1)$$

where b is the intercept and m is the slope of the calibration curve; V_s is the fixed unit volume of the standard; V_x is fixed unit volume of unknown sample; C_s is the standard concentration and C_x is the unknown sample concentration.

Christopher et al. [20] introduced the gravimetric approach to the SA considering masses instead of volumes and this strategy is more appropriated for direct solid analysis. Kelly et al. [21] reformulated the Eq. (1), considering the mass of the standard (m_S), unknown sample mass (m_x) and a diluent of mass m_D. In this new approach the x-axis was represented by Eq. (2) [21] and y- axis was represented by Eq. (3) [21] and C_x can be calculated by Eq. (4) [21].

$$x\ axis = \frac{m_SC_S + m_DC_D}{m_x} \quad (2)$$

$$y\ axis = \frac{m_x + m_S + m_D}{m_x}S \quad (3)$$

$$C_x = \frac{b}{m} \quad (4)$$

where C_D is the analyte concentration in the diluent. Usually, the diluent has high-purity and the term m_DC_D can be negligible in Eq. (2).

Barker et al. [22] used gravimetric standard addition (GSA) without using diluent for determination of sulfur in biodiesel by X-ray fluorescence adopting five successive additions in the calibration curve. Usually five points are used in the SA method, however when considering routine analysis of large batches of samples, the use of multipoint SA calibration compromises the analytical frequency, requiring a long time to prepare the calibration solid standards for each sample, and may be not feasible for routine analysis. An alternative to multipoint SA calibration is the use of one-point (OP) SA calibration. Compared to SA using multi-level additions, this alternative is low cost and compatible with high analytical throughput [23] since only two standards are used. One-point GSA calibration combined with IS was used by Gao et al. [24,25] for As and Sb determination by ICP-MS and a tailored mathematical equation was proposed to calculate the mass fraction of analytes. Despite the great advantages presented by OP GSA, there are no reports in the scientific literature about the use of this strategy as an alternative for solids analysis by LIBS.

Other alternative to compensate the mentioned drawbacks associated to multi-points SA calibration is the use of MEC. Similarly to OP SA calibration, MEC employs only two calibration standards for each sample. As originally proposed, solution 1 is composed of 50% w w^{-1} of sample and 50% w w^{-1} of a standard solution (C_S) containing the analytes; solution 2 is composed of 50% w w^{-1} of sample and 50% w w^{-1} of analytical blank solution [26]. Several signals are simultaneously or sequentially monitored for each analyte and the calibration curve is plotted using in the x-axis the instrumental response obtained in solution 1 in different wavelengths and in the y-axis the instrumental response obtained in solution 2 in different wavelengths. The analyte concentration, C_x, can be determined using Eq. (5) [26].

$$C_x = \frac{Slope.\ C_s}{1 - Slope} \quad (5)$$

Multi-energy calibration was proposed by Virgilio et al. [26] and it has been applied for metals determination in complex samples by different instrumental methods: inductively coupled plasma optical emission spectrometry (ICP OES) [26]; microwave induced plasma optical emission spectrometry (MIP OES) [26,27] and high resolution continuum source flame atomic absorption spectrometry (HR-CS FAAS) [26]. Recently, MEC was applied in LIBS to overcome matrix effects in direct analysis of mineral supplements for determination of Ca, Cu, Fe, Mn and Zn [16], dietary supplements analysis [28] and determination of Cr and Ni in ores [29].

Based on these former studies, MMC combined with IS, OP GSA and MEC were here evaluated to overcome matrix effects and allow direct determination of Ca and P in mineral supplements for cattle by LIBS. The LIBS technique presents great versatility to be applied for direct analysis of complex samples as mineral supplements for cattle. The determination of these elements in mineral supplements for cattle is important to ensure the quality control of the product, due to its direct relation with animal bone composition [7].

2. Experimental

2.1. Instrumentation

LIBS spectra were obtained using J200 LIBS system (Applied Spectra, Fremont, CA, USA), which consists of a nanosecond Nd:YAG laser at 1064 nm with a single pulse duration of 8 ns at a frequency of 5 Hz. The maximum laser pulse energy was 100 mJ, the delay time ranged from 0 to 2 μs, spot size ranged from 50 to 250 μm and the signal acquisition time was fixed at 1.05 ms. The operating parameters of this instrument were controlled by the Axiom 2.5 software using an automated XYZ stage and a 1280 × 1024 complementary metal-oxide semiconductor (CMOS) color camera imaging system. The following complementary laser settings were adopted: scan length = 10 mm, laser repetition rate = 5.0 Hz, and speed = 1.0 mm/s.

Plasma emission was collected and focused into an optical fiber bundle coupled with six-channel CCD spectrometer covering emission lines from 186 to 1042 nm. The spectral resolution (ability to separate different wavelengths) was < 0.1 nm for the ultraviolet to visible (VIS) region, and < 0.12 nm for the VIS to near-infrared (NIR) region. The most sensitive atomic (I) and ionic (II) emission lines for P and Ca, respectively, were monitored and chosen according to the Aurora software (Applied Spectra) in combination with information from the National Institute of Standards and Technology (NIST) [30]. The masses of samples and standards were accurately weighed using an analytical balance (model AY 220, Shimadzu, Kyoto, Japan). Later samples and calibration standards were pelletized using a hydraulic press (SSP-10A, Shimadzu Scientific Instruments, Columbia, USA) before analysis by LIBS.

2.2. Reagents and samples

Sodium carbonate (99.9%, Merck, Darmstadt, Germany) was used as blank or diluent, and $CaHPO_4$ (≥ 98.0%, Tennant, São Paulo, SP, Brazil) was used as solid standard to prepare the pelletized calibration mixtures used in MEC-LIBS and OP GSA LIBS determinations.

The accuracy of the methods were evaluated by analyzing the following cattle mineral supplement reference materials (RM): RM 17–03, RM 17–06, RM 17–09, RM 18–03, RM 18–06, RM 18–09 and RM SM 03–10 provided by the Empresa Brasileira de Pesquisa Agropecuária (Brazilian Agricultural Research Corporation). Student's *t*-test at 95% confidence level was adopted for data comparison.

Table 1
Matrix of experiments (based on a factorial design Box-Behnken modified) showing the variables evaluated for optimizing fluence, delay time and diluent proportion in LIBS determinations.

Experiment	Fluence (J cm^{-2})		Delay time (μs)		Diluent (%)	
	Real	Coded	Real	Coded	Real	Coded
1	1.4	–1	0.3	–1	50	0
2	3.8	1	0.3	–1	50	0
3	1.4	–1	1.8	1	50	0
4	3.8	1	1.8	1	50	0
5	1.4	–1	1	0	10	–1
6	3.8	1	1	0	10	–1
7	1.4	–1	1	0	90	1
8	3.8	1	1	0	90	1
9	2.7	0.05	0.3	-1	10	–1
10	2.7	0.05	1.8	1	10	–1
11	2.7	0.05	0.3	-1	90	1
12	2.7	0.05	1.8	1	90	1
13	2.7	0.05	1	0	50	0
14	2.7	0.05	1	0	50	0
15	2.7	0.05	1	0	50	0
16	1.4	–1	0.3	-1	10	–1
17	3.8	1	1.8	1	90	1
18	2.3	−0.31	1	0	50	0
19	1.3	−1.15	1	0	50	0
20	4.1	1.2	1	0	50	0
21*	2.7	0.05	1	0	10	−1

* Optimal condition.

Four samples of cattle mineral supplements purchased in local markets of Rio Paranaíba (Minas Gerais State, Brazil) and São Carlos (São Paulo State, Brazil) were analyzed employing all calibrations strategies. Reference values for Ca and P were obtained using ICP OES reference method developed by Babos et al. [7]. All cattle mineral supplements are composed of macro- and microminerals (e.g., Ca, P, S, Co, Se, among others), as well as < 42% protein equivalent.

2.3. Optimization of instrumental conditions

LIBS instrumental parameters were evaluated using a Box-Behnken modified factorial design with a central point. The variables evaluated were as follows: fluence at 6 levels (1.3, 1.4, 2.3, 2.7, 3.8 and 4.1 J·cm^{-2}), delay time at 3 levels (0.3, 1.05 and 1.8 μs) and diluent proportion at 3 levels (10, 50 and 90%). The variables levels were coded between −1.15 (lower level) and +1.2 (higher level), with the central point (0) used to calculate experimental errors (Table 1). The RM 18–03 mineral supplement for cattle containing 204 ± 19 g kg^{-1} Ca and 94.8 ± 5 g kg^{-1} P was used to optimize instrumental conditions used in LIBS analyses.

Three pellets were prepared following the conditions:

Pellet 1: 10% w w^{-1} of diluent, i.e. 450 mg RM 18–03 + 50 mg Na_2CO_3;

Pellet 2: 50% w w^{-1} of diluent, i.e. 250 mg RM 18–03 + 250 mg Na_2CO_3 and.

Pellet 3: 90% w w^{-1} of diluent, i.e. 50 mg RM 18–03 + 450 mg Na_2CO_3.

These mixtures were pressed for 2 min under 80 kN to form pellets with a 12 mm diameter and ca. 3 mm thickness. For each pellet (n = 3), 210 spectra were obtained at different parts of the sample surface. Thus, 630 spectra were obtained for each sample. Adopting this approach, a representative analysis was obtained.

The signal-to-background ratio (SBR) calculated for each line of Ca and P monitored were used as responses of the factorial design. A mathematical approach developed by Derringer and Suich [31], which is based on desirability functions applied to optimize multi-response experiments, was used in this study. This strategy first converts each response into an individual desirability value (d_i) ranging between $0 \leq d_i \leq 1$. In this case, $d_i = 1$ corresponds to a desired response (high SBR), while $d_i = 0$ represents a response that is outside the acceptable region (the lowest SBR).

2.4. Data collection and evaluation

Matlab software version 2017b (Matworks, Natick, MA, USA) and two labmade routines were used for preliminary data inspection. The first routine, libs_treat, was applied to detect eventual outlier spectra. In this case, the standard deviation, area, maximum and Euclidean norm were calculated for each sample (rows in the data matrix). If an outlier was detected (e.g., standard deviation equal to 0), the respective spectrum was removed, and 12 normalization modes were carried out [3,32,33].

These normalizations were tested to compensate for signal variations (area or height) and sample matrix differences during data acquisition. For each pellet, around 210 spectra were acquired for obtain a representative analysis, and 12 normalization strategies were calculated and codified as:

Norm 1 and Norm 5: average and sum of the spectra, respectively;

Norm 2 and Norm 6: each individual spectrum is divided by its Euclidean norm. After this, the average (2) or sum (6) is calculated;

Norm 3 and Norm 7: each individual spectrum is divided by its area (sum of all signal intensity). After this, the average (3) or sum (7) is calculated;

Norm 4 and Norm 8: each individual spectrum is divided by its maximum intensity value. After this, the average (4) or sum (8) is calculated;

Norm 9 and Norm 10: each individual spectrum is divided by the intensity of the C I 193.09 nm emission line (Normalization by internal standard). After this, the average (9) or sum (10) is calculated; and.

Norm 11 and Norm 12: each individual spectrum is divided by the intensity of the C I 247.85 nm emission line. After this, the average (11) or sum (12) is calculated.

No outliers were detected in all experimental measurements. The second routine, *libs_par*, was applied after normalization using *libs_treat*. It calculates the SBR as well as both the signal area and height for a specified emission line. In order to effectively use *libs_par*, it is necessary to establish the emission line intervals that contain background and analytical signals.

2.5. Calibration strategies

2.5.1. Matrix-matching calibration (MMC1) – use of a set of samples and reference materials

Using MMC, a calibration strategy using a set of six samples was tested. These samples were: MS 4 and reference materials (RM) RM 17–06, RM 18–03, RM 18–06, RM 18–09 and RM SM 03–10. The concentration of the standards used for MMC ranged from 153 (RM 17–06) to 291 g kg^{-1} (MS 4) Ca and from 29 (RM 17–09) to173 g kg^{-1} (MS 4) P. Approximately 500 mg of samples were weighed and then pressed for LIBS analysis. For Ca, the ionic emission line monitored was at 396.85 nm, and for P at 214.91 nm. Carbon atomic lines (C I 193.09 nm and C I 247.86 nm) were evaluated as internal standards.

2.5.2. Matrix-matching calibration (MMC2) – reference material diluted in Na_2CO_3

For MMC2, the reference material 18–03 of mineral supplement for cattle (204 g kg^{-1} Ca and 94.8 g kg^{-1} P) was diluted in Na_2CO_3 to obtain six solid calibration standards in the concentration range from 0 to 204 g kg^{-1} Ca and from 0 to 94.8 g kg^{-1} P. Solid standards (n = 3) with approximately 500 mg were pelletized (2 min under 80 kN) for LIBS analysis. Calcium II 396.85 nm and P I 214.91 nm were also monitored. Carbon atomic emission lines 193.09 and 247.86 nm were evaluated as internal standards.

2.5.3. Multi-energy calibration (MEC)

The MEC method requires only two calibration standards for each sample. The standard 1 (sample + blank) was composed of 400 mg of the mineral supplement sample and 100 mg of Na_2CO_3. Sodium carbonate was used as blank (diluent). The standard 2 (sample + standard) was composed of 400 mg of mineral supplement sample and 100 mg $CaHPO_4$, obtaining the concentration of 58.9 g kg^{-1} Ca and 45.4 g kg^{-1} P added to standard 2. All standards were made in triplicate ($n = 3$).

The standards were homogenized using mortar and pestle, and then pressed for LIBS analysis. To generate the linear models and calculate the angular coefficients, five lines for Ca (II 315.89, II 317.93, II 376.69, II 393.37, and II 396.85 nm) and four lines for P (I 213.62, I 214.91, I 215.34 and I 253.39 nm) were monitored.

2.5.4. One-point gravimetric standard addition – OP GSA

The OP GSA method requires also only two calibration standards (sample + blank and sample + standard). The preparation of the standards in OP GSA is the same as that used for the analysis for the MEC method (see Section *2.5.3 Multi-energy calibration – MEC*). Linear models were built using the following lines: Ca II 396.85 nm and P I 213.62 nm.

2.6. Determination of parameters of analytical performance

The main parameters of analytical performance (accuracy, linear correlation coefficient, standard error, and precision) were calculated for all calibration strategies evaluated.

Accuracy was evaluated based on the standard error (SE), according to Eq. (6):

$$SE = \sqrt{\frac{\sum_i^n (y_i - \hat{y})^2}{n - 1}} \quad (6)$$

where y_i is the analyte reference concentration (from the reported RM value, or found using ICP OES), $\hat{y}$ is the concentration determined by calibration strategy, and n is the number of samples ($n = 11$).

Recovery (%) was calculated from Eq. (7):

$$Recovery = \frac{j.\ 100\%}{j_{ref}} \quad (7)$$

where j is the concentration determined by the method described in this study (LIBS), and j_{ref} is the reference concentration of the analyte obtained by ICP OES or from the reported RM value.

3. Results and discussion

3.1. LIBS instrumental conditions

Several phenomena occurred when the laser pulse energy reaches the sample surface due to the interaction of electromagnetic radiation with matter. The laser-sample interaction is extremely dependent on the sample matrix, analyte homogeneity, and sample surface. In addition, the formation of the microplasma can be affected by the laser operating conditions (i.e., laser pulse energy, fluence and duration), and radiation emission characteristic of the species present in this plasma (ions and molecules) can be influenced by instrumental parameters, such as delay time, gate width, amplification detector gain, and emission line selection [34].

In this context, LIBS instrumental parameters were optimized to obtain high signal-to-background ratio for all emission lines monitored. In addition to the instrumental parameters, the amount of diluent added was also evaluated, since for both MEC and OP GSA methods the sample is diluted (i- sample + blank and ii- sample-standard). Therefore, we evaluated how the dilution of the sample could influence the analytical signals obtained by LIBS.

In each experiment, the individual desirability value was calculated as a function of the SBR using signal areas and heights (twelve signal normalizations) for Ca and P. In this case, each response was coded from 0 (undesired response, i.e., the lowest SBR, using area and height) to 1 (desired response, i.e., the highest SBR, using area and height). Therefore, the individual desirability value was combined into a single response after arithmetic mean calculation (the overall desirability, OD).

The model calculated for OD after monitoring Ca and P emission lines, with significant coefficients and their confidence interval at a confidence level of 95% was:

$$\text{Desirability} = 0.73 \pm 0.10 – 0.15 \pm 0.07\ \text{Dil}$$

where Dil is diluent (%). Coefficient b0 was equal to 0.73 and its confidence interval was 0.10 (this is a valid coefficient with the 95% confidence level). The model presented only two significant coefficients, b0 and b3 (diluent (%)). The highest OD value was found for experiment 21, with OD of 0.71 and OD estimated of 0.88, for both the normalizations i- by individual area and average and ii- by individual area and sum.

Fig. 1 shows the response surface plot for the proposed model. It is observed that high OD values are obtained when the lowest amount of diluent (10%) (marked with arrow) is used, because the lower the sample dilution, the higher the signal-to-background ratio for all emission lines monitored for Ca and P, which is a requirement in multielementar analysis by LIBS and when using the MEC. The fluence and delay time were not significant factors in the OD since it was observed that, in the fluence interval evaluated, the OD was constant. Thus, for all measurements performed in this study, a fluence of 2.7 J cm^{-2} (related to a 53 mJ laser pulse energy and a 50 μm laser spot size, that corresponds to an intermediary condition), a delay time of 1.0 μs (central point) and pellets containing 20% w w^{-1} diluent (400 mg sample + 100 mg Na_2CO_3 or 100 mg $CaHPO_4$), conditions marked with a star at Fig. 1.

3.2. Calibration strategies for LIBS

The main difficulty associated with direct solid analysis is caused by matrix effects, since all constituents of the sample are present in the analysis. There are many strategies to overcome this effect. Thus, different calibration strategies were applied here to get rid of these effects and to guarantee accurate and precise results.

For the matrix-matching calibration, standards were matched using a set of samples and RMs of mineral supplements for cattle (MMC1) and using the dilution of reference material of the mineral supplement in high purity Na_2CO_3, the major constituent of the sample (MMC2). The choice of the monitored emission line for Ca, P and C (used as internal standard) was made considering the least prediction error in the determinations of the analytes. Matrix effects were evaluated by recoveries obtained using different strategies and results are shown in Tables 2 (Ca) and 3 (P). Recoveries from 46 to 163% for Ca and from 26 to 127% for P were obtained using MMC1, and for Ca from 77 to 198% and from 43 to 310% for P MMC 2, both without internal standardization. These recoveries were clearly outside the acceptable range (80–120%), showing that matrix effects are compromising the results. Even when using MMC, standards may contain different characteristics when compared to the sample, such as particle size and homogeneity, and these differences may cause matrix effects.

Other calibration strategy evaluated was the combination of matrix-matching and internal standardization (IS) using C as internal standard. Carbon was adopted as IS because it is the major constituent of the sample. Best recoveries were observed when using MMC and IS. For Ca, recoveries ranged from 84 to 114% using MMC1 with IS, except for RM 17–09 (48%), and from 78 to 105% using MMC2 with IS, except for RM 18–06 (127%) and RM SM 03–10 (53%). For P, recoveries ranged from 77 to 123% using MMC1 with IS, except for the sample RM 18–06

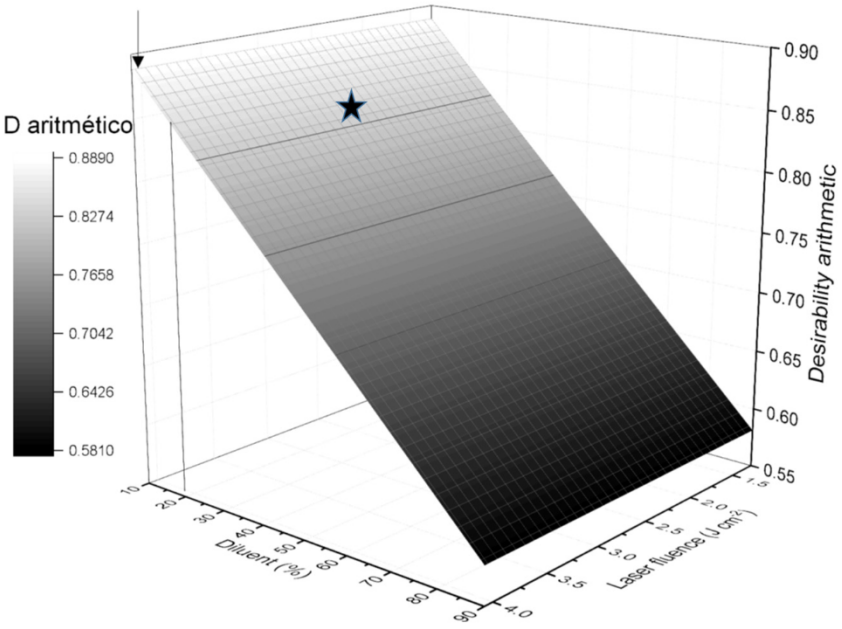

Fig. 1. Response surface plot of desirability arithmetic: diluent (%) versus laser fluence (J cm^{-2}). The star represents the selected working conditions.

(195%) and from 71 to 128% using MMC2 with IS, except for RM 17–03 (56%), RM 17–09 (21%), RM 18–03 (207%), and RM 18–06 (203%) (Tables 2 and 3).

The matrix-matching calibration combined with internal standardization is another calibration alternative for minimizing matrix effects, signal bias due to fluctuations in instrumental operational conditions, and sampling errors [13]. Some limitations of the use of IS for LIBS are (I) the choice of the IS appropriated to each analyte, (II) the incorporation of the IS in the sample in some cases, (III) similarities among physical-chemical properties of analyte and IS, and (IV) require constant concentration of IS in the samples. If these requirements are reached, the correction of matrix effects originated from laser-sample interaction is effective [13,15]. The use of IS combined with both MMCs led to better results for Ca and P when only matrix-matching was used as a calibration strategy. Although $CaCO_3$ is one of the major constituents of the mineral supplements, the formulations may have different concentrations of this salt. We suppose that the IS was not efficient for all determinations because carbon contents were not constant in all mineral supplement samples, and the C ionization and excitation energies (11.3 eV and 7.7 eV, respectively) is not similar to analytes (Ca – 6.1 eV and 3.1 eV; and P – 10.5 eV and 7.1 eV) [35] thus justifying the recoveries values outside the required range for some samples.

Thereby the alternative is the use of the sample itself as calibration standard for correcting for matrix effects, mainly when working with complex samples. The standard additions method has been used with this proposal, however the drawbacks associated with this method is the need of build an analytical curve with 5 or more addition points for each sample. One strategy to get rid of these drawbacks is the use of one-point gravimetric standard addition calibration or the use of multi-energy calibration, since in both methods only two points are used for the calibration curve and linear model, respectively.

The important parameters to be evaluated when only two calibration points are used is the concentration of the addition point, whether small or large amount of the standard is added compared to the analyte concentration present in the sample, the experimental error can be too large or the calibration method become useless [23]. Furthermore,

Table 2
Concentrations (mean ± standard deviation, g kg^{-1} Ca, $n = 3$) and recoveries (%) for Ca in samples of mineral supplements and reference materials determined by LIBS using MMC, MMC with Internal Standardization, MEC and OP GSA calibrations.

Samples	Reference value	MMC 1		MMC 2		MEC	OP GSA
	g kg^{-1} Ca	Without IS	With IS	Without IS	With IS		
MS 1	187 ± 5	189 ± 19 (101)	198 ± 23 (106)	280 ± 28 (150)	193 ± 21 (103)	160 ± 42 (86)	169 ± 30 (90)
MS 2	293 ± 23	476 ± 3 (163)	247 ± 23 (84)	346 ± 8 (118)	245 ± 12 (84)	267 ± 14 (91)	269 ± 41 (92)
MS 3	204 ± 6	94 ± 7 (46)	233 ± 17 (114)	157 ± 11 (77)	201 ± 10 (98)	192 ± 35 (94)	195 ± 24 (96)
MS 4	291 ± 2	–	–	310 ± 3 (106)	228 ± 4 (78)	283 ± 10 (97)	209 ± 82 (72)
RM 17–03	171 ± 11	235 ± 22 (137)	149 ± 11 (87)	339 ± 36 (198)	150 ± 9 (88)	186 ± 5 (109)	135 ± 46 (79)
RM 17–06	153 ± 6	–	–	255 ± 12 (167)	132 ± 5 (86)	163 ± 31 (107)	176 ± 35 (115)
RM 17–09	220 ± 6	224 ± 5 (102)	106 ± 12 (48)	336 ± 9 (166)	91 ± 9 (41)	194 ± 39 (88)	180 ± 27 (82)
RM 18–03	204 ± 19	–	–	292 ± 12 (143)	208 ± 27 (102)	199 ± 32 (98)	239 ± 43 (117)
RM 18–06	167 ± 14	–	–	264 ± 26 (158)	213 ± 32 (127)	167 ± 28 (100)	163 ± 33 (98)
RM 18–09	165 ± 19	–	–	244 ± 7 (148)	173 ± 14 (105)	165 ± 24 (86)	172 ± 26 (104)
RM SM 03–10	187 ± 36	–	–	248 ± 16 (133)	100 ± 4 (53)	167 ± 9 (89)	193 ± 6 (103)

MMC 1: Matrix-matching calibration using set sample and reference materials as calibration standards.
MMC 2: Matrix-matching calibration using reference material 18–03 diluted in Na_2CO_3 as calibration standards.
MEC: Multi-energy calibration.
OP GSA: One-point gravimetric standard addition.
-: sample or reference material (RM) used as calibration standards in MMC 1.

Table 3
Concentrations (mean ± standard deviation, g kg^{-1} P, n = 3) and recoveries (%) for P in samples of mineral supplements and reference materials determined by LIBS using MMC, MMC with Internal Standardization, MEC and OP GSA calibrations.

Samples	Reference value	MMC 1		MMC 2		MEC	OP GSA
	g kg^{-1} P	Without IS	With IS	Without IS	With IS		
MS 1	104 ± 4	115 ± 5 (111)	128 ± 9 (123)	166 ± 1 (159)	133 ± 6 (128)	92 ± 15 (89)	94 ± 8 (91)
MS 2	173 ± 6	220 ± 2 (127)	159 ± 2 (95)	215 ± 5 (124)	128 ± 2 (74)	187 ± 9 (108)	177 ± 29 (102)
MS 3	70 ± 3	18 ± 1 (26)	54 ± 7 (78)	30 ± 2 (43)	57 ± 10 (81)	62 ± 2 (88)	76 ± 3 (109)
MS 4	173 ± 6	–	–	215 ± 3 (125)	96 ± 21 (55)	168 ± 5 (97)	166 ± 2 (97)
RM 17–03	86 ± 5	80 ± 4 (93)	66 ± 9 (77)	128 ± 15 (149)	49 ± 3 (56)	87 ± 10 (102)	70 ± 9 (82)
RM 17–06	47 ± 1.2	–	–	78 ± 10 (165)	46 ± 4 (98)	47 ± 6 (101)	41 ± 5 (87)
RM 17–09	29 ± 1	–	–	16 ± 2 (54)	6 ± 4 (21)	26 ± 1.5 (90)	27 ± 1 (93)
RM 18–03	94.8 ± 5	–	–	166 ± 10 (175)	196 ± 38 (207)	76 ± 9 (80)	97 ± 9 (102)
RM 18–06	89 ± 5	90 ± 7 (101)	174 ± 13 (195)	276 ± 25 (310)	181 ± 18 (203)	83 ± 8 (94)	89 ± 8 (100)
RM 18–09	83 ± 5.4	–	–	139 ± 10 (168)	91 ± 4 (109)	77 ± 7 (93)	98 ± 5 (111)
RM SM 03–10	83 ± 1.7	–	–	138 ± 3 (163)	60 ± 1 (71)	90 ± 19 (107)	99 ± 13 (111)

MMC 1: Matrix-matching calibration using set sample and reference materials as calibration standards.
MMC 2: Matrix-matching calibration using reference material 18–03 diluted in Na_2CO_3 as calibration standards.
MEC: Multi-energy calibration.
OP GSA: One-point gravimetric standard addition calibration.
-: sample or reference material (RM) used as calibration standards in MMC 1.

precision may be compromised when small amounts of solid standards (salts) are added to the sample in a poorly homogenized mixture, since in measurements using LIBS typically sample masses around μg are analyzed. On the other hand, high concentrations of standard may lead to detector saturation and consequent loss of linear range. Thus, concentration standard was optimized to improve the trueness and accuracy of MEC and OP GSA determinations.

Four concentrations of the addition point for Ca (25, 38, 50 and 59 g kg^{-1} Ca) and P (19, 29, 39 and 45 g kg^{-1} P) were used for the reference material 18–03 when evaluating the applicability of MEC and OP GSA methods. For both methods, concentrations of 59 g kg^{-1} Ca and 45 g kg^{-1} P (100 mg $CaHPO_4$) led to the best recoveries (87% Ca and 107% P using MEC, and 103% Ca and 85% P using OP GSA). Thus, these concentrations were used in the addition point for MEC and OP GSA for the other samples.

MEC is an interesting calibration strategy for LIBS, since it is possible to monitor simultaneously several lines and bands of atomic and molecular emission of an analyte with different sensitivities. In MEC LIBS, both solid calibration standards are prepared using the same amount of sample, which contributes to correct for matrix effects.

The main advantage of the MEC is the possibility of interference detection by the observation of the outlier in the linear model calibration. Fig. 2a shows an example containing the signals for the 3 emission lines selected for P: I 213.62, I 214.91, and I 215.34 nm. Our first attempt was to calculate a calibration model with 4 P emission lines including P I 253.39 nm. In the linear model using 4 emission lines for P, it was observed one outlier (Fig. 2b). Using NIST data base [30] was observed that probably the outlier was related to the Fe interference at 253.41 nm in the P line at 253.39 nm. This hypothesis was confirmed by generating a LIBS spectra using Fe_2O_3 at 99.99% purity (Merck, Darmstadt, Germany) pelletized as the sample. As shown in Fig. 3, there is an interference caused by Fe in the P line at 253.39 nm, so this outlier was removed of the linear model and the Pearson correlation coefficient (R^2) obtained by P was 0.9991 (Fig. 2c). There was none observed outliers in the linear model for Ca and R^2 was 0.9984 (Fig. 2b). Recoveries in the acceptable range were obtained by MEC, i.e. for Ca ranged 86 (sample MS 1) from 109% (sample RM 17–03) and for P ranged 80 (sample RM 18–03) from 108% (sample MS 2), Tables 2 and 3.

The OP GSA is another interesting calibration strategy for correcting for matrix interferences in LIBS. Similarly to MEC, OP GSA combines the effectiveness of a matrix-matching procedure with the simplicity of using only two calibration standards *per* sample, but monitoring only one emission line for each analyte.

The calibration curve by OP GSA (Figs. 2d and 4b) were built using Eq. (2) in the x-axis and Eq. (3) in the y-axis and Ca and P concentrations were obtained by extrapolation method (Eq. (4)). Several studies have shown that if the instrumental method is linear, the extrapolation using only one addition point can be obtained with the same or higher precision than using multipoint additions [36]. The linearity was tested applying the test F, and in this case the ratio $F_{experimental}/F_{tabulated}$ was calculated considering the mean of square for regression (MSR) and residue (MSr). This ratio ≥ 10 demonstrated that the variances are statistically different: the MSR is statistically different when compared with the MSr, thus the model can be considered linear, and the one-point gravimetric standard addition can be used [37]. The ratios found for all samples analyzed for Ca ranged from 13 to 69 and for P from 28 to 1158, indicating that the models are linear and one-point calibration is feasible.

Recoveries in the acceptable range were obtained for Ca (72, MS4 to 117%, RM 18–03) and P (82, RM 17–03 to 111%, RM 18–03), Tables 2 and 3. The main advantage of this approach is its simplicity because only one addition point is used in the calibration curve for each sample and only one emission line is used for each analyte, hence the data treatment is easier than data treatment for MEC that uses several lines to construct the linear model. Furthermore, it is important to highlight that there is no report in the literature using OP GSA for LIBS.

The analytical performance of all calibration methods here evaluated, the normalization mode and signal type adopted (to compensate for signal variations and sample matrix differences during data acquisition), as well as emission lines monitored and used for calibrations are shown in Table 4. It is observed that the standard error values were lower for the determinations of Ca and P when using either MEC or OP GSA calibration, demonstrating good accuracies when these two calibration strategies were employed in LIBS. The relative standard deviation (RSD) values found for Ca and P determinations using all calibration strategies are in agreement with the values normally reported for determinations using LIBS [34], except for a sample when using

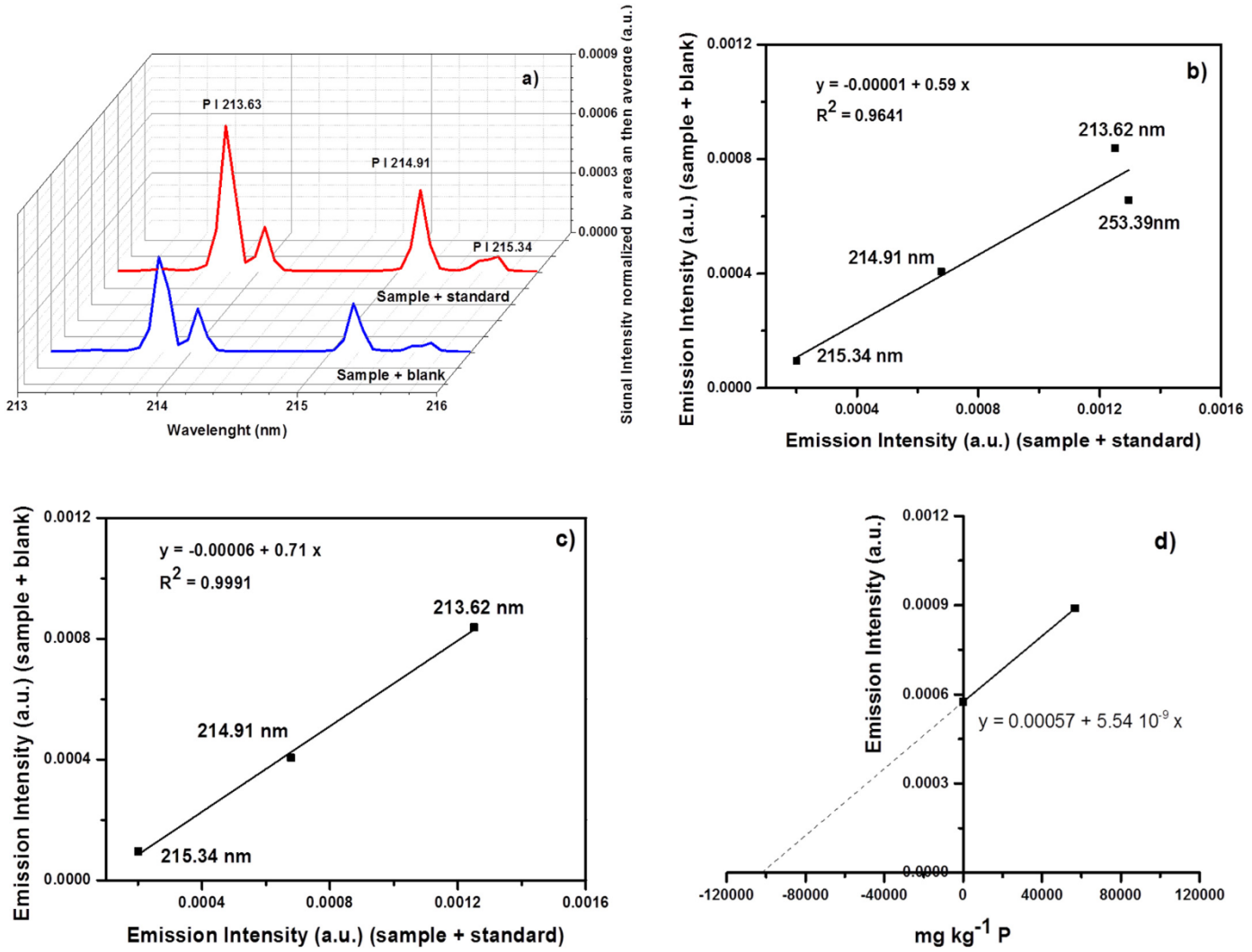

Fig. 2. LIBS spectra obtained for P with two calibration standards (a) used in multi-energy calibration – MEC with (b) and without (c) spectral interference, and one-point gravimetric standard addition – OP GSA (d) (λ = 213.63 nm).

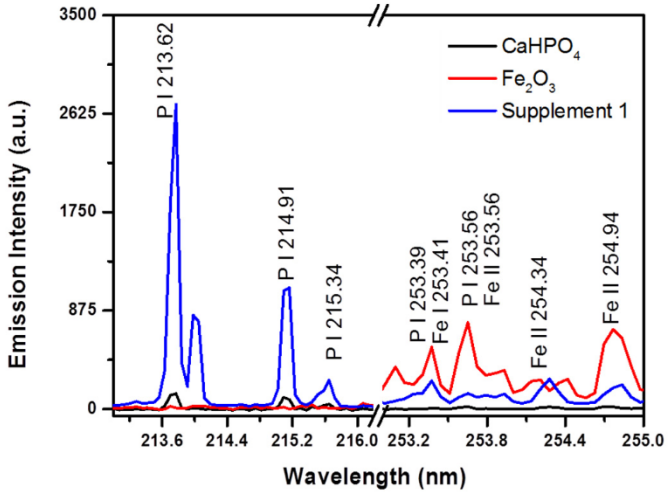

Fig. 3. Emission spectrum obtained by LIBS for the $CaHPO_4$, Fe_2O_3 salts and mineral supplement for cattle #1 sample. The spectral interference identified for P, as outlier by the MEC, is derived from Fe emission lines.

matrix-matching calibration with reference material 18–03 diluted in Na_2CO_3 without IS for P showed a 67% RSD. Furthermore, using MEC and OP GSA there were no significant difference between determined and reference values using student's *t*-test at 95% confidence level (Tables 2 and 3) for most RMs evaluated.

The Brazilian Normative Instruction No.12 of November 30, 2004, establishes the maximum levels of Ca:P ratio in the final mixture for bovine (Ca:P ratio 1:1 to 7:1) [7]. Only one sample (RM 17–09) did not present results within the specifications of the current legislation, because in its final formulation the concentration of P and Ca was 29 ± 1 g kg^{-1} and 220 ± 6 g kg^{-1}, respectively; and the ratio, 7.5 to Ca:1 to P. For the others samples evaluated the Ca:P ratio ranged from 1.6:1 to 3.2:1 in agreement with the specification of the current legislation.

4. Conclusions

The best operational conditions of LIBS were obtained using Box-Behnken modified factorial design with a central point. Several univariate calibration strategies were evaluated to overcome matrix effects in LIBS determination. Although the association of matrix-matching calibration and internal standardization allowed better recoveries in relation to matrix-matching calibration without internal standardization, for some samples or reference materials recoveries were outside

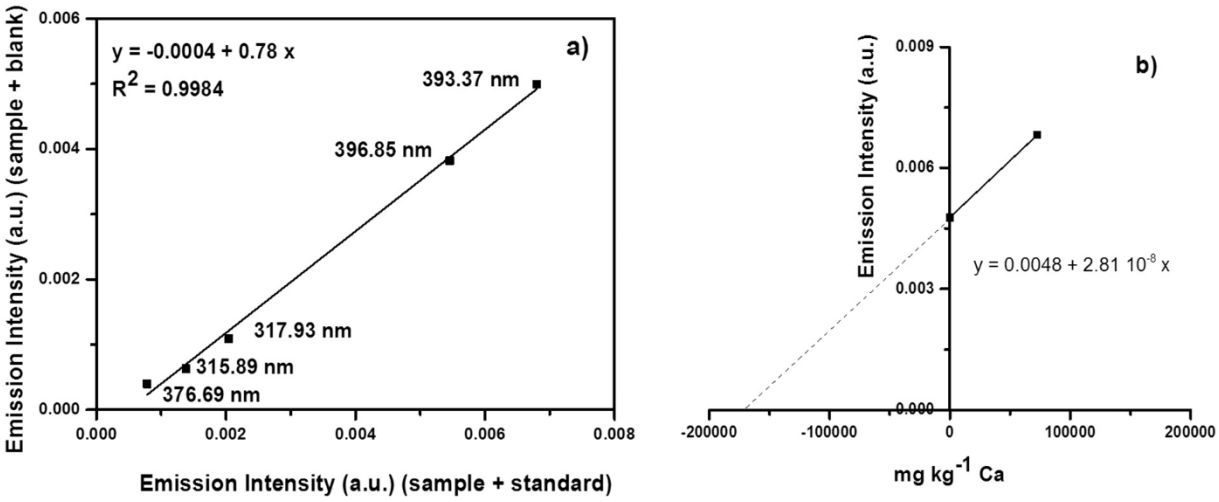

Fig. 4. Linear model for multi-energy calibration (a) and one-point gravimetric standard addition curve (b) (λ = 396.85 nm) for Ca in mineral supplement for cattle.

Table 4
Analytical performance parameters evaluated for the determination of Ca and P in cattle mineral supplements using matrix-matching calibration employing a set of samples and reference materials as calibration standards – MMC1, matrix-matching calibration using reference material 18–03 diluted in Na_2CO_3 as calibration standards – MMC2, multi-energy calibration – MEC and one-point gravimetric standard addition calibration – OP GSA.

Parameter	MMC 1		MMC 2		MEC		OP GSA
	With IS	Without IS	With IS	Without IS			
Emission analyte lines (nm)	Ca II 396.85 P I 214.91				Ca II 315.89 Ca II 317.93 Ca II 376.69 Ca II 393.37 Ca II 396.85	P I 213.62 P I 214.91 P I 215.34	Ca II 396.85 P I 213.62
Emission internal standard line (nm)	C I 193.09 (for Ca) C I 247.86 (for P)	–	C I 193.09 (for Ca and P)	–	–	–	–
Normalization selected*	Intensity IS and average for Ca and P	Area and average for Ca Maximum and average for P	Intensity IS and average for Ca and P	Area and sum for Ca and P	Area and average for Ca and P		Area and average for Ca and P
Signal type	Height for both analytes	Area for both analytes	Area for both analytes	Height for both analytes	Height for Ca	Area for P	Height for both analytes
Standard error ($g\,kg^{-1}$)	111	64	97	58	17		35
Ca	36	19	76	55	10		10
P							
RSD range (%)	1–10	7–12	1–11	2–15	4–26		3–39
Ca	1–8	1–14	1–13	2–67	3–21		1–16
P							

the acceptable range. It was demonstrated that the best calibration methods for Ca and P determinations in mineral supplements were MEC and OP GSA, these strategies were robust enough to correct for matrix effects and accurate Ca and P determinations were reached. On the one hand MEC stood out for its capability of detecting spectral interferences, for another OP GSA stood out for its straightforward data treatment. Both strategies can be used with accuracy and precision for direct determination of Ca and P in mineral supplement for cattle by LIBS, using only two standards calibration.

Acknowledgements

The authors are grateful to the Conselho Nacional de Desenvolvimento Científico e Tecnológico (CNPq – grants 141311/2017-7, 305637/2015-0) for fellowships and financial support and to the Coordenação de Aperfeiçoamento de Pessoal de Nível Superior (CAPES/PNPD – Graduate Program in Chemistry, Federal University of São Carlos). This study was financed in part by the Coordenação de Aperfeiçoamento de Pessoal de Nível Superior – Brasil (CAPES) – Finance Code 001. The authors are also grateful to São Paulo Research Foundation (FAPESP), grant number 2016/01513-0.

References

[1] W. Miziolek, V. Palleschi, I. Schechter, Laser Induced Breakdown Spectroscopy, Cambridge University Press, Cambridge, 2006.
[2] D.A. Cremers, L.J. Radziemski, Handbook of Laser-Induced Breakdown Spectroscopy, Wiley, London, 2006.
[3] V.C. Costa, J.P. Castro, D.F. Andrade, D.V. Babos, J.A. Garcia, M.A. Sperança, T.A. Catelani, E.R. Pereira-Filho, Laser-induced breakdown spectroscopy (LIBS) applications in the chemical analysis of waste electrical and electronic equipment (WEEE), laser-induced breakdown spectroscopy (LIBS) applications in the chemical analysis of waste electrical and electronic equipment (WEEE), Trends Anal. Chem. 108 (2018) 65–73 (10.1016/ j.trac.2018.08.003).
[4] G.G.A. Carvalho, M.B.B. Guerra, A. Adame, C.S. Nomura, P.V. Oliveira, H.W.P. Carvalho, D. Santos Jr., L.C. Nunes, F.J. Krug, Recent advances in LIBS and XRF for the analysis of plants, J. Anal. At. Spectrom. 33 (2018) 919–944.
[5] R. Papai, R.H. Sato, L.C. Nunes, F.J. Krug, I. Gauber, Melted paraffin wax as an innovation liquid and solid extractant for elemental analysis by laser-induced breakdown spectroscopy, Anal. Chem. 89 (2017) 2807–2815.
[6] K.H. Lepore, C.I. Fassett, E.A. Breves, S. Byrne, S. Giguere, T. Boucher, J.M. Rhodes, M. Vollinger, C.H. Anderson, R.W. Murray, M.D. Dyar, Matrix effects in quantitative analysis of laser-induced breakdown spectroscopy (LIBS) of rock powders doped with Cr, Mn, Ni, Zn, and Co, Appl. Spectrosc. 71 (4) (2017) 600–626.
[7] D.V. Babos, V.C. Costa, M.A. Sperança, E.R. Pereira-Filho, Direct determination of

calcium and phosphorus in mineral supplements for cattle by wavelength dispersive X-ray fluorescence (WD-XRF), Microchem. J. 137 (2018) 272–276.
[8] T. Takahashia, B. Thornton, Quantitative methods for compensation of matrix effects and self-absorption in laser-induced breakdown spectroscopy signals of solids, Spectrochim. Acta Part B. 138 (2017) 31–42.
[9] S.I. Gornushkin, I.B. Gornushkin, J.M. Anzano, B.W. Smith, J.D. Winefordner, Effective normalization technique for correction of matrix effects in laser-induced breakdown spectroscopy detection of magnesium in powdered samples, Appl. Spectros. 56 (4) (2002) 433–436.
[10] S.M. Clegg, E. Sklute, M.D. Dyar, J.E. Barefield, R.C. Wiens, Multivariate analysis of remote laser-induced breakdown spectroscopy spectra using partial least squares, principal component analysis, and related techniques, Spectrochim. Acta Part B 64 (2009) 79–88.
[11] T.F. Boucher, M.V. Ozanne, M.L. Carmosino, M.D. Dyar, S. Mahadevan, E.A. Breves, K.H. Lepore, S.M. Clegg, A study of machine learning regression methods for major elemental analysis of rocks using laser-induced breakdown spectroscopy, Spectrochim. Acta Part B 107 (2015) 1–10.
[12] D.M. Silvestre, F.M. Barbosa, B.T. Aguiar, F.O. Leme, C.S. Nomura, Feasibility study of calibration strategy for direct quantification measurement of K and Mg in plant material by laser-induced breakdown spectrometry, Anal. Chem. Resear. 5 (2015) 28–33.
[13] P.C. Morais, A.I. Barros, D. Santos Júnior, C.A. Ribeiro, M.S. Crespi, G.S. Senesi, J.A. Gomes Neto, E.C. Ferreira, Calcium determination in biochar-based fertilizers by laser-induced breakdown spectroscopy using sodium as internal standard, Microchem. J. 134 (2017) 370–373.
[14] A.A.C. Carvalho, F.O. Leme, M.S. Luz, P.V. Oliveira, C.S. Nomura, Internal standard fused glass beads for high silicon content sample analysis by laser-induced breakdown spectrometry, J. Anal. At. Spectrom. 33 (2018) 1243–1250.
[15] R.X. Yi, L.B. Guo, X.H. Zou, J.M. Li, Z.Q. Hao, X.Y. Yang, X.Y. Li, X.Y. Zeng, Y.F. Lu, Background removal in soil analysis using laser-induced breakdown spectroscopy combined with standard addition method, Opt. Express 24 (2016) 2607.
[16] D.V. Babos, A. Virgílio, V.C. Costa, G.L. Donati, E.R. Pereira-Filho, Multi-energy calibration (MEC) applied to laser-induced breakdown spectroscopy (LIBS), J. Anal. At. Spectrom. (2018), https://doi.org/10.1039/C8JA00109J.
[17] Y.S. Kim, B.Y. Han, H.S. Shin, H.D. Kim, E.C. Jung, J.H. Jung, S.H. Na, Determination of uranium concentration in an ore sample using laser-induced breakdown spectroscopy, Spectrochim. Acta Part B. 74–75 (2012) 190–193.
[18] S. Zivkovic, J. Savovic, M. Kuzmanovic, J. Petrovic, M. Momcilovic, Alternative analytical method for direct determination of Mn and Ba in peppermint tea based on laser induced breakdown spectroscopy, Microchem. J. 137 (2018) 410–417.
[19] M.A. Bader, Systematic approach to standard addition methods in instrumental analysis, J. Chem. Educ. 57 (1980) 703–706.
[20] S.J. Christopher, R.D. Day, C.E. Bryan, G.C. Turk, Improved calibration strategy for measurement of trace elements in biological and clinical whole blood reference materials via collision-cell inductively coupled plasma mass spectrometry, J. Anal. At. Spectrom. 20 (2005) 1035–1043.
[21] W.R. Kelly, B.S. MacDonald, W.F. Guthrie, Gravimetric approach to the standard addition method in instrumental analysis, Anal. Chem. 80 (2008) 6154–6158.
[22] L.R. Barker, W.R. Kelly, W.F. Guthrie, Determination of sulfur in biodiesel and petroleum diesel by X-ray fluorescence (XRF) using the gravimetric standard addition method-II, Energy Fuel 22 (2008) 2488–2490.
[23] J.M. Andrade, J. Terán-Baamonde, R.M. Soto-Ferreiro, A. Carlosena, Interpolation in the standard additions method, Anal. Chim. Acta 780 (2013) 13–19.
[24] Y. Gao, R.E. Sturgeon, Z. Mester, X. Hou, L. Yang, Multivariate optimization of photochemical vapor generation for direct determination of arsenic in seawater by inductively coupled plasma mass spectrometry, Anal. Chim. Acta 901 (2015) 34–40.
[25] Y. Gao, R.E. Sturgeon, Z. Mester, X. Hou, C. Zheng, L. Yang, Direct determination of trace antimony in natural waters by photochemical vapor generation ICP-MS: method optimization and comparison of quantitation strategies, Anal. Chem. 87 (2015) 7996–8004.
[26] A. Virgilio, D.A. Gonçalves, T. McSweeney, J.A. Gomes Neto, J.A. Nóbrega, G.L. Donati, Multi-energy calibration applied to atomic spectrometry, Anal. Chim. Acta 982 (2017) 31–36.
[27] R.C. Machado, A.B.S. Silva, G.L. Donati, A.R.A. Nogueira, Multi-energy calibration as a strategy for fertilizer elemental analysis by microwave-induced plasma optical emission spectrometry, J. Anal. At. Spectrom. 33 (2018) 1168–1172.
[28] A. S. Augusto, J. P. Castro, M. A. Sperança, E. R. Pereira-Filho, Combination of multi-energy calibration (MEC) and laser-induced breakdown spectroscopy (LIBS) for dietary supplements analysis and determination of Ca, Mg and K, J. Braz. Chem. Soc. Accepted for publication. 10.21577/0103-5053.20180211.
[29] F. M. Fortunato, T. A. Catelani, M. S. Pomares-Alfonso, E. R. Pereira-Filho, Application of multi-energy calibration for determination of chromium and nickel in nickeliferous ores by laser-induced breakdown spectroscopy, Anal. Sci. Accepted for publication. https://doi.org/10.2116/analsci.18P286.
[30] NIST electronic database, https://www.nist.gov/pml/atomic-spectra-database.
[31] G. Derringer, R. Suich, Simultaneous optimization of several response variables, J. Qual. Technol. 12 (1980) 214–219.
[32] J.P. Castro, E.R. Pereira-Filho, Twelve different types of data normalization for the proposition of classification, univariate and multivariate regression models for the direct analyses of alloys by laser-induced breakdown spectroscopy (LIBS), J. Anal. At. Spectrom. 31 (2016) 2005–2014.
[33] M.A. Sperança, M.S. Pomares-Afonso, E.R. Pereira-Filho, Analysis of Cuban nickeliferous minerals by laser-induced breakdown spectroscopy (LIBS): non-conventional sample preparation of powder samples, Anal. Methods 10 (2018) 533–540.
[34] R. Noll, Laser-Induced Breakdown Spectroscopy Fundamentals and Applications, Springer-Verlag, Berlin-Heidelberg, 2012.
[35] D.R. Lide (Ed.), CRC Handbook of Chemistry and Physics, CRC Press, Boca Raton, 2007.
[36] R.J.C. Brown, T.P.S. Gillam, Comparison of quantification strategies for one-point standard addition calibration: the homoscedastic case, Anal. Chim. Acta 716 (2012) 108–111.
[37] F.M.V. Pereira, E.R. Pereira-Filho, Application of free computational program in experimental design: a tutorial, Quim Nova 41 (2018) 1061–1071.

3.1.2 Direct determination of Al and Pb in waste printed circuit boards (PCB) by Laser-induced breakdown spectroscopy (LIBS): evaluation of calibrations strategies and economic-environmental questions. Journal of Hazardous Materials 399 (2020) 122831.

Journal of Hazardous Materials 399 (2020) 122831

Contents lists available at ScienceDirect

Journal of Hazardous Materials

journal homepage: www.elsevier.com/locate/jhazmat

Direct determination of Al and Pb in waste printed circuit boards (PCB) by laser-induced breakdown spectroscopy (LIBS): Evaluation of calibration strategies and economic - environmental questions

Diego Victor Babos[a,b], Andrés Cruz-Conesa[a], Edenir Rodrigues Pereira-Filho[b], Jesús M. Anzano[a,*]

[a] Laser Laboratory, Chemistry & Environment Group, Department of Analytical Chemistry, Faculty of Sciences, University of Zaragoza, Pedro Cerbuna 12, 50009, Zaragoza, Spain

[b] Group of Applied Instrumental Analysis, Department of Chemistry, Federal University of São Carlos, São Carlos, São Paulo State, 13565-905, Brazil

GRAPHICAL ABSTRACT

Evaluation of five calibration strategies for direct determination of recyclable and toxic metals in waste PCB by LIBS.

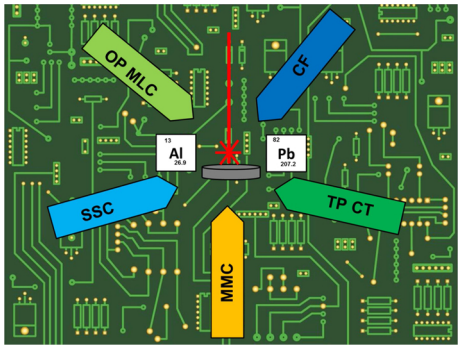

ARTICLE INFO

Editor: R. Teresa

Keywords:
WEEE
Toxic element
Environment pollution
Matrix-matching calibration
Two-point calibration transfer
Calibration free
Single-sample calibration
One-point multi-line calibration

ABSTRACT

Matrix-matching calibration (MMC), two-point calibration transfer (TP CT), one-point and multi-line calibration (OP MLC), single-sample calibration (SSC) and calibration free (CF) were evaluated in order to overcome matrix effects in laser-induced breakdown spectroscopy (LIBS). These calibration strategies were evaluated for direct determination of Al and Pb in waste printed circuit boards (PCB) using direct solids analysis by LIBS. Each strategy has limitations and advantages of its implementation, for the correction of matrix effects, so that it allows elementary determination with adequate accuracy. The MMC and CF proved to be excellent calibration strategies for the determination of strategic (Al) and toxic (Pb) elements by LIBS, with good recoveries (ranging from 80–120%) and low relative standard deviation (RSD%) values. A detailed discussion of the advantages and limitations of each of these five calibration strategies evaluated for LIBS is presented in this study. Lead concentrations in waste PCB samples are 5–12 times higher than established by Directive 2011/65/EU, and the samples analyzed contain between 3 and 55 g kg^{-1} Al, being an interesting economic and recycling source for this metal.

* Corresponding author.
E-mail address: janzano@unizar.es (J.M. Anzano).

https://doi.org/10.1016/j.jhazmat.2020.122831
Received 13 March 2020; Received in revised form 16 April 2020; Accepted 7 May 2020
Available online 23 May 2020

1. Introduction

Contemporary society utilizes several types of high-tech electrical and electronic devices and instruments. The study of waste electrical and electronic equipment (WEEE) generation is therefore of great interest due to the environmental, economic, recycling and reuse questions posed by this type of waste (Costa et al., 2018a; Tansel, 2017). According to a study published in 2017, the projection of WEEE production is expressive (Andrade et al., 2019a, 2019b, 2019c, 2019d), being 52.2 million tons in 2021 (Baldé et al., 2017).

WEEE contains a diverse, complex and valuable composition, consisting mainly of polymers, metals (base, toxic, noble and technological elements) and ceramics. Printed circuit boards (PCB), which are part of the electronic devices present in the WEEE, contain large amounts of valuable and dangerous metals such as, for example, Al and Pb. Depending on the electronic device, the metal content on PCBs can range from 2–19 % Al and 1–3% Pb, among others (Andrade et al., 2019b; Arshadi et al., 2018; Carvalho et al., 2015; Perkins et al., 2014; Yamane et al., 2011; Yang et al., 2019). Aluminum and Pb can be recycled, adding value to the WEEE and generating a source of income. Lead is a toxic metal which in high concentrations can pollute the environment. According to Directive 2011/65/EU, the maximum concentration allowed is 0.1 % by weight in homogeneous materials (RoHS, 2011).

The preparation of waste PCB samples for elemental analysis is a challenging task due to the complexity of its composition and its refractory character, being rich in oxides of Mg, Si and Ti, flame retardants, metals and polymers. Thus, the need to use vigorous conditions in the acid decomposition step is evident in order to obtain a homogeneous and representative solution for subsequent quantitative analysis by conventional analytical techniques (Arshadi et al., 2018).

LIBS technique has some advantages that could be used for the direct analysis of waste PCBs, such as: minimum sample preparation, fast multi-element analysis (μs), semi-destructive analysis (μg), and minimum waste generation. A limitation of this technique is related to matrix effects, which may compromise accuracy in quantitative analysis (Andrade et al., 2020; Carvalho et al., 2018a; Costa et al., 2019; Cremers and Radziemski, 2006b; Gondal et al., 2010; Kim et al., 2013; Lasheras et al., 2011; Miziolek et al., 2006).

As the sample is analyzed integrally (analyte and matrix simultaneously) by the LIBS instrument, the physicochemical properties of the sample and the laser-sample and/or laser-plasma interaction may influence the atomic/ionic/molecular emission phenomenon of the analyte (Cremers and Radziemski, 2006a; Miziolek et al., 2006). As in the majority of applications the goal is quantitative analysis, requiring calibration standards in some strategies. In addition, different matrix effects can occur in the plasma formed in the samples and in the calibration standards. Consequently, the figures of merit of the method can be jeopardized, and thus may make it impossible to determine the analyte with satisfactory accuracy using direct solid analysis by LIBS (Hahn and Omenetto, 2010, 2012; Sattar et al., 2019).

Matrix effects (spectral and non-spectral) can be avoided or minimized by careful peak selection or peak fitting of the analytical line and / or selecting lines that do not exhibit spectral interference, in addition the use of high resolution spectrometers in LIBS (makes it possible to identify and overcome some spectral interferences) (Takahashi and Thornton, 2017; NIST, 2020).

The non-spectral matrix effects are directly correlated to the physical and chemical properties of the sample, and these effects are more difficult to overcome because there are many possibilities of how the matrix may be influenced by the analyte emission phenomenon (Cremers and Radziemski, 2006a; Takahashi and Thornton, 2017). The main non-spectral matrix effects are related to the sample's irregular surface, inhomogeneous particle size and humidity (Carvalho et al. 2018, Takahashi and Thornton, 2017), the predominant chemical composition of the sample (organic or inorganic forms) (Eppler et al., 1996), the temperature of the sample (Lednev et al., 2019), the pressure used to compress the sample to form pellets (when necessary) (Popov et al., 2018), the presence of easily ionizable elements (EIEs) (Morais et al., 2018; Popov et al., 2018), the interaction of the laser with the sample, heat of vaporization, thermal conductivity, and the absorption coefficient, which affects the transport of an ablated mass which will be vaporized and atomized into the plasma (Takahashi and Thornton, 2017), among others (Lasheras et al., 2013; Rezaei et al., 2018). These matrix effects may contribute to the non-stoichiometric ablation of the sample and thus reduce the possibility of using LIBS for quantitative analysis.

In order to overcome these matrix effects, univariate and multivariate calibration strategies are used for LIBS: matrix-matching calibration (MMC) (Costa et al., 2018b; Gomes et al., 2013; Vieira et al., 2018), standard addition (SA) (Yi et al., 2016; Wu et al., 2019), one-point gravimetric standard addition (OP GSA) (Babos et al., 2019), internal standardization (IS) (Aquino et al., 2016; Carvalho et al., 2018b; Lasheras et al., 2013; Sperança et al., 2019) calibration free (CF) (Cavalcanti et al., 2013; Ciucci et al., 1999; Li et al., 2019; Tognoni et al., 2010), one-point and multi-line calibration (OP MLC) (Hao et al., 2018), multi-energy calibration (MEC) (Andrade et al., 2019b; Augusto et al., 2019; Babos et al., 2018; Carvalho et al., 2019; Castro et al., 2020; Fortunato et al., 2019), two-point calibration transfer (TP CT) (Castro et al., 2020), and single-sample calibration (SSC) (Yan et al., 2019).

It should be noted that many calibration possibilities are available for LIBS, but the question is what is the best calibration strategy that could be applied for the determination of Al and Pb in samples as complex, of environmental and economic interest as waste PCBs. In order to answer this question, five calibration strategies were selected and evaluated their performance based on various parameters such as standard error (SE), recovery and other figures of merit, considering the limitations and intrinsic advantages of each calibration for overcoming matrix effects and for the determination of these metals. Two strategies widely reported in the literature (MMC and CF) and three that have recently been proposed (TP CT, OP MLC and SSC) for calibration were evaluated for direct waste PCB analysis and determinations of toxic (Pb) and strategic (Al) elements by LIBS.

2. Experimental

2.1. Instrumentation

LIBS spectra were obtained using an experimental set-up based on a Q-switched Nd:YAG laser (BrilliantQuantel, model Ultra CFR) with a 1064 nm wavelength, a 7.7 ns pulse duration and a maximum laser pulse energy of 50 mJ. The sample was placed inside a sample chamber and the laser beam directly focused on it through a 150 mm focal length lens. The target surface was positioned approximately 77 mm below the focal lens. The light emitted by the plasma was collected by optic fibers connected to an Echelle spectrometer (Andor Mechelle ME5000, 195 mm focal length, F/7, l/Al 5000). The spectrometer is equipped with an intensified charge coupled device detector (Andor iStar DH734, 1024 × 1024 pixels 13.6 × 13.6 μm^2 by pixel, 18 mm of intensifier diameter). The wavelength and spectral resolution of the spectrometer were calibrated using a low pressure mercury-argon lamp by measuring both the spectral positions of the lines and their spectral profiles. The LIBS system requires some instrumental parameters to be optimized such as laser pulse energy, delay time, signal acquisition time and lens-sample distance.

An inductively coupled plasma optical emission spectrometer (ICP OES) (iCAP 7000, Thermo Scientific, Waltham, MA, USA) was used in the determination of Al and Pb in printed circuit board waste after acid digestion of the samples (n = 3). The concentrations obtained were used as reference values for the LIBS method. The emission lines monitored during ICP OES determinations were Al 167.079 nm and Pb

216.99 nm using axial viewing mode.

A scanning electron microscope (SEM) (JEOL JSM 6360-LV) (General Research Support Service of the University of Zaragoza) with voltage up to 30 kV and a maximum resolution of 3.0 nm was used for the morphological surface visualization of the waste PCBs. In order to perform the analysis, one waste PCB sample was pelletized and selected (S2). Additionally, the pellet was analyzed by SEM in order to obtain information about the crater formed by the laser pulse and then to calculate both the irradiance and laser pulse fluence values.

2.2. Reagents and samples

Standard solutions containing Al and Pb were prepared by diluting standard stock solutions containing 1000 mg L^{-1} (Specsol, São Paulo, Brazil), and acidified with HNO_3 10 % v v^{-1}, and used for ICP OES analysis.

Six PCBs from desktop computers were collected at São Carlos (São Paulo State, Brazil) and then ground in a knife mill (IKA, A11) (the particle size was estimated to be lower than 500 µm) to obtain homogeneous and representative samples. Approximately 200 mg of PCB samples were weighed and compressed using a manual hydraulic press (Perkin Elmer IR Accessory Hydraulic Press) with 10×10^4 N for 2 min, to obtain pellets (n = 3) for LIBS analysis. It is necessary to press the sample to obtain cohesive pellets that contribute to the reproducibility of the laser-sample interaction and consequently to the precision of the measurements.

2.3. Sample preparation for determination of Al and Pb by ICP OES

The samples of PCBs were digested using microwave-assisted heating for analysis and to obtain reference values of Al and Pb that were subsequently used in the proposition of the calibration models and verification of the accuracy of the proposed LIBS method. Masses of approximately 100 mg of PCB were accurately weighed directly in the perfluoroalkoxy alkanes (PFA) digestion vessels and microwave-assisted digested using a single reaction chamber oven (UltraWave™, Milestone, Sorisole, Italy). Volumes of 5 mL of concentrated HNO_3 were used as an oxidizing agent in the decomposition. The microwave heating program was applied as follows: (1) 5 min to reach 100 °C, (2) 15 min to reach 180 °C, (3) 15 min to reach 240 °C and (4) 7 min held at 240 °C. Subsequently, the digests were diluted to 50.0 mL with distilled-deionized water and filtered on qualitative filter paper 80 g m^{-2} (Unifil, Germany) for subsequent ICP OES analysis.

2.4. Optimization of LIBS instrumental parameters

Using a full factorial design 2^3 with center and axial points, the instrumental conditions (delay time, gate width and laser pulse energy) were optimized. The variables studied were evaluated at five levels: delay time (0.01, 0.4, 1.2, 2.0 and 2.54 µs), gate width (0.32, 1.0, 2.0, 3.0 and 3.68 µs) and laser pulse energy (20, 25, 35, 42.5 and 47.5 mJ). The variable levels were coded between -1.68 (lower level) and +1.68 (higher level), with the central point (coded as 0) used to calculate experimental errors. Table S1 presented at Supplementary material shows more details about the experimental design performed. Due to experimental setup limitations the delay time values were coded from -1.49 (0.01 µs) to 1.68 (2.54 µs) The S2 waste PCB sample containing 55 ± 3 g kg^{-1} Al and 11.6 ± 0.8 g kg^{-1} Pb was used to optimize the instrumental conditions used in the LIBS analyses. The Al and Pb reference concentrations were obtained after microwave digestion and ICP OES determinations.

The signal-to-background ratio (SBR) calculated for each monitored emission line of Al and Pb (besides the lines of Ca, Fe, Si and Ti used for calibration free) were used as responses of the factorial design. A mathematical approach developed by Derringer and Suich (1980), based on desirability functions applied to optimize multi-response experiments, was used in this study. This strategy first converts each experimental response into an individual desirability value (d_i), which ranges between $0 \leq d_i \leq 1$. In this case, $d_i = 1$ corresponds to a desired response (high SBR), while $d_i = 0$ represents a response that is outside the acceptable region (the lowest SBR). The individual desirability value was combined into a single response after an arithmetic mean calculation (the overall desirability, OD). In this study, was exceptionally used the arithmetic mean because some experiments resulted in di = 0.

2.5. Calibration strategies

Five calibration strategies were evaluated for the determination of Al and Pb in waste PCB samples by LIBS. For all the calibration strategies, the calibration standards and samples were pelletized (n = 3) using approximately 200 mg of waste PCB. The resulting pellets were analyzed using 50 pulses in different spots to obtain a single average spectrum. For each sample, six average spectra were obtained (total of 300 shots per sample).

Eight different strategies for normalization of the spectra (Castro and Pereira-Filho, 2016; Sperança et al., 2018) were evaluated. These normalizations are important to minimize the signal fluctuations (area or height) and sample matrix differences during data acquisition.

2.5.1. Matrix-matching calibration – MMC

For MMC method, calibration curves in the range from 3.1 to 55 g kg^{-1} Al and 0.72 to 11.6 g kg^{-1} of Pb were obtained using four samples of waste PCBs as solid standards. The curves were obtained by plotting the analytical signal (y-axis emission intensity) *versus* the analyte concentration (x-axis).

Four emission lines with different relative intensities for Al (Al I 308.21 nm, Al I 309.40 nm, Al I 394.40 nm and Al I 396.15 nm) and two lines for Pb (Pb I 363.95 nm e Pb I 405.78 nm) were evaluated to obtain the calibration curves. The choice of the best normalization mode and the most appropriate emission line was made using as a criterion the obtaining of calibration curves that enable the smallest errors of prediction of the analyte concentration in the samples.

The concentration of the analyte, using MMC, is calculated using equation 1,

$$C_{analyte} = \frac{Intensity - intercept}{slope} \quad (1)$$

where $C_{analyte}$ is the concentration of Al or Pb determined in the sample, Intensity is the analytical signal of the emission line obtained, slope and intercept, both obtained by the calibration curve.

2.5.2. Two-point calibration transfer – TP CT

For TP CT only one sample is used as the calibration standard, and the linear model is obtained with two analytical signals monitoring only one analyte emission line. The linear model plot is made using two sets of spectra in the x-axis, and in the y-axis the intensity of the emission line is obtained using only the sum of the intensity of the spectra (height or signal area) through normalization 5.

Using the reference concentration ($C_{standard}$) of the analyte in the calibration standard, and the slopes obtained in linear models for the sample ($slope_{sample}$) and for the calibration standard ($slope_{standard}$), the analyte concentration ($C_{analyte}$) can be obtained using Eq. 2 (Castro et al., 2020).

$$C_{analyte} = \frac{slope_{sample}}{slope_{standard}} \times C_{standard} \quad (2)$$

For TP CT the emission lines Al I 396.15 nm and Pb I 405.78 nm were used to obtain linear models.

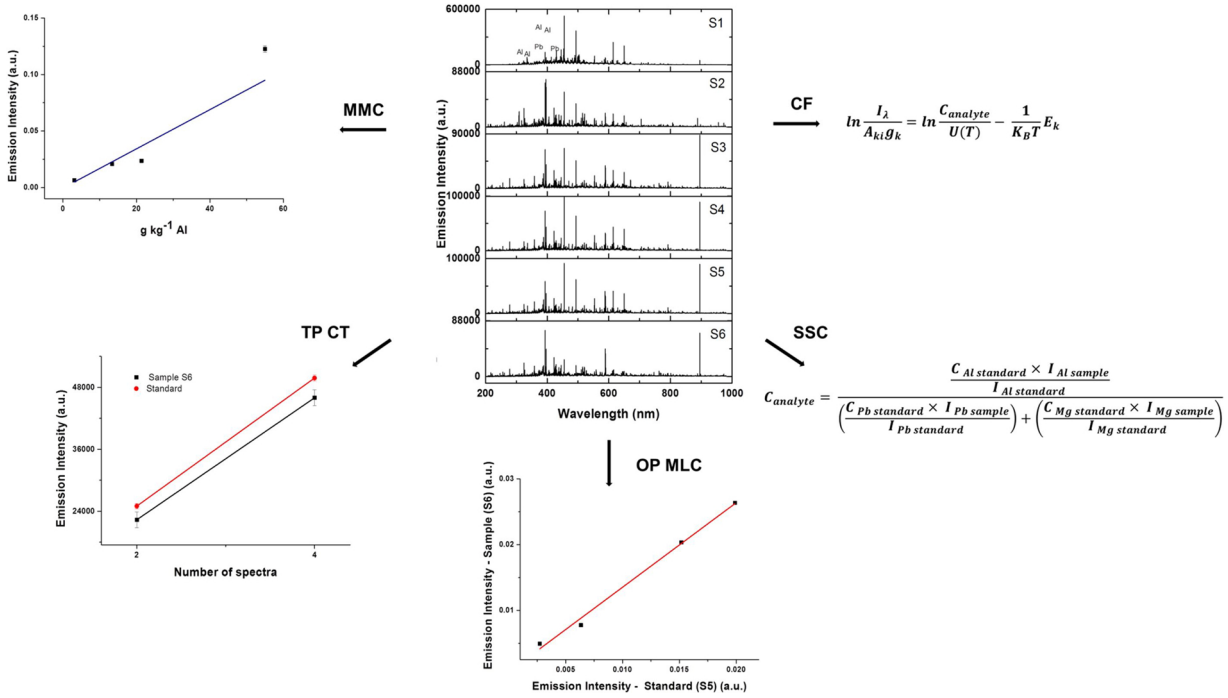

Fig. 1. Scheme representation of the calibration strategies evaluated for direct determination of Al in waste PCBs by LIBS.

2.5.3. One-point and multi-line calibration – OP MLC

For the OP MLC, only one sample is used as the calibration standard and several emission lines are used to obtain calibration linear models for Al and Pb. In the x-axis, the emission intensities are used for all the monitored analyte lines in the standard calibration, and in the y-axis the intensities are used for all the monitored lines in the sample.

The analyte concentration ($C_{analyte}$) is calculated using equation 3,

$$C_{analyte} = slope \times C_{standard} \quad (3)$$

where the slope is obtained for the linear model, and $C_{standard}$ is the concentration of the analyte in the sample used as the standard calibration (Hao et al., 2018).

Using four atomic emission lines for Al (308.21 nm, 309.27 nm, 394.40 nm and 396.15 nm) and two atomic emission lines for Pb (363.95 nm and 405.78 nm), linear models were obtained for each analyte in the respective samples.

2.5.4. Single-sample calibration – SSC

In the SSC method, only one sample is used as the calibration standard and several emission lines of the analyte present in the standard and sample (unknown) are used. The SSC does not require a calibration curve or linear models (Yan et al., 2019).

For this strategy, the emission intensities of Al I 396.15 nm, Pb I 405.78 nm and Mg II 279.55 nm were used to determine the concentration of the analyte. The S2 PCB sample containing 55 ± 3 g kg^{-1} Al, 11.6 ± 0.8 g kg^{-1} Pb and 11.4 ± 1.8 g kg^{-1} Mg (obtained after microwave digestion and ICP OES determination) was used as the calibration standard.

The analyte concentration ($C_{analyte}$) is calculated using Eq. 4,

$$C_{analyte} = \frac{\frac{C_{standard\ analyte} \times I_{analyte\ sample}}{I_{analyte\ standard}}}{\sum_{i=1}^{N} \frac{C^{N}_{standard\ element} \times I^{N}_{element\ sample}}{I^{N}_{element\ standard}}} \quad (4)$$

where $C_{standard\ analyte}$ and $I_{analyte\ standard}$ are the concentration and intensity of the emission line of the analyte in the PCB sample, respectively, used as the calibration standard (#S2 PCB). The $I_{analyte\ sample}$ is the emission intensity of the analyte in the unknown sample. The $I^{N}_{element\ sample}$ is the emission intensity of the element N in the sample of unknown concentration, and $C^{N}_{standard\ element}$ and $I^{N}_{element\ standard}$ the concentration and the emission intensity of the element N, respectively, in the sample used as the standard calibration.

2.5.5. Calibration free – CF

For CF only physicochemical parameters of the obtained plasma and from the monitored emission lines of the analytes and from all species present are necessary for the quantification. A calibration standard is not required.

The analyte concentration ($C_{analyte}$) is calculated using Eq. 5,

$$\ln\frac{I_\lambda}{A_{ki}g_k} = ln\frac{C_{analyte}}{U(T)} - \frac{1}{K_BT}E_k \quad (5)$$

where I_λ is the integrated intensity of the emission line, A_{ki} the transition probability, g_k the degeneration of the upper level, K_B the Boltzmann constant, T the temperature of the plasma, E_k the energy level of the excited state, F the experimental factor, and U(T) the partition function of the species present in the plasma (Ciucci et al., 1999; Li et al., 2019; Tognoni et al., 2010,).

All the calculations were processed using the LIBS++ software (ARWAN technology, developed by Palleschi et al.). For the calculation of the plasma temperature, the emission lines for Ba (Ba I 705.99, Ba II 614.17 and Ba II 649.69 nm), Fe (Fe I 374.55, Fe I 382.04, Fe I 405.58, Fe I 438.35, Fe II 239.92 nm) and Ti (Ti I 498.17, Ti I 499.10 and Ti II 333.94 nm) were used.

The plasma electron density (N_e) was calculated from the Hα line in 656.28 nm and using Eq. 6,

$$FWHA = 0.549nm \times \left(\frac{N_e}{10^{23}\,m^{-3}}\right)^{0.67965} \quad (6)$$

where FWHA denotes the full width at half area of this hydrogen emission line (Cavalcanti et al., 2013; Ciucci et al., 1999,).

Fig. 1 show a pictorial description of all the calibration strategies (calibration curve, linear model or correlation) used for Al.

2.6. Determination of analytical performance parameters

The precision (n = 3) was calculated using all the samples. The standard error (SE) and root mean square error of prediction (RMSEP) were calculated for analytes, using Eqs. 7 and 8, respectively:

$$SE = \sqrt{\frac{\sum (yi - \hat{y})^2}{n - 1}} \quad (7)$$

$$RMSEP = \sqrt{\frac{\sum (yi - \hat{y})^2}{n}} \quad (8)$$

where y_i is the analyte reference concentration obtained by ICP OES, $\hat{y}$ is the concentration predicted by the calibration model using LIBS, and n is the number of samples analyzed.

Slope and intercept values and respective confidence interval (95 % confidence level) obtained for linear regression for concentration reference (ICP OES method) *versus* concentration predicted (LIBS method) plots, were used for results comparison obtained in the direct determinations of analytes using five calibration strategies for LIBS. The ideal situation is a slope and intercept equals to 1 and 0, respectively.

3. Results and discussion

3.1. Optmization of LIBS instrumental conditions

The instrumental conditions of the LIBS system influence the laser-matter interaction and also the quality of the emission spectrum obtained. The laser pulse energy, delay time and gate width of the spectrometer were optimized using a full factorial design 2^3 with center and axial points (see Table S1).

The regression model based on the obtained OD (Table S1) was calculated to determine the best description of the experimental region. The quality of the model was evaluated through analysis of variance (ANOVA). After observing the values calculated for ANOVA, it was possible to verify that the regression of the model is not statistically significant at the 95 % confidence level. These results demonstrate that it is not possible to obtain a model with good predictive capacity.

By evaluating Table S1, it was observed that experiment 8 presented the highest OD value (OD = 0.89) when compared to the other experiments. Thus, the evaluated conditions of this experiment were used in all measurements by LIBS in this study, with a delay time of 2 μs, a gate width of 3 μs and laser pulse energy of 42.5 mJ.

3.2. Laser-sample interaction: energy parameters

The physical and chemical properties of the sample strongly influence the laser-sample interaction and consequently the formation of the plasma, modifying its characteristics (temperature and electronic density, among others). Using SEM analysis and laser pulse energy optimized for analyses of waste PCBs, some parameters were obtained from the laser-waste PCB pellet interaction.

The crater formed by the laser pulse over the surface of the pelletized waste PCB sample S2 (200 mg compressed using 10×10^4 N for 2 min) is shown in Fig. 2. The estimated crater diameter was 470 μm. The figure shows the heterogeneity of the morphology and composition of the sample since waste PCBs consist of several polymeric, ceramic and metallic components. The importance of a milling step to obtain a representative sample and thus enable a stoichiometric ablation is also evident, besides the need to obtain several spectra in different regions of the pelletized sample for precision in determination (low RSD values). The laser-sample interaction is complex and many phenomena occur as a result.

The irradiance (W cm^{-2}) and the laser pulse fluence (J cm^{-2}) were calculated from the diameter of the crater. Using a laser pulse of 42.5 mJ and a pulse duration of 7.7 ns, a power of 5.5 MW was generated. Even if low energies are used, it is common to obtain high power values because the pulse duration lasts for nanoseconds. The crater radius reached 235 μm, obtaining an irradiance of 3.2 GW cm^{-2} and a laser fluence of 24.5 J cm^{-2}. These parameters were calculated for the optimized instrumental conditions used to obtain all the LIBS spectra for the waste PBC samples.

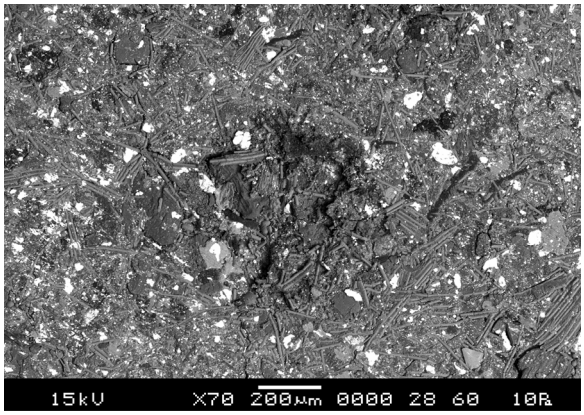

Fig. 2. Crater and superficial morphology of waste PCB sample (S2) obtained by scanning electron microscopy (SEM).

3.3. Evaluation of calibration strategies for LIBS

The matrix effects are the main sources of the linearity deviations between concentration and emission intensity in the analysis of solids by LIBS aimed at elementary determination. Thus, five calibration strategies (i- MMC, ii- TP CT, iii- OP MLC, iv- SSC and v- CF) were evaluated to overcome or minimize matrix effects in the determination of Al and Pb in six waste PCBs by LIBS. The criterion for selecting the analytes emission lines (λ) used in each calibration strategy was made considering the accuracy of the determinations based on the recovery value. Recoveries values in the range of 80–120% were considered satisfactory for all the evaluated calibration strategies.

Using matrix-matching calibration for Al, a calibration curve (coefficient of determination: $R^2 = 0.8146$) was obtained by monitoring the emission line Al I 396.15 nm in the following samples: S1, S2, S3 and S4. For the validation of the method, two samples with intermediate concentrations to the calibration standards (S5 and S6) were analyzed. Recoveries values of 99 % and 116 %, and relative standard deviation (RSD) values ≦4% were obtained, demonstrating the satisfactory accuracy of MMC for Al determinations (see Table 1).

For Pb, the calibration curve obtained monitoring the emission line Pb I 405.78 nm at samples S2, S3, S4 and S5, showed a good coefficient of determination ($R^2 = 0.8426$) using the MMC strategy. For samples S1 and S6 (used for validation), good recoveries values of 102 % and 111 % and RSD ≦ 8% were obtained for Pb determinations by LIBS (see Table 2).

For two-point calibration transfer strategy, the S4 (13.4 ± 0.7 g kg^{-1} Al) and S1 (7.6 ± 0.6 g kg^{-1}Pb) samples were used as calibration standards for Al and Pb, respectively. Since only two calibration points ("concentrations") are used, the linearity and significance of the model can be verified from the test F, and in this case the ratio $F_{experimental}/F_{tabulated}$ was calculated. This ratio ≥10 demonstrated that the variances are statistically different (the quadratic mean of the regression is statistically different when compared with the quadratic mean of the residues), thus the model can be considered linear and statistically significative, and the TP CT can be used (Pereira and Pereira-Filho, 2018). The ratio found for all samples analyzed for Al ranged from 7 to 416 and for Pb ratios of 5–116 were obtained, indicating that the models are linear and that two-point calibration is feasible.

For Al, recovery values ranging from 84 to 112 % were obtained

Table 1
Concentrations (mean ± standard deviation, g kg^{-1} Al, n = 3) and recovery (%) for Al in PCB samples determined by LIBS using matrix-matching calibration (MMC), two-point calibration transfer (TP CT), one-point and multi-line calibration (OP MLC), single-sample calibration (SSC) and calibration free (CF).

Sample	ICP OES	MMC	TP CT	OP MLC			SSC	CF
	g kg^{-1}			Theoretical slope*	Experimental Slope	g kg^{-1}		
S1	3.1 ± 0.4	–	21.2 ± 3.6 (683)	0.30	0.28 ± 0.03	2.9 ± 0.3 (93)	6.8 ± 1.1 (220)	3.3 ± 0.1 (106)
S2	55 ± 3	–	68.9 ± 8.4 (125)	5.39	5.87 ± 0.11	59.8 ± 1 (109)	–	49.8 ± 9.2 (91)
S3	21.4 ± 0.6	–	13.0 ± 1.4 (61)	2.09	1.19 ± 0.07	12.1 ± 0.6 (57)	24.8 ± 5.1 (116)	21.4 ± 3.1 (100)
S4	13.4 ± 0.7	–	–	1.32	1.02 ± 0.08	10.4 ± 0.8 (78)	13.5 ± 1.4 (101)	13.1 ± 3.4 (98)
S5	10.2 ± 1	11.8 ± 0.1 (116)	11.4 ± 0.9 (112)	–	–	–	10.4 ± 2.1 (102)	10.0 ± 2 (98)
S6	15.2 ± 0.9	15.0 ± 0.5 (99)	12.7 ± 1.4 (84)	1.49	1.23 ± 0.05	12.6 ± 0.5 (83)	12.4 ± 0.6 (82)	13.6 ± 1.2 (90)

Samples used for calibration.
* Theoretical slope: $slope = \frac{C_{analyte}}{C_{standard}}$.

using TP CT, except for S1 (683 %), S2 (125 %) and S3 (61 %). For Pb, recovery values ranging from 89 to 104 % were obtained, except for sample S4 (132 %) (Tables 1 and 2). It was not possible to determine Pb in the S3 sample using LIBS and TP CT (or any other calibration strategy evaluated), since the concentration in this sample (0.72 ± 0.09 g kg^{-1}Pb) is lower than the standard error (SE) calculated for the LIBS method (Table 3). RSD values ≦17 % and ≦22 % were obtained in the determinations of Al and Pb, respectively, using TP CT.

For one-point and multi-line calibration, the samples of waste PCBs used as solid standards for Al and Pb were S5 (10.2 ± 1 g kg^{-1} Al) and S2 (11.6 ± 0.8 g kg^{-1} Pb), respectively. Good linear models were obtained, with excellent coefficients of determination for Al (R^2 ranging from 0.9790 to 0.9960) and Pb ($R^2 = 1$), using four atomic emission lines for Al and two lines for Pb.

For Al, recoveries values ranging from 78 to 109 % were obtained using OP MLC, except for S3 (57 %). For Pb, excellent recoveries values ranging from 83 to 103 % were obtained for all the samples analyzed (Tables 1 and 2). The values of the experimental slopes calculated for the linear models do not present significant differences from the theoretical slope (see Tables 1 and 2), providing good values of recoveries and demonstrating a satisfactory accuracy of the determinations. RSD values ≦9% and ≦25 % were obtained in the determinations of Al and Pb, respectively.

Using the single-sample calibration for Al determination, the emission lines and concentrations of Al and Pb for all the samples and standard were used, except for samples S1 and S3. For these two samples, the intensity of the emission lines of Al, Pb and Mg and the respective concentrations of these elements in the calibration standard were used. Recoveries values ranging from 82 to 116 % were obtained using SSC, except for S1 (220 %).

However, for Pb determination the emission intensity of the Pb, Al and Mg lines was used for all the waste PCB samples, together with the respective concentration values of these three elements in the calibration standard, except for sample S1. Only the Pb and Mg elements were monitored for this sample, together with their respective concentrations in the standard for correlation with the S1 sample. Recoveries values ranging from 81 to 116 % were obtained using SSC, except for S6 (71 %) - see Table 2. Using the SSC as a calibration strategy, RSD values of ≦21 % and ≦25 % were obtained in the determinations of Al and Pb, respectively.

Calibration free was another strategy evaluated for the determination of the analytes in the complex and refractory waste PCB samples. For CF it is necessary to obtain some physical parameters of the plasma, such as the temperature and electronic density, to verify the local thermodynamic equilibrium (LTE) (Ciucci et al., 1999; Tognoni et al., 2010).

For the calculation of the plasma temperature using the Saha-Boltzmann equation, the emission intensities of different lines in different ionization states (atomic and ionic) for Ba, Fe and Ti were used. The average plasma temperature was 8145 ± 227 K, considering the six waste PCB samples analyzed. The physical parameters of all the elements evaluated in the CF-LIBS are shown in Table S2, see Supplementary material.

The electron density was calculated from the collision-induced enlargement of the Balmer H_α line to the hydrogen. The average plasma electron density was 0.65 ± 0.29 10^{17} cm^{-3}, considering all the samples analyzed.

From these values obtained for the temperature and electronic density of the plasma (McWhirter criterion) (Tognoni et al., 2010) it is possible to assure the existence of LTE in all the samples analyzed. Thus, also taking into account stoichiometric ablation and using optically thin plasma, the concentration of Al and Pb in the samples can be determined.

For Al, excellent recovery values ranging from 90 to 106 % were

Table 2
Concentrations (mean ± standard deviation, g kg^{-1} Pb, n = 3) and recovery (%) for Pb in PCB samples determined by LIBS using matrix-matching calibration (MMC), two-point calibration transfer (TP CT), one-point and multi-line calibration (OP MLC), single-sample calibration (SSC) and calibration free (CF).

Sample	ICP OES	MMC	TP CT	OP MLC			SSC	CF
	g kg^{-1}			Theoretical slope*	Experimental Slope	g kg^{-1}		
S1	7.6 ± 0.6	7.8 ± 0.5 (102)	–	0.655	0.574 ± 0.089	6.7 ± 1 (88)	7.3 ± 0.6 (96)	5.9 ± 0.6 (78)
S2	11.6 ± 0.8	–	11.6 ± 0.8 (100)	–	–	–	–	14.1 ± 3.6 (121)
S3	0.72 ± 0.09	–	< 1.1	0.062	0.008 ± 0.002	< 1.2	< 1.7	< 2.7
S4	4.7 ± 0.9	–	6.2 ± 0.1 (132)	0.405	0.413 ± 0.029	4.8 ± 0.3 (103)	5.4 ± 0.3 (116)	5.5 ± 0.8 (116)
S5	10.7 ± 0.6	–	9.5 ± 2.1 (89)	0.922	0.766 ± 0.059	8.9 ± 0.7 (83)	8.6 ± 2.1 (81)	10.3 ± 2.2 (97)
S6	6.9 ± 1.6	7.6 ± 0.6 (111)	7.2 ± 0.9 (104)	0.595	0.611 ± 0.160	7.1 ± 1.8 (103)	4.9 ± 0.8 (71)	11.2 ± 2.2 (162)

-Samples used for calibration.
* Theoretical slope: $slope = \frac{C_{analyte}}{C_{standard}}$.

Table 3
Analytical performance parameters.

Parameter	Matrix-matching calibration	Two-point calibration transfer	Calibration free	One point and multi-line calibration		Single-sample calibration
Emission line (nm)	Al I 396.15 Pb I 405.78	Al I 396.15 Pb I 405.78	Several lines*	Al I 308.21 Al I 309.27 Al I 394.40 Al I 396.15	Pb I 363.95 Pb I 405.78	Al I 396.15 Pb I 405.78 Mg II 279.55
Normalization selected						
Al	Each individual spectrum is divided by its Euclidean norm and the average is calculated	Sum	Average of the spectra	Each individual spectrum is divided by its Euclidean norm, and the average is calculated		Each individual spectrum is divided by its Euclidean norm and the average is calculated
Pb	Average of the spectra	Sum	Average of the spectra	Average of the spectra		Average of the spectra
Signal type						
Al	Height	Height	Area	Height		Area
Pb	Height	Height	Area	Area		Height
SE (g kg^{-1})						
Al	1.6	12.2	2.4	5.6		2.9
Pb	0.76	1.1	2.7	1.2		1.7
RMSEP (g kg^{-1})						
Al	1.1	10.9	2.2	5.0		2.6
Pb	0.49	0.87	2.4	0.91		1.3
RSD range (%)						
Al	1 - 4	8 - 17	3 - 26	2 - 9		5 - 21
Pb	6 - 8	2 - 22	10 - 26	6 - 25		6 - 25

* see Table S2 in Electronic Supplementary Information (ESI).

obtained using CF for all the samples analyzed. The recovery values for Pb ranged from 78 to 121 %, except for S6 (162 %) - see Tables 2 and 3. RSD values of ≦26 % were obtained in Al and Pb determinations.

Some parameters related to the analytical performance and processing of the data used for each of the evaluated calibration strategies are shown in Table 3. It is interesting to observe how these parameters and the processing of the spectra can change depending on the calibration strategy (SE and RMSEP, for example). This is an indication of how matrix effects can be minimized by using appropriate data processing and calibration strategies.

From the equations of the linear regression of the validation set (ICP OES concentration reference *versus* LIBS predicted concentration plot), it is possible to see that, in almost all cases the values, considering the confidence interval, that the for the angular coefficient interval includes the number 1 and the intercept includes the number 0, see Figs. S1 and S2 in Supplementary material.

3.4. What is the best calibration strategy for the determination of Al and Pb in waste PCBs by LIBS?

In the plasma induced by LIBS, physicochemical phenomena and matrix effects occur during and due to laser-sample interaction, which in turn act on the atomic emission of the analytes, directly influencing the determination of Al and Pb in the samples of waste PCBs. However, with the data obtained from the evaluated calibration strategies, it can be seen that some of these strategies were very efficient, producing results with satisfactory accuracy. It can also be seen that the intrinsic properties of each analyte and of each calibration strategy directly influence the choice of the best calibration strategy.

The matrix-matching calibration gave excellent results for the determination of both analytes, with satisfactory recovery and RSD values. The MMC proved to be an efficient calibration strategy for the analysis of solids by LIBS, because since a set of waste PCB samples were used as calibration standards, the possible matrix effects are minimized when the physical properties of the calibration standards are close to those of the analyzed samples.

One limitation of the use of MMC in this study is that there is no set of certified reference materials (CRM) of waste PCBs, with reference values for Al and Pb, which could be used as solid standards when obtaining the calibration curve. Few initiatives are observed in the literature in order to produce a reference material for WEEE and a good example was published by Andrade et al., 2019a, 2019c. Thus, it was necessary to first obtain reference values of the analytes by analyzing a set of samples by a reference technique (in this study an ICP OES was used) for use as calibration standards for the LIBS method.

In some cases it is necessary to use vigorous conditions for the decomposition of the samples (high temperatures and high volume of concentrated acid, as in this study). This represents a limitation in the use of MMC in the absence of adequate sample preparation instruments and reference values of the analytes required for later use of the samples as solid calibration standards for LIBS.

Two-point calibration transfer requires only one calibration standard (CRM or one reference value sample) and one sample with unknown concentration to determine the analyte concentration. In this calibration strategy, each set of spectra obtained in the LIBS analysis for standard and sample are divided into two sets and subsequently summed (the number of spectra composing set 2 must have approximately two-fold the number of spectra of set 1) (Castro et al., 2020).

If the standard and the sample have similar physical properties (for efficient matrix-matching), and the concentration of the standard is close to that of the sample, TP CT minimizes the matrix effects and enables a high degree of accuracy when determining the analyte concentration in the sample, using only one calibration standard and one linear model with two points. Tables 1 and 2 show that good recoveries values (ranging from 80 to 120%) were obtained for Al and Pb, when the concentration of the standard used was close to the concentration of these analytes in the sample. For samples with concentrations very different from those of the standards used, there was an under- or over-estimation of the analyte concentration.

The TP CT is an interesting simple calibration strategy for LIBS analysis when there is not a great variability of analyte concentration in the analyzed samples and when a standard with an appropriate concentration similar to that of the samples is used. This situation can be achieved in routine analysis.

Another strategy evaluated was one-point and multi-line calibration - OP MLC. Excellent results were obtained for all the determinations of Al (except for sample S3) and Pb in the waste PCB samples by LIBS. The OP MLC requires only one calibration standard and several lines of analyte emission to obtain the linear model, which facilitates the implementation of this calibration strategy when few solid calibration

standards are available in the laboratory routine. Extra care has to be taken when using the OP MLC to remove lines with low intensity that present spectral interferences, since they can harm the linear models and consequently the measurement accuracy (Hao et al., 2018).

The determination of Al and Pb was also evaluated using the single-sample calibration method - SSC, which is another recent calibration strategy for LIBS that uses only one sample as standard (reference). In this strategy, a simple correlation calculation is necessary to determine the analyte concentration in the sample with unknown concentration (Yan et al., 2019). Using SSC, good recoveries values were obtained for both Al (except sample S1) and Pb (except sample S6).

For the use of SSC, the extent of the matrix effects between the sample and the standard should be considered the same for all elements present in the LIBS-induced plasma sample and the standard, since a direct correlation between the emission intensity and concentration of these elements will be used for the determination of the analyte. In addition, it should be considered that none of the emission lines used in the SSC (analyte emission lines and other elements used in the correlation) present spectral interferences, so that results can be obtained with satisfactory precision and recovery (Yan et al., 2019).

Finally, using calibration free (CF) it was possible to obtain good results with excellent accuracy for Al and Pb determinations, except for Al determination in sample S6, using direct analysis of waste PCB samples by LIBS.

Not requiring a calibration standard is an advantage of CF, which makes it an excellent calibration strategy for use in elemental determination by LIBS in complex samples difficult to decompose. However, the quality of data acquisition and treatment in CF is a critical factor for obtaining satisfactory results. It is necessary to ensure that the emission measurements are obtained in LTE in the plasma, that the physical parameters used are correctly obtained and calculated with precision, and that only emission lines free of spectral interferences and self-absorption are employed in *cf.* Despite it is a laborious calculation procedure, CF allows the achievement of good results.

In this context, it is evident that it is difficult to choose the best calibration strategy for the direct determination of Al and Pb in waste PCBs by LIBS, since it depends on many variables. However, a knowledge of the advantages and limitations of each calibration strategy and a consideration of some intrinsic characteristics (physicochemical properties) of the sample and the analytes can help in selecting the best strategy that efficiently overcomes matrix effects and enables determination with satisfactory accuracy.

Table 4 shows some characteristics, advantages and limitations of the five calibration strategies evaluated in this study. This may help the reader to choose and evaluate the best calibration strategy for LIBS that could be used in different analytical contexts.

It is worth noting that there seems to be a tendency in recently reported new calibration strategies for LIBS to use no or few calibration standards (only 1 or 2) and to increasingly explore the physicochemical parameters and correlations of concentrations of the species present in the plasma induced by laser in each sample analyzed. Examples are TP CT, OP MLC, SSC evaluated in this study and other strategies recently reported in the scientific literature such as MEC (Babos et al., 2018) and OP GSA (Babos et al., 2019; Castro et al., 2020) calibration.

3.5. Evaluation of Al and Pb concentrations in waste PCBs: economic and environmental questions

As mentioned previously, waste PCBs can contain high concentrations of valuable and toxic metals. The recycling and appropriate disposal of this waste can both provide a source of income and contribute to environmental protection. In this context, LIBS is an excellent analytical tool for the monitoring of metals in the waste and for the development of methods for the analysis of solids and the direct determination of Al and Pb present in PCBs.

Were calculated estimations of the commercial value (in US$) per

Table 4
Advantages and limitations of the calibration strategies evaluated in this study for the determination of Al and Pb in waste PCBs by LIBS.

Calibration Method	Number of emission lines	Number of reference standard	Advantages	Limitations	Reference
Matrix-matching calibration	One	Between four and five	Efficient matching of the physical properties of the calibration standards with the samples	Difficulty in obtaining a set of commercial CRM or samples with reference values	Vieira et al., 2018, this study
Calibration free	Several	Not necessary	Does not require the use of calibration curves or matrix-matched standards	Occurrences of lines with self-absorption and spectral interferences, which compromise the determinations, laborious calculations	Tognoni et al., 2010, this study
One point and multi-line calibration	Several	One	Requires only one calibration standard	The choice of the standard with appropriate concentration, and the use of emission lines with low sensitivities	Hao et al., 2018, this study
Two-point calibration transfer	One	One	Simplicity in data processing and measurement accuracy	The choice of the standard with appropriate concentration as samples, and standards should show little variability between analyte concentrations	Castro et al., 2020, this study
Single-sample calibration	The number of lines of analytes present in the sample shall be ≤ to the number of lines used of the elements in the standard	One	No calibration curve or linear calibration model required	Samples and standards with significant variability of physico-chemical properties and analyte emission lines and reference elements with spectral interferences	Yan et al. 2019, this study

ton of each of the six samples of waste PCBs analyzed, considering only the measured concentrations of Al (ranging from 3.1 to 55 g kg^{-1} Al) and Pb (ranging from 0.72 to 11.6 g kg^{-1} Pb). Considered the prices of 1803 US$/ tonne Al and 1919 US$/ tonne Pb quoted on the London Metal Exchange, the second world center for industrial metals trading (London Metal Exchange - LME, 2019).

The commercial value per tonne of the analyzed samples, considering only the Al and Pb contents, range from 20 to 121 US$/ tonne of waste PCB (prices for the S1 and S2 samples, respectively). These are good prices for samples that are considered waste, particularly as they apply only to two metals present in the waste. Other valuable metals may also be present and thus the market price per tonne of waste PCBs may be higher.

Concerning the environmental question, only one sample (S3 PCB, 0.072 % Pb) complies with the maximum concentration value allowed (0.1 % Pb) by weight in homogeneous materials for Pb in WEEE under Directive 2011/65/EU (RoHS, 2011). The Pb concentration in the other samples is between 5 and 12 times above the maximum allowed value according to the normative instruction. This is worrying, since if these samples are inappropriately disposed of they may be a source of contamination in the environment because of the Pb metal content.

4. Conclusion

The choice of the best calibration strategy for the direct analysis of waste PCBs for LIBS when aiming to determine Al and Pb depends on the intrinsic properties of these analytes and samples, as well as the ability of each of the calibration strategies to overcome the various matrix effects. Of the five calibration strategies evaluated, MMC and CF generally allowed accurate values to be obtained for both analytes in all the samples. The LIBS technique presented itself as an excellent analytical tool in the fast, simple and direct monitoring of recyclable metals such as Al and Pb and also of potential for environmental contamination such as Pb, originating from WEEE (waste PCB). The Pb concentrations determined are of concern as only one sample was in accordance with the Directive 2011/65/EU.

CRediT authorship contribution statement

Diego Victor Babos: Conceptualization, Data curation, Formal analysis, Validation, Visualization, Writing - original draft, Writing - review & editing. **Andrés Cruz-Conesa:** Conceptualization, Data curation, Formal analysis, Validation, Visualization, Writing - original draft, Writing - review & editing. **Edenir Rodrigues Pereira-Filho:** Conceptualization, Formal analysis, Resources, Supervision, Visualization, Writing - review & editing. **Jesús M. Anzano:** Formal analysis, Funding acquisition, Project administration, Resources, Supervision, Visualization, Writing - review & editing.

Declaration of Competing Interest

The authors declare that they have no known competing financial interests or personal relationships that could have appeared to influence the work reported in this paper.

Acknowledgements

The authors are grateful to the Conselho Nacional de Desenvolvimento Científico e Tecnológico (CNPq – grants 141311/2017-7, 305637/2015-0) for fellowships and financial support. This study was financed in part by the Coordenação de Aperfeiçoamento de Pessoal de Nível Superior - Brasil (CAPES) - Finance Code 001, the Government of Aragon, the Servicio General de Apoyo a la Investigación-SAI, UNIZAR & the European Base Found, proposal E49_20R, and the Spanish Ministry of Science and Innovation, proposal #CTM2017-82929-R. The authors are also grateful to the São Paulo Research Foundation (FAPESP, grants 2016/01513-0). We would like to thank MSc. Daniel F. Andrade and Dr. Raquel C. Machado for donating the electronic waste reference material.

Appendix A. Supplementary data

Supplementary material related to this article can be found, in the online version, at doi:https://doi.org/10.1016/j.jhazmat.2020.122831.

References

Andrade, D.F., Machado, R.C., Pereira-Filho, E.R., 2019a. Proposition of electronic waste as a reference material – part 2: homogeneity, stability, characterization, and uncertainties. J. Anal. At. Spectrom. 34, 2402–2410. https://doi.org/10.1039/C9JA00284G.

Andrade, D.F., Fortunato, F.M., Pereira-Filho, E.R., 2019b. Calibration strategies for determination of the In content in discarded liquid crystal displays (LCD) from mobile phones using laser-induced breakdown spectroscopy (LIBS). Anal. Chim. Acta 1061, 42–49. https://doi.org/10.1016/j.aca.2019.02.038.

Andrade, D.F., Machado, R.C., Bacchi, M., Pereira-Filho, E.R., 2019c. Proposition of electronic waste as a reference material – part 1: sample preparation, characterization and chemometric evaluation. J. Anal. At. Spectrom. 34, 2394–2401. https://doi.org/10.1039/C9JA00283A.

Andrade, D.F., Romanelli, J.P., Pereira-Filho, E.R., 2019d. Past and emerging topics related to electronic waste management: top countries, trends, and perspectives. Environ. Sci. Pollut. Res. 26, 17135–17151. https://doi.org/10.1007/s11356-019-05089-y.

Andrade, D.F., Pereira-Filho, E.R., Amarasiriwardena, D., 2020. Current trends in laser-induced breakdown spectroscopy: a tutorial review. Appl. Spectrosc. Rev. https://doi.org/10.1080/05704928.2020.1739063.

Aquino, F.W.B., Paranhos, C.M., Pereira-Filho, E.R., 2016. Method for the production of acrylonitrile–butadiene–styrene (ABS) and polycarbonate (PC)/ABS standards for direct Sb determination in plastics from e-waste using laser-induced breakdown spectroscopy. J. Anal. At. Spectrom. 31, 1228–1233. https://doi.org/10.1039/C6JA00038J.

Arshadi, M., Yaghmaei, S., Mousavi, S.M., 2018. Recycling organics from non-metallic fraction of waste printed circuit boards by a novel conical surface triboelectric separator. Resour. Conserv. Recy. 139, 298–306. https://doi.org/10.1016/j.resconrec.2018.08.013.

Augusto, A.S., Castro, J.P., Sperança, M.A., Pereira-Filho, E.R., 2019. Combination of multi-energy calibration (MEC) and laser-induced breakdown spectroscopy (LIBS) for dietary supplements analysis and determination of Ca, Mg and K. J. Braz. Chem. Soc. 30, 804–812. https://doi.org/10.21577/0103-5053.20180211.

Babos, D.V., Virgilio, A., Costa, V.C., Donati, G.L., Pereira-Filho, E.R., 2018. Multi-energy calibration (MEC) applied to laser-induced breakdown spectroscopy (LIBS). J. Anal. At. Spectrom. 33, 1753–1762. https://doi.org/10.1039/C8JA00109J.

Babos, D.V., Barros, A.I., Nóbrega, J.A., Pereira-Filho, E.R., 2019. Calibration strategies to overcome matrix effects in laser-induced breakdown spectroscopy: direct calcium and phosphorus determination in solid mineral supplements. Spectrochim. Acta B 155, 90–98. https://doi.org/10.1016/j.sab.2019.03.010.

Baldé, C., Forti, V., Gray, V., Kuehr, R., Stegmann, P., 2017. The global E-waste monitor 2017: quantities, flows. Resour. Nat. Resour. Manag.

Carvalho, R.R.V., Coelho, J.A.O., Santos, J.M., Aquino, F.W.B., Carneiro, R.L., Pereira-Filho, E.R., 2015. Laser-induced breakdown spectroscopy (LIBS) combined with hyperspectral imaging for the evaluation of printed circuit board composition. Talanta 134, 278–283. https://doi.org/10.1016/j.talanta.2014.11.019.

Carvalho, G.G.A., Guerra, M.B.B., Adame, A., Nomura, C.S., Oliveira, P.V., Carvalho, H.W.P., Santos Jr, D., Nunes, L.C., Krug, F.J., 2018a. Recent advances in LIBS and XRF for the analysis of plants. J. Anal. At. Spectrom. 33, 919–944. https://doi.org/10.1039/C7JA00293A.

Carvalho, A.A.C., Leme, F.O., Luz, M.S., Oliveira, P.V., Nomura, C.S., 2018b. Internal standard fused glass beads for high silicon content sample analysis by laser-induced breakdown spectrometry. J. Anal. At. Spectrom. 33, 1243–1250. https://doi.org/10.1039/C8JA00112J.

Carvalho, A.A.C., Cozer, L.A., Luz, M.S., Nunes, L.C., Rocha, F.R.P., Nomura, C.S., 2019. Multi-energy calibration and sample fusion as alternatives for quantitative analysis of high silicon content samples by laser-induced breakdown spectrometry. J. Anal. At. Spectrom. 34, 1701–1707. https://doi.org/10.1039/C9JA00149B.

Castro, J.P., Pereira-Filho, E.R., 2016. Twelve different types of data normalization for the proposition of classification, univariate and multivariate regression models for the direct analyses of alloys by laser-induced breakdown spectroscopy (LIBS). J. Anal. At. Spectrom. 31, 2005–2014. https://doi.org/10.1039/C6JA00224B.

Castro, J.P., Babos, D.V., Pereira-Filho, E.R., 2020. Calibration strategies for the direct determination of rare earth elements in hard disk magnets using laser-induced breakdown spectroscopy. Talanta 208, 120443. https://doi.org/10.1016/j.talanta.2019.120443.

Cavalcanti, G.H., Teixeira, D.V., Legnaioli, S., Lorenzetti, G., Pardini, L., Palleschi, V., 2013. One-point calibration for calibration-free laser-induced breakdown spectroscopy quantitative analysis. Spectrochim. Acta B 87, 51–56. https://doi.org/10.1016/j.sab.2013.05.016.

Ciucci, A., Corsi, M., Palleschi, V., Rastelli, S., Salvetti, A., Tognoni, E., 1999. New

procedure for quantitative elemental analysis by laser-induced plasma spectroscopy. Appl. Spectrosc. 53, 960–964. https://www.osapublishing.org/as/abstract.cfm?URI=as-53-8-960.
Costa, V.C., Castro, J.P., Andrade, D.F., Babos, D.V., Garcia, J.A., Sperança, M.A., Catelani, T.A., Pereira-Filho, E.R., 2018a. Laser-induced breakdown spectroscopy (LIBS) applications in the chemical analysis of waste electrical and electronic equipment (WEEE). Trends Analyt. Chem. 108, 65–73. https://doi.org/10.1016/j.trac.2018.08.003.
Costa, V.C., Babos, D.V., Aquino, F.W.B., Virgilio, A., Amorim, F.A.C., Pereira-Filho, E.R., 2018b. Direct determination of Ca, K and Mg in cassava flour samples by laser-induced breakdown spectroscopy (LIBS). Food Anal. Methods 11, 1886–1896. https://doi.org/10.1007/s12161-017-1086-9.
Costa, V.C., Augusto, A.S., Castro, J.P., Machado, R.C., Andrade, D.F., Babos, D.V., Sperança, M.A., Gamela, R.R., Pereira-Filho, E.R., 2019. Laser induced-breakdown spectroscopy (LIBS): history, fundamentals, applications and potentialities. Quim. Nova 42, 527–545. https://doi.org/10.21577/0100-4042.20170325.
Cremers, D.A., Radziemski, L.J., 2006a. Handbook of Laser-Induced Breakdown Spectroscopy. Wiley, London.
Cremers, D.A., Radziemski, L.J., 2006b. History and fundamentals of LIBS. In: Miziolek, A.W., Palleschi, V., Schechter, I. (Eds.), Laser-Induced Breakdown Spectroscopy. Cambridge University Press, New York.
Derringer, G., Suich, R., 1980. Simultaneous optimization of several response variables. Int. J. Qual. Assur. Eng. Technol. Educ. 12, 214–219. https://doi.org/10.1080/00224065.1980.11980968.
Eppler, A.S., Cremers, D.A., Hickmott, D.D., Ferris, M.J., Koskelo, A.C., 1996. Matrix effects in the detection of Pb and Ba in soils using laser-induced breakdown spectroscopy. Appl. Spectrosc. 50, 1175–1181. https://doi.org/10.1366/0003702963905123.
Fortunato, F.M., Catelani, T.A., Pomares-Alfonso, M.S., Pereira-Filho, E.R., 2019. Application of multi-energy calibration for determination of chromium and nickel in nickeliferous ores by laser-induced breakdown spectroscopy. Anal. Sci. 35, 165–168. https://doi.org/10.2116/analsci.18P286.
Gomes, M.S., de Carvalho, G.G.A., Junior, D.S., Krug, F.J., 2013. A novel strategy for preparing calibration standards for the analysis of plant materials by laser-induced breakdown spectroscopy: a case study with pellets of sugar cane leaves. Spectrochim. Acta B 86, 137–141. https://doi.org/10.1016/j.sab.2013.03.009.
Gondal, M.A., Seddigi, Z.S., Nasr, M.M., Gondal, B., 2010. Spectroscopy detection of health hazardous contaminants in lipstick using Laser induced breakdown spectroscopy. J. Hazard. Mater. 175, 726–732. https://doi.org/10.1016/j.jhazmat.2009.10.069.
Hahn, D.W., Omenetto, N., 2010. Laser-induced breakdown spectroscopy (LIBS), part I: review of basic diagnostics and plasma-particle interactions: still-challenging issues within the analytical plasma community. Appl. Spectrosc. 64, 335–366. https://doi.org/10.1366/000370210793561691. 2010.
Hahn, D.W., Omenetto, N., 2012. Laser-induced breakdown spectroscopy (LIBS), part II: review of instrumental and methodological approaches to material analysis and applications to different fields. Appl. Spectrosc. 66, 347–419. https://doi.org/10.1366/11-06574.
Hao, Z.Q., Liu, L., Zhou, R., Ma, Y.W., Li, X.Y., Guo, L.B., Lu, Y.F., Zeng, X.Y., 2018. One-point and multi-line calibration method in laser-induced breakdown spectroscopy. Opt. Express 26, 22926–22933. https://doi.org/10.1364/OE.26.022926.
Kim, G., Kwak, J., Kim, K.R., Lee, H., Kim, K.W., Yang, H., Park, K., 2013. Rapid detection of soils contaminated with heavy metals and oils bylaser induced breakdown spectroscopy (LIBS). J. Hazard. Mater. 263, 754–760. https://doi.org/10.1016/j.jhazmat.2013.10.041.
Lasheras, R.J., Bello-Gálvez, C., Rodríguez-Celis, E.M., Anzano, J., 2011. Discrimination of organic solid materials by LIBS using methods of correlation and normalized coordinates. J. Hazard. Mater. 192, 704–713. https://doi.org/10.1016/j.jhazmat.2011.05.074.
Lasheras, R.J., Bello-Gálvez, C., Anzano, J.M., 2013. Quantitative analysis of oxide materials by laser-induced breakdown spectroscopy with argon as an internal standard. Spectrochim. Acta B 82, 65–70. https://doi.org/10.1016/j.sab.2013.01.005.
Lednev, V.N., Grishin, M.Y., Sdvizhenskii, P.A., Asyutin, R.D., Tretyakov, R.S., Stavertiy, A.Ya., Pershin, S.M., 2019. Sample temperature effect on laser ablation and analytical capabilities of laser induced breakdown spectroscopy. J. Anal. At. Spectrom. 34, 607–615. https://doi.org/10.1039/C8JA00348C.
Li, T., Hou, Z., Fu, Y., Yu, J., Gu, W., Wang, Z., 2019. Correction of self-absorption effect in calibration-free laser-induced breakdown spectroscopy (CF-LIBS) with blackbody radiation reference. Anal. Chim. Acta 1058, 39–47. https://doi.org/10.1016/j.aca.2019.01.016.
London Metal Exchange - LME. https://www.lme.com/, 2019.
Miziolek, W., Palleschi, V., Schechter, I., 2006. Laser Induced Breakdown Spectroscopy. Cambridge University Press, Cambridge.
Morais, C.P., Barros, A.I., Bechlin, M.A., Silva, T.V., Santos Júnior, D., Senesi, G.S., Crespi, M.S., Ribeiro, C.A., Gomes Neto, J.A., Ferreira, E.C., 2018. Laser-induced breakdown spectroscopy determination of K in biochar-based fertilizers in the presence of easily ionizable element. Talanta 188, 199–202. https://doi.org/10.1016/j.talanta.2018.05.089.
NIST electronic database, (2020) https://www.nist.gov/pml/atomic-spectra-database.
Pereira, F.M.V., Pereira-Filho, E.R., 2018. Application of free computational program in experimental design: a tutorial. Quim. Nova 41, 1061–1071. https://doi.org/10.21577/0100-4042.20170254.
Perkins, D.N., Drisse, M.-N.B., Nxele, T., Sly, P.D., 2014. E-waste: a global hazard. Ann. Glob. Health 80, 286–295. https://doi.org/10.1016/j.aogh.2014.10.001.
Popov, A.M., Zaytsev, S.M., Seliverstova, I.V., Zakuskin, A.S., Labutin, T.A., 2018. Matrix effects on laser-induced plasma parameters for soils and ores. Spectrochim. Acta B 148, 205–210. https://doi.org/10.1016/j.sab.2018.07.005.
Restriction of Hazardous Substances Directive (RoHS) Directive 2011/65/EU Restriction of the Use of Certain Hazardous Substances in Electrical and Electronic Equipment, 2011. The European Parliament and the Council of the E. Union. http://data.europa.eu/eli/dir/2011/65/oj.
Rezaei, A.H., Keshavarz, M.H., Tehrani, M.K., Darbani, S.M.R., 2018. Quantitative analysis for the determination of aluminum percentage and detonation performance of aluminized plastic bonded explosives by laser-induced breakdown spectroscopy. Laser Phys. 28, 065605. https://doi.org/10.1088/1555-6611/aab660.
Sattar, H., Sun, L., Imran, M., Hai, R., Wu, D., Ding, H., 2019. Effect of parameter setting and spectral normalization approach on study of matrix effect by laser induced breakdown spectroscopy of Ag–Zn binary composites. Plasma Sci. Technol. 21, 034019. https://doi.org/10.1088/2058-6272/aaf712.
Sperança, M.A., Pomares-Afonso, M.S., Pereira-Filho, E.R., 2018. Analysis of Cuban nickeliferous minerals by laser-induced breakdown spectroscopy (LIBS): non-conventional sample preparation of powder samples. Anal. Methods 10, 533–540. https://doi.org/10.1039/C7AY02521A.
Sperança, M.A., Andrade, D.F., Castro, J.P., Pereira-Filho, E.R., 2019. Univariate and multivariate calibration strategies in combination with laser-induced breakdown spectroscopy (LIBS) to determine Ti on sunscreen: a different sample preparation procedure. Opt. Laser Technol. 109, 648–653. https://doi.org/10.1016/j.optlastec.2018.08.056.
Takahashi, T., Thornton, B., 2017. Quantitative methods for compensation of matrix effects and self-absorption in Laser induced Breakdown Spectroscopy signals of solids. Spectrochim. Acta B 138, 31–42. https://doi.org/10.1016/j.sab.2017.09.010.
Tansel, B., 2017. From electronic consumer products to e-wastes: global outlook, waste quantities, recycling challenges. Environ. Int. 98, 35–45. https://doi.org/10.1016/j.envint.2016.10.002.
Tognoni, E., Cristoforetti, G., Legnaioli, S., Palleschi, V., 2010. Calibration-free laser-induced breakdown spectroscopy: state of the art. Spectrochim. Acta B 65, 1–14. https://doi.org/10.1016/j.sab.2009.11.006.
Vieira, A.L., Silva, T.V., de Sousa, F.S.I., Senesi, G.S., Santos Júnior, D., Ferreira, E.C., Gomes Neto, J.A., 2018. Determinations of phosphorus in fertilizers by spark discharge-assisted laser-induced breakdown spectroscopy. Microchem. J. 139, 322–326. https://doi.org/10.1016/j.microc.2018.03.011.
Wu, C., Sun, D.X., Su, M.G., Yin, Y.P., Han, W.W., Lu, Q.F., Dong, C.Z., 2019. Quantitative analysis of Pb in soil samples by laser-induced breakdown spectroscopy with a simplified standard addition method. J. Anal. At. Spectrom. 34, 1478–1484. https://doi.org/10.1039/c9ja00059c.
Yamane, L.H., de Moraes, V.T., Espinosa, D.C.R., Tenório, J.A.S., 2011. Recycling of WEEE: characterization of spent printed circuit boards from mobile phones and computers. Waste Manage. 31, 2553–2558. https://doi.org/10.1016/j.wasman.2011.07.006.
Yan, R., Tang, Y., Zhu, Z., Hao, Z., Li, J., Yu, H., Yu, Y., Guo, L., Zeng, X., Lu, Y., 2019. Accuracy improvement of quantitative analysis for major elements in laser-induced breakdown spectroscopy using single-sample calibration. Anal. Chim. Acta 1064, 11–16. https://doi.org/10.1016/j.aca.2019.02.056.
Yang, J., Wang, H., Zhang, G., Bai, X., Zhao, X., He, Y., 2019. Recycling organics from non-metallic fraction of waste printed circuit boards by a novel conical surface triboelectric separator. Resour. Conserv. Recy. 146, 264–269. https://doi.org/10.1016/j.resconrec.2019.03.008.
Yi, R.X., Guo, L.B., Zou, X.H., Li, J.M., Hao, Z.Q., Yang, X.Y., Li, X.Y., Zeng, X.Y., Lu, Y.F., 2016. Background removal in soil analysis using laser- induced breakdown spectroscopy combined with standard addition method. Opt. Express 24, 2607–2618. https://doi.org/10.1364/OE.24.002607.

Electronic Supplementary Information (ESI):

Direct determination of Al and Pb in waste printed circuit boards (PCB) by Laser-induced breakdown spectroscopy (LIBS): evaluation of calibration strategies and economic - environmental questions

Diego Victor Babos,[1,2] Andrés Cruz-Conesa,[1] Edenir Rodrigues Pereira-Filho[2] and Jesús M. Anzano[1*]

[1]Laser Laboratory, Chemistry & Environment Group, Department of Analytical Chemistry, Faculty of Sciences, University of Zaragoza, Pedro Cerbuna 12, 50009 Zaragoza, Spain

[2]Group of Applied Instrumental Analysis, Department of Chemistry, Federal University of São Carlos, São Carlos, São Paulo State, 13565-905, Brazil

*Corresponding author:
Jesús M. Anzano
Laser Laboratory, Chemistry & Environment Group, Department of Analytical Chemistry, Faculty of Sciences, University of Zaragoza, Pedro Cerbuna 12, 50009 Zaragoza, Spain
Phone number: +34 9 7676 2684
E-mail: janzano@unizar.es (J. Anzano).

This ESI contains:

- 2 Tables
- 2 Figures

Table S1. Matrix of experiments showing the variables evaluated for optimizing delay time, gate width and laser pulse energy in LIBS determinations. The overall desirability (OD) was used as experimental response.

Experiment		Delay time (μs)		Gate width (μs)		Laser pulse energy (mJ)		OD
		Real	Coded	Real	Coded	Real	Coded	
Full factorial design 2^3	1	0.4	-1	1.0	-1	25	-1	0.49
	2	2.0	1	1.0	-1	25	-1	0.73
	3	0.4	-1	3.0	1	25	-1	0.67
	4	2.0	1	3.0	1	25	-1	0.55
	5	0.4	-1	1.0	-1	42.5	1	0.57
	6	2.0	1	1.0	-1	42.5	1	0.62
	7	0.4	-1	3.0	1	42.5	1	0.30
	8	2.0	1	3.0	1	42.5	1	0.89
Central point	9	1.2	0	2.0	0	35	0	0.44
	10	1.2	0	2.0	0	35	0	0.56
	11	1.2	0	2.0	0	35	0	0.77
	12	1.2	0	2.0	0	35	0	0.61
	13	1.2	0	2.0	0	35	0	0.62
Axial point	14	0.01	-1.49	2.0	0	35	0	0.41
	15	2.54	1.68	2.0	0	35	0	0.74
	16	1.2	0	0.32	-1.68	35	0	0.63
	17	1.2	0	3.68	1.68	35	0	0.64
	18	1.2	0	2.0	0	20	-1.68	0.69
	19	1.2	0	2.0	0	47.5	1.68	0.69

Table S2. Spectroscopic parameters λ (wavelength), E_i (energy of the lower level of transition), E_k (energy of the upper level of transition), A_{ki} (transition probability), and g_k (degeneracy factor of state k) of atomic (I) and ionic (II) lines used in the CF-LIBS calculation. Source: NIST DataBase.

Elements	Line	λ (nm)	E_i (eV)	E_k (eV)	g_k	A_{ki} .10^8 (s^{-1})
Al	I	309.271	0.01	4.02	6	0.730
Al	I	783.531	4.02	5.60	6	0.057
Al	I	783.613	4.02	5.60	6	0.004
Ba	II	614.172	0.70	2.72	4	0.412
Ba	II	649.690	0.60	2.51	2	0.130
Ba	I	705.994	1.19	2.95	9	0.500
C	I	247.856	2.68	7.68	3	0.180
Ca	II	317.933	3.03	7.05	6	3.600
Ca	I	558.876	40.05	43.51	7	0.409
Ca	I	612.222	1.89	3.91	3	0.287
Ca	I	616.217	1.90	3.91	3	0.477
Co	I	356.938	0.92	4.40	8	1.500
Cr	II	283.563	1.55	5.92	12	2.000
Cr	I	360.533	0.00	3.44	5	1.620
Cu	I	510.554	1.39	3.82	4	0.020
Cu	I	521.820	3.82	6.19	6	1.220
Cu	I	578.213	1.64	3.79	2	0.019
Fe	II	239.924	0.08	5.25	6	1.400
Fe	I	373.532	0.86	4.18	7	0.270
Fe	I	382.042	0.86	4.10	9	0.668
Fe	I	404.581	1.48	4.55	9	0.863
Fe	I	438.354	1.48	4.31	11	0.500
Mg	I	518.361	2.72	5.11	3	0.561
Mn	II	293.306	1.17	5.40	3	2.040
Ni	I	341.476	0.03	3.66	9	0.550
Ni	I	351.505	0.11	3.64	7	0.420
Ni	I	352.454	0.03	3.54	5	1.000
Pb	I	405.780	1.32	4.38	3	0.912
Sb	I	259.805	1.06	5.83	2	0.210
Si	I	288.158	0.78	5.08	3	1.890
Sn	I	317.050	0.42	4.33	3	0.838
Ti	II	334.941	0.05	3.75	12	1.680
Ti	I	498.173	0.85	3.34	13	0.660
Ti	I	499.107	0.84	3.34	11	0.584
Zn	I	481.053	4.08	6.65	3	0.700

Figure S1. Comparison of Al concentrations determined in waste PCBs samples by the proposed LIBS method using different calibration strategies (a- MMC, b- TP CT, c- OP MLC, d- SSC and e- CF) and the ICP OES reference method. The SE and RMSEP were added as lines parallel to the X-axis.

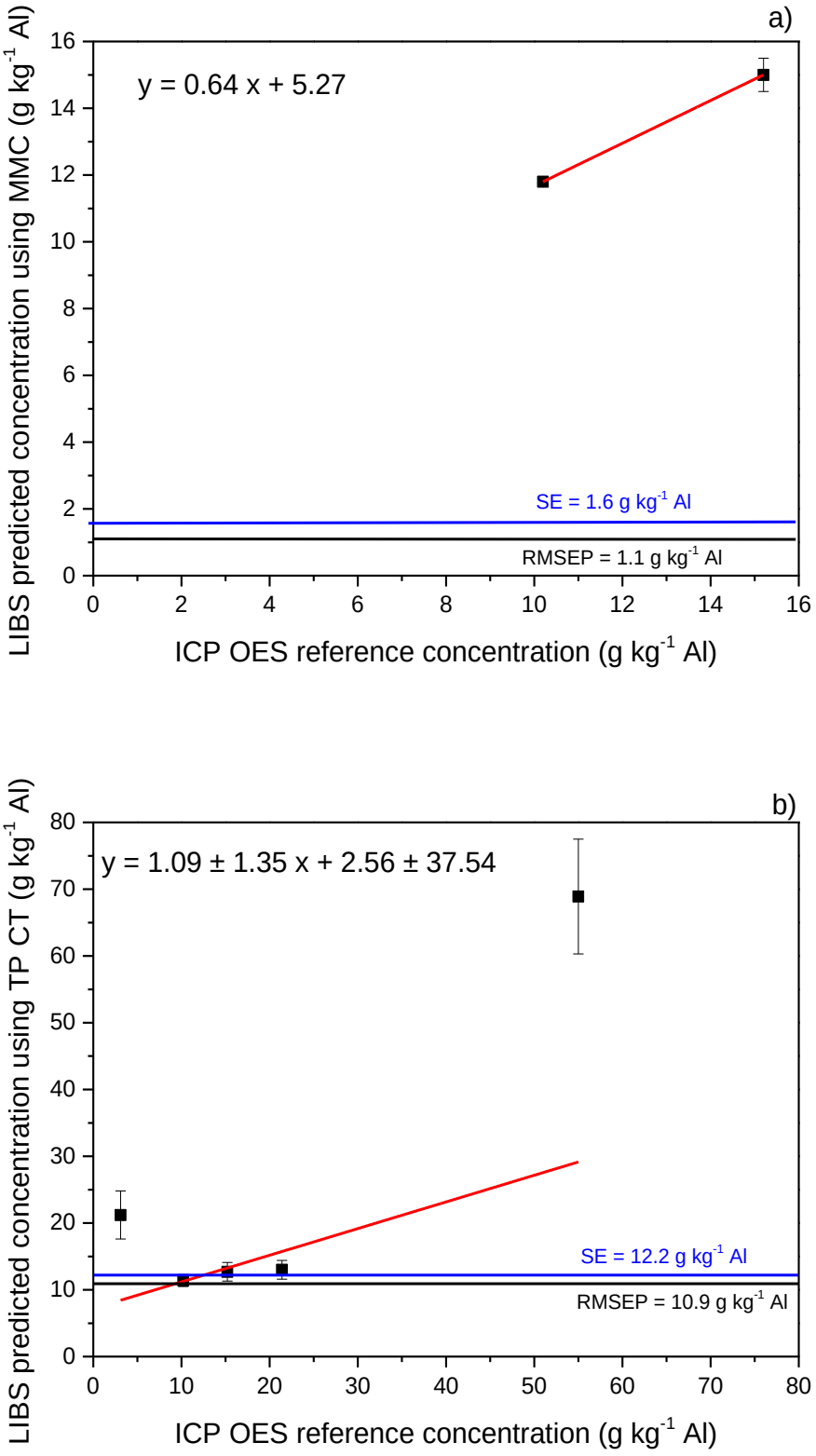

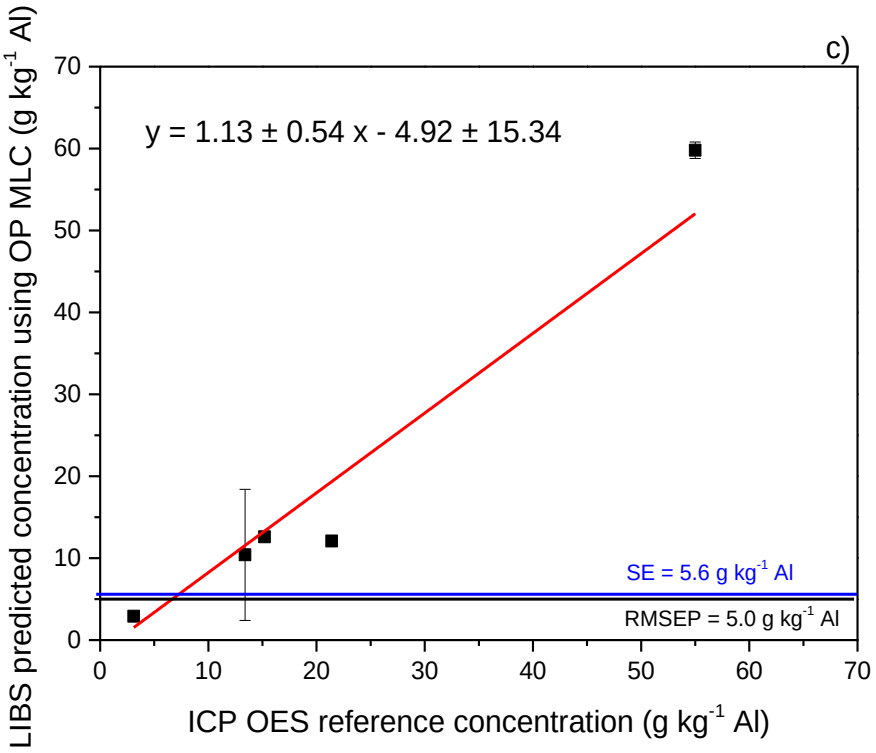
c)
y = 1.13 ± 0.54 x - 4.92 ± 15.34
SE = 5.6 g kg-1 Al
RMSEP = 5.0 g kg-1 Al
LIBS predicted concentration using OP MLC (g kg-1 Al)
ICP OES reference concentration (g kg-1 Al)
0
10
20
30
40
50
60
70

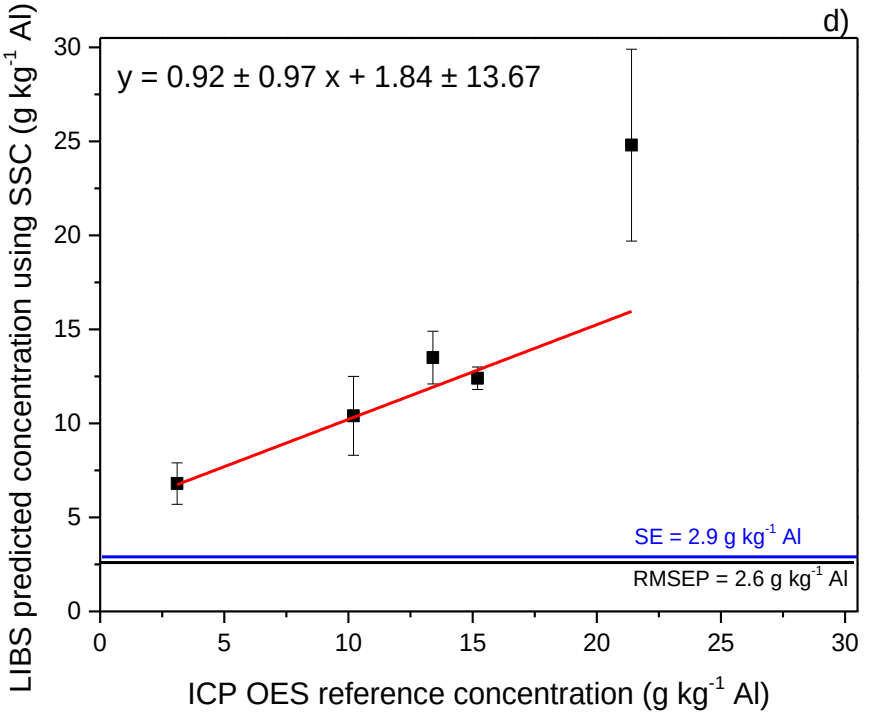
d)
y = 0.92 ± 0.97 x + 1.84 ± 13.67
SE = 2.9 g kg-1 Al
RMSEP = 2.6 g kg-1 Al
LIBS predicted concentration using SSC (g kg-1 Al)
ICP OES reference concentration (g kg-1 Al)
0
5
10
15
20
25
30

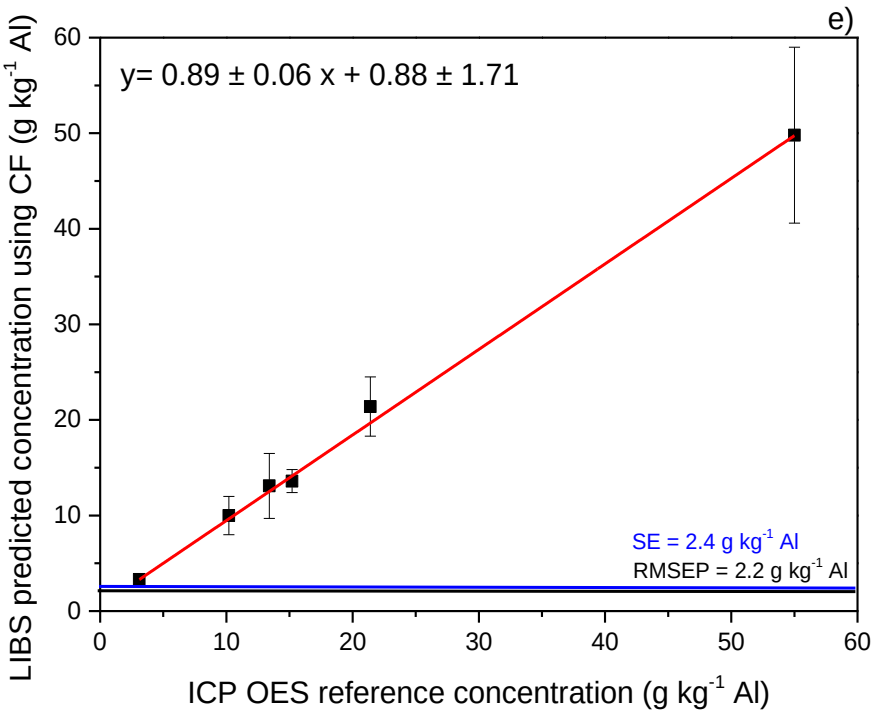
e)
y= 0.89 ± 0.06 x + 0.88 ± 1.71
SE = 2.4 g kg-1 Al
RMSEP = 2.2 g kg-1 Al
LIBS predicted concentration using CF (g kg-1 Al)
ICP OES reference concentration (g kg-1 Al)
0
10
20
30
40
50
60

Figure S2. Comparison of Pb concentrations determined in waste PCBs samples by the proposed LIBS method using different calibration strategies (a- MMC, b- TP CT, c- OP MLC, d- SSC and e- CF) and the ICP OES reference method. The SE and RMSEP were added as lines parallel to the X-axis.

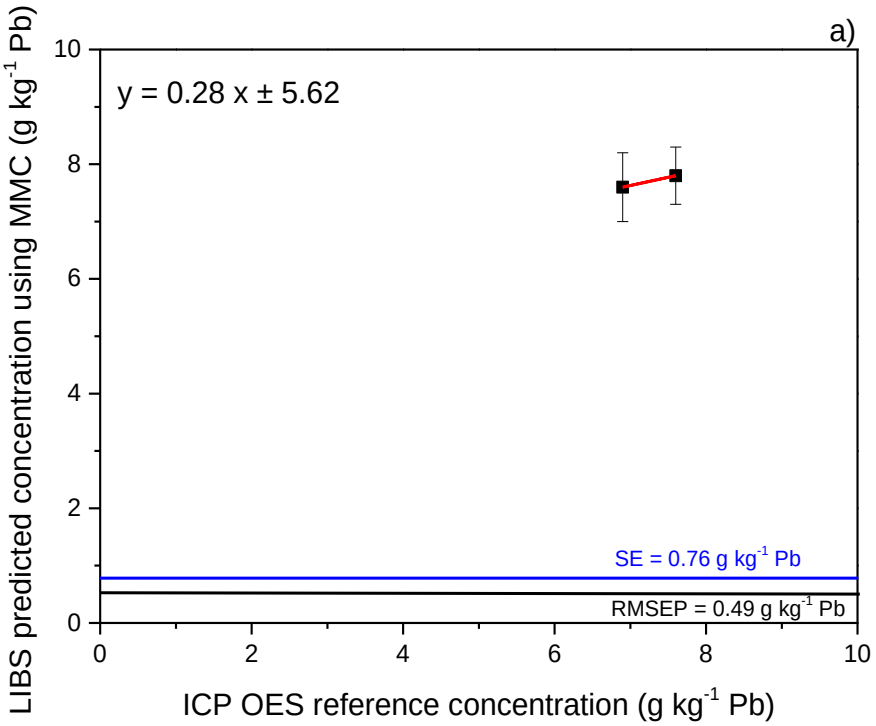

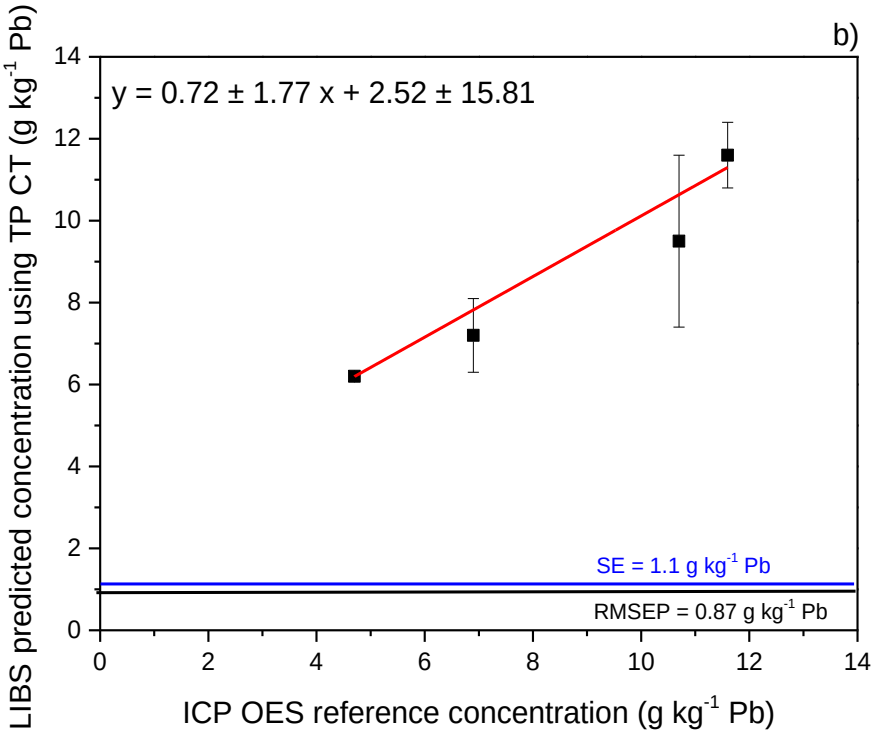

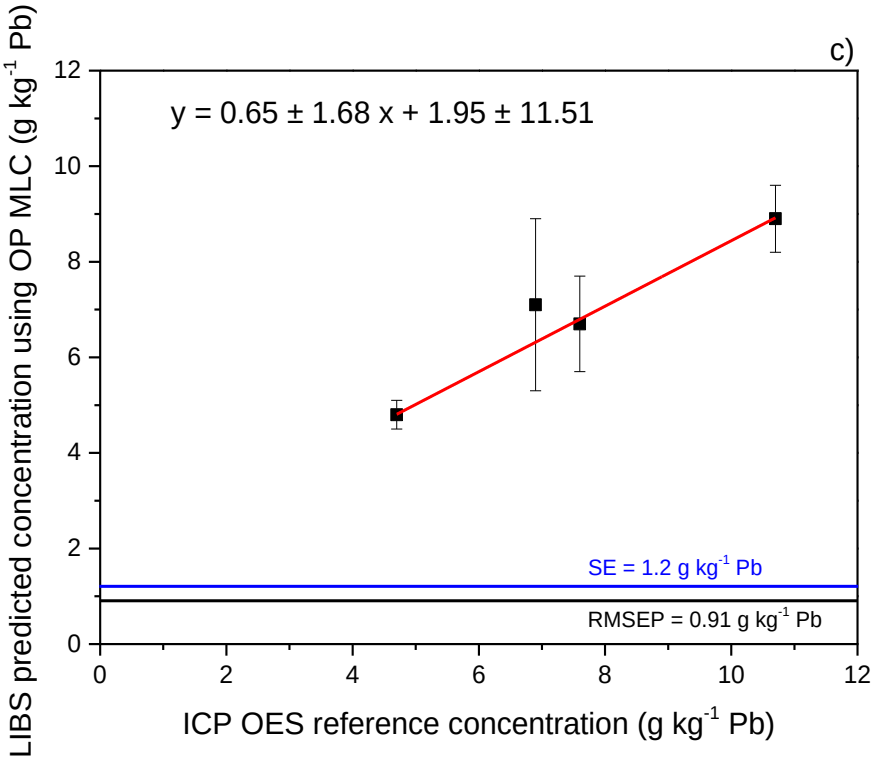
c)
y = 0.65 ± 1.68 x + 1.95 ± 11.51
SE = 1.2 g kg-1 Pb
RMSEP = 0.91 g kg-1 Pb
LIBS predicted concentration using OP MLC (g kg-1 Pb)
ICP OES reference concentration (g kg-1 Pb)
0
2
4
6
8
10
12

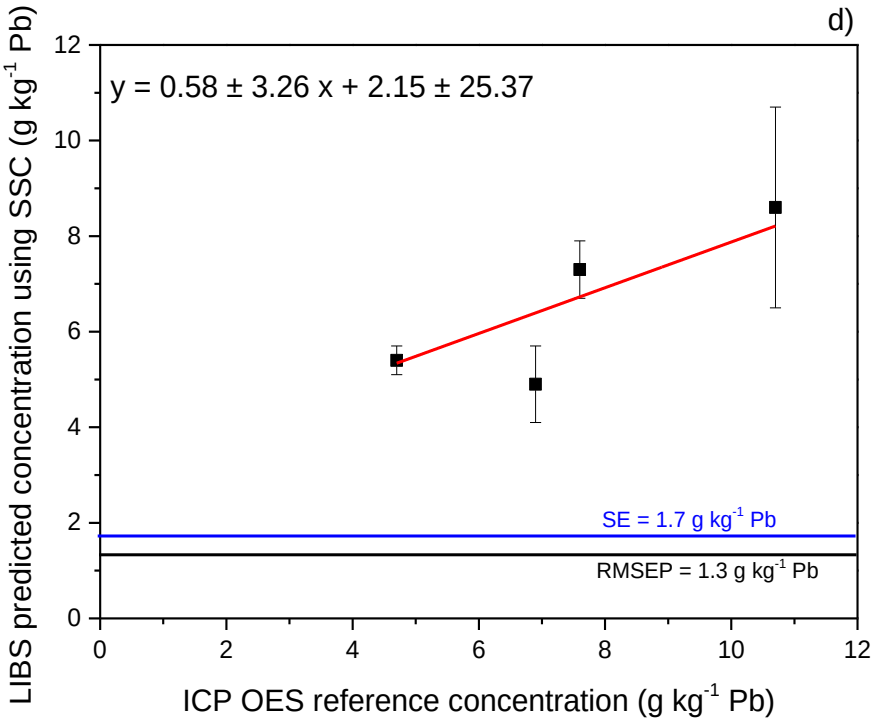
d)
y = 0.58 ± 3.26 x + 2.15 ± 25.37
SE = 1.7 g kg-1 Pb
RMSEP = 1.3 g kg-1 Pb
LIBS predicted concentration using SSC (g kg-1 Pb)
ICP OES reference concentration (g kg-1 Pb)
0
2
4
6
8
10
12

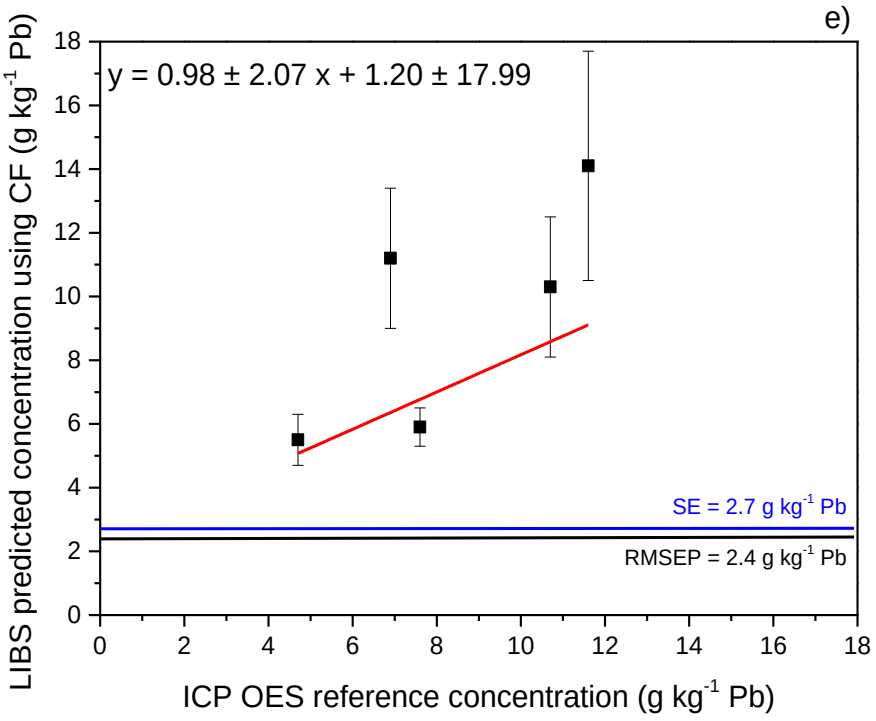
e)
y = 0.98 ± 2.07 x + 1.20 ± 17.99
SE = 2.7 g kg-1 Pb
RMSEP = 2.4 g kg-1 Pb
LIBS predicted concentration using CF (g kg-1 Pb)
ICP OES reference concentration (g kg-1 Pb)
0
2
4
6
8
10
12
14
16
18

Chapter 4 – Conclusion

Considering the advantages and limitations of the various calibration strategies (univariate and multivariate) evaluated and associated with the adequate preparation of the solids calibration standards, it was possible to overcome one of the main difficulties of the direct analysis of solids: the matrix effects.

In the direct determination of Ca and P in mineral supplements for cattle by WD XRF, the preparation of the calibration standards by matrix-matching enabled determinations with satisfactory precision (RSD ≤3%) and accuracy for analytes. It is possible to prepare standards for the determination of Ca using only a reference material diluted in constituents of the sample matrix (NaCl and Na_2CO_3) or using a set of reference materials. However, for P it is mandatory to use a set of reference materials as standards.

In speciation analysis and direct determination of S in mineral supplements for cattle by WD XRF, the strong matrix and chemical effects can be overcome by preparing solid standard for matrix-matching using standards that contain the predominant specie of S in the samples and employing the PLS regression and Matrix-matching calibration - MMC. For samples containing predominantly elemental sulfur (S 0), the calibration standards were prepared from simple dilutions of S_8 in NaCl and Na_2CO_3; or using a sample set with analyte reference values. And for samples containing the predominant sulphate specie (S +VI), only one set of samples should be used with reference values for the determination of total S. Using PCA and the S Kβ and S Kβ' transitions, it was possible to identify the mineral supplements for cattle that contained predominantly S 0 or S +VI species.

Using the XANES associated with the chemometric tools, PLS regression, PCA and LCF; was possible to perform the speciation analysis of P (phosphate and phosphite) from the simple dilution in water of the samples of fertilizers and mineral supplements for cattle. The chemometric tools used enabled the determination of the analytes and the recognition of patterns that help to verify the authenticity of the information contained in the labels of these agricultural inputs.

The macronutrients Ca and P, contained in mineral supplements for cattle, were determined with precision and accuracy by LIBS using the MEC and OP GSA methods. For the use of these strategies, only two calibration

standards are required for each sample, which enable efficient matrix-matching and to overcome matrix effects, because a portion of the sample is used in the preparation of the calibration standards. Better analytical parameters were obtained using MEC and OP GSA, when compared to MMC and IS. In addition, the use of MEC permits to identify a spectral interference for P line due to the presence of Fe.

Using LIBS was possible to determine Al and Pb in waste PCB samples (both metals can be recyclable, and Pb must be monitored as it is toxic). Of the five calibration strategies evaluated (MMC, CF, SSC, TP CT and OP MLC), some of which have recently been reported in the literature; MMC and calibration-free - CF, allowed satisfactory results for both analytes. The direct solid analysis by LIBS, and the use of these calibration strategies allow, from the determined concentrations, to evaluate and assist the correct segregation of waste PCBs, aiming at economic (recycling) and environmental protection questions.

Chapter 5 – References

1. MACHADO, R. C.; ANDRADE, D. F.; BABOS, D. V.; CASTRO, J. P.; COSTA, C. C.; SPERANÇA, M. A.; GARCIA, J. A.; GAMELA, R. R. & PEREIRA-FILHO, E. “Solid sampling: advantages and challenges for chemical element determination - a critical review”. J. Anal. At. Spectrom., 35: 54-77, 2020.

2. KRUG, F. J. & ROCHA, F. R. P. “Métodos de preparo de amostras para análise elementar”. EditSBQ – Sociedade Brasileira de Química, São Paulo, 2016.

3. NOMURA, C. S.; DA SILVA, C. S. & OLIVEIRA, P. V. “Análise direta de sólidos por espectrometria de absorção atômica com atomização em forno de grafite: uma revisão”. Quim. Nova, 31 (1): 104-113, 2008.

4. CARVALHO, R. R. V.; COELHO, J. A. O.; AQUINO, F. W. B.; CARNEIRO, R. L. & PEREIRA-FILHO, E. R. “Laser-induced breakdown spectroscopy (LIBS) combined with hyperspectral imaging for the evaluation of printed circuit board composition”. Talanta, 143: 278-283, 2015.

5. WILLIS, J. P.; FEATHER, C. E. & TURNER, K. “Guidelines for XRF analysis”. James Willis Consultants cc, Cape Town, 2014.

6. WILLIS, J. P. & DUCAN, A. R. “Understanding XRF spectrometry. Basic concepts and instrumentation”. Volume 1. PANalytical B.V., Almelo, 2008.

7. CARVALHO, G. G. A.; GUERRA, M. B. B.; ADAME, A.; NOMURA, C. S.; OLIVEIRA, P. V.; CARVALHO, H. W. P.; SANTOS JÚNIOR, D.; NUNES L. C. & KRUG, F.J. “Recent advances in LIBS and XRF for the analysis of plants”. J. Anal. At. Spectrom., 33: 919-944, 2018.

8. TAKAHASHI, T. & THORNTON, B. “Quantitative methods for compensation of matrix effects and self-absorption in laser induced breakdown spectroscopy signals of solids”. Spectrochim. Acta B, 138: 31-42, 2017.

9. MORAIS, C. P.; BARROS, A. I.; BECHLIN, M. A.; SILVA, T. V.; SANTOS JÚNIOR, D.; SENESI, G. S., CRESPI, M. S., RIBEIRO, C. A., GOMES NETO, J. A. & FERREIRA, E. C. “Laser-induced breakdown spectroscopy

determination of K in biochar-based fertilizers in the presence of easily ionizable element". Talanta, 188: 199-202, 2018.

10. COSTA, V. C.; AUGUSTO, A. S.; CASTRO, J. P.; MACHADO, R. C.; ANDRADE, D. F.; BABOS, D. V.; SPERANÇA, M. A.; GAMELA, R. R. & PEREIRA-FILHO, E. R. "Laser induced-breakdown spectroscopy (LIBS): history, fundamentals, applications and potentialities". Quim. Nova, 42: 527-545, 2019.

11. WILLIS, J. P. & DUCAN, A. R. "Understanding XRF spectrometry. Quantitative analysis and special sample preparation and presentation methods". Volume 2. PANalytical B.V., Almelo, 2008.

12. ANDRADE, D. F.; PEREIRA-FILHO, E. R. & AMARASIRIWARDENA, D. "Current trends in laser-induced breakdown spectroscopy: a tutorial review". Appl. Spectrosc. Rev., DOI: 10.1080/05704928.2020.1739063, 2020.

13. BABOS, D.V.; BARROS, A. I.; NÓBREGA, J. A. & PEREIRA-FILHO, E. R. "Calibration strategies to overcomed matrix effects in laser-induced breakdown spectroscopy: direct calcium and phosphorus determination in solid mineral supplements". Spectrochim. Acta B., 155: 90-98, 2019.

14. BABOS, D. V.; VIRGILIO, A.; COSTA, V. C.; DONATI, G. L. & PEREIRA-FILHO, E. R. "Multi-energy calibration (MEC) applied to laser-induced breakdown spectroscopy (LIBS)". J. Anal. At. Spectrom., 33: 1753-1762, 2018.

15. VIEIRA, A. L.; SILVA, T. V.; DE SOUSA, F. S. I.; SENESI, G. S.; SANTOS JÚNIOR, D.; FERREIRA, E. C. & GOMES NETO, J. A. "Determinations of phosphorus in fertilizers by spark discharge-assisted laser-induced breakdown spectroscopy". Microchem. J., 139: 322-326, 2018.

16 COSTA, V. C.; AMORIN, F. A. C.; BABOS, D. V. & PEREIRA-FILHO, E. R. "Direct determination of Ca, K, Mg, Na, P, S, Fe and Zn in bivalve mollusks by wavelength dispersive X-ray fluorescence (WDXRF) and laser-induced breakdown spectroscopy (LIBS)". Food Chem., 273: 91-98, 2019.

17. YI, R. X.; GUO, L. B.; ZOU, X. H.; LI, J. M.; HAO, Z. Q.; YANG, X. Y.; LI, X. Y.; ZENG, X. Y. & LU, Y. F. “Background removal in soil analysis using laser-induced breakdown spectroscopy combined with standard addition method”. Opt. Express, 24: 2607-2618, 2016.

18. WU, C.; SUN, D. X.; SU, M. G.; YIN, Y. P.; HAN, W. W.; LU, Q. F. & DONG, C. Z. “Quantitative analysis of Pb in soil samples by laser-induced breakdown spectroscopy with a simplified standard addition method’. J. Anal. At. Spectrom., 34: 1478-1484, 2019.

19. CARVALHO, A. A. C.; LEME, F. O.; LUZ, M. S.; OLIVEIRA, P. V. & NOMURA, C. S. “Internal standard fused glass beads for high silicon content sample analysis by laser-induced breakdown spectrometry”. J. Anal. At. Spectrom., 33: 1243-1250, 2018.

20. MORAIS, P. C.; BARROS, A. I.; SANTOS JÚNIOR, D.; RIBEIRO, C. A.; CRESPI, M. S.; SENESI, G. S.; GOMES NETO, J. A. & FERREIRA, E. C. “Calcium determination in biochar-based fertilizers by laser-induced breakdown spectroscopy using sodium as internal standard”. Microchem. J., 134: 370-373, 2017.

21. MZYK, Z.; ANYSZKIEWICZ, J. & GOREWODA, T. “Special tablets containing cellulose binder and Sr internal standard for simplifying X-ray fluorescence analysis of powder samples”. Spectrochim. Acta B, 114:15-19, 2015.

22. PASHKOVA, G. V.; AISUEVA, T. S.; FINKELSHTEIN, A. L.; IVANOV, E. V. & SHCHETNIKOV, A. A. “Analytical approaches for determination of bromine in sediment core samples by X-ray fluorescence spectrometry”. Talanta, 160: 375-380, 2016.

23. MALHERBE, J. & CLAVERIE, F. “Toward chromium speciation in solids using wavelength dispersive X-ray fluorescence spectrometry Cr Kβ lines”. Anal. Chim. Acta, 773: 37-44, 2013.

24. ROMERA, J. P. R.; BARSANELLI P. L. & PEREIRA. F. M. V. “Expeditious prediction of fiber content in sugar cane: an analytical possibility with LIBS and chemometrics”. Fuel, 166: 473-476, 2016.

25. CASTRO, J. P.; BABOS, D. V. & PEREIRA-FILHO, E. R. “Calibration strategies for the direct determination of rare earth elements in hard disk magnets using laser-induced breakdown spectroscopy”. Talanta, 208: 120443, 2020.

26. SPERANÇA, M. A.; ANDRADE, D. F.; CASTRO, J. P. & PEREIRA-FILHO, E. P. “Univariate and multivariate calibration strategies in combination with laser-induced breakdown spectroscopy (LIBS) to determine Ti on sunscreen: a different sample preparation procedure”. Opt. Laser Technol., 109: 648–653, 2019.

27. GAMELA, R. R.; COSTA, V. C.; SPERANÇA, M. A. & PEREIRA-FILHO, E. R. “Laser-induced breakdown spectroscopy (LIBS) and wavelength dispersive X-ray fluorescence (WDXRF) data fusion to predict the concentration of K, Mg and P in bean seed samples”. Food Res. Int., 132: 109037, 2020.

28. DE OLIVEIRA, M. D.; FONTES, L. M. & PASQUINI, C. “Comparing laser induced breakdown spectroscopy, near infrared spectroscopy, and their integration for simultaneous multi-elemental determination of micro- and macronutrients in vegetable samples”. Anal. Chim. Acta, 1062: 28-36, 2019.

29. KUMAR, N.; BANSAL, A.; SARMA, G. S. & RAWAL, R. K. “Chemometrics tools used in analytical chemistry: an overview”. Talanta, 123: 186-199, 2014.

30. BRO, R. “Multivariate calibration. What is in chemometrics for the analytical chemist?”. Anal. Chim. Acta, 500: 185-194, 2003.

31. FERREIRA, M. M. C. “Quimiometria – conceitos, métodos e aplicações”. Editora da Unicamp, Campinas, 2015.

32. YAROSHCHYK, P.; DEATH, D.L. & SPENCER S.J. “Comparison of principal components regression, partial least squares regression, multi-block partial least squares regression, and serial partial least squares regression

algorithms for the analysis of Fe in iron ore using LIBS". J. Anal. At. Spectrom., 27: 92-98, 2012.

33. PANCHUK, V.; YAROSHENKO, I.; LEGIN, A.; SEMENOV, V. & KIRSANOV, D. "Application of chemometric methods to XRF-data - a tutorial review". Anal. Chim. Acta, 1040: 19-32, 2018.

34. HENDERSON, G. S.; DE GROOT F. M. F. & MOULTON, B. J. A. "X-ray absorption near-edge structure (XANES) spectroscopy" Rev. Mineral. Geochem., 78: 75-138, 2014.

35. ULERY, A. L. & DREES, L. R. "Methods of soil analysis part 5 - mineralogical methods". Soil Science of America, Madison, 2008.

36. WEST, M.; ELLIS, A. T.; STRELI, C.; VANHOOF, C. & WOBRAUSCHEK, P. "2017 atomic spectrometry update - a review of advances in X-ray fluorescence spectrometry and its special applications". J. Anal. At. Spectrom., 32:1629-1649, 2017.

37. OHMORI, T.; KATO, S.; DOI, M.; SHOJI, T & TSUJI, K. "Wavelength dispersive X-ray fluorescence imaging using a high-sensitivity imaging sensor". Spectrochim. Acta B., 83-84: 56-60, 2013.

38. TSUJI, K.; MATSUNO,T.; TAKIMOTO, Y.; YAMANASHI, M.; KOMETANI, N.; SASAKI, Y. C.; HASEGAWA, T.; KATO, S.; YAMADA, T.; SHOJI, T. & KAWAHARA, N. "New developments of X-ray fluorescence imaging techniques in laboratory". Spectrochim. Acta B.,113: 43-53, 2015.

39. ALEXANDRINA, E. C.; BABOS, D. V.; ANDRADE, D. F.; COSTA, V. C.; LUI, E. S.; CORRÊIA, N. A.; AGUIAR, M. L. & PEREIRA-FILHO, E. R. "Particulate matter (PM10) from São Carlos-SP (Brazil): spectroanalytical techniques to evaluated and determine chemical elements". Int. J. Environ. Anal. Chem., 99(7): 653-669, 2019.

40. SANTOS, M. C.; SPERANÇA, M. A. & PEREIRA, F. M. V. "Wavelength dispersive X-ray fluorescence (WDXRF) and chemometric investigations of human hair after cosmetic treatment". X-Ray Spectrom., 47 (3): 252-257, 2018.

41. BABOS, D. V.; COSTA, V. C. & PEREIRA-FILHO, E. R. “Wavelength dispersive X-ray fluorescence (WD-XRF) applied to speciation of sulphur in mineral supplements for cattle: evaluation of the chemical and matrix effects.” Microchem. J., 147:628-634, 2019.

42. ZHAO, W, Z.; LU, B.; YU, J. B.; ZHANG, B. B. & ZHANG, Y. “Determination of sulfur in soils and stream sediments by wavelength dispersive X-ray fluorescence spectrometry”. Microchem. J., 156:104846, 2020.

43. CHUBAROV, V. M.; AMOSOVA, A. A. & FINKELSHTEIN, A. L. “Determination of iron and sulfur valence state in coal ashes by wavelength-dispersive X-ray fluorescence spectrometric technique”. Spectrochim. Acta B., 163: 105745, 2020.

44. CHUBAROV, V.; SUVOROVA, D.; MUKHETDINOVA, A. & FINKELSHTEIN, A. “X-ray fluorescence determination of the manganese valence state and speciation in manganese ores.” X-ray Spectrom., 44:436-441, 2015.

45. OZDEMIR, Y.; BOREKCI, B.; LEVET, A & KURUDIREK, M. “Assessment of trace element concentration distribution in human placenta by wavelength dispersive X-ray fluorescence: effect of neonate weight and maternal age”. Appl. Radiat. Isot., 67:1790-1795, 2009.

46. MARGUÍ, E.; HIDALGO, M. & QUERALT, I. “Multielemental fast analysis of vegetation samples by wavelength dispersive X-ray fluorescence spectrometry: possibilities and drawbacks”. Spectrochim. Acta B., 60:1363- 1372, 2005.

47. KRISHNA, A. K.; KHANNA, T. C. & MOHAN, K. R. “Rapid quantitative determination of major and trace elements in silicate rocks and soils employing fused glass discs using wavelength dispersive X-ray fluorescence spectrometry”. Spectrochim. Acta B., 122: 165-171, 2016.

48. CASTRO, J. P.; SPERANCA, M. A.; BABOS, D. V.; ANDRADE, D. F. & PEREIRA-FILHO, E. R. “Neodymium determination in hard drive disks magnets using different calibration approaches for wavelength dispersive X-ray fluorescence”. Spectrochim. Acta B., 164:105763, 2020.

49. NAKAYAMA, K. & WAGTSUMA, K. “Absorption-free calibration on X-ray fluorescence analysis of high-speed steel with glass bead preparation”. X-ray Spectrom., 49(2): 332-337, 2020.

50. SHE, X.; ZHU, Z.; GAO, J.; QIAN, R.; SHENG, C.; SHEN, R. & ZHUO, S. “Application of Kβ / Kα in selecting calibration standards for X-ray fluorescence analysis”. X-ray Spectrom. 48:664-673, 2019.

51. GRÄFE, M.; DONNER, E.; COLLINS, R. N. & LOMBI, E. “Speciation of metal(loid)s in environmental samples by X-ray absorption spectroscopy: A critical review”. Anal Chim. Acta., 822: 1-22, 2014.

52. PORCARO, F.; ROUDEAU, S.; CARMONA, A. & ORTEGA, R. “Advances in element speciation analysis of biomedical samples using synchrotron based techniques”. Trend Anal. Chem., 104: 22-41, 2018.

53. HENDERSON, G. S.; DE GROOT, F. M. F. & MOULTON, B. J. A. “X-ray absorption near-edge structure (XANES) spectroscopy”. Rev. Mineral. Geochem., 78:75-138, 2014.

54. GUDA, A. A.; GUDA, S. A.; LOMACHENKO, K. A.; SOLDATOV, M. A.; PANKIN, I A.; SOLDATOV, A. V.; BRAGLIA, L.; BUGAEV, A. L.; MARTINI, A.; SIGNORILE, M.; GROPPO, E.; PIOVANO, A.; BORFECCHIA, E. & LAMBERTI, C. “Quantitative structural determination of active sites from *in situ* and *operando* XANES spectra: from standard *ab initio* simulations to chemometric and machine learning approaches.” Catal. Today, 366: 3-21, 2019.

55. BAVA, Y. B.; GERONÉS, M.; GIOVANETTI, L. J.; ANDRINI, L. & ERBEN, M. F. “Speciation of sulphur in asphaltenes and resins from Argentinian petroleum by using XANES spectroscopy”. Fuel, 256:115952, 2019.

56. SZCZERBOWSKA-BORUCHOWSKA, M.; LANKOSZ, M.; CZYZYCKI, M. & ADAMEK, D. “An integrated experimental and analytical approach to the chemical state imaging of iron in brain gliomas using X-ray absorption near edge structure spectroscopy”. Anal. Chim. Acta, 699:153-160, 2011.

57. SHAFFER, R. E.; CROSS, J. O.; ROSE-PEHRSSON, S. L. & ELAM, W. T. “Speciation of chromium in simulated soil samples using X-ray absorption spectroscopy and multivariate calibration”. Anal. Chim. Acta, 442: 295-304, 2001.

58. TERZANO, R.; AL CHAMI, Z.; VEKEMANS, B.; JANSSENS, K.; MIANO, T. & RUGGIERO, P. “Zinc distribution and speciation within rocket plants (*Eruca vesicaria L. Cavalieri*) grown on a polluted soil amended with compost as determined by XRF microtomography and micro-XANES”. J. Agric. Food Chem. 56: 3222-3231, 2008.

59. KAPPEN, P.; FERRANDO-MIGUEL, G.; REICHMAN, S. M.; INNES, L.; WELTER, E. & PIGRAM, P. J. “Antimony leaching and chemical species analyses in an industrial solid waste: Surface and bulk speciation using ToF-SIMS and XANES”. J. Hazard. Mater., 329: 131-140, 2017.

60. CHITPIROM, K.; AKARACHARANYA, A.; TANAWUPAWAT, S.; LEEPTPATPIBOON N.; KIM, K. W.; HORMES, J. & PRANGE, A. “Characterization of arsenic speciation using XANES spectroscopy in *Comamonas terrae*, an arsenite-oxidizing bacterium isolated from agricultural soil in Thailand”. J. Food. Agric. Environ., 15: 44-47, 2017.

61. BELISSONT, R.; MUÑOZ, M.; BOIRON, M. C.; LUAIS, B. & MATHON, O. “Distribution and oxidation state of Ge, Cu and Fe in sphalerite by µ-XRF and K-edge µ-XANES: insights into Ge incorporation, partitioning and isotopic fractionation”. Geochim. Cosmochim. Acta, 177: 298-314, 2016.

62. TANNAZI, F. & BUNKER, G. “Determination of chemical speciation by XAFS”. Phys. Scr. T115: 953-956, 2005.

63. ERIKSSON, A. K.; HESTERBERG, D.; KLYSUBUN, W. & GUSTAFSSON, J. P. “Phosphorus dynamics in Swedish agricultural soils as influenced by fertilization and mineralogical properties: Insights gained from batch experiments and XANES spectroscopy”. Sci. Total Environ., 566-567: 1410-1419, 2016.

64. BABOS, D. V.; CASTRO, J. P.; ANDRADE, D. F.; COSTA, V. C. & PEREIRA-FILHO, E. R. “Determination and speciation of phosphorus in fertilizers and mineral supplements for cattle by X-ray absorption near-edge structure spectroscopy: a simple nondestructive method”. Anal. Methods, 11: 1508-1515, 2019.

65. LEVINA, A.; McLEOD, A. I.; GASPARINI, S. J.; NGUYEN A.; DE SILVA, W. G. M.; AITKEN, J. B.; HARRIS, H. H.; GLOVER, C.; JOHANNESSEN, B. & LAY, P. A. “Reactivity and speciation of anti-diabetic vanadium complexes in whole blood and its components: the importance role of red blood cell”. Inorg. Chem., 54: 7753-7766, 2015.

66. SIEBERS, N.; KRUSE, J.; ECKHARDT, K. U.; HU, Y. & LEINWERBER, P. “Solid-phase cadmium speciation in soil using L3-edge XANES spectroscopy with partial least-squares regression”. J. Synchrotron Rad., 19: 579-585, 2012.

67. VORONOV, A.; URAKAWA, A.; VAN BEEK, W.; TSAKOUMIS, N. E.; EMERICH, H. & RØNNING, M. “Multivariate curve resolution applied to in situ X-ray absorption spectroscopy data: an efficient tool for data processing and analysis”. Anal. Chim. Acta., 840: 20-27, 2014.

68. CASSINELLI, W. H.; MARTINS, L.; PASSOS, A. R.; PULCINELLI, S. H.; SANTILLI, C. V.; ROCHET, A. & BRIOIS, V. “Multivariate curve resolution analysis applied to time-resolved synchrotron X-ray absorption spectroscopy monitoring of the activation of copper alumina catalyst”. Catal. Today, 229: 114-122, 2014.

69. NIKULSHINA, M.; BLANCHARD, P.; LANCELOT, C.; GRIBOVAL-CONSTANT, A.; MARINOVA, M.; BRIOIS, V.; NIKULSHIN, P. & LAMONIER, C. “Genesis of active phase in MoW/Al_2O_3 hydrotreating catalysts monitored by HAADF and in situ QEXAFS combined to MCR-ALS analysis”. Appl. Catal. B. Environ, 269: 118766, 2020.

70. ROCHET, A.; BAUBET, B.; MOIZAN, V.; PICHON, C. & BRIOIS, V. “Co-K and Mo-K edges Quick-XAS study of the sulphidation properties of Mo/Al_2O_3 and $CoMo/Al_2O_3$ catalysts.” C. R. Chimie, 19: 1337-1351, 2016.

71. RAVEL, B. & NEWVILLE, M. “ATHENA, ARTEMIS, HEPHAESTUS: data analysis for X-ray absorption spectroscopy using IFEFFIT.” J. Synchrotron Radiat. 12: 537-541, 2005.

72. KUNO, A.; MATSUO, M. & NUMAKO, C. “*In situ* chemical speciation of iron in stuarine sediments using XANES spectroscopy with partial least-squares regression”. J. Synchrotron Rad., 6: 667-669, 1999.

73. NOLL, R. “Laser-induced breakdown spectroscopy: fundamentals and applications”, Springer, Berlin, Heidelberg, 2012.

74. COSTA, V. C.; CASTRO, J. P.; ANDRADE, D. F.; BABOS, D. V.; GARCIA, J. A.; SPERANÇA, M. A.; CATELANI, T. A. & PEREIRA-FILHO, E. R. “Laser-induced breakdown spectroscopy (LIBS) applications in the chemical analysis of waste electrical and electronic equipment (WEEE)”. Trend Anal. Chem., 108: 65-73, 2018.

75. MIZIOLEK, A. W.; PALLESCHI, V. & SCHECHTER, I. “Laser-induced breakdown spectroscopy: fundamentals and applications”, Cambridge, UK, 2006.

76. SERRANO, J.; MOROS, J. & LASERNA, J. J. “Sensing signatures mediated by chemical structure of molecular solids in laser-induced plasmas”. Anal. Chem., 87: 2794−2801, 2015.

77. KALAM, S. A.; MURTHY, N. L.; MATHI, P.; KOMMU, N.; SINGH, A. K. & RAO, S. V. “Correlation of molecular, atomic emissions with detonation parameters in femtosecond and nanosecond LIBS plasma of high energy materials”. J. Anal. At. Spectrom. 32: 1535-1546, 2017.

78. SERRANO, J.; MOROS, J. & LASERNA, J. J. “Exploring the formation routes of diatomic hydrogenated radicals using femtosecond laser-induced breakdown spectroscopy of deuterated molecular solids”. J. Anal. At. Spectrom., 30: 2343-2352, 2015.

79. SERRANO, J.; MOROS, J. & LASERNA, J. J. “Molecular signatures in femtosecond laser-induced organic plasmas. comparison with nanosecond laser ablation”. Phys. Chem. Chem. Phys., 18: 2398-2408, 2016.

80. DELGADO, T.; VADILLO, J. M. & LASERNA, J. J. “Isomer discrimination in condensed phase by laser-induced breakdown spectrometry and laser-ionization mass spectrometry using a tailored paired-pulse excitation scheme”. J. Anal. At. Spectrom., 28: 1377-1384, 2013.

81. PIETSCH, W.; PETIT, A. & BRIAND, A. “Isotope ratio determination of uranium by optical emission spectroscopy on a laser-produced plasma - basic investigations and analytical results”. Spectrochim. Acta B, 53: 751-761, 1998.

82. RUSSO, R. E.; BOL'SHAKOV, A. A.; MAO, X.; MCKAY, C. P.; PERRY, D. L. & SORKHABI, O. “Laser ablation molecular isotopic spectrometry”. Spectrochim. Acta B 66: 99-104, 2011.

83. JOLIVET, L.; LEPRINCE, M.; MONCAYO, S.; SORBIER, L.; LIENEMANN, C. -P. & MOTTO-ROS, V. “Review of the recent advances and applications of LIBS-based imaging”. Spectrochim. Acta B, 151: 41-53, 2019.

84. GAMELA, R. R.; SPERANÇA, M. A.; ANDRADE, D. F & PEREIRA-FILHO, E. R. “Hyperspectral images: a qualitative approach to evaluate the chemical profile distribution of Ca, K, Mg, Na and P in edible seeds employing laser-induced breakdown spectroscopy”. Anal. Methods, 11: 5543-5552, 2019.

85. NARDECCHIA, A.; FABRE, C.; CAUZID, J.; PELASCINI, F.; MOTTO-ROS, V. & DUPONCHEL, L. “Detection of minor compounds in complex mineral samples from millions of spectra: a new data analysis strategy in LIBS imaging.” Anal. Chim. Acta, 11141: 66-73, 2020.

86. CASTRO, J. P & PEREIRA-FILHO, E. R. “Twelve different types of data normalization for the proposition of classification, univariate and multivariate regression models for the direct analyses of alloys by laser-induced breakdown spectroscopy (LIBS)”. J. Anal. At. Spectrom., 31: 2005-2014, 2016.

87. BELLOU, E.; GYFTOKOSTAS, N.; STEFAS, D.; GAZELI, O. & COURIS, S. “Laser-induced breakdown spectroscopy assisted by machine learning for olive oils classification: the effect of the experimental parameters”. Spectrochim. Acta B, 163: 105746, 2020.

88. SPERANÇA, M. A.; POMARES-ALFONSO, M. S. & PEREIRA-FILHO, E. R. “Analysis of cuban nickeliferous minerals by laser-induced breakdown spectroscopy (LIBS): non-conventional sample preparation of powder samples”. Anal. Methods, 10: 533-540, 2018.

89. DIB, S. R.; NESPECA, M. G.; SANTOS JUNIOR, D.; RIBEIRO, C. A.; CRESPI, M. S.; GOMES NETO, J. A. & FERREIRA, E. C. “CN diatomic emission for N determination by LIBS”. Microchem. J., 157: 105107, 2020.

90. ZHANG, S.; CHU, Y.; MA, S.; CHEN, F.; ZHANG, D.; HU, Z.; ZHANG, Z.; JIN, H. & GUO, L. “Highly accurate determination of Zn and Cu in human hair by ultrasound-assisted alkali dissolution combined with laser-induced breakdown spectroscopy”. Microchem. J., 157: 105018, 2020.

91. CIUCCI, A.; CORSI, M.; PALLESCHI, V.; RASTELLI, S.; SALVETTI, A. & TOGNONI, E. “New procedure for quantitative elemental analysis by laser-induced plasma spectroscopy”. Appl. Spectrosc., 53: 960-964, 1999.

92. TOGNONI, E.; CRISTOFORETTI, G.; LEGNAIOLI, S. & PALLESCHI, V. “Calibration-free laser-induced breakdown spectroscopy: state of the art”. Spectrochim. Acta B, 65: 1-14, 2010.

93. GRIFONI, E.; LEGNAIOLI, S.; LORENZETTI, G.; PAGNOTTA, S.; POGGIALINI, F. & PALLESCHI, V. “From calibration-free to fundamental parameters analysis: a comparison of three recently proposed approaches”. Spectrochim. Acta B 124: 40.46, 2016.

94. CHEN, C.-T.; BANARU, D.; SARNET, T. & HERMANN, J. “Two-step procedure for trace element analysis in food via calibration-free laser-induced breakdown spectroscopy”. Spectrochim. Acta B, 150: 77-85, 2018.

95. LI, T.; HOU, Z.; FU, Y.; YU, J.; GU, W. & WANG, Z. “Correction of self-absorption effect in calibration-free laser-induced breakdown spectroscopy (CF-LIBS) with blackbody radiation reference". Anal. Chim. Acta, 1058: 39-47, 2019.

96. PRAHER, B.; PALLESCHI, V.; VISKUP, R.; HEITZ, J. & PEDARNIG, J. D. "Calibration free laser-induced breakdown spectroscopy of oxide materials". Spectrochim. Acta B, 65: 671-679, 2010.

97. CAVALCANTI, G. H.; TEIXEIRA, D. V.; LEGNAIOLI, S.; LORENZETTI, G.; PARDINI, L. & PALLESCHI, V. “One-point calibration for calibration-free laser-induced breakdown spectroscopy quantitative analysis”. Spectrochim. Acta B, 87: 51-56, 2013.

98. GAUDIUSO, R.; DELL'AGLIO, M., DE PASCALE, O.; SANTAGATA, A. & DE GIACOMO, A. “Laser-induced plasma analysis of copper alloys based on local thermodynamic equilibrium: an alternative approach to plasma temperature determination and archeometric applications”. Spectrochim. Acta B, 74-75: 38-45, 2012.

99. ARAGÓN, C. & AGUILERA, J. A. “CSigma graphs: a new approach for plasma characterization in laser-induced breakdown spectroscopy”. J. Quant. Spectrosc. Radiat. Transf., 149: 90-102, 2014.

100. GAUDIUSO, R. “Calibration-free inverse method for depth-profile analysis with laser-induced breakdown spectroscopy”. Spectrochim. Acta B, 123: 105-113, 2016.

101. ARAGÓN, C. & AGUILERA, J. A. “Direct analysis of aluminum alloys by CSigma laser-induced breakdown spectroscopy”. Anal. Chim. Acta, 1009:12-19, 2018.

102. HAO, Z.Q.; LIU, L.; ZHOU, R.; MA, Y.W.; LI, X. Y.; GUO, L. B.; LU, Y. F. & ZENG, X. Y. “One-point and multi-line calibration method in laser-induced breakdown spectroscopy”. Opt. Express, 26: 22926-22933, 2018.

103. GAMELA, R. R.; COSTA, V. C.; BABOS, D. V.; ARAÚJO, A. S. & PEREIRA-FILHO, E. R. “Direct determination of ca, k, and mg in cocoa beans by laser-induced breakdown spectroscopy (LIBS): evaluation of three univariate calibration strategies for matrix matching”. Food. Anal. Methods, 13:1017-1026, 2020.

104. BABOS, D. V.; CRUZ-CONESA, A.; PEREIRA-FILHO, E. R. & ANZANO, J. M. “Direct determination of Al and Pb in waste printed circuit boards (PCB) by laser-induced breakdown spectroscopy (LIBS): evaluation of calibration

strategies and economic - environmental questions". J. Hazard. Mater., 399:122831, 2020.

105. YAN, R.; TANG, Y.; ZHU, Z.; HAO, Z.; LI, J.; YU, H.; YU, Y.; GUO, L.; ZENG, X. & LU, Y. "Accuracy improvement of quantitative analysis for major elements in laser-induced breakdown spectroscopy using single-sample calibration". Anal. Chim. Acta, 1064:11-16, 2019.

106. NUNES, L. C.; ROCHA, F. R. P. & KRUG, F. J. "Slope ratio calibration for analysis of plant leaves by laser-induced breakdown spectroscopy". J. Anal. At. Spectrom., 34: 2314-2324, 2019.

107. VIRGILIO, A.; GONÇALVES, D. A.; McSWEENEY, T.; GOMES NETO, J. A.; NOBREGA, J. A. & DONATI, G. L. "Muti-energy calibration applied to atomic spectrometry". Anal. Chim. Acta., 982:31-36, 2017.

108. AUGUSTO, A. S.; CASTRO, J. P.; SPERANÇA, M. A. & PEREIRA-FILHO, E. R. "Combination of multi-energy calibration (MEC) and laser-induced breakdown spectroscopy (LIBS) for dietary supplements analysis and determination of Ca, Mg and K". J. Braz. Chem. Soc., 30: 804-812, 2019.

109. CARVALHO, A. A. C.; COZER, L. A.; LUZ, M. S.; NUNES, L. C.; ROCHA, F. R. P. & NOMURA, C. S. "Multi-energy calibration and sample fusion as alternatives for quantitative analysis of high silicon content samples by laser-induced breakdown spectrometry". J. Anal. At. Spectrom., 34: 1701-1707, 2019.

110. ANDRADE, D. F.; FORTUNATO, F. M. & PEREIRA-FILHO, E. R. "Calibration strategies for determination of the In content in discarded liquid crystal displays (LCD) from mobile phones using laser-induced breakdown spectroscopy (LIBS)". Anal. Chim. Acta, 1061: 42-49, 2019.

111. FORTUNATO, F. M.; CATELANI, T.A.; POMARES-ALFONSO, M. S. & PEREIRA-FILHO, E. R. "Application of multi-energy calibration for determination of chromium and nickel in nickeliferous ores by laser-induced breakdown spectroscopy". Anal. Sci., 35:165-168, 2019.

112. PEREIRA, F. M. V. & PEREIRA-FILHO, E. R. “Application of free computational program in experimental design: a tutorial”. Quim. Nova, 41: 1061-1071, 2018.

113. MILLAR, S.; GOTTLIEB, C.; GÜNTHER, T.; SANKAT, N.; WILSCH, G. & KRUSCHWITZ, S. "Chlorine determination in cement-bound materials with laser-induced breakdown spectroscopy (LIBS) - a review and validation". Spectrochim. Acta B, 147: 1-8, 2018.

114. MARTINEZ, M. & BAUDELET, M. “Matrix-matched calibration material for zinc analysis of human nails by laser-induced breakdown spectroscopy”. Spectrochim. Acta B, 163: 105732, 2020.

115. DUPONCHEL, L.; BOUSQUET, B.; PELASCINI, F. & MOTTO-ROS, V. "Should we prefer inverse models in quantitative LIBS analysis?" J. Anal. At. Spectrom., 35: 794-803, 2020.

116. FERREIRA, E. C.; MILORI, D. M. B. P.; FERREIRA, E. J.; DA SILVA, R. M. & MARTIN-NETO, L. “Artificial neural network for Cu quantitative determination in soil using a portable laser induced breakdown spectroscopy system”. Spectrochim. Acta B, 63: 1216-1220, 2008.

117. EL HADDAD, J.; VILLOT-KADRI, M.; ISMAËL, A.; GALLOU, G.; MICHEL, K.; BRUYÈRE, D.; LAPERCHE, V.; CANIONI, L. & BOUSQUET, B. “Artificial neural network for on-site quantitative analysis of soils using laser induced breakdown spectroscopy”. Spectrochim. Acta B, 79-80: 51-57, 2013.

118. EL HADDAD, J.; LIMA FILHO, E. S.; VANIER, F.; HARHIRA, A.; PADIOLEAU, C.; SABSABI, M.; WILKIE, G. & BLOUIN, A. “Multiphase mineral identification and quantification by laser-induced breakdown spectroscopy”. Miner. Eng., 134: 281-290, 2019.

119. EL RAKWE, M.; RUTLEDGE, D. N.; MOUTIERS, G. & SIRVEN, J. -B. “Analysis of time-resolved laser-induced breakdown spectra by mean field-independent components analysis (MFICA) and multivariate curve resolution-alternating least squares (MCR-ALS)”. J. Chemom., 31: e2869, 2017.

120. ZHANG, Y.; SUN, C.; GAO, L.; YUE, Z.; SHABBIR, S.; XU, W.; WU, M. & YU, J. “Determination of minor metal elements in steel using laser-induced breakdown spectroscopy combined with machine learning algorithms”. Spectrochim. Acta B, 166: 105802, 2020.

121. BOUCHER, T. F.; OZANNE, M. V.; CARMOSINO, M. L.; DYAR, M. D.; MAHADEVAN, S.; BREVES, E. A.; LEPORE, K. H. & CLEGG, S. M. “A study of machine learning regression methods for major elemental analysis of rocks using laser-induced breakdown spectroscopy” Spectrochim. Acta B, 107: 1-10, 2015.

122. BREIMAN, L. “Rondom forests”. Machine Learning 45: 5-32, 2001.

123. ZHANG, T.; LIANG, L.; WANG, K.; TANG, H.; YANG, X.; DUAND, Y. & LI, H. "A novel approach for the quantitative analysis of multiple elements in steel based on laser-induced breakdown spectroscopy (LIBS) and random forest regression (RFR)". J. Anal. At. Spectrom, 29: 2323-2329, 2014.

124. WU, S.; ZHANG, T.; TANG, H.; WANG, K.; YANG, X. & LI, H. "Quantitative analysis of nonmetal elements in steel using laser-induced breakdown spectroscopy combined with random forest". Anal. Methods, 7: 2425-2432, 2015.

125. Wang, T.; Jiao, L.; Yan, C.; He, Y.; Li, M.; Zhang, T. & Li, H. "Simultaneous quantitative analysis of four metal elements in oily sludge by laser induced breakdown spectroscopy coupled with wavelet transform-random forest (WT-RF)". Chemom. Intell. Lab. Syst., 194: 103854, 2019.

126. CASTRO, J. P.; PEREIRA-FILHO, P. F. & BRO, R. “Laser-induced breakdown spectroscopy (LIBS) spectra interpretation and characterization using parallel factor analysis (PARAFAC): a new procedure for data and spectral interference processing fostering the waste electrical and electronic equipment (WEEE) recycling process”. J. Anal. At. Spectrom., 35: 1115-1124, 2020.

127. BRO, R. "PARAFAC. Tutorial and applications". Chemom. Intell. Lab. Syst., 38: 149-171, 1997.